Reverse Engineering the Tree

Nicholas T. Davies
University of Canterbury

New Zealand School of Forestry
College of Engineering
University of Canterbury

Thesis submitted in partial fulfilment of the requirements for the
Degree of Master of Forestry Science at the
University of Canterbury

· 2014 ·

Abstract

The aim of this thesis was to investigate the typical radial pattern of density and microfibril angle within *Pinus radiata* with respect to structural stability. In order to investigate changes in mechanical stability with different radial patterns, first experimental work was carried out in order to obtain elastic constants, Poisson ratios and limits of proportionality for green corewood and outerwood, these values, a discussion on their accuracy and the implications of the values are included along with a comparison to previous literature. These constants were used to parametrise a finite element model of a tree stem with different radial patterns, including patterns not observed in nature, wind loadings were applied to the stem and failure evaluated. It was found that patterns consisting of high density stiff wood and/or low density high flexibility wood could withstand the greatest wind speeds for a given stem and canopy, while high density flexible and low density stiff profiles generally performed poorly. The analysis was considered at ages 5, 10 and 15 years, each providing similar results. Why these profiles perform best, what errors need to be considered, and other evolutionary pressures which could narrow this list of profiles were discussed. The need for further research, and the directions for this research are suggested.

Contents

List of Figures

List of Tables

Acknowledgments

I would like to acknowledge a number of people and organisations for their monetary, motivational and academic support throughout this research. The work would not have been possible without all of them. The FRST Compromised Wood Quality project and the T.W. Adams scholarship both provided financial assistance for course fees, living costs, travel and other sundry items. Dr. Luis Apiolaza and Dr. Clemens Altaner provided supervisory roles for the project, giving advise, criticism, guidance and support even with some of my slightly esoteric or obscure approaches. I would also like to include Dr. Jonathan Harrington for warning me of pitfalls in this area of research and lending his thoughts on a number of topics including the mathematical implementation, without your advise this work would have been a lot more trying. Nigel Pink and Lochlan Kirk for the hours they put in with me in the laboratory. Last but not least my parents Heather and Meric Davies for their continued financial and motivational support.

Chapter 1

Introduction

1.1 Introduction

Previous work which has been completed in relevant fields such as wood structure, loading effects on wood, stem design, modelling attempts and the effect of wind damage are discussed below. Following this the objectives of this research are defined, the experimental and modelling work discussed and conclusions drawn.

The primary focus of this work was the relationship between the mechanical stability of tree stems in living (green) condition with respect to variations in the Typical Radial Pattern (TRP) under wind loading. The TRP in *Pinus radiata* has growth rings near the pith containing larger proportions of early wood tracheids which gradually decreases towards the bark. Early wood tracheids also increase in diameter with cambial age. These two properties are at least partially responsible for the typical variation in density observed (Meinzer et al., 2011). MicroFibril Angle (MFA), the angle at which the cellulose fibrils wind around the cell axis, generally declines rapidly in the first few growth rings out from the pith before it approaches a minimum value asymptotically (Cave and Walker, 1994). Other wood properties such as chemical composition are also observed to follow a TRP (Larson, 1966). While it is likely that there is a combination of mechanisms involved in producing the TRP, there are three common hypothesizes

(and a number of variants on these) which have been presented in order to explain these trends. Corewood and outerwood are defined as presented by Burdon et al. (2004). The first hypothesis is developmental; this simply argues that the cambium is not capable of producing outerwood cells until it has divided a number of times. The second is hydraulic, which argues that trees grow cells in a way to maximise water distribution and the third is mechanical, arguing that trees produce cellular properties in order to maintain structural integrity (Meinzer et al., 2011). There are others such as the auxin hypothesis which argue for different mechanistic controls, however essentially equate to one or a combination of the three main hypothesis. In the case of the auxin hypothesis it is argued that mechanical strains influence the distribution of auxin within forming cells creating particular patterns of cellular growth (Asnacios and Hamant, 2012).

The TRP of decreasing MFA and increasing density of *Pinus radiata* can be seen in Figure 1.1. By contrast the TRP of density for Sugi decreases with distance from the pith, as can be seen in Figure 1.2, even though both are softwoods. Within the Sugi species this density pattern can also vary by cultivar, ranging from near flat to having a negative gradient as shown by Yamashita et al. (2009). The MFA pattern also varies from near constant to a negative gradient, similar to what is observed in radiata.

While trees or parts of trees have small diameter stems it is advantageous for them to be able to bend in order to dissipate forces such as wind. Stem which remain rigid in wind require a much higher stiffness and strength in order to resist failure. Corewood has a high fracture strain which allows it to bend though large angles without rupturing the wood fibres, in order to dissipate loads. As the stem diameter increases in order to prevent buckling under self weight the second moment of area increases and strength must increase. By changing the properties of the wood produced to be stiffer a lower amount of material needs to be added in order to gain the same strength (Meinzer et al., 2011).

Most existing studies with the goal of obtaining material constants focus on dried timber, usually 12% moisture content outerwood. Little information available for corewood and greenwood presents a challenge for biomechanical investigation of living tree structures.

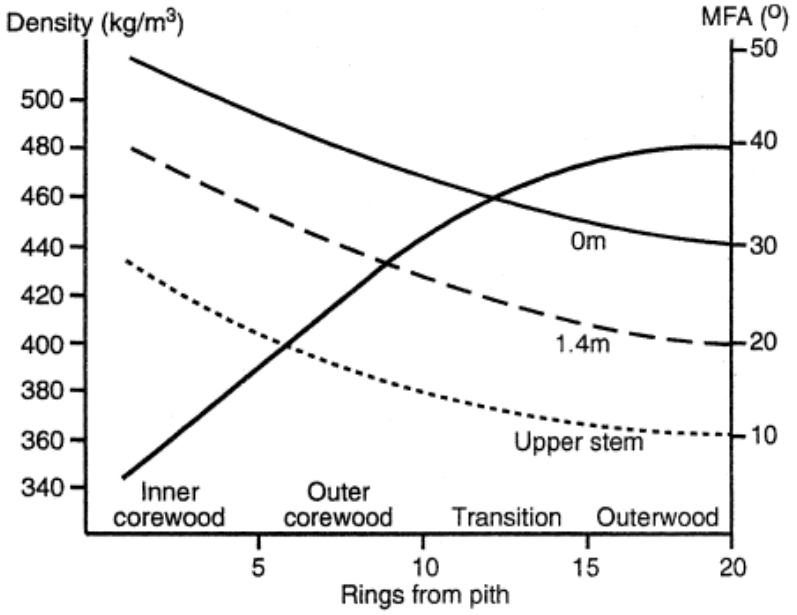

Figure 1.1: The TRP of density and MFA in *Pinus radiata* at varying heights. Reproduced from Burdon et al. (2004).

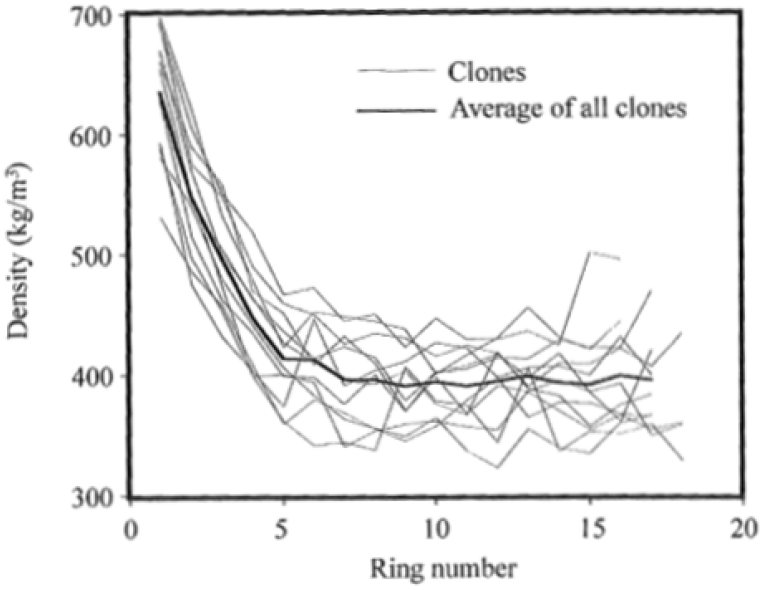

Figure 1.2: TRP for density of *Cryptomeria japonica*. Reproduced from Walker (2006).

1.2 Background

Current research into trees' biomechanical behaviour has had two main focuses, the focus on cells and their functions and the focus on the tree as an engineering structure. The term 'macroscopic' is used to refer to an engineering approach to tree biomechanics, which usually regards the tree as made from a homogeneous material. 'Microscopic' is used to descibe aspects of cells and structure inside the wood, these models are often unconcerned with the bio-mechanics of the whole tree instead focusing in more detail on particular aspects of the material. Some statistical techniques have been applied in an attempt to correlate microscopic attributes with final timber attributes, while these studies do not directly examine the biomechanical properties of the tree its-self they provide valuable insight into correlations which exist. Other studies have investigated wind forces required to damage individual trees and stands, while this does not directly investigate wood structure, it gives indications as to some of the formation attributes which may effect the structural integrity of the stem.

1.2.1 The structure of wood

The microscopic structure of living organisms such as trees is very complex with a lot of questions currently unanswered. When considering particular properties of trees, such as their mechanical behaviour, only a small subset of cells and their properties can be investigated. To understand tree stem mechanical behaviour both the mechanical properties and the geometry of wood as a cellular solid must be considered. Further cells, tissues and organs' mechanical properties can't be dissociated from their anatomical configuration. Wood is one of humans' oldest engineering materials (Mishnaevsky Jr. and Qing, 2008), however there is still a substantial lack of understanding of woods' material behaviour from the microscopic to macroscopic level (Holmberg et al., 1999).

Wood cells mainly consist of cellulose, lignin and hemi-celluloses. The cellulose is arranged into long micro-fibrils which have high tensile strength (Butterfield and Meylan, 1980) and are the principal tensile load bearing members in land plants (Niklas and Spatz, 2012). At a micrometre scale wood is a fibre reinforced composite, the cell walls

are made up of cellulose fibres embedded in a matrix of hemi-celluloses and lignin (Gibson, 1997). These cellulose reinforced cell walls are comparable to engineered composites such as kevlar for tensile strength for their weight (Niklas and Spatz, 2012).

Important factors such as fibre shape, cell wall thickness, MFA, cell shape, geometry and relative density must be considered (Mishnaevsky Jr. and Qing, 2008; Holmberg et al., 1999). Wood at the scale of micro to millimeters is a cellular solid with highly elongated cells made up from tracheids (in softwoods) and ray's (radially orientated parenchyma cells and in some cases radially orientated tracheids) (Walker, 1993; Gibson, 1997). The wood made up of tracheids can be considered a closed wall cellular solid with cylindrical units (Niklas and Spatz, 2012), others have suggested that hexagonal prism units are more appropriate (Gibson, 1997). In cellular solids the relative density, that is the density of the cellular material over the density of the solid making up the walls, largely dictates the attributes of the material. This is why late wood tends to be stronger and stiffer than early wood as it tends to have a greater volume of cell wall materials (Niklas and Spatz, 2012). Similarly a reduction in width of the cell wall creates the larger cell lumans' associated with the characteristics of earlywood.

When cells are created they form a primary cell wall, and after some expansion, when final size is reached a layered secondary wall is formed. The S_2 layer in the secondary cell wall largely determines the strength and stiffness of the wood (Niklas and Spatz, 2012). The cell wall needs to fulfil a number of mechanical and physiological requirements, initially the primary cell wall must be able to expand plastically during the growth phase, and resist large tensile stress (Schopfer, 2006). The tracheids provide support for the tree mechanically as well as conduct water (Reiterer et al., 1999).

The S_1 and S_3 layers tend to have more perpendicularly (to the vertical axis of the cell) arranged micro-fibrils than the S_2 layer (Niklas and Spatz, 2012). The strength of the cell wall is dependent on a number of characteristics, one of the most important variables is the water content of the cell wall which has effects on the mechanical and elastic behaviour of the cell, as it effects the adhesion between microfibrils. The cell wall is stiffer and stronger when it is dry rather than wet (Reiterer et al., 1999; Niklas and Spatz, 2012).

Lignin is deposited in the cell walls for two reasons; first it bolsters the cell wall increas-

ing the compressive strength by preventing buckling of the cellulose fibrils. Secondly it acts as a barrier and limits the moisture content of the cell wall due to its hydrophlic properties.

1.2.2 Loading of wood

When wood is under compressive loading it follows the typical pattern of most cellular solids, linear elastic deformation followed by a period of plastic deformation, where a stress plateau forms and finally the stress rises steeply resulting in a complete breakdown of the structure. Under compression cells undergo localized plastic buckling (Gibson, 1997). Buckling results in a slip plane beginning to form at approximately half the breaking load (Niklas and Spatz, 2012).

Wood is not technically a linear-elastic solid, it exhibits visco-elastic properties and because of this the standard tests of linear-elastic fracture dynamics do not always give consistent results. Cracks are stable and do not propagate for low sub-critical loads, once this load is exceeded the crack will propagate by one to a few cell diameters at a time, and finally become unstable and propagate rapidly over hundreds of cell diameters at a time (Gibson, 1997). Cracks in low density or earlywood (which is typically of low density) tend to propagate by cell wall breaking; this is when the cell is split open across the wall which loads the other side of the cell wall and it breaks, which in turn loads the cell wall of the next cell and so on. Crack advance in high density woods are characterised by both cell wall breaking and peeling. Cell wall peeling occurs when cells de-bond along the middle lamella (Gibson, 1997).

The first in-depth modelling attempt of the cellular structure from a mechanical view point was completed by Mark (1967) who developed a method for analysing stresses in cell walls. Models of cells range from considering a homogeneous block of elastic material to including the heterogeneity and geometry of the individual cells, in extreme cases the individual molecules are taken into account (Mishnaevsky Jr. and Qing, 2008).

1.2.3 Hypothesis to explain the TRP

While being able to insinuate the way in which wood behaves under load and fracture is useful, it begs the question; why is wood created this way? Currently there are three competing theories as to why trees develop their cells to have various properties. These are the mechanical hypothesis, which states that trees form in such a way as to maximise their resistance to mechanical loads with the minimum amount of material required, the second is the developmental hypothesis which simply argues that the cambium is unable to produce some cellular attributes until it reaches a certain age, and the third is the hydraulic hypothesis which argues that cells are formed with properties in order to maximise water transport without embolism (Meinzer et al., 2011).

The mechanical hypothesis states that the change in wood properties over the radius of the tree is a strategy to allow small trees and branches to bend out of the wind or to release snow while providing larger stems and branches the ability to withstand their own self weight as well as the applied loads such as wind. This hypotheses explains why corewood tends to have a large MFA which reduces toward the outer edge of the tree as the corewood requires a high fracture strain to allow for large bending angles without rupture of the wood fibres and the outer growth has a lower MFA to form stiffer wood to support the trees self weight (Meinzer et al., 2011).

The developmental hypothesis states that the cambium must mature before it can produce the most adaptive wood. The assumption of this hypothesis is that outerwood is universally superior to corewood. There is some support for this hypothesis such as the first few growth rings produced in the pith are often the same size regardless of the environment. However there is evidence that corewood is superior to outerwood for some functions such as its high resistance to embolism, its higher maximum strain and the abundance of compression wood which provides the ability to re-orient stems when they are bent, all of which are vital to survival during the early stages of growth (Meinzer et al., 2011).

The hydraulic hypotheses states that the TRP acts to maintain adequate water distribution for the tree giving corewood the ability to withstand high negative pressures and the outerwood high specific conductivity. Corewood is required to withstand higher

negative pressures as young trees have less developed root systems and lower water storage capability, while old trees have higher transport demands requiring a higher specific conductivity (Meinzer et al., 2011).

Approaches such as the auxin hypothesis are mechanistic, in the case of auxin it is argued that the distribution of the growth hormone auxin is responsible for the TRP, however it is also hypothesized that the distribution of auxin is related the mechanical stress in surrounding cell walls (Asnacios and Hamant, 2012). This may in effect provide an intermediate step in forming a more complete hypotheses incorporating stresses from both the mechanical and hydraulic hypothesis into a more complete theory to explain the formation of the TRP.

1.3 Stem Design

Various classical mechanics techniques have been used in order to study tree stems as a whole. However these approaches make a number of problematic assumptions in order to disregard the complexities of cellular behaviour described above. In particular the fact that plant cells, tissues and organs are typically complex composites or microstructures that are both chemically and structurally heterogeneous is overlooked in order to maintain the ability to make general statements about the structure and behaviour of the trees and wood (Niklas and Spatz, 2012). While these methods can provide some general statements about stems such as stem A is stronger than stem B it lacks any ability for details to be discerned about why this is the case. The approach also disregards the important variations of cellular structure within the wood reducing the accuracy of the outcomes.

While the structural mechanics aspects of the stem are the main focus it of this work is worth noting that mechanical properties are not the only influencing factor in stem design, they may not even be the most prevalent as there are many physiological requirements which need to be met along with other non-structural requirements such as water transport. Further the assumption of homogeneity and that trees are made of idealized solids or fluids are often made in order to decrease the complexity of the

model (Niklas and Spatz, 2012) further reducing accuracy in order to retain simplicity.

The way in which trees grow is thought to be governed by the constant stress hypothesis. Niklas and Spatz (2012) and Gartner (1995) suggested a combination of the constant stress hypothesis and the minimization of external loads. Mattheck and Kubler (1995) went even further suggesting the previous two, along with the minimization of shear stresses, the strength of wood governed by mechanical stresses and growth stresses induced to counterbalance weak points.

The axiom of uniform stress (the constant stress hypothesis) states that stresses are distributed uniformly over the surface of the tree for an average over time (Mattheck and Kubler, 1995). Unfortunately, it is unknown how trees average stresses over time (Niklas and Spatz, 2012), hence making this statement difficult to prove. The result of the axiom of uniform stress being applied is that the tree becomes as light as possible (minimising self weight) and as strong as necessary (Gartner, 1995). It is worth noting that from a theoretical standpoint, the axiom of uniform stress leads to optimum tree design (Niklas and Spatz, 2012), with regard to its structural integrity. There is argument against this theory however, Niklas and Spatz (2000) found that wind load stress levels vary along the stem even for the same wind speed profile. Domec and Gartner (2002) found that mechanical safety factors were higher than hydraulic safety factors along with evidence that the variation in the hydraulic safety factor would impact survival while the mechanical safety factor wouldn't. Further the properties of juvenile and mature wood influence the hydraulic safety factors to a larger extent throughout the tree than the mechanical safety factors.

The principal of minimum leaver arms states that the tree acts to minimize external loads by minimizing the loaded length of its leaver arms. This manifests in a number of ways, the reduction of crown on the windward side, spiral grain, twisting branches away from the wind etc. (Gartner, 1995). The most noticeable effect is the tendency for trees to bend their long leaver arms toward the load axis (Mattheck, 1991). If trees were unable to do this it would greatly increase the load which they must counteract, increasing the use of valuable materials to maintain a similar level of strength. Niklas and Spatz (2000) stated that trees are capable of self pruning of small branches in extreme conditions in order to reduce the load on the stem. An example where both the axiom of uniform stress and the principal of minimum leaver arms are apparent is

in the production of stem taper (Mattheck, 1991; Gartner, 1995).

1.3.1 Applying external loads

Any externally applied force can be broken down into two components, tangential (parallel to the surface of interest) and normal (perpendicular to the surface of interest). Shear stresses are formed by tangential forces, tension and compression are formed by normal forces (Niklas, 1992). Compressive, tensile and shear forces and their associated stresses are only governed by the cross-sectional area of the surface. However when both tangential and normal forces are applied at once bending and torsion result, these are dependent on the geometry, shape and size of the object under investigation (Niklas and Spatz, 2012). When these various forces are applied to the tree the reaction is at the cellular level as described above, but due to the increasing complexity of modelling individual cells these effects are not taken into account in models which are designed to investigate the macroscopic biomechanical nature of the tree.

Due to the nature of the way wood fails, in order to gain a true understanding, failure would need to be modelled at the cellular level to incorporate the various fracture mechanics which have been described above. This is further complicated as trees self repair over time, so buckling and some cellular collapse can be repaired and not significantly reduce the structural integrity of the stem or branch.

1.3.2 Growth Stresses

Cambial cells divide, make the transition to xylem and die. As the cells go through these changes growth stresses develop. The magnitude of growth stresses varies between individuals and species, but the pattern remains constant. At the outer periphery of the stem the cells are under tension with the core being under compression (Gartner, 1995). It has been hypothesised that the lignification of the S_2 cell wall layer causes tangential swelling resulting in longitudinal shrinkage (Archer, 1987, 1989) it has also been proposed that the cellulose content may be a factor through cellulose fibril con-

traction (Yamamoto, 1998). As the cells are attached to the stem there is resistance from the older growth for this shrinkage to occur, equally there is a force placed on the older growth from the new cells trying to contract. More recently Yamamoto (1998) introduced a new model taking into account time dependence of the maturation of the secondary cell wall, including both lignification and cellulose micro-fibril contraction.

A number of theories have been put forward to describe how growth stresses are likely to be distributed within the stem, most build on each other. One of the most comprehensive discussions on growth stress is available from Archer (1986), along with his series 'On the Distribution of growth stresses' (Archer and Byrnes, 1974; Archer, 1976, 1979, 1981, 1985). Other authors at a similar time also presented similar theories on how the stresses are distributed (Gillis, 1973; Gillis and Hsu, 1979). Gillis and Hsu (1979) fixed an issue that plagued previous studies by introducing plastic deformation of corewood in order to remove the vertical asymptote at the centre of the stem.

1.3.3 Wind breakage mortality

A number of papers have been published on the issue of wind damage and wind-throw in commercial forests, clearly severe wind events can have a significant impact of the profitability of a commercial forestry enterprise with wind-throw accounting for significant financial loss in many countries such as France, Great Britten and New Zealand (Ancelin et al., 2004; Moore and Quine, 2000). A number of software products are available for predicting wind damage (for example GALES and HWIND) and have been applied to forests in both New Zealand and overseas. GALES was developed in England, and has been used for comparing wind risk between Great Britain and New Zealand (Moore and Quine, 2000). Moore and Quine (2000) found significant losses in both areas due to wind throw events. It should be noted however that GALES relies on tree pulling experiments in order to calibrate the software for different locations and species.

While statistical methods for predicting windthrow provide useful information to scientists and managers for risk analysis, tree pulling experiments are expensive and provide limited information on how failure occurs. Gardiner et al. (2000) compared HWIND

and GALES and found (with a small number of exceptions) that usually trees are more resistant to stem breakage than to uprooting with values depending on diameter and height. Ancelin et al. (2004) created a model which predicted wind speeds ranging from 23.3 to 26.7m/s are required to break the stems while only 20.8 to 22.8m/s to uproot in individual Norway spruce trees within stands, however these varied depending on diameter and height as with the Gardiner et al. (2000) model. The two authors also suggested that stem tapper also played a critical role in whether the tree would break or overturn, for trees with low tapper critical wind speeds were reduced and the tree became more likely to break than overturn. Gardiner et al. (2000) also concluded that HWIND and GALES provided relatively low differences in predictions of critical wind speed, however they also noted that these small differences can lead to large differences in damage probability.

While there is a lot of literature produced on proposed mechanisms for the creation of stiff wood from genetic, physiological and silvicultural viewpoints there has been little literature published with regard to how these particular changes may effect tree mortality rates within commercial forests. This is something which needs to be investigated as further refinements are made in tree breading and silvicultural techniques with the intent of increasing wood stiffness particularly in corewood. If the stiffness of corewood is increased beyond a particular point it may increase mortality rates due to wind throw and breakage events.

Low stiffness timber is often related to a high MFA angle and low density. While in the timber industry low stiffness products are usually considered to be of lower quality, from a growing trees standpoint this may not be the case. Low stiffness corewood has a higher fracture strain which allows the stem to bend though larger angles without rupture, while outerwood has a much higher stiffness. Because of the larger diameter of the stem the higher stiffness material reduces the quantity of material needed for a given strength at the larger diameters, this optimises strength for a given amount of growth (Meinzer et al., 2011). The TRP may influence the relationship between stiffness and maximum strain to provide the most desirable ratios for survival at different points in the trees lifetime.

In order to parametrise many of the models used for wind throw prediction tree pulling experiments are needed. These experiments typically involve fixing a strop to the stem

and winching the stem until it breaks or uproots. A measurement of the maximum resistive moment is obtained along with the elastic modulus of the stem. Numerous studies such as Peltola et al. (2000) and Papesch et al. (1997) have been completed for commercial species using these methods. Wind tunnel experimentation has also been used in order to better understand how stems react to wind events. By using wind tunnel and tree pulling experiments along with mechanistic modelling approaches could provide information on the causation of failure due to wind loading which statistical methods can not provide (Peltola, 2006). Mattheck et al. (2006) used an interesting approach to study failure mechanisms. Selecting hollow stemmed trees they showed stem breakage due to bending was not the primary failure and instead suggested failure was due to longitudinal shear. They did show however that shear stresses increase with hollowness.

1.4 Modelling

1.4.1 Microscopic models

There have been a number of attempts at modelling individual cells and small cellular blocks (for examples see (Astley et al., 1998; Geitmann, 2010; Fourcaud et al., 2003; Watanabe et al., 2000) and (Moden, 2008)). The use of hierarchical modelling techniques with multiple scales is common. This is achieved using multiple modelling layers, such as at the nano-structural, ultra-structural, cellular and mesoscopic scales.

Astley et al. (1998) created models of individual cells for seven species. The models in this case used tapered beam cell models to account for variation of axial cell wall thickness. The result was a higher tangential elastic moduli for the tapered cells compared with uniform cell thickness for a given density. The curvilinearly increasing thickness (in the axial direction) of cell walls resulted in the best approximation to experimentally obtained results. Other models investigating radiata pine have been developed to take into account not only the characteristics of the cell wall layers but also the effect of spiral grain. Spiral grain is an important consideration as it reorientates cells in all directions, Watanabe et al. (2000) found that for low MFA cells spiral grain has a significant effect

reducing the stiffness. Late wood was also reported to increase stiffness in the tangential direction (Watanabe et al., 2000). Mixed numerical-experimental methods have been used to investigate cellular mircostructures effects on wood. These attempts tend to use relatively simplistic mechanical relationships coupled with experimental results in order to increase the accuracy of the experiments, or gain more information than what the experimental results themselves provide (Gamstedt et al., 2013; Moden and Berglund, 2008).

1.4.2 Macroscopic modelling

A common approach to investigating tree structural biomechanics is to use a variant of classical beam theory called rod theory and usually the assumption is that the tree is made of a homogeneous material with constant elastic modulus, Poison ratio etc. and are subjected to loads. This is analogous to the way an engineer would treat a simple beam made of a material such as steel. However due to the heterogeneous nature of tree structures this overlooks the TRP and the impacts the changes in MFA, density and other structural attributes have on the mechanical properties of wood.

A variant of beam theory, rod theory (Green and Laws, 1966) has been used in order to model tree stem and branch behaviour, under a number of assumptions such as the homogeneity of wood and that the structure does not change in time (i.e. no growth). Rod theory provides no ability for the reference configuration to change with time, this has caused problems for a number of authors. The common solution when attempting to include both primary and secondary growth is for authors to step time, with each step increasing the thickness of all existing rods and adding a new rod to the end of the current configuration (Yamamoto et al., 2002; Fourcaud et al., 2003). The problem with this approach is that the time domain is discontinuous and does not allow for new material to be added to a pre-stressed stem.

More recently it was suggested by Fourcaud et al. (2011) that this difficulty resulting from the tight coupling between space and time in growth problems could be overcome. As trees grow and add material to themselves under loads such as gravity and growth stresses, new material is added without stress onto an existing pre-stressed structure.

Recently the suggested modification to rod theory has been made by Guillon et al. (2012a) and tested by Guillon et al. (2012b) which allows for primary and secondary growth of a rod structure. This was developed for the purpose of modelling tree stems and branches and allows for the stem or branch to grow in a continuous time domain, something which previously could not be achieved and was usually circumvented by using unit time additions of growth under discontinuous time steps, at each step a new rod was added for primary growth and the other rods diameters were increased. This modification allows for new growth to be added to a stem in a pre-stressed state. However these new techniques do not take into account internal structure of the trees or cells and assume complete homogeneity within the structure.

Ormarsson et al. (2010) produced an axisymmetric model considering one-dimensional gravitational and orthotropic maturation strains to create growth stresses. This study also provided the ability for the Elastic moduli to be varied depending on the radial position in the tree stem. The model showed significant variations of stress in the radial direction along with stress profile differences during growth. Archer (1986) presents a number of different approaches to collecting experimental evidence for particular growth stress patterns, various mathematical models presented by a number of authors (Skatter and Archer, 2001; Fourcaud et al., 2003; Archer and Byrnes, 1974; Archer, 1979) have been used with varying degrees of experimentally obtained data and mathematical modelling predict similar growth stresses patterns. Ormarsson et al. (2010) provided similar theoretical stress patterns to the experimental observations however the absolute values varied significantly. It is thought this is likely to be due to assumptions made in the study which effects the modulus of elasticity such as the MFA. The stress patterns predicted by the model showed growth stresses consisting of compression in the centre of the stem while tension stresses forming at the outer edge. Mattheck (1990) analysed a number of unusual formations observed as a result of adaptive growth in trees and animals using FEA. From this analysis he argued that biological load carriers self-optimized growth in order to achieve constant stress over their surface. If this equilibria is disturbed adaptive growth is used to repair the perturbation and restore the optimum state.

A number of more simplistic models have also been used. These models ignore time entirely and effectively treat the tree as a simple engineering object in order to deduce critical dimensions under the assumptions of homogeneity. Morgan and Cannell (1987)

used successive thinner non-tapered beams to imitate taper of a stem. They found that with only 20 segments good agreement with experimental values for large deformations using point loads. If stems are too slender for their own weight they become mechanically unstable, this leads to Euler buckling. The likelihood of buckling can be calculated as a ratio of actual height over critical bucking height, this metric is often used as a safety factor to compare different individuals or species for their susceptibility to mechanical failure. Spatz and Bruechert (2000) investigated Norway spruce trees for different wind loads presenting safety factors of approximately six for gravitational loads and ranging from three to ten (approximately) for various wind profiles and stem heights. Generally the safety factors reduced with height with the exception of 20+m tall stems where the factors appear to start increasing. Using a similar technique Jaouen et al. (2007) analysed 236 samples of 16 species of saplings and used these results to produce a simplified calculation for assessing bucking risk. While most studies have ignored dynamical forces, although often stating their importance England (2000) investigated dynamic loading from gusting winds generating impulsive forces in Sitka spruce, the study focused on the likelihood of uprooting.

These simplistic models have been used to show the mass efficiency of trees to better inform engineering design. Burgess and Pasini (2004) suggested in the future engineering design should draw on the lessons learned from trees refined structural hierarchies, adaptive growth and non-structural functions begin employed in structural members to construct multi-functioning structures with adaptable behaviour.

1.4.3 Attempts to incorporate microscopic and macroscopic models

Holmberg et al. (1999) attempted to incorporate modelled behaviours on the microscopic level into a macroscopic model in two dimensions with infinitely long cells. The approach taken was to measure and generalize the cellular structure properties of early, transition and late wood, with the cells modelled as hexagons. Homogenisation with FEA was used in order to solve the models and they found reasonable agreement between simulations and experiments when considered with spruce. However they pointed out the importance of modelling the different types of wood within the growth rings

and suggested that both modelling and experimentation were needed to advance the simulation. It should be noted that these simulations were based off micrographs of surfaces of the woods tested experimentally.

Raffaele et al. (2011) created models of timber using image analysis techniques to capture the growth increment boundaries, followed by the creation of a morphological FEA. These consisted of two generalized elements which represented early and late wood, again in spruce and modelled as a square block. They found that weak layer and spaced column theories could be used to explain radial and tangential compression, showing that the weak early wood layer controls most of the deformation in radial compression, however under tangential compression the load is distributed according to the early and late woods relative stiffness. It is worth noting that in this model MFA was not taken into account. Moden (2008) used experimental analysis combined with FEA of honeycomb structures to investigate the transverse shear modulus, but again only using small blocks.

Ormarsson et al. (2010); Persson (2000) and Harrington (2002) attempted to combine microscopic and macroscopic models to some extent, with Persson (2000) and Harrington (2002) going from the molecular scale to small wood blocks (10s of cells) and Ormarsson et al. (2010) going from small cell blocks to the entire stem. All of these approaches relied on homogenisation and assumptions of homogeneous blocks of material to provide an estimate of the final structure. At this date no known attempts have been successful in incorporating models with resolutions of sub cellular wall materials into full tree stem models. This is likely to be due to the limitations of current experimental and computing technology along with currently established mathematical techniques.

Qing and Mishnaevsky (2009) used composite theory to develop multilayer cell models in order to predict macroscopic elastic properties and stiffness for particular cellular geometries and MFA distributions within the various cell wall layers. From this study they concluded that for transverse elastic properties the MFA in the S_1 and S_3 layers were most important as oppose to the S_2 layer as for the longitudinal direction. Qing and Mishnaevsky (2009) also found the variation of micro-structure and thickness in the S_2 layer had the largest effect on the macroscopic properties of the cell wall layers.

A good review of major wood modelling projects as of 2003 with discussion around

the concepts involved can be found in Gustafsson (2003) and a more recent review of hierarchical modelling of wood structure is also available (Hofstetter and Gamstedt, 2008).

1.4.4 Elastic plastic models

As a tree approaches failure, whether it be under stress from mechanical forces (for example wind), or from hydrological forces such as those which exist within the stem as pressure differentials to move water from the roots up the stem, as the material breaks, it follows the common trend of most solids. An elastic region into plastic deformation and finally into rupture. This is evident from stress strain curves such as those found in Tabarsa and Chui (2000) and Gibson (1997). Because the linear elastic portion of the stress strain curve is mathematically simpler to deal with than plastic or nonlinear deformation the majority of models in the literature trend to only use this region. However this inherently relies on one of two problematic assumptions; either that plastic deformation is equivalent to breakage in terms of tree survival which is unlikely as trees often continue to grow and self repair after minor breakage events, or that the point of the beginning of plastic deformation is linearly proportional to the point of rupture. Evidence against the second can be seen in experimentally derived stress strain curves of separate pieces of timber, for example see (Tabarsa and Chui, 2000; Gibson, 1997). This is not to argue that the approach is unreliable with a number of examples showing results with various degrees of concordance with experimental work such as Ormarsson et al. (2010),Holmberg et al. (1999) and Raffaele et al. (2011)

Plastic deformation has been less widely adopted, likely because of the inherently more difficult mathematics and larger computational loads needed to solve the problems. Ormarsson et al. (2010) produced models which took into account elastic strain, maturation strain, visco-elastic strain and progressive stiffening of wood in order to investigate creep and progressive stiffening caused by growth stresses. Persson (2000) attempted the use of elastic-plastic models over a single growth ring and showed that under compression early wood cells will begin to fail first. However it was also stated that due to numerical convergence issues surrounding the problem that a number of crude assump-

tions had to be made and the numerical solvers would only converge for a very limited number of analyses.

The study of timber in an engineering sense has led most of the elasto-plastic modelling attempts of wood. Mackenzie-Helnwein and Hanhijrvi (2003) and Hanhijrvi and Mackenzie-Helnwein (2003) suggested a model which takes into account viscoelastic-machanosorptive-plastic behaviour in order to investigate distortion during the drying process. Schniewind and Barrett (1972) investigated tensile creep in the longitudinal planes for Douglas fir and concluded that because creep at angles to the grain could be predicted using standard transformations, wood is a linear orthotropic viscoelastic material. However Yeh and Schniewind (1992) argued this was not the case and applied the J-integral method, (a method commonly used for steel analysis) to show that increasing moisture content and temperature increased the nonlinearity. A number of other authors have also presented various methods for evaluating plasticity of blocks or boards of timber in various species and directions (Henrik and Gustafsson, 2013; Yoshihara, 2009; Mackenzie-Helnwein and Hanhijrvi, 2003). An excellent discussion of plasticity and plastic strains within wood can be found in Barkas (1949) although no models for plastic deformation within wood are produced in this text.

1.5 Objectives

Two related research projects are presented here, in two chapters. The goal of Chapter 2 is to describe and present the methods and results from testing green *Pinus radiata* for elastic constants for both core and outerwood. Chapter 3 presents a finite element model used to investigate the effect of different MFA and density radial patterns on structural integrity of tree stems. In order for this model to cover extremes for *Pinus radiata* in terms of elastic constants the boards for experimental work were selected on this basis. Using the values obtained from the experiments, the finite element model was parameterised and solved for a number of unusual radial profiles to investigate the extent of an effect the radial pattern of MFA and density has on the structural integrity of the stem.

Chapter 2

Experimental work

2.1 Introduction

While density and acoustic tests are common practice for obtaining dynamic modulus (which can in turn be used to estimate the static modulus (Barker, 1998; Lindström et al., 2004)) in both timber research and industry, little information about the underlying structure of wood is obtained from these tests. Wood is often dried to 6-12% moisture content before conducting any experimental work, which has been observed to alter the mechanical properties (Skaar, 1988; Ozyhar et al., 2013). Investigating dry wood gives a poor representation of the living organism, leaving scientists interested in the growth of trees somewhat in the dark when considering the way trees react to mechanical phenomena. Unfortunately there is a lack of information on both green (the state of wood when it is inside a living tree) and corewood (wood produced by a young cambium).

Wind loading can cause mechanical failure which can decrease the value of processed timber due to defects, the associated financial loss has led to a substantial amount of research on predicting wind throw and wind damage risk for commercial species (Gardiner et al., 2008). However, these models do not investigate the structural failure within the tree, they only attempt to identify how likely failure is to occur in a particular

environment. In areas with less pronounced prevailing wind directions there may be an effect on the stiffness of the trees in order to compensate for the multi-directional loadings (Apiolaza et al., 2011; Kern et al., 2005), this reduction in stiffness can result in a timber product of lower value.

One way of investigating mechanical phenomena present in tree stems is the use of mathematical models. However because of the size, modelling an entire tree from the molecular level is infeasible, so homogenization is used. In order to use these methods experimental data is required to parametrize them. Full sets of constants even for dry timber are hard to find and to the best of our knowledge there are no full sets available for green or corewood radiata. Proportional limit and ultimate failure surfaces for all directions in green and corewood have also not been reported previously. Lack of available data is an issue for a number of current problems in plant biophysics.

The purpose of this chapter is to present a number of necessary material constants for describing green corewood and outerwood as an orthotropic material. A set of static moduli and Poisson ratios for green corewood and outerwood in the radial, tangential and longitudinal (to the grain) directions were obtained. The small study was completed with *Pinus radiata* selected from plantations in Canterbury, New Zealand.

2.2 Experimental Method

Current standards such as BS 373:1957 (BS, 1957) and AS/NZS 4063.1:2010 (AUS/NZS, 2010) apply for dry timber and have been developed for testing timber for engineering applications. Because of this design consideration, and the large differences in testing procedures between some of these standards they are not necessarily the most appropriate when considering green wood for use in biomechanics or biophysics investigations. The techniques used in this paper do borrow from these standards however have been modified in order to make them more applicable to the current task and equipment.

Table 2.1: The four samples shown along with their properties known at the time of selection. Green density was measured using a measuring tape to get an approximate volume and field scales to get the weight of the board. Tree tap was used to get the acoustic velocity. Ring number and wood type from visual inspection (Note visual inspection for sapwood and heartwood rather than corewood and outerwood as they were much harder to distinguish visually).

Sample	Green Density	Acoustic velocity	Approximate ring number	Type of wood
HS	high	high	> 15	Sapwood
HW	high	low	> 15	Sapwood
LS	low	high	< 15	Heartwood
LW	low	low	< 15	Heartwood

2.2.1 Sample selection and preparation

One consideration when using the FEM is the assumption that the field variable inside the elements can be approximated by a simple function, usually a polynomial (Rao, 1999), because of this it is necessary to be testing samples as close to homogeneous as possible. The samples were machined to sample sizes which were as small as practically possible for the available equipment. The goal was to minimize the variation in MicroFibril Angle (MFA), green density and other properties within a sample, because of the differences between early and late wood variation is evident in all samples tested. All samples were sourced as green as possible from the sorting table at a local mill and the boards chosen to give extreme values of green density and stiffness combinations for the species as can be seen in Table 2.1. This was achieved by using tree tap (Chauhan et al., 2013) and portable scales at the mill to estimate the dynamic modulus of the entire board.

The samples were docked into approximately 500 mm lengths and stored in sealed bags with excess water in a refrigerated room. The samples were cut using a bandsaw and precision milled into the required shapes as described in the following sections. Each test was repeated 6 times for each sample (i.e. 6 specimens of each sample were made for each test). When specimens were selected they were chosen to have no knots or other visual defects, with grain as straight as possible. These shapes were again stored in sealed bags with excess water until their testing. The specimens showed no signs of deterioration during storage. At this time the samples were also measured for acoustic

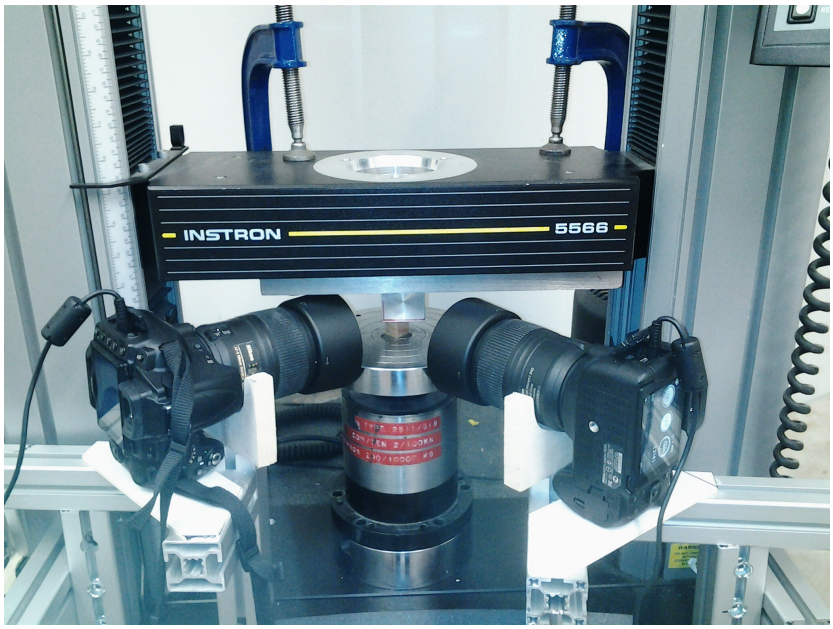

Figure 2.1: The layout of the instron and cameras for compression testing. The other setups are similar.

velocity using the NZSOF disk scanner.

2.2.2 Testing

Samples were removed from their sealed bags at testing time, weighed and volume measured using the displacement method. The samples were placed into an Instron 5566 set-up for the appropriate test. Two cameras (a Nikion D5000 and a D5200 with 60mm micro lenses) were used to take images during the test in order to track displacements within the sample. These cameras were focused on the sample, one imaging each plane perpendicular to the axis of loading. The setup can be seen in Figure 2.1, timelapse photography was used taking images every 3 seconds during the test, controlled via gphoto2 (Contributors, 2013).

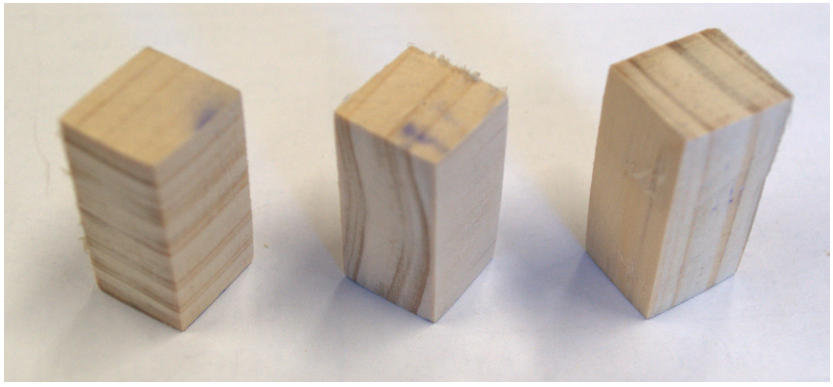

Figure 2.2: Examples of the sample shapes used for compression properties. The samples, labelled in the direction of load applied from left to right are radial (r), tangential (t) and longitudinal (l). The vertical direction is 30 mm with the two other sides being 15 mm each.

Pure compression

Samples approximately 15 x 15 x 30 mm were used as is shown in Figure 2.2, cut so that three different compression axis (the 30 mm axis of the specimens) could be investigated (longitudinal, radial and tangential to the grain). All three directions are tracked for each orientation using the digital cameras. The Universal Testing Machine (UTM) was run at a constant velocity applying compression to the top of the sample at a velocity of 1.5 mm per minute. During this time the load cell which the sample was resting on takes load measurements at a minimum of 1 reading per second, with more frequent recordings as the load increases. The accuracy of the load cell is 0.1 N. The test is run for a period of 300 seconds, giving a displacement of 7.5 mm which equates to a strain of approximately 0.25. During the test, images of the sample are taken every 3 seconds (100 images for the test).

Pure tension

Samples were created in a 'bone' shape as shown in Figure 2.3 with the total dimensions approximately 50 x 25 x 6.5 mm with the breakage plane having an area of approximately 6.5 x 6.5 mm. With the exception of the longitudinal direction, where a straight

Figure 2.3: Examples of the sample shapes used for tensile property testing. The samples, labelled in the direction of load applied from left to right are r (radial), t (tangential) and l (longitudinal). Samples have a cross sectional area of 6.5 x 6.5 mm at the fracture point. The radial and tangential samples are 100 x 25 x 6.5 mm overall. The longitudinal sample is 200 x 6.5 x 6.5 mm.

stick test was used. The reasoning for the two different sample shapes is that in the radial or tangential direction the jaws of the testing machine damage the samples causing an artificial fracture point. In the longitudinal direction this is not an issue however the samples fail in shear along the grain before tension across it when the bone shape was used. Again the tests in all three directions were captured as above.

Shear

Shear stresses within orthotropic materials are assumed to be independent of other stresses within the material. Again the three directions were considered, however perpendicular displacements were not tracked for the off axis terms. Figure 2.4 shows the layout of the samples. In this case the shear plane is approximately 15 x 15 mm. The data from the UTM is used directly to obtain the strain measurements.

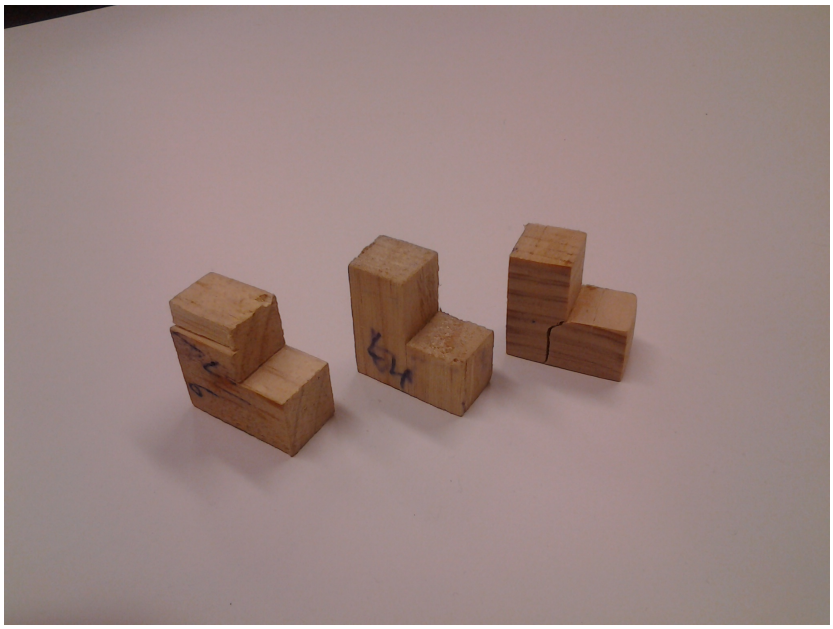

Figure 2.4: Examples of the sample shapes used for testing shear properties. The samples, labelled from left to right are the radial tangential plane rt, tangential longitudinal plane tl and the longitudinal radial plane lr. The samples are 30 mm long by 30 mm high and 15 mm wide, resulting in a 15 x 15 mm shear plane.

2.2.3 Post testing mechanical properties

Once the specimens had been mechanically tested they were oven dried at $104°C$ until a representative sample was no longer losing weight 48 hours apart. Each sample was weighted and volume measured using the displacement method. From one specimen of each sample and test (ie 12 in total) a small strip approximately 1 x 5 x 10 mm was taken for x-ray diffraction testing. The microfibril angle and standard deviation of the microfibrils were obtained using the methods described in Cave and Robinson (1998b) and Cave and Robinson (1998a).

2.3 Computation

The time and load applied was extracted from the UTM data for use with the photo collections to create stress strain curves. This was implemented using Digital Image Correlation and Tracking with Matlab scripts (Chris Eberl, 2006) to track identifiable points within the photos throughout each series to obtain strain versus photo number curves. The time of each photo was extracted from the EXIF data attached to the photo using the Python Imaging Library (Lundh et al., 1995) and used to match the corresponding load applied by the UTM along with the dimension measurements which are used to calculate the stress strain curves.

During the process of extracting strain information from the images, a visual inspection of the data was undertaken. This involved using displacement versus image number, displacement vs neighbour's displacement and area of interest selection (available from Chris Eberl (2006)) to determine the points which have been tracked correctly within the photo series. One-Dimensional average strains are taken in both the vertical and horizontal direction.

Because the UTM runs at a set velocity it is possible to estimate the strain on the sample, although this tends to slightly overestimate the strain. Initially there is a period of motion before the compression plate comes into contact and re-orientates the sample, (although this is minimal) providing a good estimation to select the accuracy

tracked points. The horizontal direction within the photographs is used to track the displacement perpendicular to the applied load. Here the assumption is made that points tracked accuracy in the vertical direction are also tracked reliably in the horizontal direction.

2.3.1 Calculation of the Elastic modulus

For each test of each specimen a visual inspection of the stress strain curves is undertaken, the initial reorientation of the sample, resulting in a curve before the linear elastic region is discarded, and the linear portion of the stress strain curve identified by overlaying a linear model $y = mx$ to the data being considered. Once there was as little deviation between the data and model as possible, this was considered the elastic region with the Elastic modulus E being the gradient m of the model. The end point of the fitted model is considered the limit of proportionality, and it is assumed this is equal to the yield point. This may provide a slightly lower yield point estimate than some other techniques for determining the yield point, such as taking the intersection between this line and the line tangent to the peak of the plastic curve.

2.3.2 Calculation of the Poisson ratios

Poisson ratios defined as $v = -d\epsilon_x/d\epsilon_y$ (Bodig and Jayne, 1982) (where ϵ is strain, x is transverse direction and y is axial direction) from the method in Section 2.3.1 the slope of the elastic region of the stress strain curve is known for both the x and y directions. In y this is the elastic Modulus, defined as $E_y = \sigma_y/\epsilon_y$ (where σ is stress) (Bodig and Jayne, 1982) and in the x direction $S_x = \sigma_y/\epsilon_x$ (i.e. the force per unit area applied in the y direction results in a displacement in the y and a different displacement in the x direction related by the Poisson ratio). Therefore $S_x = \sigma_y/\epsilon_x$ and $E_y = \sigma_y/\epsilon_y$ so $-\epsilon_x/\epsilon_y = E_y/S_x$ giving $v_{yx} = -E_y/S_x$

2.3.3 Determining Elastic moduli and Poisson ratios for use with the orthotropic assumption

Orthotropic materials have symmetry giving rise to the following equalities (Salenon, 2001):

$$\frac{v_{yx}}{E_y} = \frac{v_{xy}}{E_x}, \quad \frac{v_{zx}}{E_z} = \frac{v_{xz}}{E_x}, \quad \frac{v_{yz}}{E_y} = \frac{v_{zy}}{E_z} \tag{2.1}$$

However from the experiments the equalities presented in Equation 2.1 do not hold. This is probably due to a number of reasons, such as the errors inherent in the method of measurements. While the difference between the experimental and predicted values (by the equalities) is usually around 30-50% of experimental value it does range from near 0% to near 200%. In order to ensure these equalities hold (which is necessary for the assumption of wood being an orthotropic material) optimisation is used to find the values which deviate least from all of the experimental values while still satisfying the equality constraints above. Due to the larger absolute values of some constants (for example E_l) the deviation is considered as normalized against the 95% confidence intervals of the mean values in order to give every variable an even weighting for its accuracy. The optimisation uses the above constraints and the following objective function:

$$min \sum \frac{|\delta_i - \gamma_i|}{\theta_i} \quad i = E_r, E_t, E_l, v_{rt}, v_{tr}, v_{tl}, v_{lt}, v_{lr}, v_{rl} \tag{2.2}$$

Where δ_i is the experimental value of i, γ_i is the new value and θ_i is the 95% confidence interval of δ_i. This optimisation was implemented in a least squares sense using the python algorithm scipy.optimize.fmin_slsqp (Jones et al., 2001). It should be noted that setting the 95% confidence intervals as bounds worked for all but one case. The HS sample when tested under tension fails to converge, due to the inequality constraints being incompatible with any combination within the bounds. This is redeemed by increasing the bound to the 99.9% confidence intervals. An average of Elastic moduli obtained from both compression and tension tests was also undertaken. For the radial (r) and tangential (t) directions the values from the non axial plane for each tension and compression were averaged, whereas for the longitudinal (l) direction all measurements were averaged. The Poisson ratios from compression tests were used. The reasons for

using these particular values are discussed in Section 2.5.2.

2.3.4 Proportional limit (yield point) criteria and ultimate failure

The failure criterion presented by Tsai and Wu (1971) provides a general theory of strength for anisotropic materials, other papers have since used this failure criterion and it has been suggested as an appropriate failure criterion for wood and wood products (Mackenzie-Helnwein et al., 2005a,b). Due to the use and acceptance of the theory in other research along with its treatment of experimental results allowing for pure tension and compression to be regarded separately make it a good choice for investigation into the properties of green wood. The separate treatment of pure tension and compression is needed as wood has been reported to behave substantially differently under the two regimes (Ozyhar et al., 2013; Bodig and Jayne, 1982). Shear loading is extremely difficult to test within wood due to the material structure being very week in planes perpendicular to the longitudinal axis (i.e. separation between cells requires much less force than breakdown of the cells themselves). The problem of separation is evident in shear tests where the samples are likely to split under the rotational loading (although this loading is assumed to be negligible, it is often significant (Bodig and Jayne, 1982)) between the cells rather than fracture through the desired plane. In the future this could be overcome by using different equipment and more sophisticated shear tests such as those presented in (BS, 1957) or Kollmann and Cote (1968). It has also been suggested that shear properties are best derived from torsion or various bending tests (Moden, 2008).

The full power of Tsai and Wu (1971) failure criterion was not utilised in this paper. The off axis interaction terms are either ignored or a modified Hills criterion (Hill, 1950)) was used within the P matrix described in Equations 2.3 to 2.12. This paper did not consider interaction from experimentally obtained tests, as is suggested by Tsai and Wu. Using Hills criterion interaction is considered, however the method is essentially arbitrary (Tsai and Wu, 1971).

$$\boldsymbol{\sigma}^T \boldsymbol{q} + \boldsymbol{\sigma}^T \boldsymbol{P} \boldsymbol{\sigma} - 1 = 0 \tag{2.3}$$

Where:

$$\boldsymbol{\sigma} = \begin{bmatrix} \sigma_r \\ \sigma_t \\ \sigma_l \\ \sigma_{tl} \\ \sigma_{lr} \\ \sigma_{rt} \end{bmatrix} \tag{2.4}$$

$$\boldsymbol{q} = \begin{bmatrix} F_{rr} \\ F_{tt} \\ F_{ll} \\ 0 \\ 0 \\ 0 \end{bmatrix} \tag{2.5}$$

$$\boldsymbol{P} = \begin{bmatrix} F_{rrrr} & F_{rrtt} & F_{rrll} & 0 & 0 & 0 \\ F_{rrtt} & F_{tttt} & F_{ttll} & 0 & 0 & 0 \\ F_{rrll} & F_{ttll} & F_{llll} & 0 & 0 & 0 \\ 0 & 0 & 0 & F_{tltl} & 0 & 0 \\ 0 & 0 & 0 & 0 & F_{lrlr} & 0 \\ 0 & 0 & 0 & 0 & 0 & F_{rtrt} \end{bmatrix} \tag{2.6}$$

Where $\boldsymbol{\sigma}$ is the stress vector, F_{ii}, F_{ij}, F_{iiii} and F_{ijij} were described in Equations 2.7 to 2.10:

$$F_{ii} = \frac{1}{f_{it}} - \frac{1}{f_{ic}} \quad i = r, t, l \tag{2.7}$$

$$F_{ij} = \frac{1}{f_{ijt}} - \frac{1}{f_{ijc}} \quad i, j = r, t, l \ \ (i \neq j) \tag{2.8}$$

$$F_{iiii} = \frac{1}{f_{it} f_{ic}} \quad i = r, t, l \tag{2.9}$$

$$F_{ijij} = \frac{1}{f_{ij}^2} \quad i, j = r, t, l \ \ (i \neq j) \tag{2.10}$$

Where f_{it} and f_{ic} are the tensile and compressive strengths in the i direction with f_{ij} the shear strengths. In a simplified case F_{iijj} is ignored giving the following $\boldsymbol{P}$ matrix with no interaction terms:

$$\boldsymbol{P} = \begin{bmatrix} F_{rrrr} & 0 & 0 & 0 & 0 & 0 \\ 0 & F_{tttt} & 0 & 0 & 0 & 0 \\ 0 & 0 & F_{llll} & 0 & 0 & 0 \\ 0 & 0 & 0 & F_{tltl} & 0 & 0 \\ 0 & 0 & 0 & 0 & F_{lrlr} & 0 \\ 0 & 0 & 0 & 0 & 0 & F_{rtrt} \end{bmatrix} \tag{2.11}$$

The $\boldsymbol{P}$ matrix can also be built using quadratic approximations for the interaction terms. F_{iijj} presented in Equation 2.12 uses a modified Hills criterion to account for the differences in tensile and compressive strength:

$$F_{iijj} = -\frac{1}{2}(F_{iiii} + F_{jjjjj} - F_{kkkk}) \quad i,j,k = r,t,l \quad where \quad i \neq j \neq k \tag{2.12}$$

Regardless of whether interaction is considered, the system of equations was solved using optimisation techniques. As only two of the six stresses are of interest at any one time (due to visualisation requirements), one is set as the independent variable and a linear space set-up to provide each point that will be evaluated ($n = 1000$), the other four stress directions which are not of interest are set to 0, and the dependent variable is calculated by maximising the distance $\sqrt{\sigma^2_{independent} + \sigma^2_{dependent}}$ subject to Equation 2.3, completed using the scipy.optimize.fmin_ slsqp algorithm (Jones et al., 2001). The proportional limit criterion (assumed to be the same as the yield criterion) is reported in all directions, however the ultimate failure criterion is only reported for the tensile tests. In the tensile direction ultimate failure is characterised by very quick drop in stress to near zero, this happens when the sample breaks into two parts. In the compressive direction ultimate failure is harder to define, if it is considered as the start of sample densification, the experimental results in this study are unable to provide the required information. The tests were limited to a maximum strain of 0.25. Other studies in dry wood have shown densification starts at strains greater than 0.5 (Gibson,

1997). When considering the tree as a living structure it is hard to conserve of a case in nature where densification would occur without ultimate tensile failure occurring on the opposite side of the stem.

2.4 Results

2.4.1 Initial properties

A number of descriptive properties of the samples are presented in Table 2.2. Dry density is reported for comparison with green density, the difference in density between corewood and outerwood is consistent with the change in moisture content. Acoustic velocity follows the same trend as MFA with the samples HW and LS having similar values. The standard deviation of the MFA is an estimate of the spread of angles which the S_2 layer contains, which has an influence on stiffness (Cave and Robinson, 1998a). LS is labelled as corewood, however given its MFA it may well be outer heart wood, or possibly a stiff sample of mature corewood.

2.4.2 Elastic moduli

Table 2.3 shows the experimentally obtained elastic moduli. It can be seen that in a number of cases there is a significant difference between the value of the constants and the method used to obtain them. The cellular structure of wood when sheared across the grain appears to act as if under compression, cellular breakdown occurs in compression rather than shear during this test.

2.4.3 Poisson ratios

Differences in the Poisson ratios presented in Table 2.4 clearly show variation between the testing procedures.

Table 2.2: Table showing the wood properties of the samples. Densities are averages from measuring all of the specimens individually. Disk scanner velocities are averages from individual specimens or a block of no more than six specimens depending on the size and shape. Wood spec velocities are from sections of board 500 mm in length, which were not used for specimens, taken in wet condition. MFA is obtained from x-ray diffraction after testing and drying.

Property	HS	HW	LS	LW
Green Density, kg/m^3	1143 (3)	1099 (9)	933 (21)	818 (22)
Dry Density, kg/m^3	531 (5)	458 (9)	438 (8)	393 (5)
Acoustic Velocity m/s Disk Scanner (green)	4651 (8)	4221 (26)	4191 (34)	3413 (14)
Acoustic Velocity m/s Wood Spec (green)	3490	3470	3470	2700
Wood Type	outerwood	outerwood	corewood?	corewood
Ring Number	> 15	> 15	< 15	< 15
MFA, *Degrees*	7	8	9	21
Standard Deviation of MFA *Degrees*	9	12	11	12

Table 2.3: Elastic moduli obtained from various UTM tests. The first letter is the direction of force, the second, the face which was recorded and the third t is a tension force and c is a compressive force. Capital letters indicate the shear moduli in the given plane.

Direction	HS		HW		LS		LW	
	E	SE	E	SE	E	SE	E	SE
rt_t in GPa	0.40	0.11	0.24	0.05	0.13	0.01	0.16	0.01
rt_c in GPa	0.58	0.08	0.36	0.10	0.39	0.03	0.47	0.13
rl_t in GPa	0.62	0.10	0.13	0.04	0.37	0.11	0.12	0.02
rl_c in GPa	0.57	0.07	0.58	0.09	0.45	0.07	0.54	0.10
tr_t in GPa	0.13	0.01	0.22	0.04	0.20	0.02	0.09	0.01
tr_c in GPa	0.33	0.03	0.35	0.07	0.29	0.07	0.26	0.02
tl_t in GPa	0.30	0.11	0.08	0.01	0.14	0.01	0.14	0.02
tl_c in GPa	0.37	0.04	0.36	0.03	0.22	0.02	0.29	0.05
lr_t in GPa	10.74	1.83	3.78	0.93	3.03	0.90	4.33	1.51
lr_c in GPa	3.10	0.11	1.02	0.50	3.76	0.80	4.04	0.61
lt_t in GPa	11.74	2.18	4.69	1.13	3.23	1.50	4.05	1.17
lt_c in GPa	7.47	1.60	1.74	0.61	4.65	1.06	5.85	1.18
TL in MPa	111.7	7.3	211.1	3.9	107.0	1.2	125.8	5.4
LR in MPa	59.7	1.9	34.4	1.2	38.5	1.7	29.5	1.1
RT in MPa	45.9	1.3	22.8	1.7	22.5	1.4	39.0	0.8

Table 2.4: v is the Poisson ratio and SE is the standard error on the ratio. First letter is the direction of force, the second the face which was recorded and the third t is a tension force and c is a compressive force.

Direction	HS		HW		LS		LW	
	v	SE	v	SE	v	SE	v	SE
rt_t	0.21	0.10	0.30	0.08	0.27	0.12	0.08	0.01
rt_c	0.64	0.04	0.52	0.09	0.60	0.05	0.49	0.17
rl_t	0.26	0.08	0.04	0.02	0.31	0.15	0.15	0.06
rl_c	0.14	0.04	0.15	0.05	0.22	0.14	0.17	0.13
tr_t	0.20	0.03	0.19	0.05	0.53	0.22	0.02	0.01
tr_c	0.47	0.10	0.33	0.04	0.39	0.08	0.42	0.05
tl_t	0.15	0.05	0.09	0.03	0.04	0.02	0.62	0.08
tl_c	0.10	0.02	0.08	0.04	0.18	0.08	0.08	0.03
lr_t	0.24	0.08	0.42	0.18	0.30	0.01	0.35	0.14
lr_c	0.26	0.05	0.41	0.13	0.36	0.08	0.44	0.09
lt_t	0.48	0.14	0.29	0.10	0.39	0.17	0.21	0.05
lt_c	0.41	0.08	0.16	0.06	0.37	0.09	0.42	0.14

2.4.4 Orthotropic assumption

If treating the material as anisotropic Tables 2.3 and 2.4 give a variety of options along with standard error to use. Depending on the application averaging multiple values may be appropriate. Often wood is assumed to be orthotropic, when this is the case using the above values is not an option due to the assumed symmetry of the material. Table 2.5 shows the outcome of the optermisation described in Section 2.3.3.

The Elastic moduli and Poisson ratios here were obtained through the optimisation. Both optimisations in Table 2.5 used Poisson ratios from the compression tests, as is discussed later in Section 2.5.1, the Elastic moduli were split into tension or compression values. Table 2.6 uses Poisson ratios from the compressive tests, the Elastic moduli from nonlongitudinal faces where possible and all four faces for the axial direction. Tension and compression values are averaged and optimised.

Table 2.5: Optimised values for the orthotropic assumption. All Poisson ratios used are from compression tests for reasons described in Section 2.3.3. The moduli are reported from both the compression and tension tests

Compression								
Axial direction	Long-rad				Long-tan			
Constant	HS	HW	LS	LW	HS	HW	LS	LW
E_r in GPa	0.58	0.39	0.43	0.29	0.66	0.49	0.39	0.29
E_t in GPa	0.33	0.35	0.29	0.26	0.37	0.35	0.29	0.26
E_l in GPa	3.10	1.04	4.17	4.04	4.33	1.45	4.63	3.56
v_{rt}	0.64	0.36	0.60	0.49	0.64	0.46	0.60	0.49
v_{rl}	0.06	0.15	0.04	0.03	0.06	0.15	0.03	0.04
v_{tr}	0.37	0.33	0.41	0.42	0.36	0.33	0.45	0.42
v_{tl}	0.05	0.05	0.03	0.04	0.05	0.04	0.03	0.04
v_{lr}	0.30	0.41	0.36	0.44	0.36	0.45	0.36	0.44
v_{lt}	0.45	0.16	0.37	0.57	0.56	0.16	0.41	0.50

Tension								
Axial direction	Long-rad				Long-tan			
Constant	HS	HW	LS	LW	HS	HW	LS	LW
E_r in GPa	0.40	0.34	0.14	0.16	0.22	0.34	0.14	0.16
E_t in GPa	0.16	0.22	0.16	0.09	0.16	0.23	0.16	0.09
E_l in GPa	5.06	3.73	2.26	1.37	4.98	2.76	2.26	1.76
v_{rt}	0.64	0.52	0.50	0.75	0.64	0.52	0.50	0.73
v_{rl}	0.02	0.05	0.02	0.05	0.01	0.05	0.02	0.04
v_{tr}	0.26	0.33	0.56	0.42	0.47	0.34	0.56	0.42
v_{tl}	0.02	0.01	0.03	0.04	0.02	0.01	0.03	0.04
v_{lr}	0.26	0.55	0.36	0.44	0.26	0.41	0.36	0.44
v_{lt}	0.64	0.16	0.37	0.55	0.64	0.16	0.37	0.69

Table 2.6: Optimised values for the orthotropic assumption. All Poisson ratios used are from compression tests for reasons described in Section 2.5.2. The moduli are reported calculated from averages of tension and compression. In the radial (r) and tangential (t) directions this is the average of tension and compression from the cameras viewing the radial tangential planes (rt) and tr. In the longitudinal direction it is the average of all four image sets.

Average Direction	HS	HW	LS	LW
E_r in GPa	0.49	0.30	0.26	0.31
E_t in GPa	0.25	0.19	0.24	0.17
E_l in GPa	4.36	2.81	3.50	2.38
v_{rt}	0.64	0.54	0.60	0.77
v_{rl}	0.03	0.05	0.03	0.06
v_{tr}	0.33	0.33	0.55	0.42
v_{tl}	0.03	0.01	0.03	0.04
v_{lr}	0.29	0.47	0.36	0.44
v_{lt}	0.60	0.16	0.37	0.50

Table 2.7: Proportional limit values. The first letter is the direction of force, the second the face which was recorded and the third t is a tension force and c is a compressive force. Capital letters are the planes of shear.

Direction	HS		HW		LS		LW	
	S	SE	S	SE	S	SE	S	SE
rt_t in MPa	0.8	0.2	1.3	0.5	1.2	0.3	0.9	0.1
rt_c in MPa	-3.2	0.1	-2.5	0.2	-2.1	0.1	-3.2	0.3
rl_t in MPa	1.0	0.1	0.8	0.2	1.7	0.4	0.5	0.1
rl_c in MPa	-3.3	0.2	-2.6	0.1	-2.3	0.1	-3.3	0.2
tr_t in MPa	0.8	0.2	0.7	0.2	0.9	0.1	0.6	0.1
tr_c in MPa	-2.7	0.1	-2.4	0.3	-1.8	0.2	-2.0	0.2
tl_t in MPa	1.0	0.3	0.5	0.1	0.8	0.2	0.8	0.2
tl_c in MPa	-2.6	0.2	-2.8	0.2	-2.0	0.1	-2.3	0.3
lr_t in MPa	46.0	7.5	26.0	1.3	7.6	1.8	21.8	4.1
lr_c in MPa	-17.4	1.0	-6.6	2.9	-14.0	1.1	-17.6	1.9
lt_t in MPa	35.3	3.8	27.0	4.5	9.6	2.4	20.6	2.4
lt_c in MPa	-15.5	1.5	-8.5	3.5	-13.6	1.6	-21.4	2.8
TL in MPa	2.2	0.4	4.5	0.3	2.7	0.2	3.2	0.3
LR in MPa	1.8	0.1	0.9	0.2	1.6	0.3	1.3	0.1
RT in MPa	1.1	0.2	0.6	0.2	0.7	0.1	0.9	0.1

2.4.5 Proportional limits (yield points)

The failure surfaces displayed in Figures 2.5, 2.6 and 2.7 use the values from Table 2.7 with measurements of the direction averaged. As the plots are two dimensional it is assumed for each plot that there are only forces acting in two directions, although it is possible to evaluate up to six directions using the criterion it cannot be displayed.

Figure 2.5 shows the failure planes calculated as described in Section 2.3.4 with no interaction terms. The behaviour of the two corewood samples are of interest, while the outerwood samples are stronger in longitudinal tension than compression, the corewood samples are much more centred on the zero axis. When interaction is included as in Figure 2.6 by way of the modified Hills criterion the system provides some unusual behaviour, particularly in the longitudinal direction. Possible explanations for this behaviour are discussed in Section 2.5.1. A constant of 0.05 is also used and displayed in Figure 2.7. With a small amount of interaction rotation of the failure surfaces is observed.

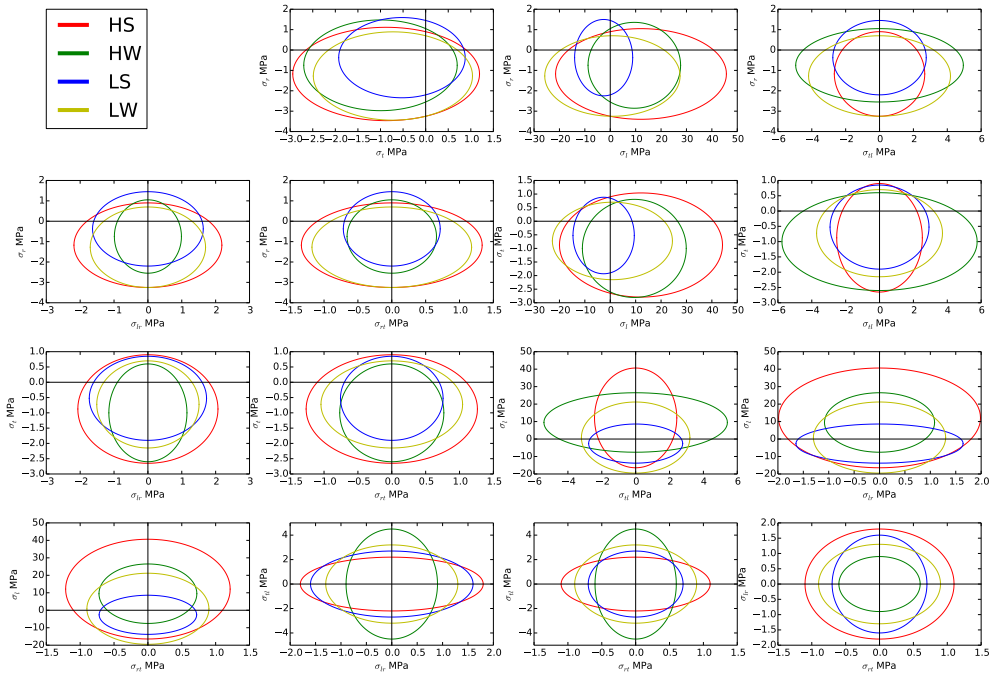

Figure 2.5: Proportional limit surfaces calculated using Tsai and Wu (1971)'s failure criterion with no interaction for all failure planes.

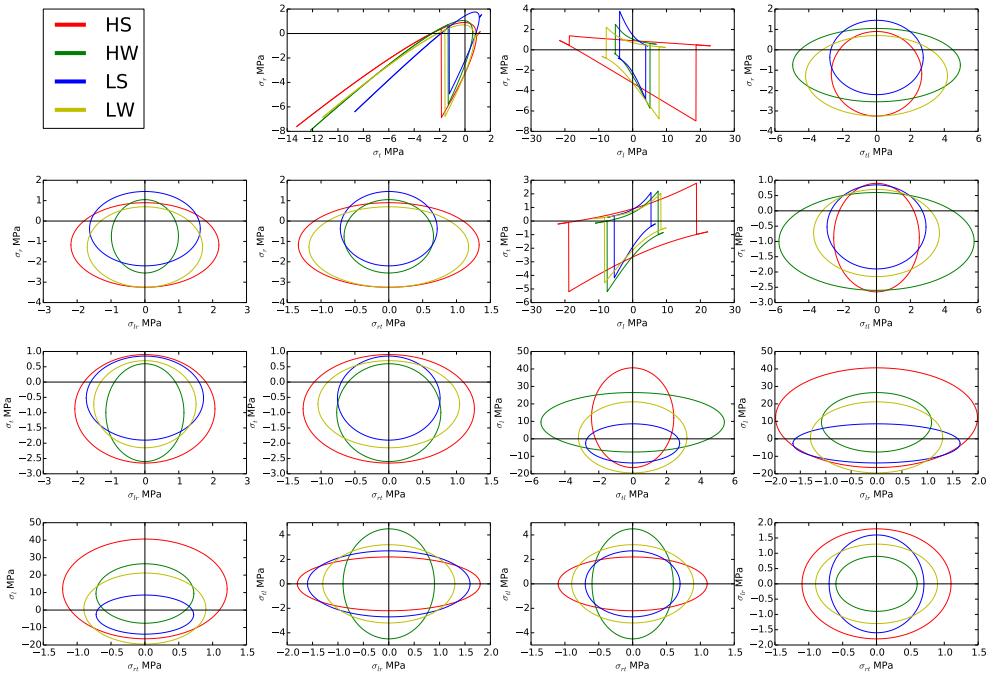

Figure 2.6: Proportional limit surfaces calculated using Tsai and Wu (1971)'s failure criterion and Hills interaction terms for all failure planes with a constant of 0.5.

2.4.6 Ultimate strength

Experimentally obtained values are reported in Table 2.7. Measurements of the same directional force (eg, lr_t and lt_t could be averaged, as they are both measurements of the same phenomenon.

Table 2.8 presents multiple measurements of the same tests, reported here as radial direction, rt and rl, the tangential direction tr and tl and the longitudinal direction lr and lt. These pairs can be averaged to calculate the three ultimate strengths, but are reported separately for completeness.

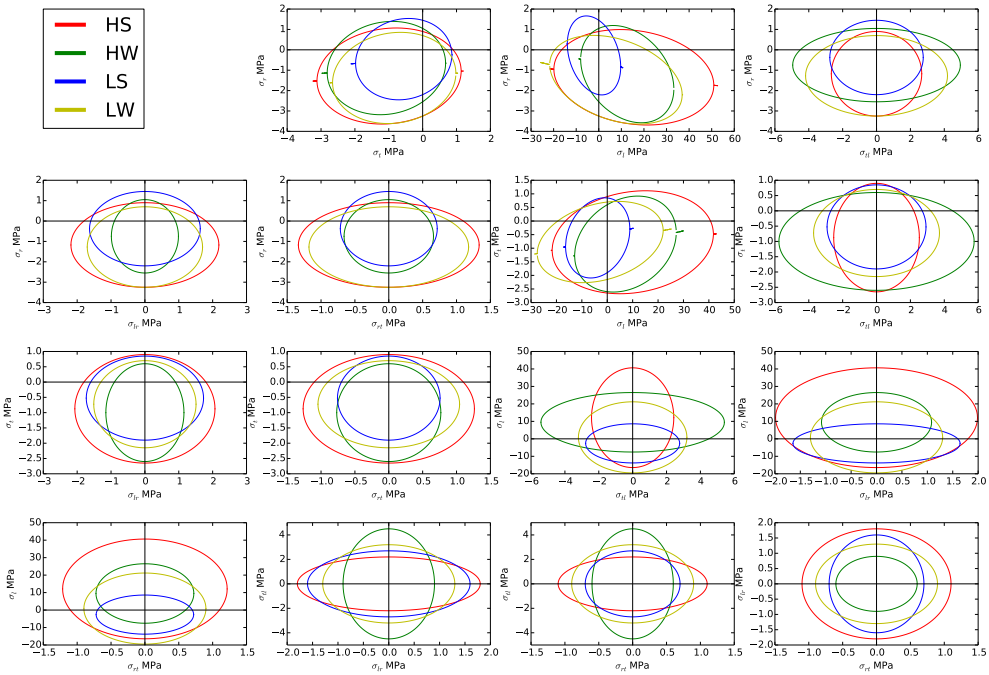

Figure 2.7: Proportional limit surfaces calculated using Tsai and Wu (1971)'s failure criterion and Hills interaction terms for all failure planes with a constant of 0.05.

2.5 Discussion

2.5.1 Discussion of the results

The proportional limit surfaces with no interaction terms clearly show the propensity for wood to be stronger in the axial tensile direction than any other when considering high density (outerwood) samples. An interesting phenomenon occurs with decreasing density, the samples become more centred or even favour compression in the longitudinal direction. The two low density samples are both expected to be corewood (although LS may not be). Focusing on the two corewood samples (LS and LW) the LS sample shows a low proportional limit in the longitudinal direction while having a high Elastic modulus. By contrast LW has a much higher proportional limit in most directions, while having a lower Elastic modulus (in the longitudinal direction). Both samples indicate the compressive strength is much more important than it is in the outerwood samples (which follow the more traditional idea of higher strength in tension). It could

Table 2.8: Ultimate strength reported in MPa. Only tensile strength is reported, the first letter is the direction of the force, second is the plane of imaging.

Direction	HS		HW		LS		LW	
	S	SE	S	SE	S	SE	S	SE
rt in MPa	3.1	0.3	3.1	0.3	2.9	0.2	2.2	0.2
rl in MPa	3.1	0.3	3.0	0.3	2.8	0.3	2.2	0.2
tr in MPa	2.1	0.4	1.6	0.3	1.9	0.1	2.1	0.2
tl in MPa	2.1	0.5	1.4	0.3	1.9	0.1	2.1	0.2
lr in MPa	64.2	5.9	45.2	4.6	21.2	1.6	32.6	2.9
lt in MPa	65.0	5.7	43.6	5.1	20.0	1.9	32.8	2.9

be speculated that this decrease in tensile proportional limit compared to compression strength is partially due to the environmental demands placed on young trees (if the samples are in fact corewood). Some examples that might have an impact on this are the low second moment of area from the thin stem meaning the tree must withstand much more movement from wind, resulting in more compression wood like cells being produced at young ages. Animals stepping on stems causing compressive destruction may have an effect. The trend may also be a by product of a non mechanical pressure. It is possible that because these samples were taken from fully growth trees, (typically 25-30 years old) that over time the material structure has been degraded by growth stresses, wind induced microfracture, or other time/growth dependent phenomena resulting in a reduction in tensile strength, which is not present if the wood is tested from a young tree.

All samples show that under radial or tangential loading that compressive stress is favoured. This may be due to the different failure mechanisms in tension and compression, with tension causing peeling between the cells, while compression must act on the cells themselves. If there has been no evolutionary pressure causing the cells to reinforce the connection to resist tension it may result in a significantly lower proportional limit than in compression where the geometry of the cellular structure gives it more strength.

When interaction is considered rotation of the failure planes can be observed in the σ_r σ_t plot to further favour compression in these directions. This rotation is also observable in the other two sub-plots only involving pure stresses. The sub-plots involving longitudinal samples show erratic behaviour which is likely to have come from numerical instability induced by the interaction term of 0.5. It is suspected this is because

the interaction term is too large for the given differences in magnitude between the longitudinal and other directions. Figure 2.7 using the lower 0.05 interaction constant still shows the rotation, however the erratic behaviour is removed.

While Tsai and Wu suggest the use of experimentation to find the appropriate interaction terms for use within their strength criterion, other options are available. In this case a modified version of Hills criterion (Hill, 1950) was used. The original criterion assumes that the compressive and tensile strengths are equal. The Tsai and Wu criterion differentiates between compressive and tensile strengths, so the modification to Hills criterion makes it more suitable for use with the Tsai and Wu criterion. However when the proportional limit surfaces are solved using these interaction terms, with Hills 0.5 constant the three failure planes associated with σ_r, σ_t and σ_l show erratic behaviour.

Failure planes with σ_l show severally decreased strength in the l direction, and become nonelliptical. It is likely to be the case the the constant of 0.5 is not appropriate when there is such a large disparity between strengths in two of the directions. Other authors have suggested varying the constant, and when reproduced here at a value of -0.05 shows rotation of the failure surfaces. Hills criterion is essentially arbitrary (Tsai and Wu, 1971) and bears no resemblance to the materials structure, the generalisation of Hills criterion in this manner has no physical basis for the choice. Additionally the generalisation does not increase the methods realism. The deformation of these two strength planes away from elliptical is likely to be evidence of the breakdown of the criterion caused by the incorrect interaction terms being used.

The Tsai and Wu criterion has been used in a number of papers as discussed in Section 2.3.4 however it has been suggested that the criterion is insufficient (Mackenzie-Helnwein et al., 2003, 2005a). Because we have assumed linear elastic deformation, with the yield point defined as the end of the linear section of the stress strain curve, no nonlinear elastic effects have been considered. These authors suggested that the nonlinearity which is usually considered to be nonlinear elastic is due to an inelastic portion of the the total strain, so these findings should have little effect on these results.

The Elastic and Shear moduli are low although similar to published values for dry wood, as are the Poisson ratios, as can be seen in Tables 2.9 and 2.10. The lower values presented here are not unexpected due to the samples being in green condition and from

Pinus radiata. In order to accurately quantify the differences between green and dry wood values more accurate testing procedures along with a higher number of samples are needed.

Corewood needs further investigation as this study provides some interesting results, particularly the failure planes in the longitudinal direction. With the corewood samples providing a higher ratio of compressive to tensile strength than outerwood samples. Investigation is needed to determine if this is a property of corewood produced by seedlings and young trees, or if it forms differently and is modified over time while the tree grows. Again to accurately quantify the difference between dry and green wood properties a larger number of more accurate tests are needed.

Table 2.9: Comparison of literature values with the findings in this study. Values are aproximate as a number of them were taken from published plots. All Moduli in GPa.

Reference	Test	Species	E_r	E_t	E_l	G_{tl}	G_{lr}	G_{rt}	v_{rt}	v_{rl}	v_{tr}	v_{tl}	v_{lr}	v_{lt}
This work	Static	*Pinus radiata*	0.26	0.17	2.38	0.11	0.03	0.02	0.54	0.03	0.33	0.01	0.29	0.16
(Range)			0.49	0.25	4.36	0.21	0.06	0.05	0.77	0.06	0.55	0.04	0.47	0.60
Ozyhar et al. (2013)	Static	*Fagus sylvatica*	1.14	0.53	9.14				0.19	0.39	0.47	0.5	0.04	0.03
(Range)			2.33	1.05	14.54				0.41	0.55	0.76	0.87	0.2	0.11
Henrik and Gustafsson (2013)			0.8	0.5	12	0.7	0.7	0.05		0.02	0.3	0.02		
Raffaele et al. (2011)	Hybrid	*Picea Abies*	0.236	0.387	10.4	0.65	0.597	0.029	0.42	0.018		0.017		
Mackenzie-Helnwein et al. (2005a)	Hybrid	Spruce	0.7	0.5	13	0.47	0.63	0.22	0.38			0.013	0.5	
Ormarsson and Cown (2005)	Hybrid	*Pinus radiata*	0.7	0.2	5	0.6	1	0.05						
(Range)			2.2	0.7	19	1.2	2	0.15						
Qing and Mishnaevsky (2009)	Theoretical			2.202	20.25	1.94		1.4						
Harrington (2002)	Theoretical	*Pinus radiata*	0.56	0.23	5.61	1.0	1.20	0.08		0.42	0.38	0.37		
(Range)			3.08	3.08	9.33	2.18	2.07	0.79		0.48	1.23	0.45		
Persson (2000)	Theoretical	Spruce	0.67	0.08	7.7	0.40	0.68	0.009		0.009	0.124	0.006		
(Range)			1.57	2.1	36.4	1.77	1.76	0.043		0.057	0.241	0.054		

Table 2.10: Literature values for the longitudinal Elastic moduli. Values are aproximate as a number of them were taken from published plots. All moduli in GPa.

Reference	Test	Species	E_l
Watt et al. (2006)	Dynamic	*Pinus radiata*	2 - 7
Waghorn et al. (2007b)	Dynamic		5 - 9
Lindström et al. (2004)	Dynamic		2 - 4.8
Xinguo et al. (2011)	Dynamic		3 - 6
Watt et al. (2008)	Dynamic		2.4 - 5.9
Lasserre et al. (2009)	Dynamic		2.7 - 4.2
Watt et al. (2011)	Silviscan		3 - 15
Downes et al. (2002)	Silviscan		11.5 - 13.5
Watt et al. (2010)	Silviscan		1.4 - 21.6
Watt and Zoric (2010)	Silviscan		3 - 18
Xu et al. (2004)	Static		4.8 - 14.9
Lindström et al. (2002)	Static		2.5 - 6

2.5.2 Sources of error in this study

It should be kept in mind that only four boards were tested during this experiment and those boards were selected as extreme cases of green density and acoustic velocity. The selection criteria and low sample number result in the selected samples not being representative of the species in general. In order to gain an understanding of the 'average' stem further testing is needed.

It can be noted from Table 2.1 that for the given green densities and acoustic velocities obtain using the disk scanner if one were to calculate the dynamic modulus, which has been reported to have a strong correlation to static modulus in the axial direction (Lindström et al., 2004, 2002) at usually around a $1:1$ linear relation the predicted values for the axial modulus become very high. The disk scanner has not been used for samples of this shape before and as a consequence may not have been providing accurate velocities as they differ substantially from those obtained from wood spec. The use of green wood may also have had an effect. The ranking of the samples does however fit with the persevered ranking when the boards were selected at the mill, and the density values. Acoustic velocities, green and dry densities, in general, have higher values for higher strength and stiffness boards. Low density corewood samples have a low strength and stiffness compared to the outerwood samples.

Because in many cases a number of constants could be obtained by different methods from one or more tests there is a need to select the measurements which best resemble the real underlying physical characteristics. While all of the results are reported above for completeness, the following is a discussion to consider which are the more accurate solutions.

Measurements in the horizontal direction can be ignored when considering tensile tests, this is due to the resolution of the cameras not being high enough to resolve the contraction on the samples in the horizontal direction. The low tensile strength in the radial and tangential directions results in very low dimension changes before both the proportional limit and the rupture of the sample. Although in the longitudinal direction the samples have a much higher breaking strength the reliability of the measurements of contraction in the horizontal direction is also suspect. Generally tracking of the longitudinal face of the samples is more error prone than the other two faces, it is suspected this is because of the uniformity of the image over the samples in this direction, whereas in the other two directions early and late wood give identifiable points within the images used by the point tracking algorithm. In the vertical direction the samples are tracked more reliably due to the greater number of pixels and the greater displacement of the sample due to its shape. In the future artificially adding a random speckle pattern should be considered to increase the accuracy of point tracking.

Extension data extracted from the UTM can be ignored for all tension tests as the jaws which hold the sample are self tightening using a mechanism which provides an increase in extension reading at the machine without it being transferred to the sample. On samples of this size the effect was significant.

Compression tests are used for calculating all of the Poisson ratios. Absolute values of constants obtained from tracking on longitudinal faces appear to be low, however the Poisson ratios generally agree with the ratios gained from the other tests. Due to the implementation of the image tracking algorithm, if the algorithm does not detect the identifiable group of pixels in the new image it simply leaves the point with no displacement. It is suspected that the assumption that points tracked well in the vertical direction will also be tracked well in the horizontal direction holds true, along with its corollary, points which remain stationary due to poor tracking in the vertical direction will also remain stationary in the horizontal direction. The result of this is that although

the absolute values for the displacement in both directions is highly suspect the ratio of observed displacement in the vertical and horizontal direction still provides a good estimate of the true value of the ratio because every time a displacement is observed in one direction, the associated displacement in the other direction is also observed. Because of the errors in magnitude of the displacements when it can be avoided these values were not used. This not possible when calculating Poisson ratios, or the Elastic modulus when force is applied in the longitudinal direction, as both cameras image a longitudinal face. For the radial and tangential directions of compression and tension the Elastic modulus was calculated from the camera which had a view of the growth rings and hence provided more robust image tracking.

The nature of shear tests means some of the force applied is dissipated through rotation of the sample block, the magnitude of this is expected to be significant due to the unexpectedly low values for the shear moduli. In some cases this rotational force results in breakage of the sample specimen via cell wall peeling in the plane perpendicular to the desired shear plane. Where the shear plane attempts to break the cells directly (ie shear plane perpendicular to the cell axis) bowing is observed around the bottom sample rest, this also dissipates energy further reducing the accuracy of the tests. It is worth noting that other testing methods for determining shear characteristics such as those presented in (BS, 1957) and (Kollmann and Cote, 1968) may provide more reliable solutions however these require more specialist equipment. The difficulty in obtaining accurate shear measurements has been reported on before (Kollmann and Cote, 1968; Bodig and Jayne, 1982). Kollmann and Cote (1968) reported shearing stress perpendicular to grain are three to four times higher than parallel to it.

It can be seen from the data tables that generally the compressive tests result in higher Elastic modulus values than the tension tests. One explanation for this may be the documented dependence of the moduli on the dimensions of the sample (Niklas, 1997), with the tension tests being smaller than the compression tests this may lead to lower outcomes. However what this does not explain is why the tension tests in the longitudinal direction of the two outerwood samples (HS and HW) are substantially larger than those in compression. Another possible reason for this is that it is a genuine material property which is accentuated in outerwood indicating it may be less well described by the assumption of an orthotropic material than corewood.

When testing in pure compression or tension producing samples which are exactly in the desired direction is near impossible due to the variations in properties during the growth of the tree. While every effort was taken to minimise the effect of this, in some cases, particularly in corewood with wide grain spacing it is not possible for the given sample size, due to the radius of the rings. The Poisson ratios may be affected by the specimen not having all three directions perfectly perpendicular. Some samples may be cut from boards with spiral grain but no samples with visible spiral grain were used. It is thought that while this is an issue to note, it is unlikely to be substantially decrease the accuracy of the measurements given the magnitude of other errors also discussed here.

During compression testing it was observed that samples compressed in the tangential direction tend to bow in the same direction as the grain, this is much more evident in corewood where the curvature of the grain is larger. The bending may have some effect on the accuracy of the findings, but to what extent is unknown.

It has been reported that the size of samples of wood when tested for elastic constants can have an effect on the result (Niklas, 1997). While size dependence is an important note to be aware of controlling for this would require using samples which do not necessarily provide a good representation of a homogeneous piece of wood. The sample sizes in this study most likely also suffer when compared to other tests utilising different sized samples. It is important to use data collected from specimens which best represent the level of homogenisation required for the particular end use. Given current personal computing resources, this size specimen provides a good resolution for finite element models of an entire stem in the horizontal plane. The vertical direction shows much lower deviation of material properties per unit length, so the sample dimension is less important, hence can be reduced in order to give clean samples without defects.

Experimental errors from changing dimensions within the UTM under loading are assumed to be negligible (with the exception of the mechanisms of the jaws used for tension tests). The load cells are reported to be accurate to 0.1N and hence are also negligible when compared to the major sources of error in these tests, the image tracking.

Chapter 3

Model

3.1 Introduction

The stiffness and strength of timber is important to industries which rely on it as a building material. As a consequence of high variability in these properties when trees are milled, timber is graded. There has been interest and research in breeding trees which reliably produce this higher value timber.

Trees are subjected to multiple environmental mechanical loads and adapt the mechanical properties of their stems to an environment changing over time. Wind is one of the most important (Timell, 1986a). Wind loading can cause mechanical failure making the tree worthless in a commercial sense. A substantial amount of research on predicting wind throw and wind damage risk for commercial species has been conducted (Ancelin et al., 2004; Peltola et al., 1999; Mayer et al., 1989; Gardiner et al., 2000; Dunham and Cameron, 2000). These models do not investigate the structural failure within the tree, but attempt to identify how likely failure is to occur in a particular environment. Wind also has less obvious effects. Continued wind loadings from a prevailing direction can cause compression wood production on the lee side of the pith in order to compensate for this loading (Timell, 1986a).

One way of investigating the time phenomenon is the use of mathematical models, such as finite element models. However because of the size of the tree, modelling an entire tree from the molecular level is infeasible, so homogenisation is used. This is the case for a number of current problems in plant biophysics. In order to use finite element methods experimental data is required for parametrization.

While MFA controls the stiffness of the cell wall, basic density measures the amount of cell wall in the tissue. Therefore overall mechanical wood properties rely on both features. For a more detailed description of the TRP of MFA and density or these modelling and experimental attempts see Chapter 1.

When investigating living trees from a structural standpoint other requirements need to be considered. Structural integrity of both greenwood and corewood have had little attention in literature at the scale of small cellular blocks. Investigating the TRP requires testing at scales small enough to separate corewood and outerwood. Most experimental work investigating the structural stability of whole stems is undertaken for use in failure prediction models for wind throw (statistical models such as HWIND and GALES, see Chapter 1). Classical mechanics theories have been used, sometimes in conjunction with experimental data from tree pulling and wind tunnel experiments (Rudnicki et al., 2004; Peltola et al., 1999; Spatz and Bruechert, 2000). Neither take into account changes in material properties within the stem.

Over the last century or so there have been a number of suggested explanations for why trees grow with the typical radial patterns observed. The mechanical hypothesis which is investigated in this study, asserts that the TRP is a result of the tree needing to respond to different mechanical loadings from its environment as it grows. For a seedling being highly flexible could be important in order to bend out of the path of animals and reduce wind and snow loads. However when the tree grows and a significant size is reached along with a large canopy greater stiffness could be an advantage in outerwood as bending becomes difficult due to the stem diameter. Note that there are other hypotheses, see Chapter 1 for more details or for a good review see Meinzer et al. (2011). This thesis endeavours to in investigate the mechanical hypothesis in further detail by including the ability for material properties to vary within the stem to represent the TRP. The approach used is to construct a finite element model of a tree with different radial patterns and subject it to wind loadings. In Section 3.2 the

required mathematical and physical principles are briefly introduced along with the implementation of these principles to this particular problem. Finally comparisons are discussed between the various wood structure profiles.

Elastic deformation of a material occurs when the magnitude of loads applied to a sample are small enough that when released the sample returns to its original state (Hibbeler, 2000). Here we need to define some particular terminology and assumptions. The proportionality limit is the point at which the relationship between stress and strain stops being linear, although not necessarily elastic. The end of the elastic state is characterised by the yield point (elastic limit), after the yield point plastic (irreversible) deformation occurs, although this deformation does not necessarily result in a loss of stiffness (Reiterer et al., 1999).

It was assumed that the proportionality limit and the yield point are equal and the terms yield point, proportionality limit and failure point are used interchangeably to indicate what is strictly the proportionality limit. There is argument for and against the assumption that wood is a linear elastic material in literature (Mackenzie-Helnwein et al., 2005a). Within this work models are restricted to the limit of proportionality in order to retain simplicity.

3.2 Method

3.2.1 Mesh construction

As trees grow, cells in the cambium divide and produce new cells on the outside of the current wood, or the apical meristem grows vertically. Because the apical growth is not expanding the stem horizontally as the cambium is on lower parts of the stem, taper develops. Here taper is included at a ratio dependent on the stocking being investigated. However the taper for individual cells was not considered and they were assumed to be vertically orientated. Data presented in Waghorn et al. (2007a) was used to create a regression to estimate stem radius from stocking rates based on the slenderness ratios. The regression presented in Equation 3.1 was calculated from reported slenderness

ratios for stocking rates of between 275 and 1457 stems per hectare and assuming a stem height of 15 m. The size of the elements is dependent on the size of the stem being modelled. Elements are quadratic tetrahedral and have a width and height one fifth the radius and height of the stem and cover an angle of 22.5 degrees.

$$r_s = e^{-0.000328S-1.868} \tag{3.1}$$

Where S is the stocking rate, assumed to be either open grown, one stem per hectare or 741 stems per hectare.

Gravity is the only external force considered during the growth phase, as the tree grows it compresses under self weight, resulting in the lower parts of the stem becoming successively compressed by the new growth.

When cells mature within the tree they attempt to change shape. The molecular basis behind this potentially involves lignin swelling of the cell wall and/or cellulose contraction such as presented by Yamamoto et al. (2002). The new cells dividing from the cambium are born into a un-stressed state. During differentiation the cells become more stout, shrinking along the cell axis and expanding radially (Archer, 1987). If there is nothing stopping this swelling there are no resulting stresses, in a living tree however the existing mature cells resist the change. Cellular contraction results in a stress profile forming within the tree, longitudinal compression in the centre, where older wood is compressed by the needs of newly contracting cells, and tension at the outer edge, as the centre wood is resisting the contraction of the maturing cells.

The pre-stressed state of the cambium from gravity and growth stresses produces the need to successively 'grow' the mesh which is to be used so that each mesh addition is added in a non stressed state on top of a stressed surface. Mesh growth is achieved by first defining an initial state, this state can be thought of as a seedling. The seedling is subjected to gravitational forces, deformation occurs and a new deformed mesh is created. The positions of the nodes and vertices of the deformed mesh are used to calculate the positions of new vertices and nodes to be added in order to represent cambial growth in a non stressed state onto the stressed surface along with apical growth to a predefined height. The newly calculated outer layer nodes and vertices are

then added to the original un-stressed mesh, creating a new mesh in a relaxed state (there are no stresses in it) with the growth layers added as though to a stressed surface, removing the need to track accumulative stresses through the growth phase.

The result of the addition is a mesh with no internal stresses, and new elements added as though they were added to a stressed state. Keeping the reference mesh without stress is important as the next iteration now reapplies the forces to the whole mesh, resulting in deformation of the new mesh. The growth process was repeated for five time steps. The final result was a mesh of age t (where $t = 5, 10, 15$) which when the gravitational forces and growth stresses are reapplied has the appropriate internal stress profile ready for a wind load to be applied. The description above is presented as a flow chart in Figure 3.1. Figure 3.2 is (a simplified representation of) the original, 'seedling' mesh used. The seedling mesh is deformed and then has new growth positions calculated from its deformed configeration. These new nodes and vertices are added to the existing mesh as can be seen in Figure 3.3. Note the green section of the mesh is the original mesh shown in Figure 3.2 with the new cambial growth added shown in red, and apical growth shown in blue.

3.2.2 Material constants, microfibril angle and density

Experimental constants described in Chapter 2 were used to parametrise the model. Four wood samples of *Pinus radiata* were chosen to represent a range of extreme values of green density and stiffness for the species. Linear interpolation was used to approximate material constants between two samples to provide a gradient of material properties from the corewood to the outerwood. The TRP of cellular properties was investigated using the gradient of elastic constants and Poisson ratios from different samples by applying simulated wind loads to stems with different radial profiles.

A linear interpolation was used between two samples in order to provide the TRP over the stem. While the TRP of *Pinus radiata* usually follows a non-linear increase for density and a non-linear decrease for MFA (Burdon et al., 2004), during the first 15 years the trend can be approximated as linear, after this however the non-linear behaviour becomes more prevalent as the properties stabilise. It should be noted that

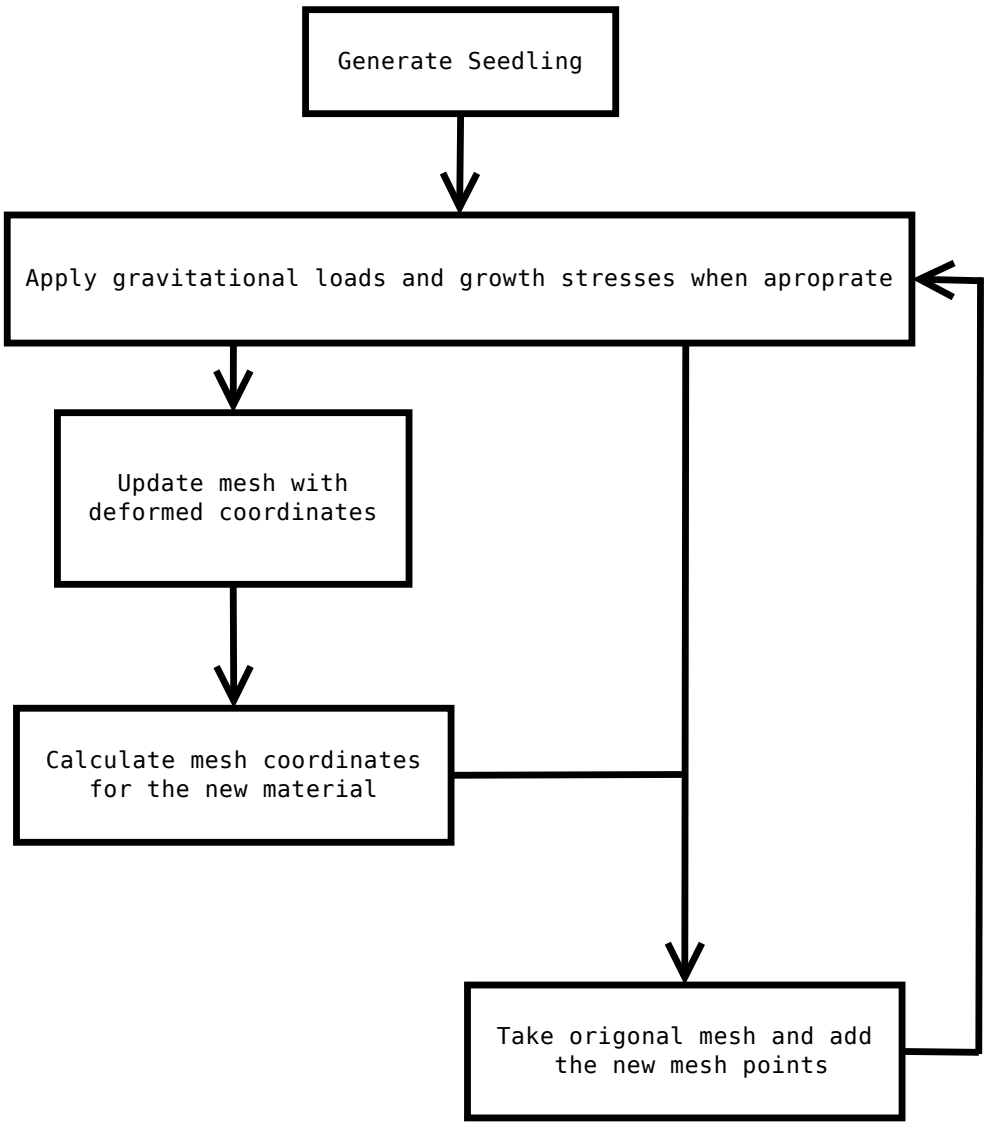

Figure 3.1: Flow chart showing the construction of the mesh described in Section 3.2.1.

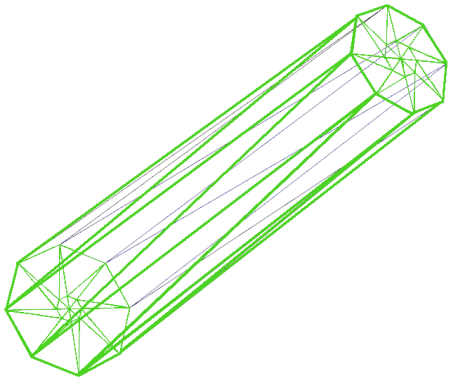

Figure 3.2: The initial mesh. This mesh represents the initial seedling which is then grown.

there is much variation between individuals and this is not universal. After 15 years the properties produced by older cambial tissues become fairly consistent for a given individual and are not considered here. As the radius increases and the pattern becomes consistent the inner radial pattern will have less influence on the structural stability of the stem. The TRP was investigated by calculating the appropriate elastic and shear moduli along with Poisson ratios for each point in the stem based on a linear interpolation. The linear interpolation was calculated between two samples chosen to represent corewood and outerwood, Equation 3.2 shows the general form.

$$\lambda = \frac{-r}{r_t}(\lambda_i - \lambda_o) + \lambda_i \tag{3.2}$$

Where r is the stem radius at the current point, r_t is the total radius at 15 years, λ_i and λ_o are the values of the material properties obtained in Chapter 2 at $r = 0$ and $r = r_t$ respectively.

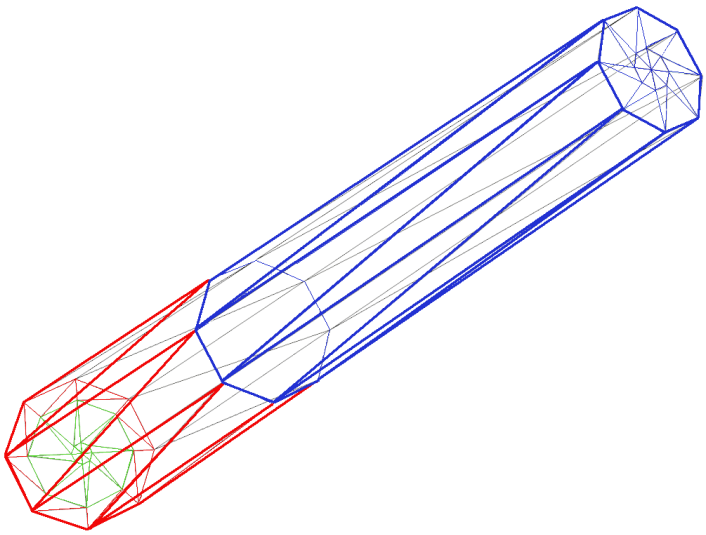

Figure 3.3: The mesh at age two. Note that the green section in the base is the base of the seedling shown in Figure 3.2. Blue is the new apical growth and red is the cambial growth elements.

3.2.3 Coordinate transformations

Due to the microstructure of wood the native coordinate system for describing material properties is not the same as the global coordinates system used to impose external forces on the stem. Transformation between the two systems is needed. The *rtl* local system used for experimental work presented in Chapter 2 is used in combination with the interpolations presented in Equation 3.2 and presented as the stiffness matrix in Equation 3.4 using Voigt (engineering) notation at any point in the stem. Because the stiffness matrix is calculated in the local coordinates it needs to be converted into an xyz system in order to apply wind loadings in a sensible fashion, Equation 3.5 provides the transformation matrix. The use of Voigt notation allows for transformation of the elastic constants into the global system, via Equations 3.6 and 3.8. It is assumed that there is no spiral grain occurrence within the stem, the local l axis is always parallel with the global z axis. Material constants in the longitudinal direction are parallel with the z axis, i.e. there is no correction angle applied to account for taper.

$$S_l = \begin{bmatrix} \frac{1}{E_r} & -\frac{v_{tr}}{E_t} & -\frac{v_{lr}}{E_l} & 0 & 0 & 0 \\ -\frac{v_{rt}}{E_r} & \frac{1}{E_t} & -\frac{v_{lt}}{E_l} & 0 & 0 & 0 \\ -\frac{v_{rl}}{E_r} & -\frac{v_{tl}}{E_t} & \frac{1}{E_l} & 0 & 0 & 0 \\ 0 & 0 & 0 & \frac{1}{2G_{tl}} & 0 & 0 \\ 0 & 0 & 0 & 0 & \frac{1}{2G_{lr}} & 0 \\ 0 & 0 & 0 & 0 & 0 & \frac{1}{2G_{rt}} \end{bmatrix} \tag{3.3}$$

$$C = S^{-1} \tag{3.4}$$

$$G = \begin{bmatrix} a_r^x a_r^x & a_r^y a_r^y & a_r^z a_r^z & a_r^y a_r^z & a_r^x a_r^z & a_r^x a_r^y \\ a_t^x a_t^x & a_t^y a_t^y & a_t^z a_t^z & a_t^y a_t^z & a_t^x a_t^z & a_t^x a_t^y \\ a_l^x a_l^x & a_l^y a_l^y & a_l^z a_l^z & a_l^y a_l^z & a_l^x a_l^z & a_l^x a_l^y \\ 2a_t^x a_l^x & 2a_t^y a_l^y & 2a_t^z a_l^z & a_t^y a_l^z + a_t^z a_l^y & a_t^x a_l^z + a_t^z a_l^x & a_t^x a_l^y + a_t^y a_l^x \\ 2a_r^x a_l^x & 2_r^y a_l^y & 2a_r^z a_l^z & a_r^y a_l^z + a_r^z a_l^y & a_r^x a_l^z + a_r^z a_l^x & a_r^x a_l^y + a_r^y a_l^x \\ 2a_r^x a_t^x & 2a_r^y a_t^y & 2a_r^z a_t^z & a_r^y a_t^z + a_r^z a_t^y & a_r^x a_t^z + a_r^z a_t^x & a_r^x a_t^y + a_r^y a_t^x \end{bmatrix} \tag{3.5}$$

Where a_i^j is the directional cosine from j to i (global to local), $j = x, y, z$ and $i = r, t, l$.

$$\boldsymbol{C = G^T C_l G} \tag{3.6}$$

$$\boldsymbol{G^T = D^{-1}} \tag{3.7}$$

$$\boldsymbol{\sigma_l = D\sigma} \tag{3.8}$$

The stiffness matrix $\boldsymbol{C}$, stress vector $\boldsymbol{\sigma}$ and strain vector $\boldsymbol{\epsilon}$ are in the global coordinate system while $\boldsymbol{C_l}$,$\boldsymbol{\sigma_l}$,$\boldsymbol{\epsilon_l}$ are in the local system.
The forces being applied in the global system (through the transformation of the elastic constants) results in stresses being calculated in the global system. As the experimental work was conducted in the local system the proportionality limit stresses are in the local system. Equation 3.8 was used in order to transform the stresses in the global system (calculated by the model) back into the local system in order to evaluate failure.

3.2.4 Gravitational forces

The forces due to gravity from self weight of the stem and canopy were applied to appropriate domains. The force due to gravity from self weight of the stem was applied as a body force to the whole domain Ω (i.e. the whole stem) in Equation 3.11. Green density ρ is calculated as per Section 3.2.2 and g is gravity. The canopy is assumed to take the geometry of the upper half of an ellipsoid described in Equation 3.12, where z_0 is the height at the bottom of the current element and z_1 is the height at the top of the current element, with the top of the ellipsoid at the top of the stem, height h. The start height S_c of the canopy was estimated using Equation 3.9 which was derived from data presented by Waghorn et al. (2007a). In order to estimate crown radius, r_c, Equation 3.10 is used, which was derived from the assumption that the maximum radius which can be achieved by the crown is half the distance between two trees evenly spaced in the stand. Note the predicted radius for open grown trees is 0.36 m smaller using Equation 3.10 than the regression presented by Leech (1984) which was not used as it predicts excessive crown overlap at higher stockings. The weight of the canopy on the stem is applied as a body force described in Equation 3.14.

$$S_c = -123.4r_s + 20.6 \tag{3.9}$$

$$r_c = 34.4r_s - 2.07 \tag{3.10}$$

$$B_s = \rho g \tag{3.11}$$

$$V_c = \pi r_c^2 \left(z_1 \left(\frac{1 - z_1^2}{3(h - S_c)^2} \right) - z_0 \left(\frac{1 - z_0^2}{3(h - S_c)^2} \right) \right) \tag{3.12}$$

$$V_s = \frac{\pi}{3} \left(r_{\|_{z_0}}^2 z_0 - r_{\|_{z_1}}^2 z_1 \right) \tag{3.13}$$

$$B_c|_{\mathbf{\Omega_1}} = V_c \rho_c g \frac{1}{V_s} \tag{3.14}$$

$$\mathbf{\Omega_1} = \{(x, y, z) \in \mathbf{\Omega} : z > S_c\} \tag{3.15}$$

Where r_s is the radius of the stem (from Equation 3.1), $r_{\|z_0}$ is the radius of the stem at height z_0, $r_{\|z_1}$ is the radius of the stem at height z_1 and g is gravity. ρ_c is the canopy density of 5.6 kg/m^3 estimated from data in Beets and Whitehead (1996) at a stocking of 741 stems per hectare and converted to green density assuming the same relationship as for wood presented in Chapter 2. The canopy force due to gravity is only applied to the subdomain Ω_1, defined in Equation 3.15, where z is the vertical coordinate of any point. $\frac{1}{V_s}$ is needed in order transform the canopy's gravitational force into a force per unit stem volume.

3.2.5 Drag

In order to stress the stem a constant wind profile was applied to the canopy. The crown sail area was assumed to be the upper half of an ellipse attached to the stem on the surface Γ_1 (defined by Equation 3.20) a surface subregion of total surface Γ. The common drag model presented in Equation 3.19 has been used previously (Spatz and Bruechert, 2000; Rudnicki et al., 2004; Mayer et al., 1989) and is used to approximate the wind load. It should be noted that more complex models are available (Coutts and Grace, 1995). The drag coefficient ς in Equation 3.16 was produced from data reported by Mayhead (1973), for Scotts pine as no data was available for radiata. The use of the Mayhead (1973) Scotts pine data set has previously been suggested as a suitable substitute (Moore and Gardiner, 2001).

$$\varsigma = e^{-0.377\omega - 0.306} \tag{3.16}$$

$$A_c = \int_{z_0}^{z_1} 2r_c \sqrt{1 - \frac{z^2}{(h - S_c)^2}} dz \tag{3.17}$$

$$A_s = \frac{\pi}{2} \left(r_{\|_{z_0}} \sqrt{z_0^2 + r_{\|_{z_0}}^2} - r_{\|_{z_1}} \sqrt{z_1^2 + r_{\|_{z_1}}^2} \right) \tag{3.18}$$

$$T_w|_{\mathbf{\Gamma_1}} = \frac{1}{2} \rho_{air} \varsigma \omega^2 A_c \frac{1}{A_s} \tag{3.19}$$

$$\mathbf{\Gamma_1} = \{(x, y, z) \in \mathbf{\Gamma} : x > 0, z > S_c\} \tag{3.20}$$

T_w is the force induced on the stem via the canopy for a given wind speed ω. Air density ρ_{air} is constant at 1.226 kg/m^3 (Mayhead, 1973). The canopy area A_c is calculated as per Equation 3.17 and stem area A_s is calculated as per Equation 3.18. $\frac{1}{A_s}$ is needed in order to transform the wind induced force into a force per unit stem surface area. T_w is imposed on the stem as a boundary force in the sub-domain Γ_1 as described by Equation 3.20.

The constant velocity wind profile used is simplistic, more complex profiles, gust factors and dynamic loading simulations have been suggested by other authors (Coutts and Grace, 1995; Spatz and Bruechert, 2000; Peltola et al., 1999; James, 2003). A combination of factors such as the wind speed profile and the canopy implementation induce unknown magnitudes of error.

Papesch et al. (1997) reported statistical regressions (reproduced in Equations 3.21 and 3.22) in order to predict the maximum bending moment and the angle of deflection at the maximum applied bending moment. Assuming the deflection when a stem first reaches its proportionality limit stress coincides with the angle of deflection at the maximum bending moment, by calculating the expected deflection at the maximum bending moment and comparing with the results the model produces gives insight into the general accuracy of the model. The force imposed by the canopy can also be converted into a bending moment at the first wind speed which breaks proportionality and compared to Equation 3.21's prediction for further insight.

$$ln(M_c) = 2.5578 ln(h) - 3.18 \tag{3.21}$$

$$D_{M_c} = -0.5416h + 21.099 \tag{3.22}$$

Where M_c is the maximum bending moment, h is the height and D is deflection.

3.2.6 Growth stresses

Growth stresses are represented in a simplified fashion. Gillis and Hsu (1979) provide Equation 3.25 to describe growth stress profiles. The growth stress profile presented in Equations 3.23 to 3.25 are imposed on the stem at each growth step, and the new growth added to the pre-stressed stem as described in Section 3.2.1. Growth stresses are imposed by adding the growth stress vector directly onto the stress vector during its calculation (in a similar way to how temperature dependent stresses are often represented) the growth stress vector, $\boldsymbol{\sigma_{gs}}$ is presented in Equation 3.26. It should be noted that the growth stresses are only added into the longitudinal direction, it is assumed that the resulting deformation through the interaction of the stiffness matrix will result in an appropriate stress profile in the other material directions. At the periphery of the stem in a 15 year old tree the tensile growth stresses calculated here ranges from 0.8 to 2 MPa depending on the outerwood used, this is similar to the values reported by Timell (1986b) for *Pinus taeda* of 1.2 MPa in tension at the periphery, however they also report similar values for compression at the centre of the stem, which is somewhat lower than the assumption used here.

r_{core} is the radius which the growth stress model assumes the stress strain relationship is flat at the limit of proportionality under compression. Y_l is the yield limit set to 0.1 as presented by Gillis and Hsu (1979) and is the radial proportion of the stem at the compressive proportionality limit. R is the maximum radius of the stem for the height of the point being evaluated. When the point being evaluated is the apex, R is set to 0, as the apical growth from the current time step is assumed not to have gone through the maturation process.

$$r_{core} = Y_l R \tag{3.23}$$

$$IT_{stress} = \frac{Y_{cs}}{\frac{R}{r_{core}}(1 - \frac{r_{core}}{R})} \tag{3.24}$$

IT_{stress} is the initial longitudinal tensile stress and Y_{cs} is the compressive stress at the

limit of proportionality calculated as per Section 3.2.2.

$$G_s = \begin{cases} 0, & \text{if } r_{core} = 0 \\ -IT_{stress}\frac{R}{r_{core}}(1 - \frac{r_{core}}{R}), & \text{else if } r \leq r_{core} \\ -IT_{stress}\frac{R}{r_{core}}\frac{(\frac{r_{core}}{r} - 2\frac{r_{core}}{R} + \frac{r_{core}^2}{R^2})}{1-\frac{r_{core}}{R}}, & \text{otherwise} \end{cases} \tag{3.25}$$

$$\boldsymbol{\sigma_{gs}} = \begin{bmatrix} 0 \\ 0 \\ G_s \\ 0 \\ 0 \\ 0 \end{bmatrix} \tag{3.26}$$

The original authors of this growth stress model Gillis and Hsu (1979) presented a graphic to show the growth stress profile. The figure is reproduced in Figure 3.4.

3.2.7 Elasticity

Hooks law can be used to characterise elastic relationships in mathematical terms. Generalised Hook's law (Equation 3.28) is used here to describe the mechanical elastic characteristics of wood. Because the characterisation of the proportionality limit is the point at which the stress strain curve is no longer linear, stress is only proportional to the strain and not the strain rate. Above this point non-linear elastic and plastic effects need to be considered, which was beyond the scope of this study.

Stress, $\boldsymbol{\sigma}$, is calculated from strain $\boldsymbol{\epsilon}$ and the stiffness matrix $\boldsymbol{C}$. When growth stresses were not considered Equation 3.28 was used, when growth stresses were considered $\boldsymbol{\sigma_{gs}}$ was defined by Equation 3.26 and $\boldsymbol{\sigma}$ was calculated through Equation 3.29.

$$\boldsymbol{\epsilon} = \frac{1}{2}(\bigtriangledown \boldsymbol{u} + \bigtriangledown \boldsymbol{u}^T) \tag{3.27}$$

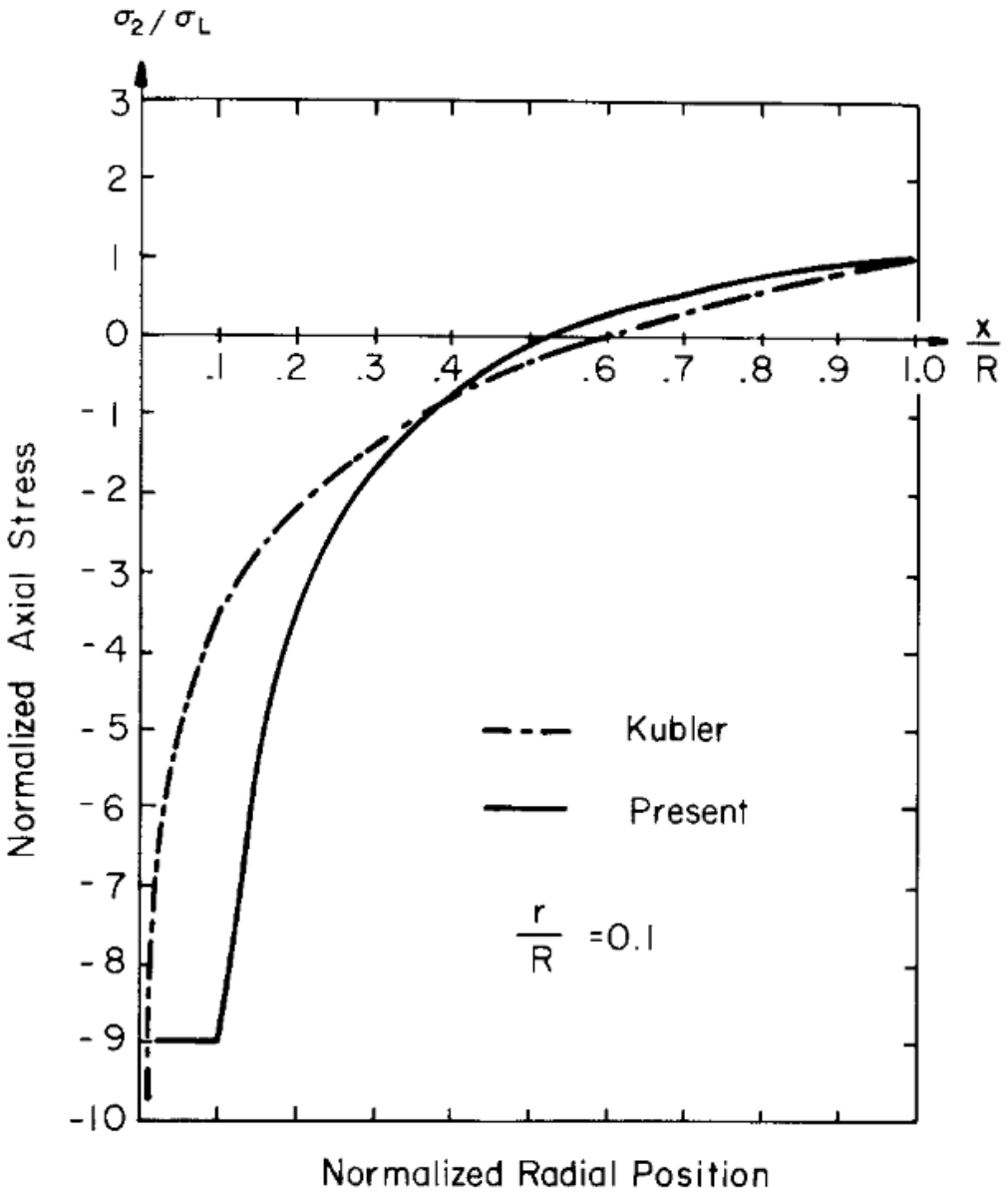

Figure 3.4: Plot showing the longitudinal growth stress profile used. Image is reproduced from Gillis and Hsu (1979).

$$\boldsymbol{\sigma} = \boldsymbol{C\epsilon} \tag{3.28}$$

$$\boldsymbol{\sigma} = \boldsymbol{C\epsilon} + \boldsymbol{\sigma_{gs}} \tag{3.29}$$

Strain energy density can then be calculated

$$W = \frac{1}{2}\boldsymbol{\sigma\epsilon} \tag{3.30}$$

and the total potential energy found

$$\prod = \int_{\boldsymbol{\Omega}} W \, d\boldsymbol{\Omega} - \int_{\boldsymbol{\Omega}} \boldsymbol{B_s}.\boldsymbol{u} \, d\boldsymbol{\Omega} - \int_{\boldsymbol{\Omega_1}} \boldsymbol{B_c}.\boldsymbol{u} \, d\boldsymbol{\Omega_1} - \int_{\boldsymbol{\Gamma_1}} \boldsymbol{T_s}.\boldsymbol{u} \, d\boldsymbol{\Gamma_1} \tag{3.31}$$

$$\boldsymbol{\Omega_1} = \{(x, y, z) \in \boldsymbol{\Omega} : z > S_c\}$$

$$\boldsymbol{\Gamma_1} = \{(x, y, z) \in \boldsymbol{\Gamma} : x > 0, z > S_c\}$$

By taking the directional derivative of $\prod$ with respect to the change in u and setting it to zero the displacement field u can be calculated at the minimum potential energy.

$$F = \bigtriangledown_{\boldsymbol{u}} \prod(\boldsymbol{u}) = 0 \tag{3.32}$$

Subject to the Dirichlet boundary conditions, Equations 3.33 and 3.34.

$$\boldsymbol{u}|_{\boldsymbol{\Omega_{bc1}}} = \begin{bmatrix} u_x \\ u_y \\ 0 \end{bmatrix} \tag{3.33}$$

$$\boldsymbol{\Omega_{bc1}} = \{(x, y, z) \in \boldsymbol{\Omega} : z > tol_z\}$$

and

$$\boldsymbol{u}|_{\boldsymbol{\Omega_{bc2}}} = \begin{bmatrix} 0 \\ 0 \\ 0 \end{bmatrix} \tag{3.34}$$

$$\boldsymbol{\Omega_{bc2}} = \{(x, y, z) \in \boldsymbol{\Omega_{bc1}} : (x, y) < tol, (x, y) > -tol\}$$

Where tol_z is the tolerance required to select all points at the boundary between the base of the stem and the ground, and where tol is the tolerance sufficient to select only

the points at the boundary between the base of the stem and the ground for the initial seedlings' radius.
By solving Equation 3.32 for displacement $\boldsymbol{u}$ subject to the boundary conditions (Equations 3.33 and 3.34) and internal and external loadings (Equations 3.11, 3.14, 3.19 and 3.25) the displacement field was obtained. Hook's law (Equation 3.28) was used to find the stresses. Solving of the system is achieved through the FEM as disused in Section 3.2.8.

3.2.8 Finite element analysis

The finite element method is a common mathematical tool used in many fields of engineering. It is a mathematical process which can be used to approximate the solutions of partial differential equations. The technique involves creating a mesh to represent a physical problem, partial differential equations are solved at nodes of the mesh. For a full introduction to FEM see any number of FEM textbooks (e.g. Rao (1999) or Liu (2010)).

Equation 3.32 is solved for displacement (u) at the minimum potential energy using the FEM. Quadratic interpolation models were used over tetrahedral (10 node 3 dimensional) Lagrange elements. Two boundary conditions were used, the first (Equation 3.33) to set all points at the interface with the ground (i.e. all points with a global z coordinate at zero before deformation) to have zero displacement in the vertical (z) direction. This boundary condition is needed in order to ensure that when wind loads were applied the stem does not rotate and growth stresses do not cause the stem to contract at the edges and extend in the centre. The other boundary condition (Equation 3.34) is to stop horizontal movement, by stopping the original seedling base from moving, this boundary condition is needed in order to make sure the tree does not simply slide when the wind load is applied. In nature trees are able to deform the soil around them up to a few centimetres in order to reduce some of the stress. The boundary conditions used here do not allow for soil deformation, in further work the root structure and soil could be included in order to investigate this effect.

3.2.9 Linear and quadratic elements

Both linear and quadratic tetrahedral elements were tested in this analysis. Each element has with it associated trade offs, in particular linear regimes assume a linear displacement function within the element, while on the other hand quadratic elements allow for a quadratic displacement field. Quadratic tetrahedral elements are prone to volume locking, so in this work reduced integration was used to avoid this phenomenon. The main trade off using quadratic elements is that the size of the global matrix equations rapidly become unsolvable within current personal computer hardware limitations. Linear tetrahedral elements are not prone to volume locking and because of the lower number of nodes per element, greater resolution can be used providing more detail about the problem. Because of the computational limitations linear elements were used with a resolution of one per year, while quadratic elements were reduced to one every three years (at age 15), this is partially compensated for by the increased flexibility of the local functions within quadratic elements. Higher resolution linear systems were numerically unstable for larger deformations and consequently not used for wind induced bending.

3.2.10 Breakage criteria

Failure surfaces were created using Tsai and Wu's failure criterion (Tsai and Wu, 1971) and calculated for every point in the stem for all wind speeds. Each point is evaluated for its safety factor, where a factor of one is on the failure surface, with a lower than one factor being before the limit of proportionality and higher than one factor after the limit. The values are the observed stress over the proportional limit stress given the other five stress states. Due to the dependence of each direction of failure on the other directions, as demonstrated in Chapter 2, for this calculation all but the variable in question are held constant at their modelled values. Once passed the proportional limit the linear stress strain curves were still assumed, this is not physically accurate. The proportional limit stresses were calculated from the linear interpolation described in Section 3.2.2.

From the experimental work in Chapter 2 and the relationships presented in Section

3.2.2 proportional limit surfaces for each point were calculated using Tsai and Wu's criterion. Because the proportional limit surfaces are defined in the local rtl coordinate system and the stresses provided by the model are in the global xyz system Equation 3.8 was used to convert each stress vector into the local system at its given global location. The failure criterion was applied through Equation 3.35 and the maximum and minimum stress values which could be obtained without failure calculated for each point assuming all other stresses stay fixed (Equations 3.37 and 3.36). With the maximum tensile and compressive stresses a safety factor was calculated as per Equations 3.38 and 3.39. The stress bounds can be used to investigate how much redundant strength is available at failure by both position in the stem and direction of stress. Note, no interaction terms are considered in the $\boldsymbol{P}$ matrix. For more details see Chapter 2.

$$\boldsymbol{\sigma^T q} + \boldsymbol{\sigma^T P \sigma} - 1 = 0 \tag{3.35}$$

$$\boldsymbol{\sigma_{max}} = max(\sigma_i) \text{ subject to } \boldsymbol{\sigma^T q} + \boldsymbol{\sigma^T P \sigma} - 1 = 0 \tag{3.36}$$

$$\boldsymbol{\sigma_{min}} = min(\sigma_i) \text{ subject to } \boldsymbol{\sigma^T q} + \boldsymbol{\sigma^T P \sigma} - 1 = 0 \tag{3.37}$$

Where σ_i is a single entry in the stress vector $\boldsymbol{\sigma}$

$$SF_{ten} = |\frac{\boldsymbol{\sigma}}{\boldsymbol{\sigma_{max}}}| \tag{3.38}$$

$$SF_{comp} = |\frac{\boldsymbol{\sigma}}{\boldsymbol{\sigma_{min}}}| \tag{3.39}$$

3.2.11 Example of stress bounds

Throughout this analysis the Tsai and Wu (1971) failure criterion was used to determine failure of points within the stem. The reasons for using this criterion are discussed in Section 3.4.1. A failure in any direction is dependent on other loadings in the material. By use of the failure criterion as disused in Section 3.2.10 maximum and minimum bounds can be placed on the value of stress in a direction at a point subject to all of the other stresses acting at that point. Figure 3.5 shows these upper and lower bounds along with the curve of the observed stress for a single point (arbitrarily chosen to illustrate the concept). At a wind speed of between 23 and 24 m/s the observed

point breaks proportionality in tension along the radial and tangential directions and compression in the longitudinal direction. The bounds reducing in separation occurs because of the other stresses on the point. As the other stress values increase, the value which any direction can vary by reduces, because of the coupling of material directions.

At wind speeds of 23 m/s or more depending on the direction, the two bounds cross, indicating no mater what value the stress takes it will still exceed the proportionality limit. In order to be able to compare how close different points are to failure, safety factors were calculated as per Equations 3.36 and 3.37. These values compare the current stress value with the maximum or minimum potential value which could be achieved before reaching the proportionality limit given the other five stresses.

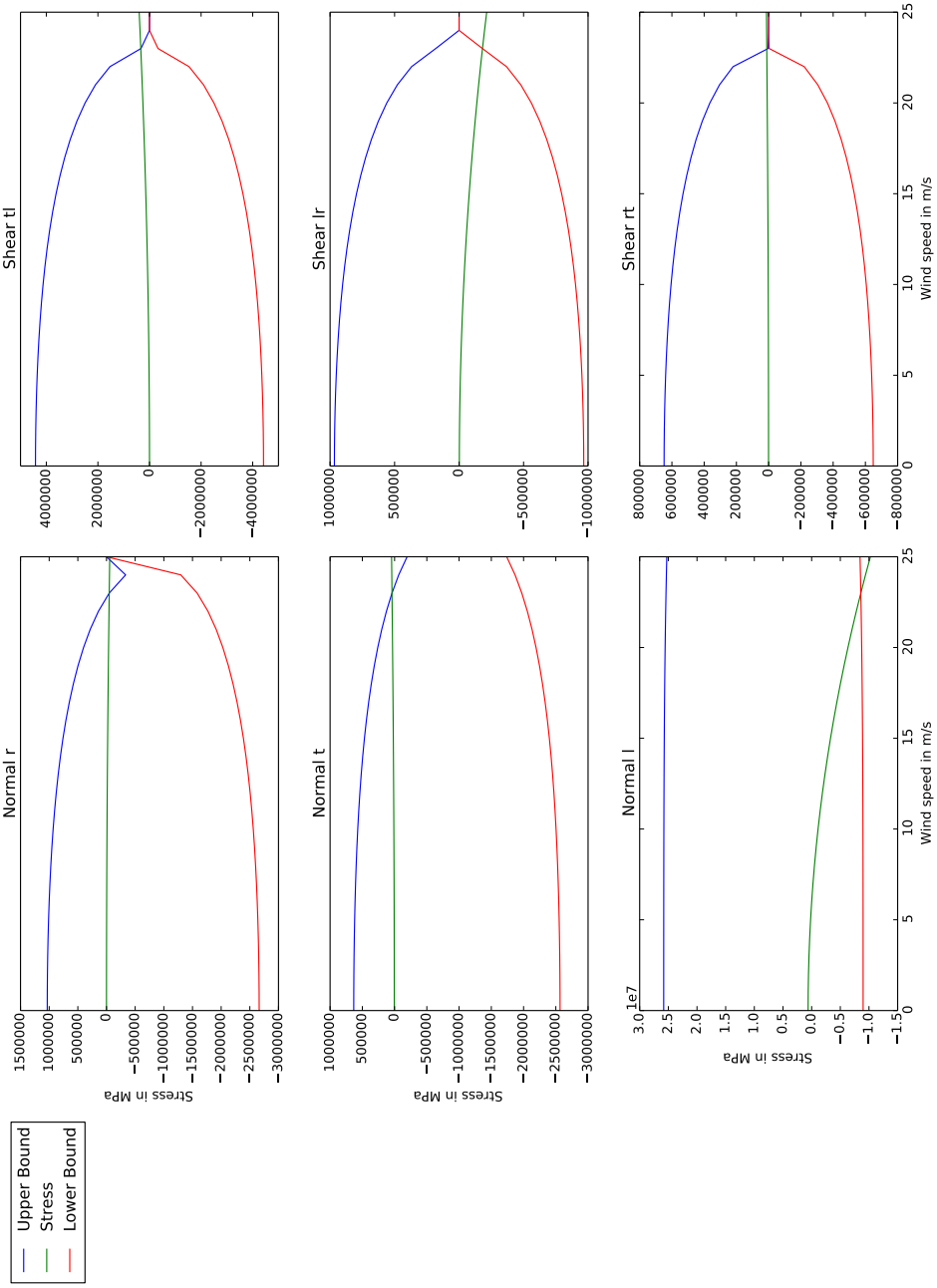

Figure 3.5: The failure criterion seen used here is from Tsai and Wu (Tsai and Wu, 1971). The green line is the observed stress for a single point. Upper and lower bounds on stress define the limit of proportionality in either direction. These bounds are calculated as per Equations 3.35, 3.36 and 3.37. As the wind speed increases and the other material directions become stressed the window between the bounds with which the stress can occupy and not break proportionality becomes smaller because of the coupling between material directions. This point breaks proportionality between 23 and 24 m/s.

Table 3.1: Stem and crown dimensions for open grown trees. Calculated from Equations 3.1, 3.9 and 3.10.

Height (m)	Stem radius (m)	Crown start height (as proportion of stem height)	Crown radius (m)
5	0.051	0.10	1.1
10	0.10	0.10	2.2
15	0.15	0.10	3.2

3.2.12 Fenics Numpy and Python

Python, version 2.7 (`http://www.python.org`) was used for all of the computation within this project. Numpy 1.8.0 (Ascher et al., 1999) and scipy 0.13.3 (Jones et al., 2001) were used extensively. Fenics version 1.2 (Anders Logg and Wells, 2011) is an open source general PDE solver which focuses on the FEM. Fenics was used to solve the potential energy minimization presented in Equations 3.31 and 3.32.

3.3 Results

Two stem and crown profiles were investigated. An open grown stem, assumed to have no light competition, at a stocking rate of one stem per hectare and a stem under competition at a stocking rate of 741 stems per hectare. The dimensions of the open grown stem and crown for different ages are available in Table 3.1. Stems grown in the open tend to produce a lower taper and a wider crown which protrudes further to the base of the stem. The open grown stem and crown dimensions are extrapolated from measurements reported by Waghorn et al. (2007a). Table 3.2 presents the stem and crown dimensions used under considerable light competition. These dimensions represent architecture for a stem grown at a stocking rate of 741 stems per hectare. The stocking rate of 741 stems per hectare was chosen as it is the stocking rate used to estimate crown density and it falls within the bounds of the data from Waghorn et al. (2007a).

Table 3.2: Stem and crown dimensions for trees stocked at 741 stems per hectare. Calculated from Equations 3.1, 3.9 and 3.10.

Height (m)	Stem radius (m)	Crown start height (as proportion of stem height)	Crown radius (m)
5	0.051	0.10	1.1
10	0.081	0.38	2.1
15	0.12	0.38	2.1

3.3.1 Initial check with reported values

In order to ensure that the values being presented were realistic Equations 3.22 and 3.21 from Papesch et al. (1997) were solved with $h = 15$ resulting in a maximum bending moment of 42 MPa at a deflection of 13 degrees. Solving the equations presented in Section 3.2.5 with wind speed ω as the unknown, the wind speed at maximum bending moment (42 MPa) was calculated to be 15.5 m/s. From these equations and the assumption that the maximum bending moment will occur at the lowest wind speed needed to surpass the proportional limit it is seen that at a stocking rate of 741 stems per hectare the FEM model predicts the stem with the radial profile $LW \rightarrow HS$ will fail at approximately 16 m/s, however the deflection angle is approximately 21 degrees at this point. The radial profiles at a stocking rate of 741 stems per hectare fall on either side of the 13 degree deflection at 15.5 m/s wind speed from Papesch et al. (1997). Open grown stems withstand higher wind speeds, however they break at lower deflection angles than stems at a stocking of 741. Open grown stems also fail at higher and lower wind speeds and deflections than the predictions from Papesch et al. (1997), with the radial profiles performing in a similar order as for the higher stocking rate. If growth stresses are not considered a reduction in the wind speeds to below the predicted value of 15.5 m/s is observed, for both stocking rates. The deflection angle at first failure is also reduced with radial profile $LW \rightarrow HS$ to approximately 14 degrees (from 21 degrees). Radial profiles fall on either side of the prediction of 13 degrees from Papesch et al. (1997).

3.3.2 Where failure occurs

The stress profiles within the stems are fairly consistent regardless of the TRP used. All profiles show compression in the longitudinal direction and slight stresses in the other directions, when growth stresses are not considered. As the wind load increases tension stresses start to become visible in the longitudinal direction on the windward side of the stem, along with compressive stresses on the leeward side. The largest of these appearing in the bottom third of the stem, with little appearing at the top. The longitudinal-tangential and longitudinal-radial shear planes also develop significant stresses, with the maximum magnitude usually occurring at similar heights in the stem as longitudinal stresses, as can be seen in Figure 3.6.

Stress distributions within the stem don't indicate points of failure because of the relationship between material directions, the change in strength with material direction and the change in strength of the material as the TRP evolves. To visualise when and where failure occurs Equations 3.39 and 3.38 were solved at each point in order to give a safety factor, with a value of less than one being before the point of failure and greater than one being after failure. Figure 3.7 indicates that once a point breaks proportionality in one direction the same is likely to occur in other directions soon after. Typically failure occurs on the leeward side of the stem in the bottom half in multiple directions at a similar time. A horizontal slice is also taken through the stem at a height of 3 m. The longitudinal stresses again dominate, being in compression from self weight at zero wind, as the wind increases the progression of tensile stresses from the windward side is visible moving from the outer edge of the stem toward the centre. The increase in compression at the leeward side of the stem is also visible following the same trend. Shear and normal stresses both increase with increasing wind speed, and the propagation can be seen in Figure 3.8. Failure is also evident in the cross section shown in Figure 3.9. Note the longitudinal-tangential and longitudinal-radial shear planes show slightly lower stresses in the centre of the stem than at the periphery the reason for this is unknown. These patterns vary but are typical for all TRPs, ages and stocking rates investigated.

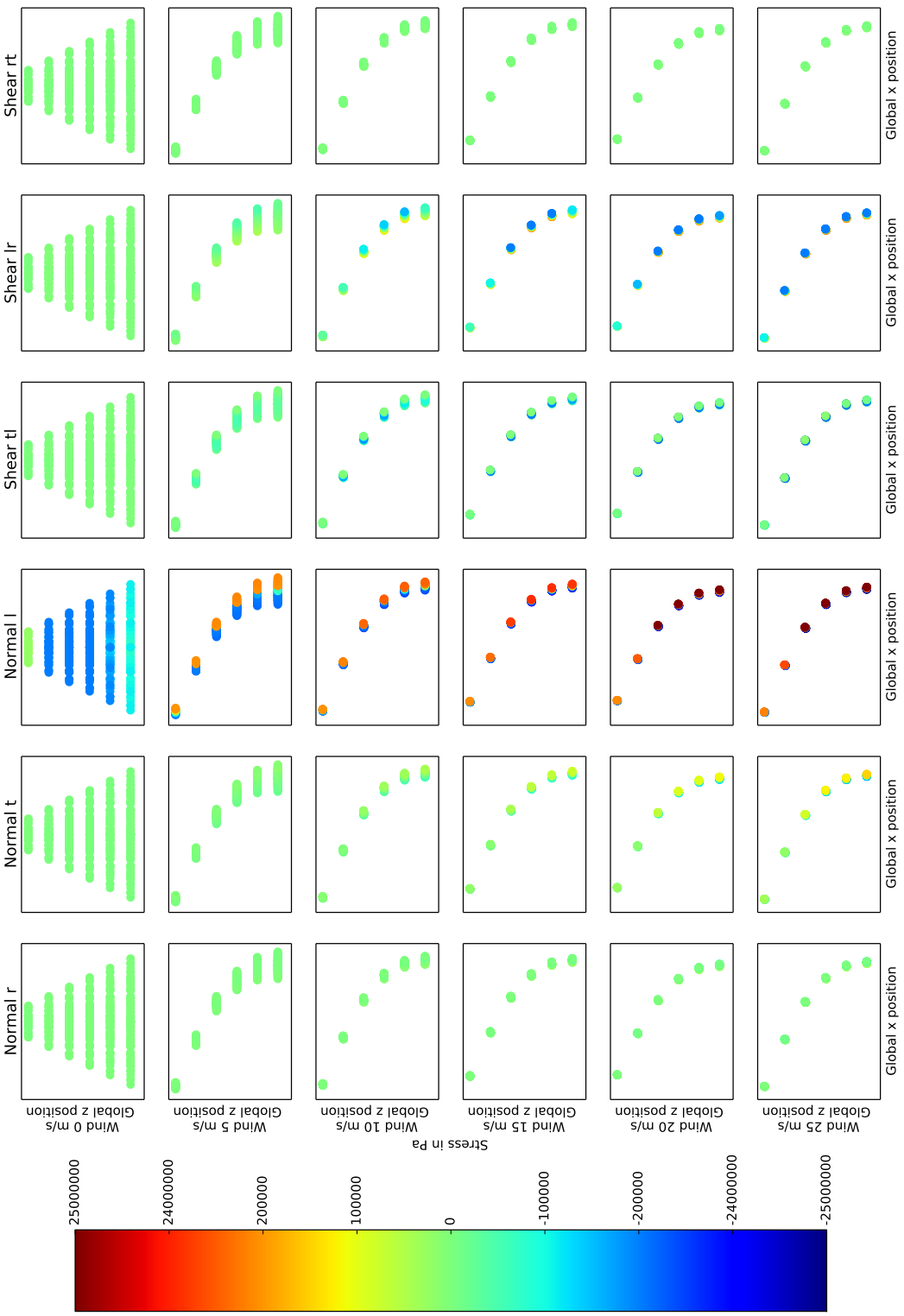

Figure 3.6: Stress profile of the stem for increasing wind loads to show stress distribution in the longitudinal direction. Taken from the TRP $LW \rightarrow HS$ at age 15. The plot shows the surface of the stem, some inner points are visible due to the geometry. Note that the x axis uses a variable scale.

Figure 3.7: Safety factor profile of the stem for increasing wind loads to show failure distribution in the longitudinal direction. Taken from the TRP $LW{\rightarrow}HS$ at age 15. The plot shows the surface of the stem, some inner points are visible due to the geometry. Note that the x axis uses a variable scale.

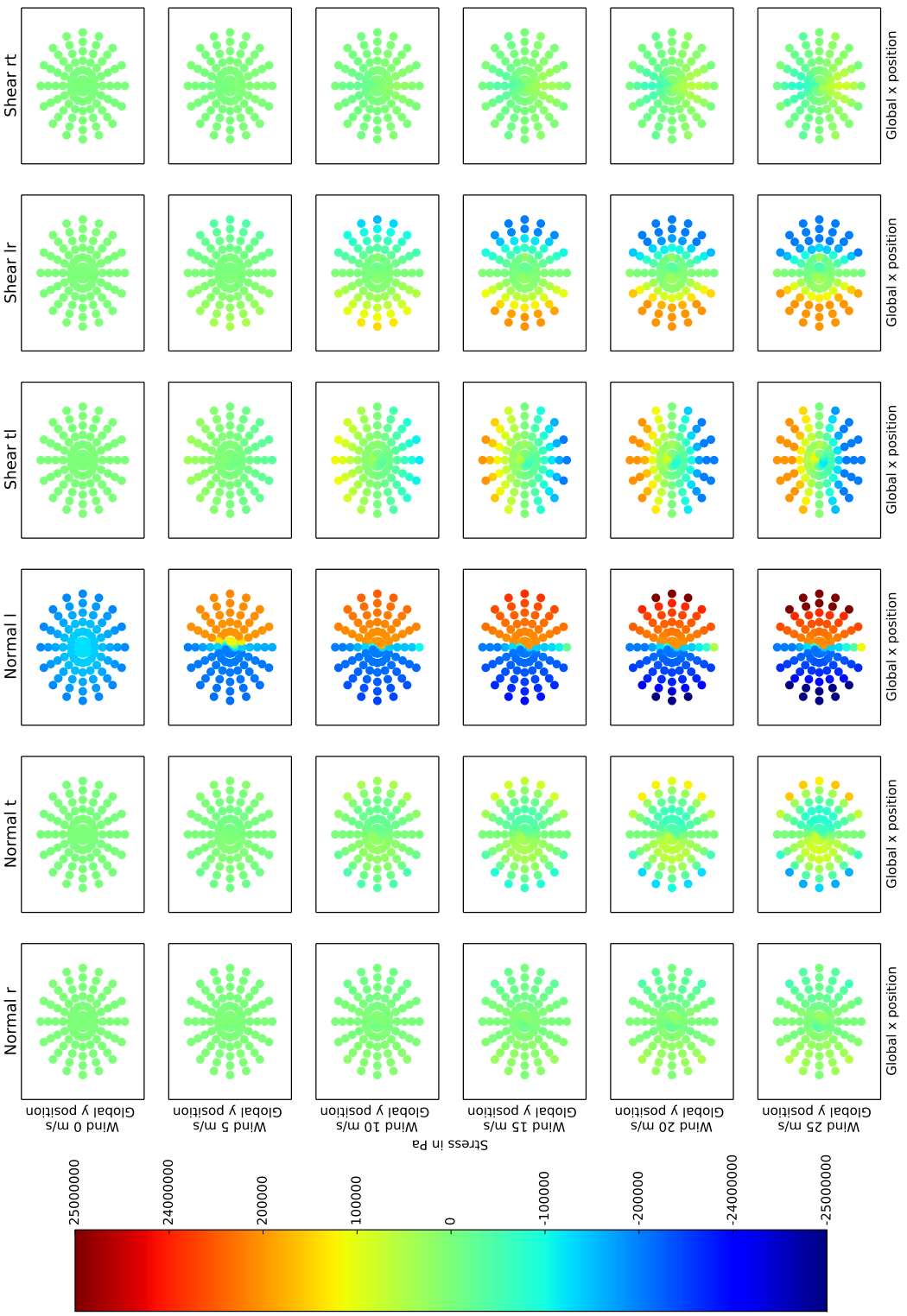

Figure 3.8: Stress profile of the stem for increasing wind loads to show stress distribution in the horizontal plane, taken at a height of 3 m. Taken from TRP $LW \rightarrow HS$.

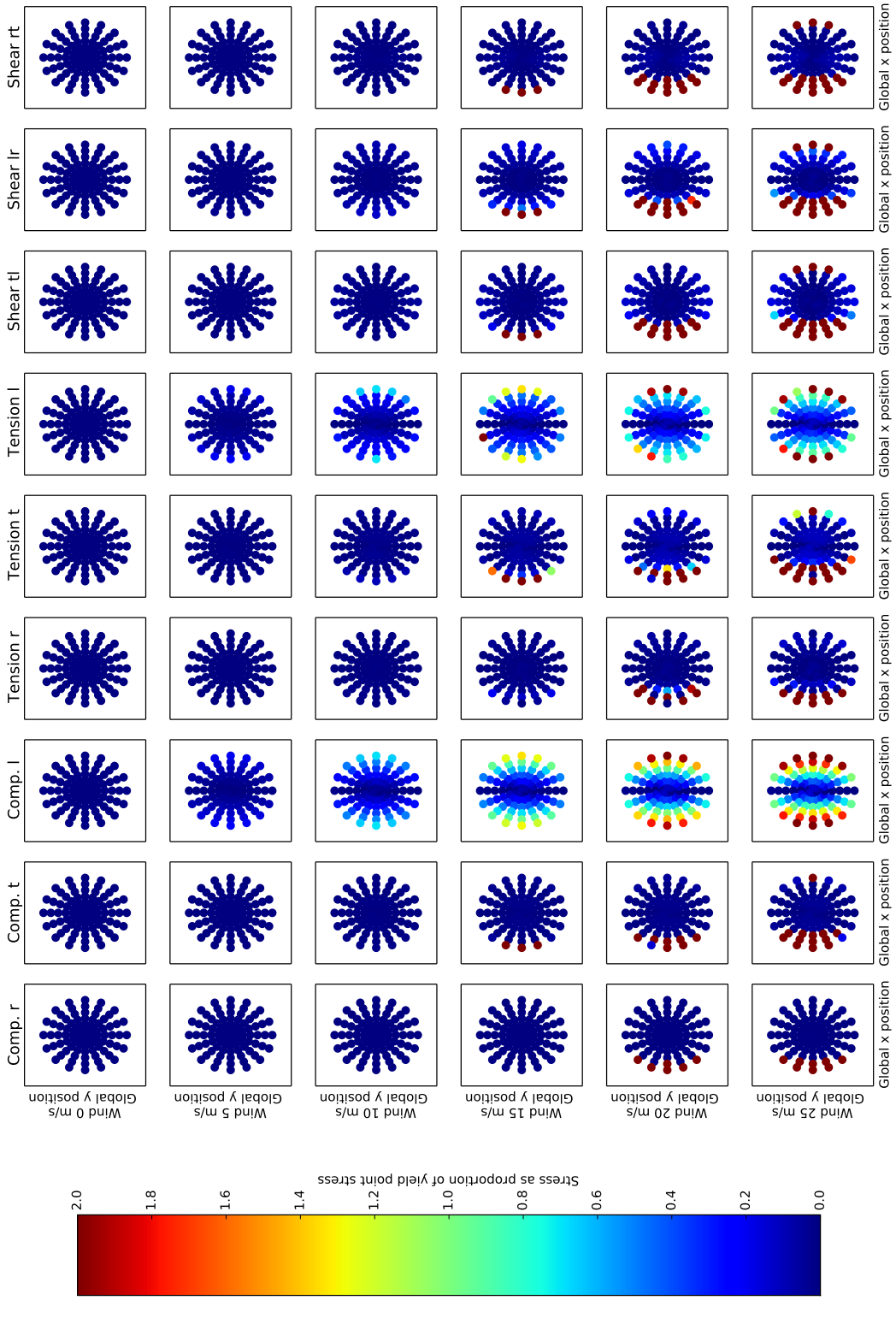

Figure 3.9: Safety factor profile of the stem for increasing wind loads to show failure distribution in the horizontal plane, taken at a height of 3 m. Taken from TRP $LW \rightarrow HS$ at age 15.

3.3.3 Growth stresses

The growth stress implementation described in Section 3.2.6 provides similar surfaces strains to that reported for *Pinus taeda* (Timell, 1986b). However the assumptions around the implementation are untested and caution should be applied when interpreting these results. In particular the growth stress profile is added into the stress vector as a constant state, only implemented in longitudinal direction and not accumulative. Not accumulating the growth stresses through successive growth steps, instead reapplying them at each time step results in stems of all ages having the same growth stress profile (as magnitude only varies by wood properties). It may not be the case that young trees (eg 5 years old) have the same growth stresses as their 15 year old counterparts. The growth stress profile causes some points to break proportionality in the core of the stem, the structural affect is assumed to be negligible, instead the point at which the proportion of failed points starts to increase is taken as the start of structure breakdown. The progression of points passing the proportional limit can be seen in Figures 3.11 and 3.13. Note the tension at the periphery of the stem and compression in the centre caused by the growth stresses. Figures 3.10 and 3.12 show how the implementation of growth stresses effects the stress in the different material directions.

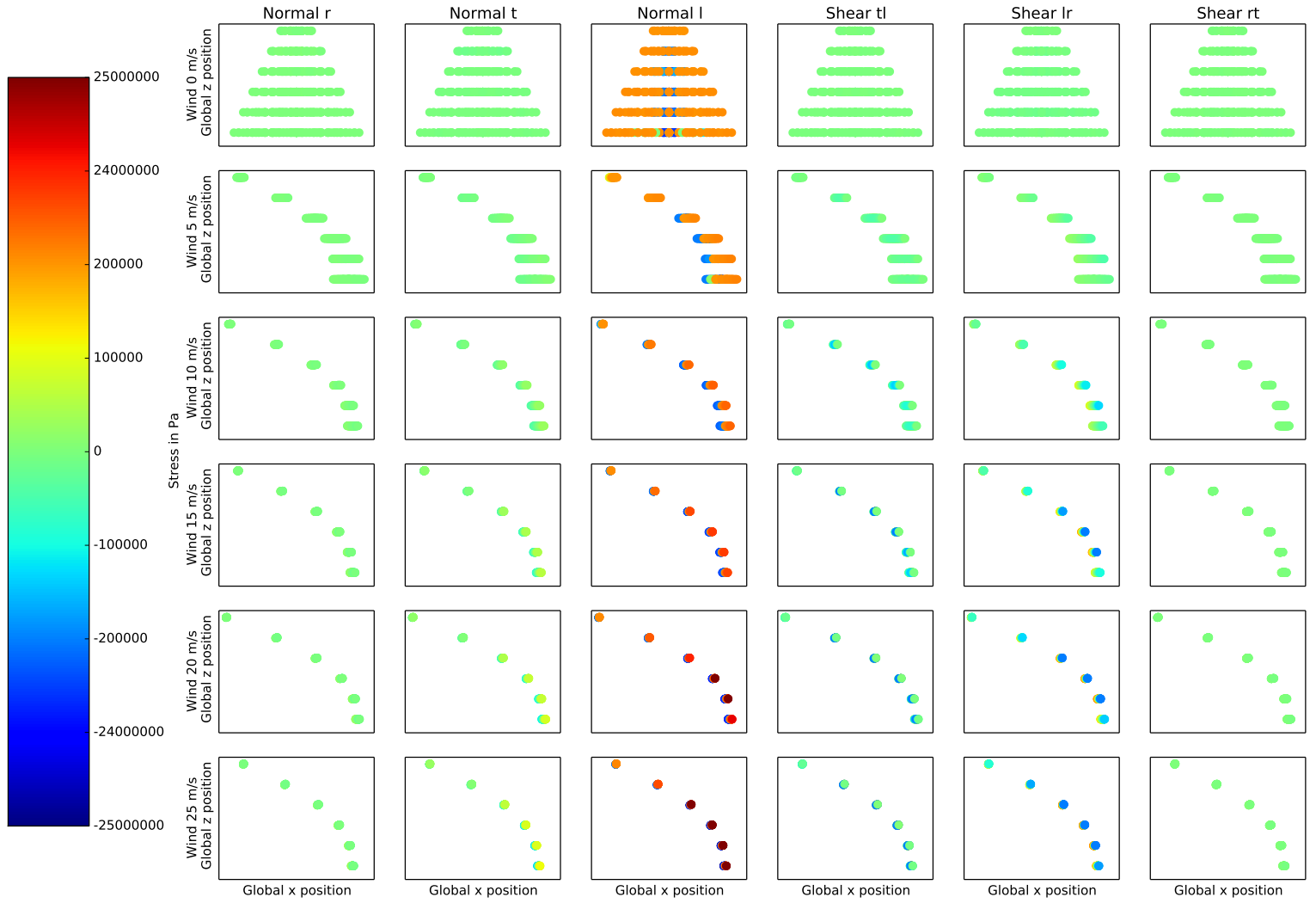

Figure 3.10: Stress profile of the stem for increasing wind loads to show stress distribution in the longitudinal direction. Taken from the TRP $LW \rightarrow HS$ at age 15 with growth stresses implemented. The plot shows the surface of the stem, some inner points are visible due to the geometry. Note that the x axis uses a variable scale.

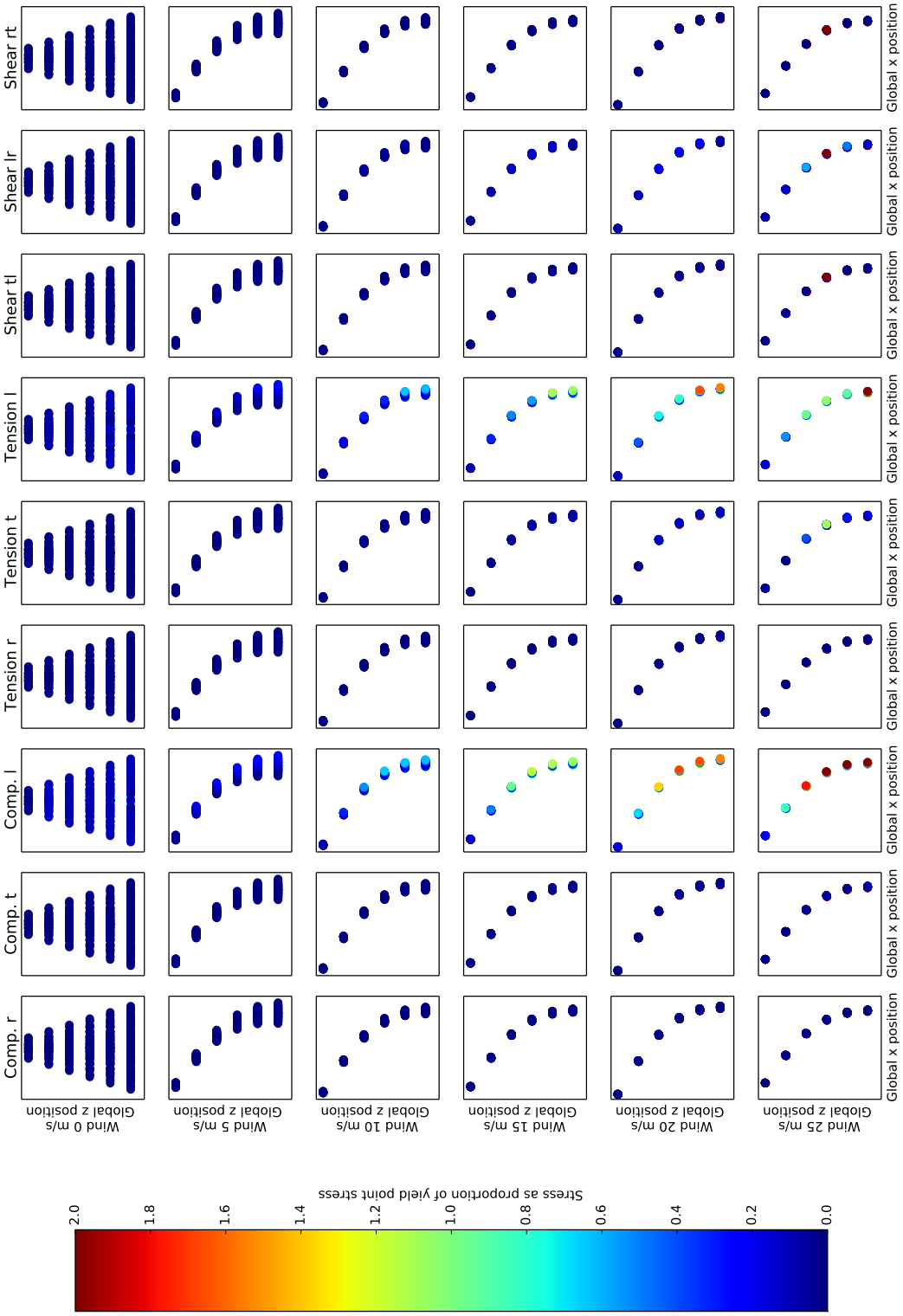

Figure 3.11: Safety factor profile of the stem for increasing wind loads to show failure distribution in the longitudinal direction. Taken from the TRP $LW{\rightarrow}HS$ at age 15 with growth stresses implemented. The plot shows the surface of the stem, some inner points are visible due to the geometry. Note that the x axis uses a variable scale.

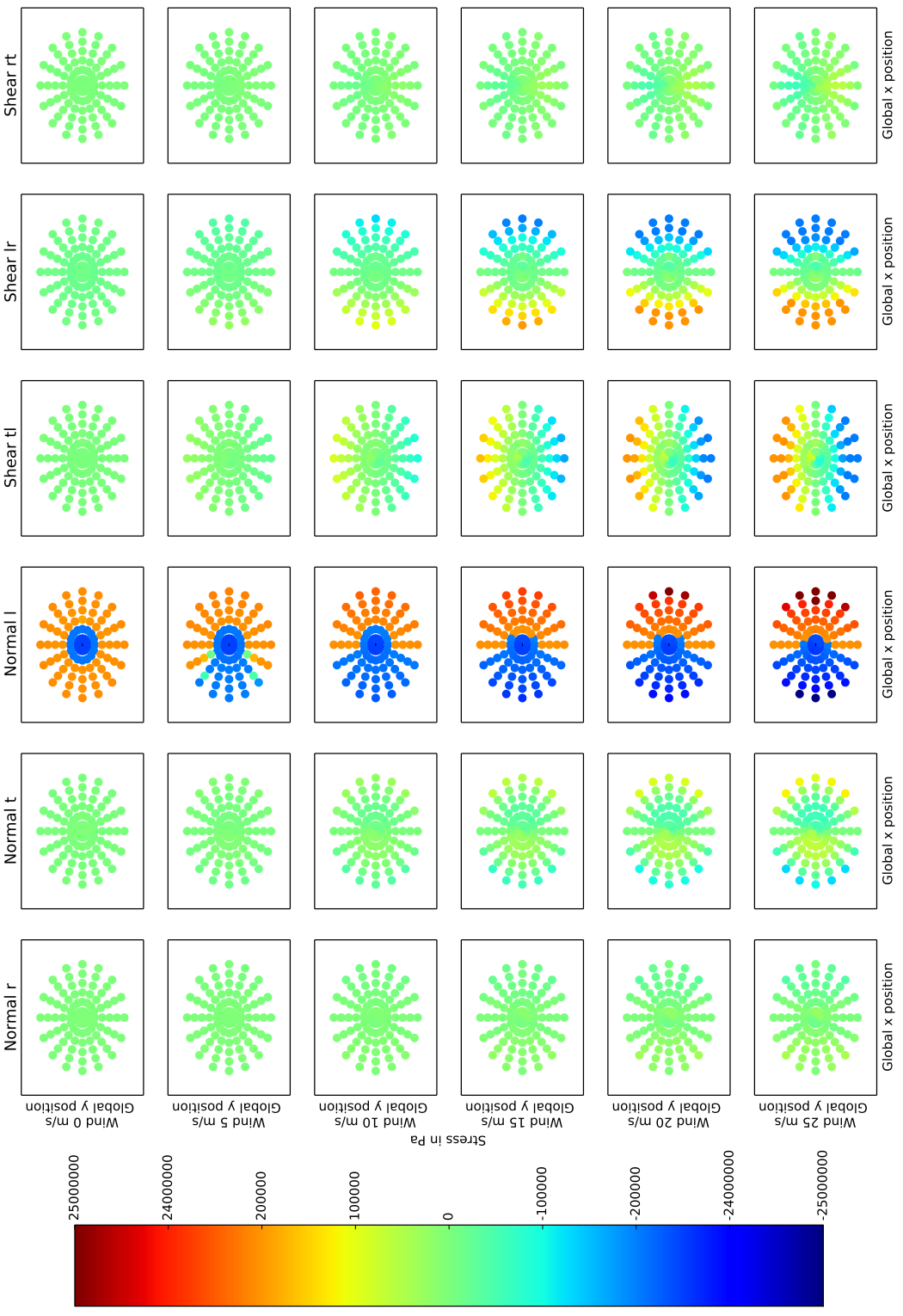

Figure 3.12: Stress profile of the stem for increasing wind loads to show stress distribution in the horizontal plane, taken at a height of 3 m. Taken from the TRP $LW \rightarrow HS$ at age 15 with growth stresses implemented.

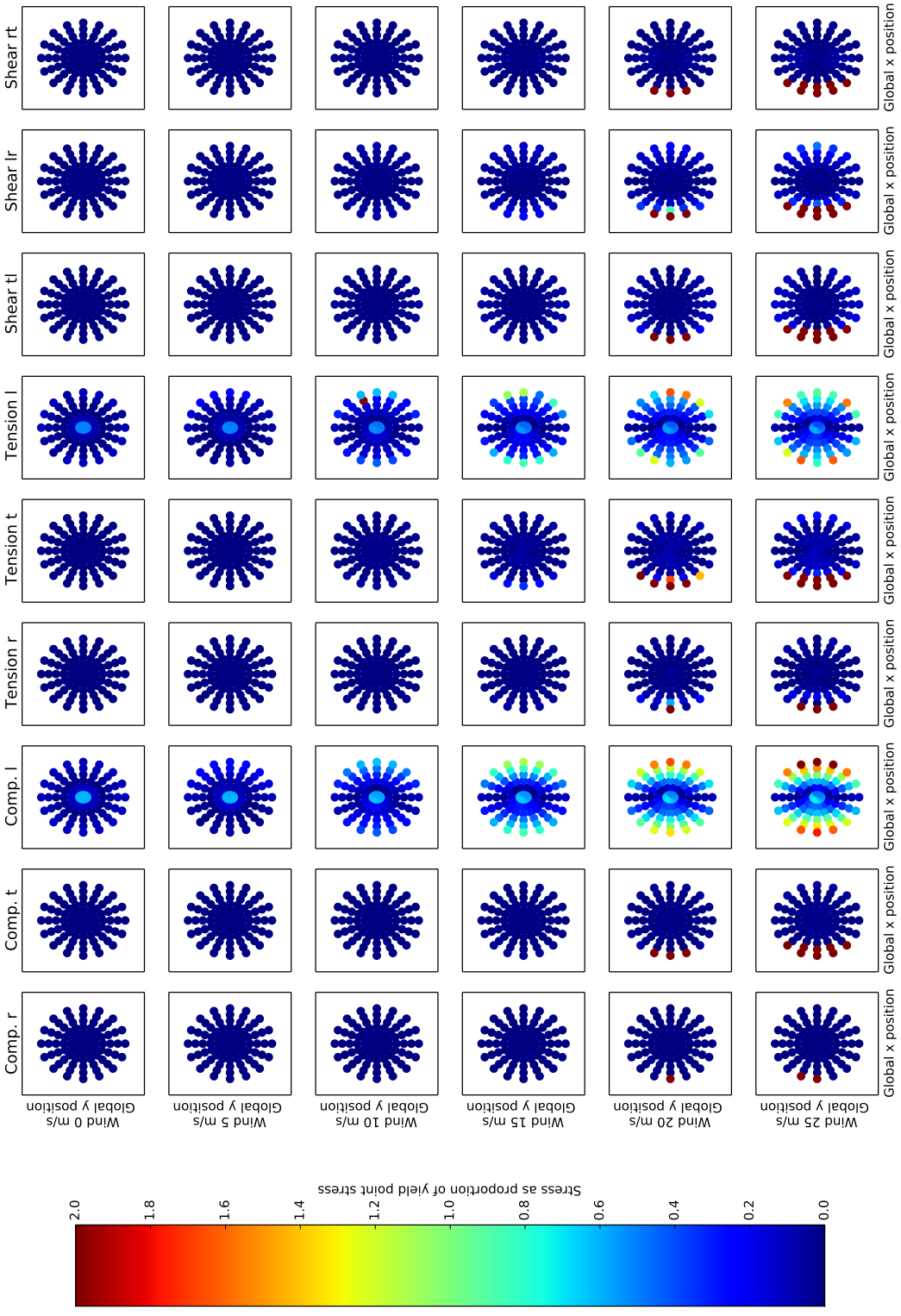

Figure 3.13: Safety factor profile of the stem for increasing wind loads to show failure distribution in the horizontal plane, taken at a height of 3 m. Taken from the TRP $LW \rightarrow HS$ at age 15 with growth stresses implemented.

Figure 3.14 is a plot of two samples, ($LW \rightarrow HS$ and $HW \rightarrow LS$), with and without growth stresses, at a wind speed of 20 m/s. The plot shows the failure criterion value for each point separated by their height. The two samples were chosen to show contrast between TRPs (plots of all the other TRPs are available in Appendix A.1). Although the samples LW and HS show the largest contrast in material properties, they both exhibit similar strength properties, HW and LS show lower strengths in most directions, as can be seen in Chapter 2. In general samples which more closely follow the natural TRP show a more constant variation in the number of failed points with height. The implementation of growth stresses appears to cause the differences between the TRPs to become more accentuated in this respect. TRPs which perform better tend to have more constant failure profiles in the lower half to two thirds of the stem, both with and without growth stresses.

The implementation of growth stresses clusters the average height of first failure when compared to stems without growth stresses, as can be seen in Figure 3.15. Potential reasons for this are discussed in Section 3.4.1. In stems with observed radial profiles, the wind speeds at which the first points break proportionality increase substantially more than stems with unnatural profiles when growth stresses are implemented. Younger stems gain the most strength from having growth stresses, although younger trees may produce lower growth stresses than larger older ones, which was not considered, all stems have the same growth stress profiles governed by the martial properties of the wood within the stem.

Including growth stresses causes a marked increase in tensile failure and decrease in compressive failure for the longitudinal direction. The effect is strongest for young trees, and is less pronounced at higher stockings in older stems, although still evident, and shown in Figures 3.16 and 3.17. Even with the increase in tensile failure, most stems still fail in longitudinal compression and/or various shear planes. In TRPs which perform best longitudinal tensile failure is nearly as common as compressive failure, by contrast in the poorer performing TRPs (with the exception of the low density high stiffness profile) there is a much larger gap. See Appendix B and C for a number of plots expressing this relationship.

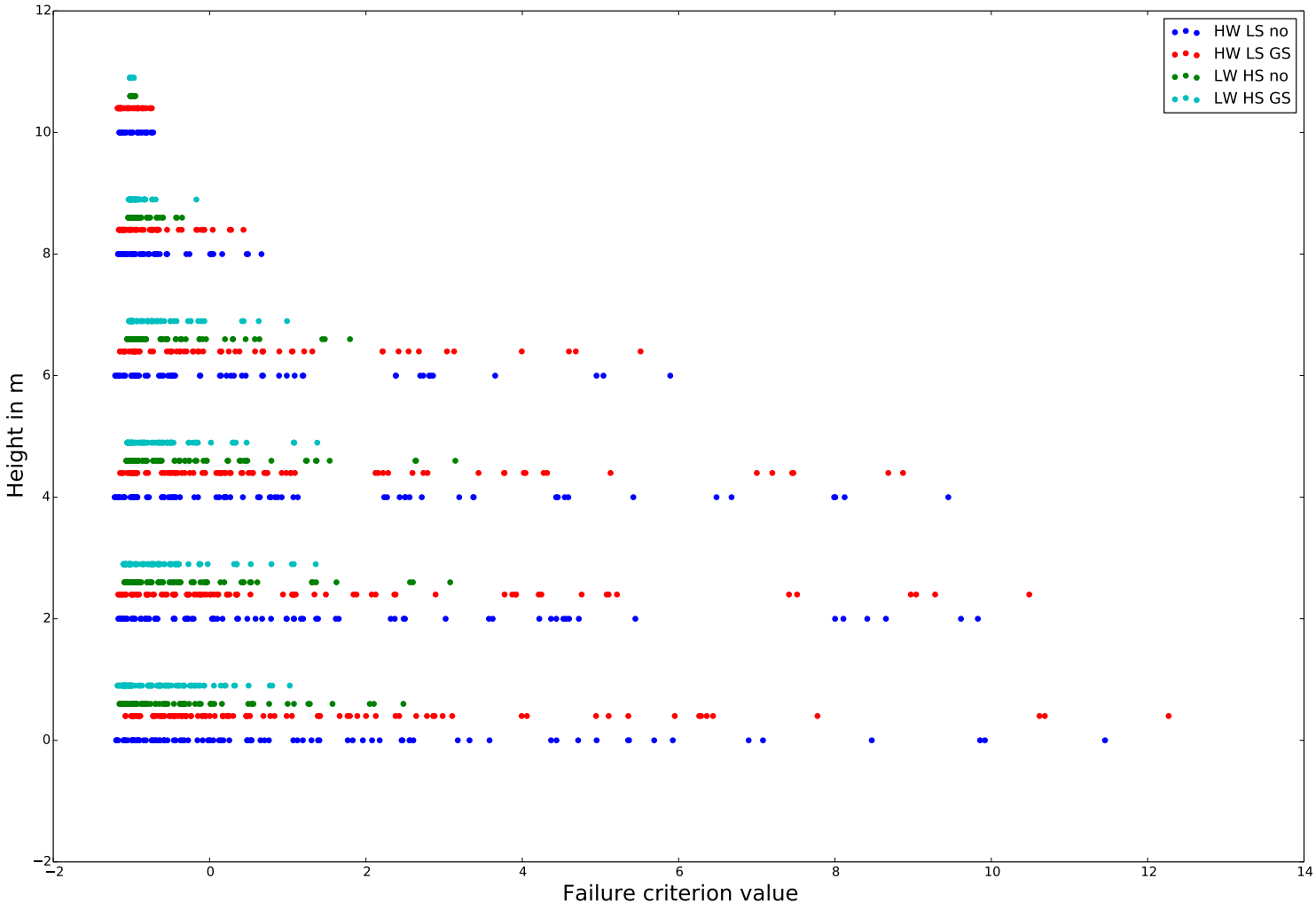

Figure 3.14: Comparison for both with and without growth stresses for contrasting TRPs, $LW \rightarrow HS$ and $HW \rightarrow LS$ at age 15 with a stocking of 741 stems per hectare and a wind speed of 20 m/s. Note the $LW \rightarrow HS$ profile has a much more constant state in the lower half of the stem. All TRPs are available in Appendix A.2

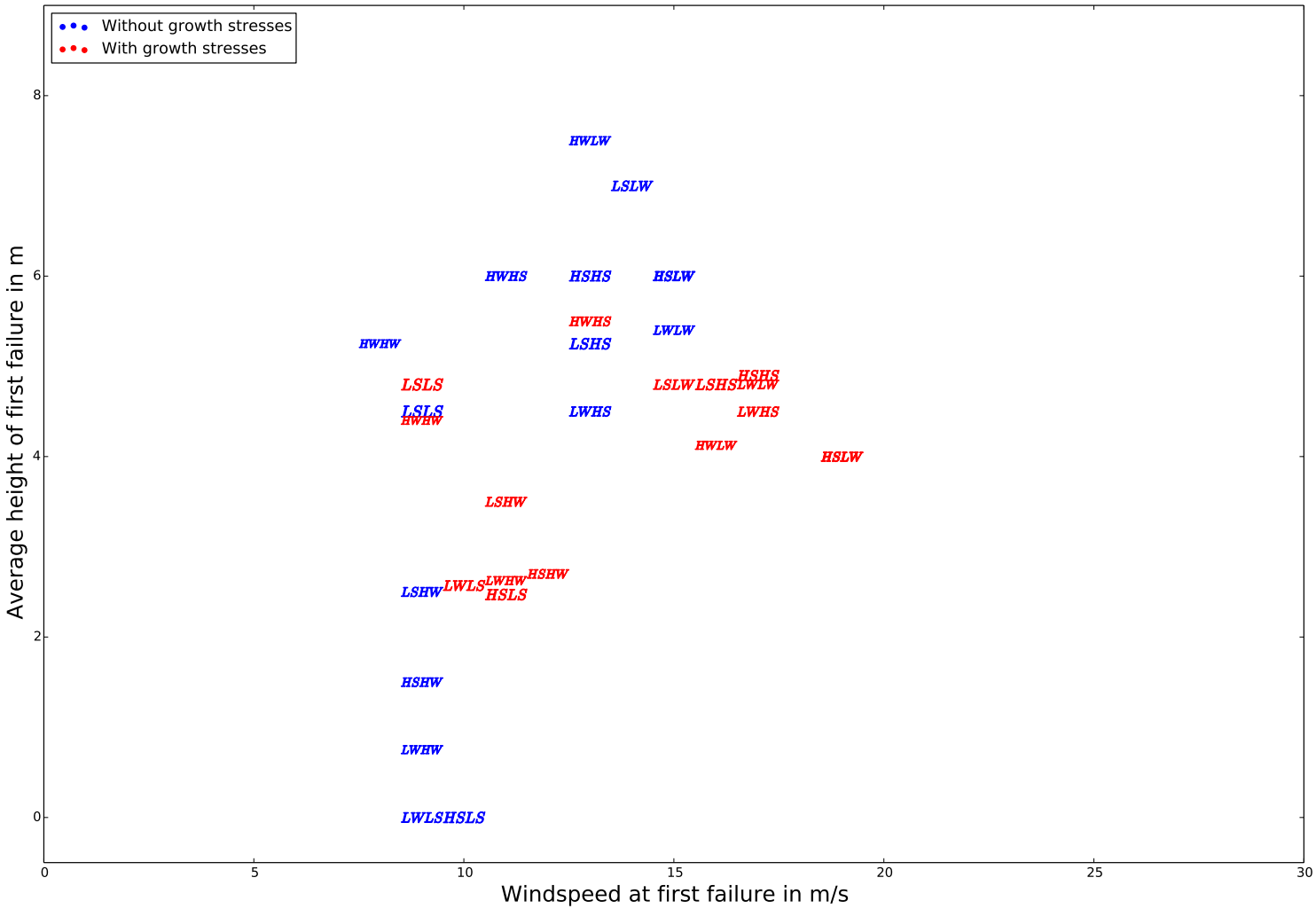

Figure 3.15: The height at the lowest wind speed at which failure occurs. In the cases where multiple failures occur at the first wind speed failure is observed the heights are averaged. Taken at a stocking of 741 stems per hectare and at age 15. Other ages are available in Appendix A.1

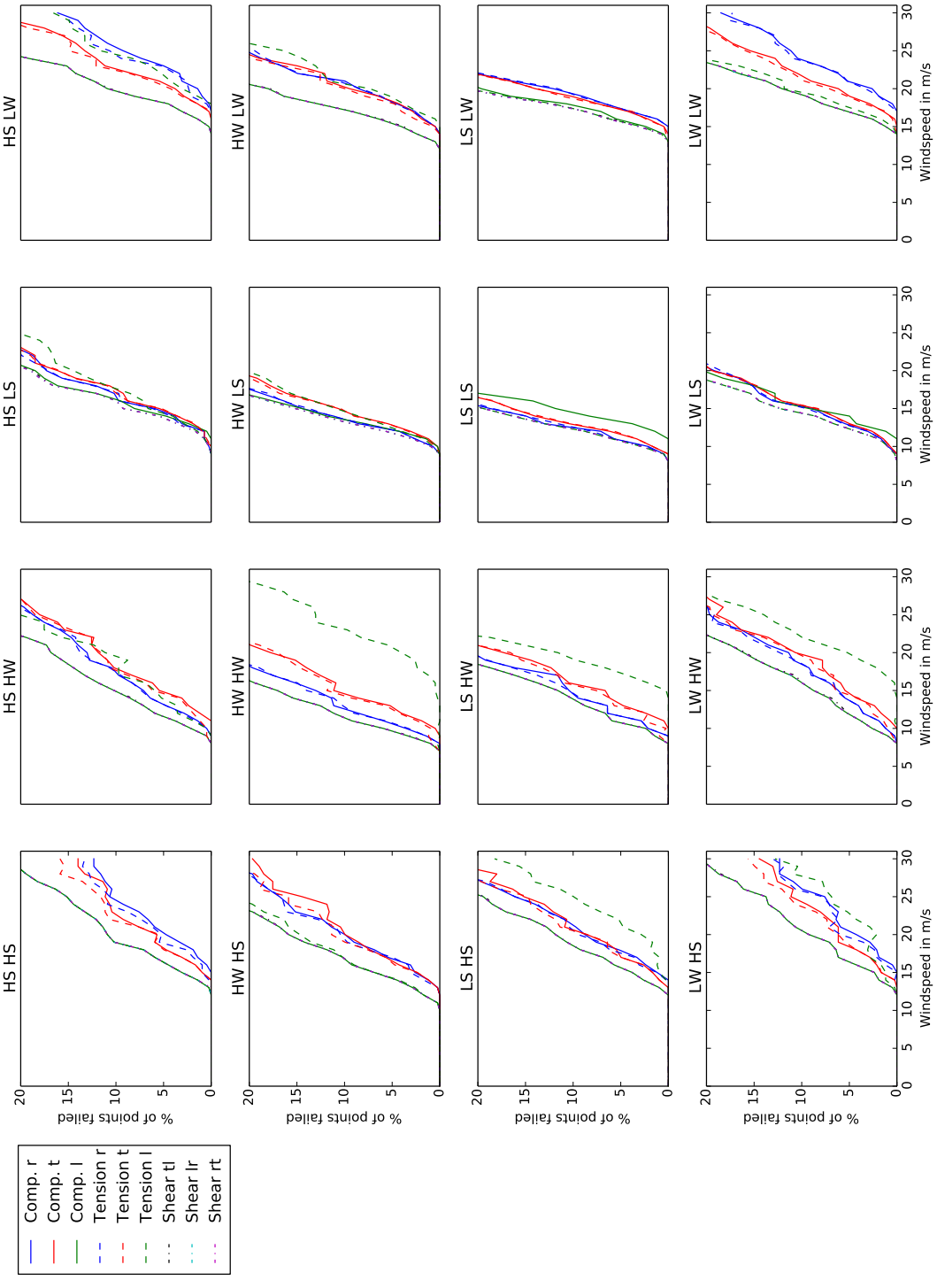

Figure 3.16: Comparison of the direction of failure at age 15, without growth stresses and a stocking of 741 stems per hectare.

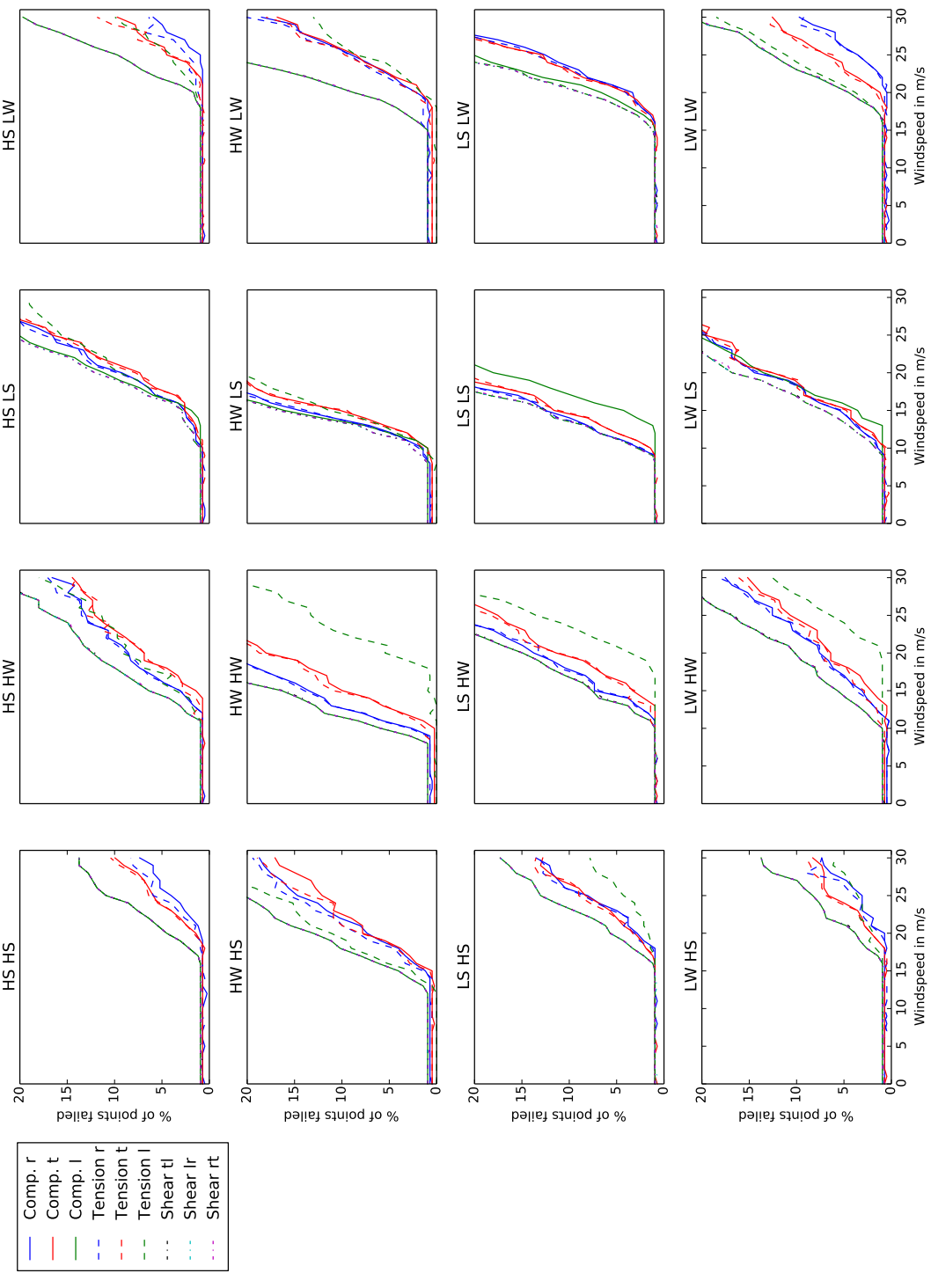

Figure 3.17: Comparison of the direction of failure at age 15, with growth stresses and a stocking of 741 stems per hectare.

3.3.4 Effect of stocking rate

The environment a tree experiences is largely effected by its surroundings, trees inside forests experience lower wind loads than those grown on open plains. For this reason the two scenarios were considered and it can be seen in Figures 3.18 and 3.19 that while stocking rate effects at what wind speed stems will fail, the order TRPs failure remains fairly constant. Stems at a stocking of 741 stems per hectare fail significantly earlier than the open grown trees, even though their crowns are smaller. The change in slenderness ratio from 97 to 124 caused a reduction in wind speed at first failure from 20 to 16 m/s for the TRP LW $\rightarrow$ HS (at age 15). By comparison, for the open grown stem removing growth stresses causes a reduction from 20 to 15 m/s and from 16 to 12 m/s for a stocking of 741. The TRP still has the most influence with a spread of up to 10 m/s at 15 years.

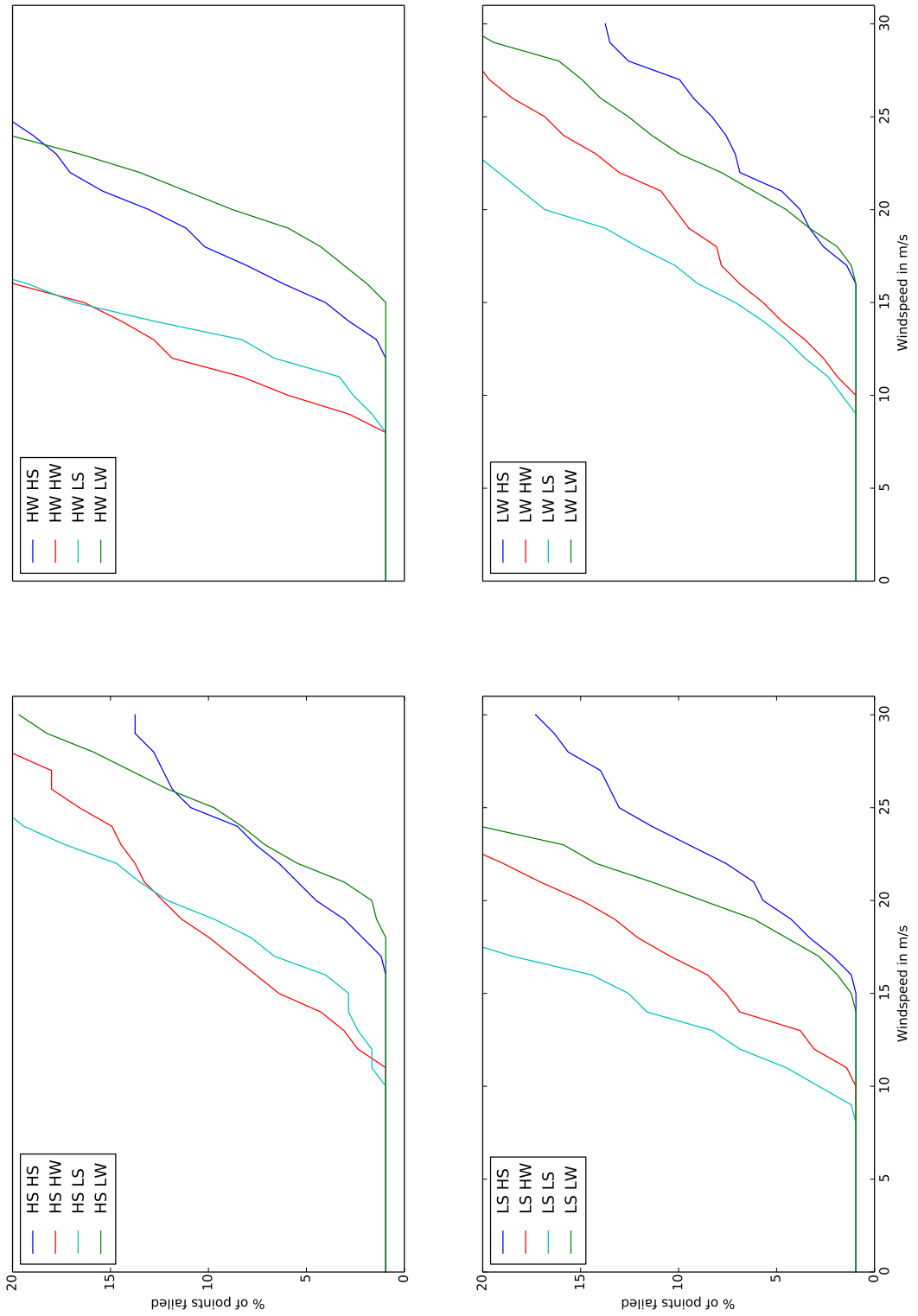

Figure 3.18: Number of failed points at given wind speeds for a 15 year old stem with growth stresses implemented at a stocking rate of 741 stems per hectare. Other ages are available in Appendix A.1

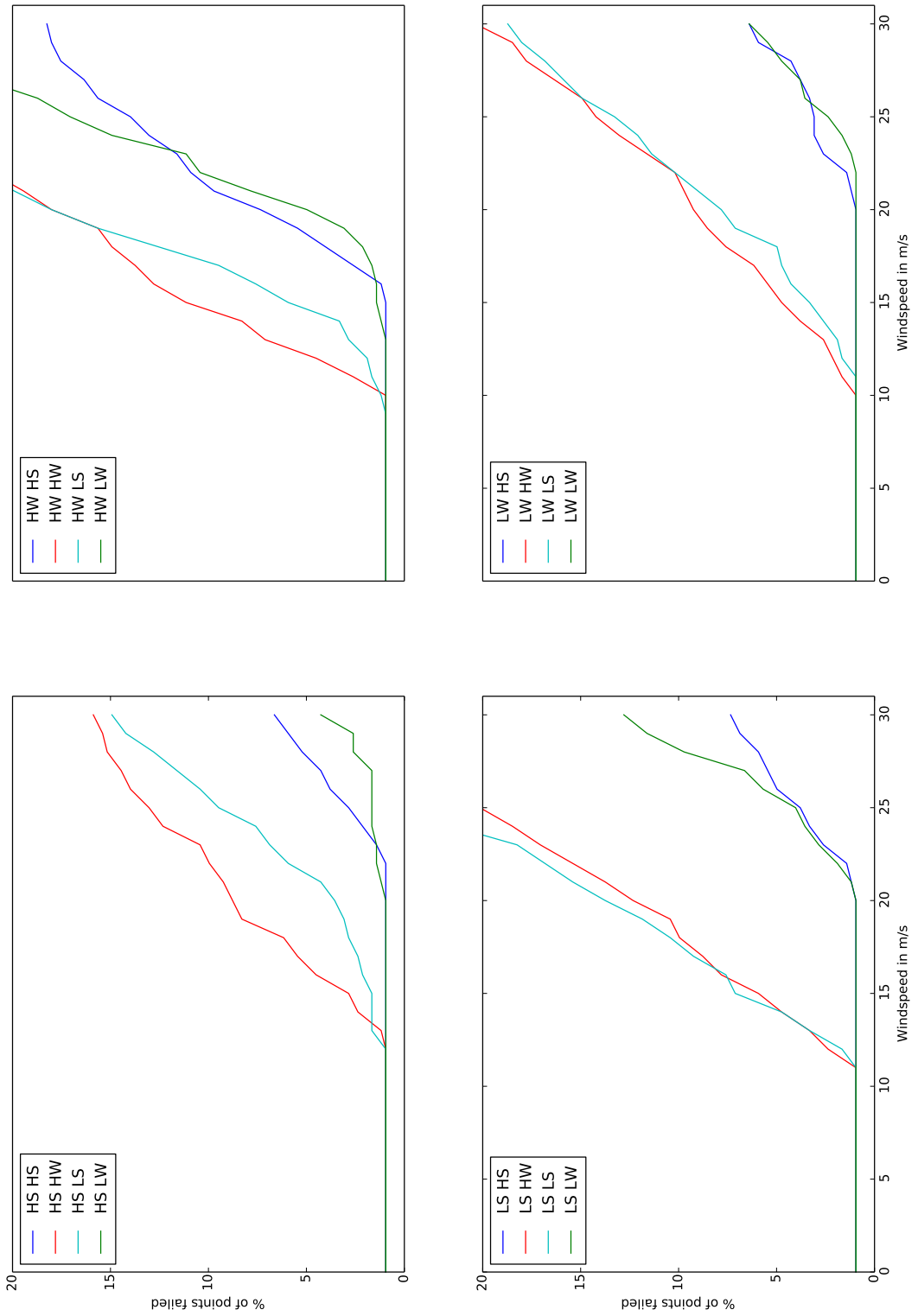

Figure 3.19: Number of failed points at given wind speeds for a 15 year old stem with growth stresses implemented for an open grown tree. Other ages are available in Appendix A.1

Table 3.3: Categorising the TRPs which have the lowest incidence of failure (High resilients), to those that have the highest (Low resilients) across all time steps. Bold indicates naturally occurring profiles.

High resilients	Moderate resilients	Low resilients
LW → LW	**LS → HS**	LS → LS
HS → HS	HS → LS	HW → HW
LW → HS	LS → LW	**LS → HW**
HS → LW	HW → LW	HW → LS
	HW → HS	LW → LS
		LW → HW

3.3.5 Comparison of the TRP over time

Throughout a trees lifetime its structure changes as it grows and adapts to its current environmental setting. The simulation was run for a tree at ages 5, 10 and 15 years old. TRPs which perform well (have a low proportion of failed points at a given wind speed) at one time perform well at all other times. Table 3.3 categorises the TRPs into the groups of how well they performed over all time. Note that the top four TRPs consists of every permutation of the HS and LW samples while the bottom six TRPs contains all permutations of LS and HW, reasons for this are discussed in Section 3.4.1.

When the TRP is split into its stress direction constituents the tendency to fail in longitudinal compression is evident for a number of TRPs, and is often accompanied or closely followed by a number of other directions. Discussion with regard to this clustering of failure in a number of stress directions is in Section 3.4.1 and Appendix B presents a number of plots showing the differences in the magnitude and direction of failure for different TRPs over time.

For younger stems the spread in deflection is much lower, this could be contributed to the lower radial variation between samples as only the first third of the TRP is used in the five year old stems because of the lower radius.

3.4 Discussion

3.4.1 Observed results

There are a number of instances within this work where errors and assumptions need to addressed and their implications considered, see Section 3.4.2 for this. Here it is assumed that the results given are reliable and a discussion of the results is given assuming the errors discussed in Section 3.4.2 are minimal and do not alter general trends.

TRPs involving the samples which had properties that are more normally associated with *Pinus radiata* and had no anomalies produced the stems most resistant to breaking proportionality ($LW \rightarrow HS$ tends to perform best over all ages, closely followed by $HS \rightarrow HS$, $LW \rightarrow LW$, $HS \rightarrow LW$ and $LS \rightarrow HS$). Stem breakage may have (partially) driven the development of wood structure changes, but this study indicates that a number of other TRPs may provide similar amounts of mechanical stability. The argument could be made that the constant profile $HS \rightarrow HS$ while appearing to be mechanically stable, may be more likely to become uprooted and break at a young age, hence there is an evolutionary driver away from this profile, the same argument could be made for the inverse profile of $HS \rightarrow LW$.

Given the assumption that breaking proportionality is counter productive this indicates there is an advantage in using these wood types for stems which are under no unusual mechanical loads (e.g. strong prevailing winds). We can speculate to reasons why some TRPs are disadvantageous to survival. High stiffness in the center of stems may increase the chances of uprooting or breakage while the tree is young making high stiffness corewood profiles undesirable. High stiffness corewood is desirable for commercial forest operations where logs are graded on stiffness, as long as the trees can survive until harvest. The LS sample has an unusually low longitudinal tensile strength, this may be significant in why it does not perform well as outerwood.

By excluding the HS and LS samples as suitable corewood (due to their stiffness making them vulnerable to uprooting or breakage while young) only low stiffness corewood

samples remain. Why high density high stiffness outerwood is most profitable for the stem is unknown, but it could be a result of a need to reduce bending in larger stems. Stiffer outerwood will require less material to reduce the deflection for a given load than lower stiffness material. The low stiffness low density corewood to high stiffness high density outerwood performed best in most scenarios, although closely followed by stems made entirely of low density low stiffness corewood. The low density low stiffness corewood stems exhibited a lot more deflection at given wind speeds than the other profiles, which may cause crown damage when situated near other trees.

Influence from growth stresses is apparent when comparing between model runs with and without growth stresses implemented. What growth stresses achieved which may be an advantage to survival is increase the height of the first points to break proportionality over all TRPs tested. The better performing TRPs both with and without growth stresses break proportionality highest within the stem, however when growth stresses are introduced poorer performing profiles which typically break low on the stem, break at a similar height to the better performing profiles. At high wind speeds better performing profiles exhibit a lower proportion of failed points within the stem, and the amount of failed points is much more constant at different heights in the stem than poorer performing profiles. Adding growth stresses accentuates differences between good and poor profiles, with poor profiles typically having more points fail lower in the stem than higher while better performing profiles have a more even distribution in the lower two thirds of the stem, with the maximum number of failed points near half the total height of the stem. The concentration of first failure around half the height of the stem when growth stresses are included may on the other hand indicate a less obvious mechanical advantage of growth stresses. A tree breaking at the base either dies, or must reproduce a substantial amount of biomass to become competitive again, however if a stem snaps at half its height, there are likely to be a number of branches which could take over as new leaders reducing the time it takes to become light competitive again. Multiple leaders may have an advantage if wind breakage is common due to the lower force on each leader from the canopy.

Pinus radiata grow in both forests and open plains. The two regimes experience different environmental impacts because of their soundings. A tree in a dense forest is sheltered from wind, however must compete strongly for light, whereas a tree in the open must withstand higher wind loads, however does not have to compete for light.

Light competition and shelter from wind results in stems with higher slenderness ratios as they put more biomass into growing taller to out compete other trees along with higher crowns with lower crown radii. Open grown trees have lower slenderness ratios to withstand the higher wind speeds they are subjected to as they grow. Crowns form lower on the stem, with larger radii because they are not restricted by the surrounding trees. When the two regimes are compared open grown stems are substantially more resistant to wind loadings, even with their larger crowns.

The constant stress hypothesis (Mattheck and Kubler, 1995) argues that trees grow in such a way as to preserve constant surface stress. Some of the results presented here provide some support for this idea, particularly that stems with natural TRPs have a more consistent profile of failed points in the vertical direction than non natural profiles do.

The TRP and the wood properties it consists of have a substantial influence on the structural stability of the stem. For a given tree the variability in the wind speed required to break proportionality has a range of 10 m/s. By comparison, for a stem with the TRP ($LW \rightarrow HS$) growth stresses and slenderness only cause half this variation in the wind speeds required to break proportionality, indicating the TRP plays a significant roll in a stems ability to withstand wind loads. Given the magnitude of changes in both stocking and growth stresses, both of these effects also need to be considered.

3.4.2 Errors and assumtions

Having stiff corewood or flexible outerwood are both unusual, as a result, these samples used may provide some slightly unusual results. The comparatively high value for the tangential longitudinal plane shear modulus in the HW sample and the LS sample being stronger in compression than tension both give credence to these being slightly unusual samples. The reasons for these anomalies are unknown, but the speculation could be made that HW has a high proportion of rays or an angle within the grain (for an unknown reason) and possibly LS is not normal wood. The consequence of having samples exhibiting unusual mechanical properties; that the profiles involving these samples are inferior, may be a result of the individual samples used and not

necessarily the wood properties they were chosen to represent. In order to remove doubt associated with these individuals a larger sample size is needed to be confident of the average wood with these properties. If the assumption is made that these samples are representative, there must be a reason why the HW and LS produce stems which are less structurally sound.

Yield point and the limit of proportionality have different mechanical consequences when exceeded, Reiterer et al. (1999) showed high MFA wood is more highly non-linear elastic than low MFA wood. The assumption that yield point and the limit of proportionality are equal may be better suited to outerwood than corewood. If the non-linear elastic section of the stress strain curve is larger for corewood the yield point is not reached until a significantly larger deflection than what was assumed here.

Failure tends to occur in clusters, when a point fails in one direction, it is quickly followed by other directions. Considering the discussion in Section 3.2.11 this is not surprising. The clustering of failure points in most directions may indicate to some extent that there has been a driver for making the material as strong as necessary, although it may also simply be an attribute of the material structure. Note that when growth stresses are applied the failure in the longitudinal tension direction does increase for all TRPs however there are still very few TRPs where it is the primary form of failure.

One of the most limiting assumptions made in this work was that wood is a linear elastic material which has a limit of proportionality equal to its yield point. By excluding the possibility of non-linear stress strain relationships the deflection at the yield point has been underestimated. Further because the assumption of proportionality was included even when points passed the proportionality limit an over prediction of stiffness is observed above this point. Without non-linear elasticity relationships being accounted for the possibility of corewood and outerwood performing differently in the non-linear region of the stress strain curve can not be considered. Differing relationships between stress and strain after the point of proportionality for corewood and outerwood could significantly effect the outcomes of these simulations.

Corewood in these cases was taken from the centre of stems of felled trees. It is likely these trees were felled around 28 to 32 years old. It may be the case that the mechanical properties of corewood taken from a 5 year old tree and corewood taken from the same

tree at age 30 will not have the same mechanical properties, due to phenomenan such as creep due to gravity and growth stresses and microfracture due to extreme wind events (although no visible defects were observed in the samples). Taking samples from the centre of felled trees to represent the mechanical properties of corewood may not be appropriate when considering a five year old stem. Testing how much the mechanical properties do change over the age of a tree would be useful, however due to variation between individuals, even clones, this may be problematic to test experimentally.

The corewood samples, particularly *LS* were taken from rings further out than ring five, approximately ring ten, although as they were selected as milled boards their ring number is only an estimate based on growth ring curvature within the board. When modelling a five year old stem this corewood may be too stiff, resulting in an over prediction of stiffness and potentially an under prediction of deflection which can be withstood before breakage.

Numerical instabilities were pronounced when using growth stresses on the high resolution linear element model. The entire system is not highly numerically stable even when using quadratic elements and often results in oscillations within the newton solver, the system is always solved to a minimum relative error (calculated by Fenics (Anders Logg and Wells, 2011)) of 10^{-5}. Growth stresses increase numerical instability regardless of the element type or resolution used.

Spiral grain has not been considered, instead the assumption was made that the grain always lies along the axial direction. The lack of spiral grain may further increase the stiffness of the simulated stems, particularly for the stiff TRPs. Astley et al. (1998) found that as MFA reduces, spiral grain has an increased effect on stiffness. Other effects such as the difference in cellular geometries within each sample were not accounted for. Spiral grain may also cause growth stresses to operate at an angle to the vertical axis of the stem, due to the cells being orientated at the grain angle. How this would effect the growth stress profile is unknown.

The stem radius, and other tree architecture measurements were approximated from measurements presented by Waghorn et al. (2007a). While there is a strong relationship between these properties for trees within forestry stands, the relationships were extrapolated to predict architecture of open grown stems. Given open grown trees are

out side of the data used to create the relationships, there is an unknown amount of uncertainty associated with the predictions of stem and crown architecture for both young and open grown stems.

Chapter 4

Summary

4.1 Conclusions

Chapter 1 provides an overview of the current literature in the field, Chapter 2 presents elastic constants, Poisson ratios and limits of proportionality obtained experimentally. Chapter 3 presents a number of different sets of numerical evidence to add information to the investigation of why the TRP exists.

It was found that the typical radial pattern of low density low stiffness corewood tending to high density high stiffness outerwood performs best through a range of ages, however a number of other profiles which do not all follow the naturally observed trend also perform well. These are constant profiles of high density high stiffness, low density low stiffness and the inverse profiles of what naturally occurs, high density high stiffness to low density low stiffness, these are closely trailed by low density high stiffness high density high stiffness, which is ideal for commercial forestry products. A warning should be noted that high stiffness saplings may increase the likelihood of toppling, even if the risk of failure does not change much. TRPs which perform well also tend to have more constant longitudinal stress profiles in the lower half of the stem. Interestingly TRPs which perform worst, when growth stresses are applied also find their initial failure point moves toward the mid height of the stem where the most resilient profiles first

start to fail. The assumptions, accuracy and improvements which are applicable to the work were also discussed.

4.2 Future work

Work presented in this thesis should be thought of as a proof of concept. A number of issues with regard to the implementation of this work were discussed, however the results are promising in applying these techniques to plant biomechanics problems.

The experimental work presented here is limited to only four samples, future work needs a much larger data set to reduce the problems associated with using individual boards as representative samples. The experimental techniques used were crude, and did not provide very accurate results. Suggestions are made as to how these techniques could be improved in Chapter 2. Even with improved experimental techniques substantially more samples need to be processed in order to investigate anomalies and trends between properties in different material directions and the materials placement within the stem. Further work considering the mechanical properties of corewood obtained from stems at a young age should also be conducted to allow for comparisons between how corewood changes though a stems life time. In order to investigate corewood at young ages sample sizes need to be reduced due to the geometry of growth rings. In its self changing sample sizes causes variation in experimental results (Niklas, 1997). A fine balance exists between representative homogeneous samples and samples too small to account for woods cellular geometries and growth rings. One of the main goals of this research was to present complete sets of constants for green corewood and outerwood, future work is needed in order to increase the accuracy and size of the set of these constants.

Unfortunately the problem of computational power, without using computing clusters or general purpose graphics processing is still a limiting factor. Moving into parallel computation will provide the ability to reduce the physical size of samples during experimental work. The finer resolution will provide greater control for modelling the effects of the TRP and potentially allow for the effect of cellular geometry to be simulated directly, rather than relying on homogenisation from macro-scale experimentation. An

important piece of missing information here is how to accurately incorporate micro and nano-scale features of wood structure into an accurate and reliable homogenisation scheme. In this work these issues were ignored, instead assuming that the sample blocks tested were homogeneous material.

The ideas of nonlinear elasticity and plasticity were touched on within this work, however were not explicitly considered. The next extension of this work should be to extend the experimental work into these domains, and redo the analysis to include these effects. The separation of the limit of proportionality and the yield point need to be considered in order to calculate the accuracy of the assumption that the limit of proportionality and the yield point are equivalent. Further because of trees ability to self repair, plasticity needs to be considered along with a prevision for self repair over time.

Spiral grain and branching were both ignored here. Spiral grain has been shown to have an influence on stiffness (Astley et al., 1998) and will likely have an influence on strength as well as the way failure planes propagate through the stem. Incorporating spiral grain will provide insight into a number of current problems, particularly problems associated with why spiral grain exists.

Branching was not considered in this work, instead the canopy was assumed to be attached uniformly to the surface of the stem. There are a number of reasons to include branching into structural models, it has been suggested that the branching structure provides significant dampening to wind loads (Coutts and Grace, 1995), the ability for branches to bend and self prune to reduce wind loadings (Niklas and Spatz, 2000) and the complex grain patterns which evolve around branch attachment will all have an effect on internal stress profiles and failure of the stem.

Wind and canopy profiles have a significant effect on the force applied onto the stem. A more realistic canopy profile and wind profile are needed, ideally this would include branching to predict changes in the drag coefficient and dynamic damping in a mechanistic manner.

Incorporating more complex functions at boundaries to let the base move in strong winds will result in larger deflections without failure. It could also be possible to produce a rooting system and soil interface model in an attempt to predict toppling

rather than breakage.

Appendix A

Failure height variation

A.1 Windspeed and height at first failure

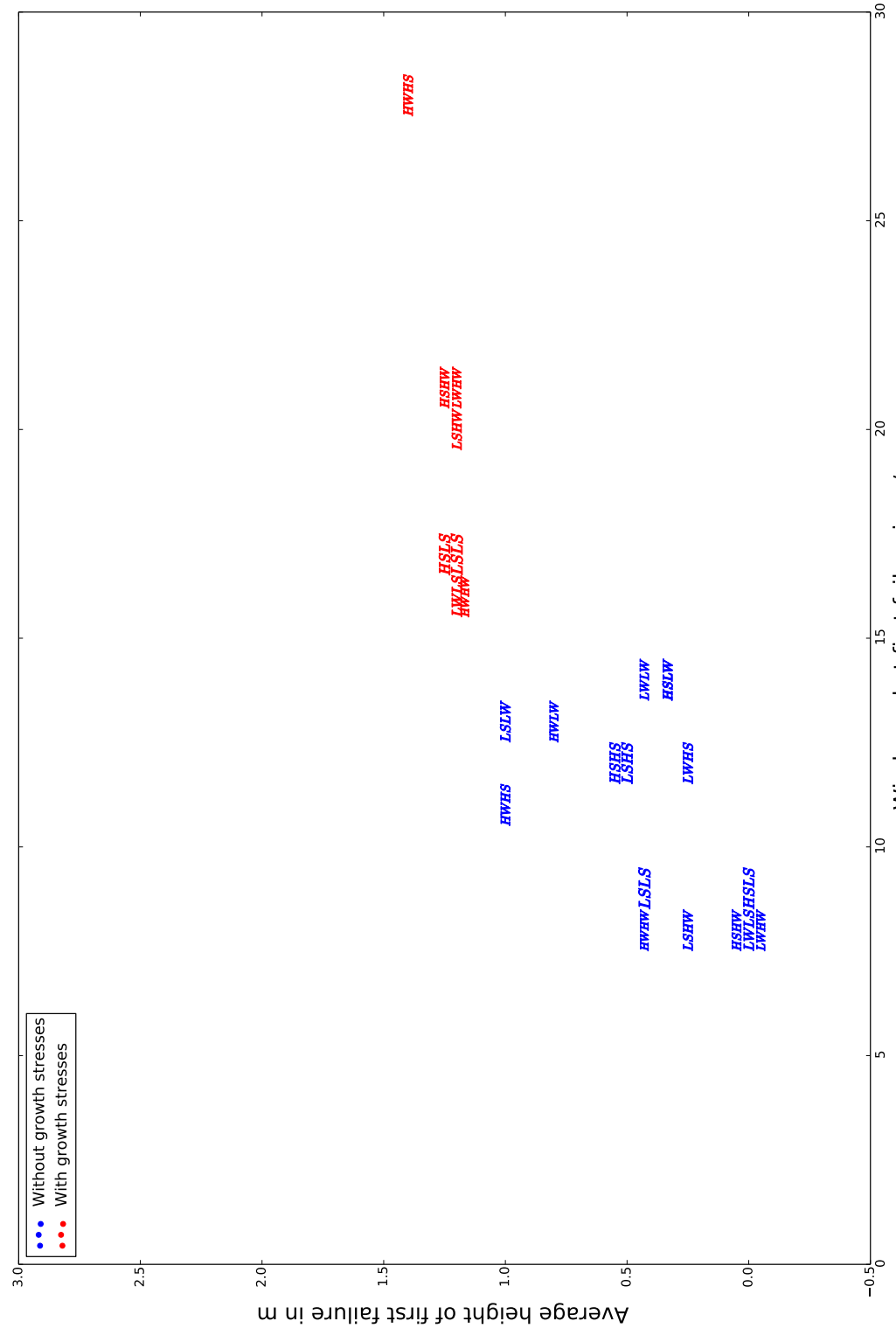

Figure A.1: The height at lowest wind speed at which failure occurs. In the cases where multiple failures occur at the first wind speed the average height of failure for that wind speed was taken. Taken at age 5 for an open grown tree.

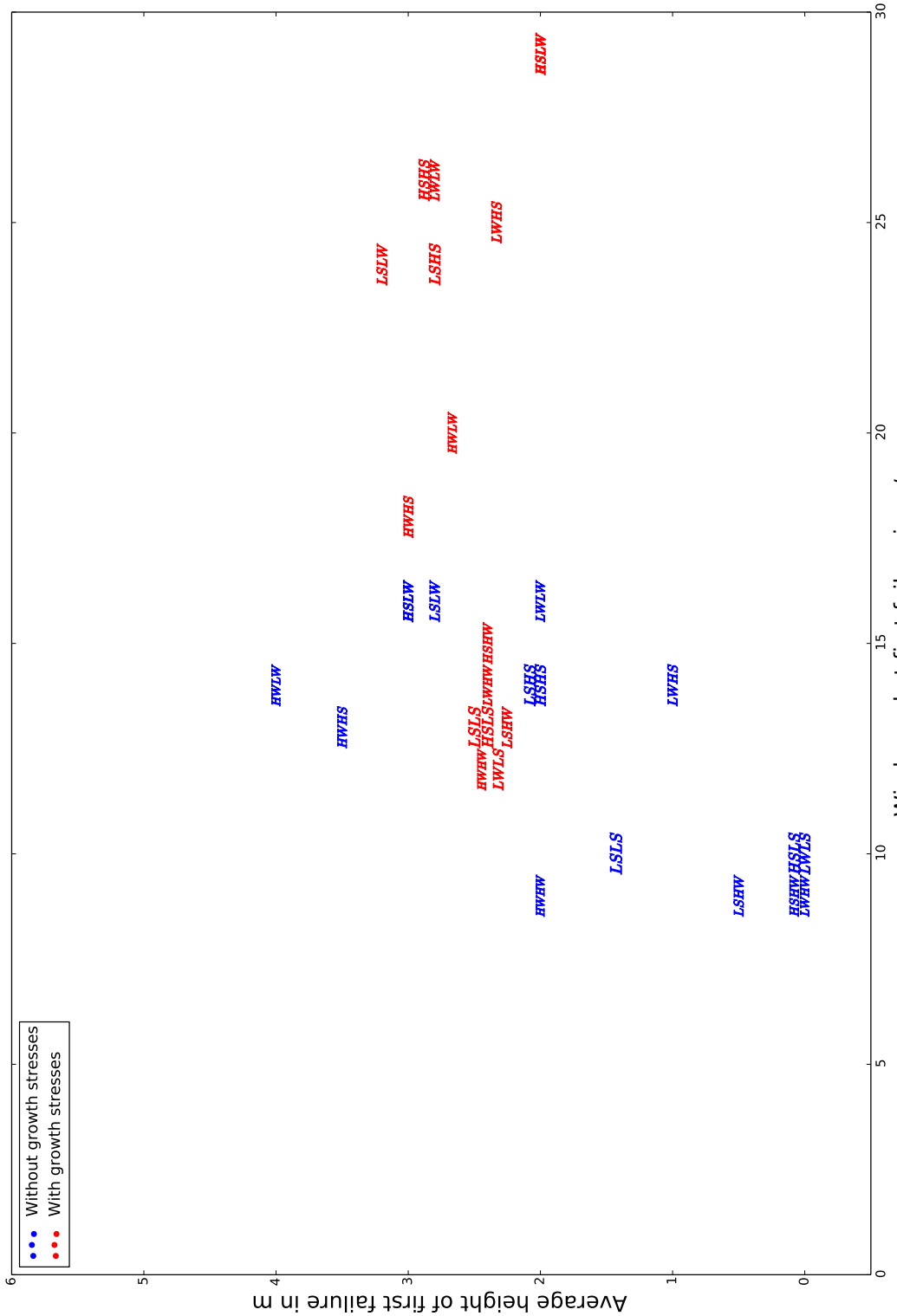

Figure A.2: The height at lowest wind speed at which failure occurs. In the cases where multiple failures occur at the first wind speed the average height of failure for that wind speed was taken. Taken at age 10 for an open grown tree.

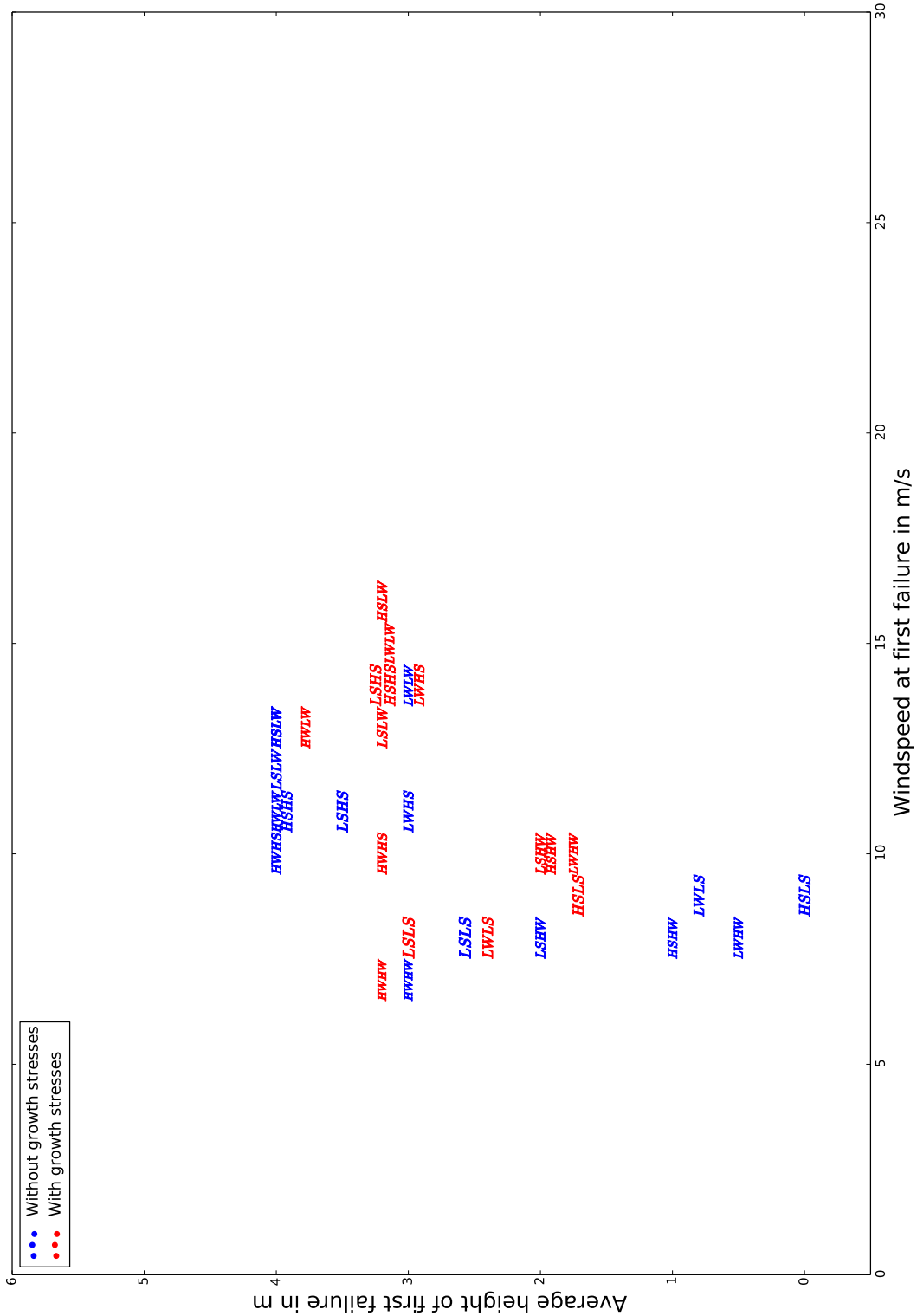

Figure A.3: The height at lowest wind speed at which failure occurs. In the cases where multiple failures occur at the first wind speed the average height of failure for that wind speed was taken. Taken at age 10 for an trees grown at a stocking of 741 stems per hectare.

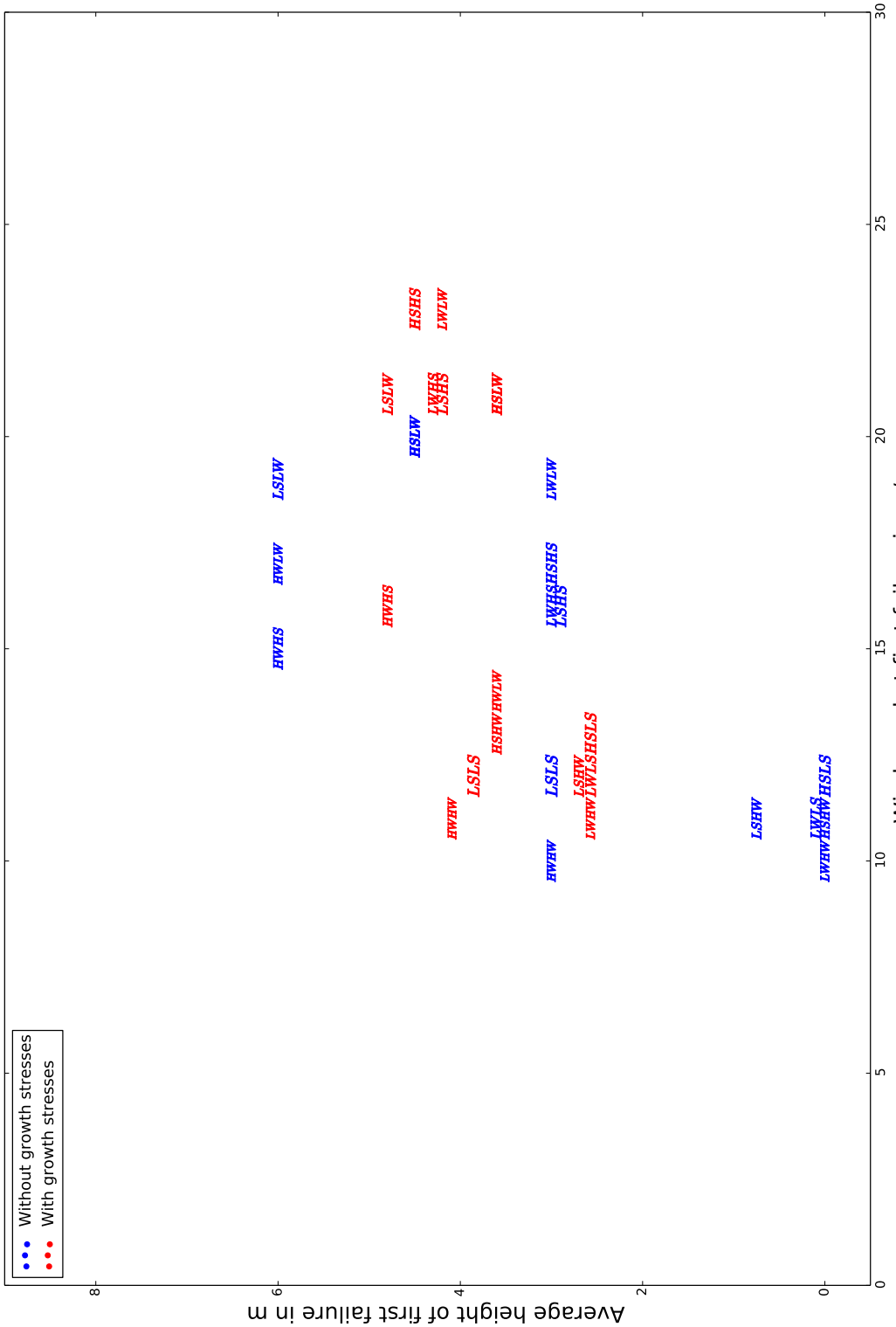

Figure A.4: The height at lowest wind speed at which failure occurs. In the cases where multiple failures occur at the first wind speed failure is observed the heights are averaged. Taken at age 15 for an open grown tree.

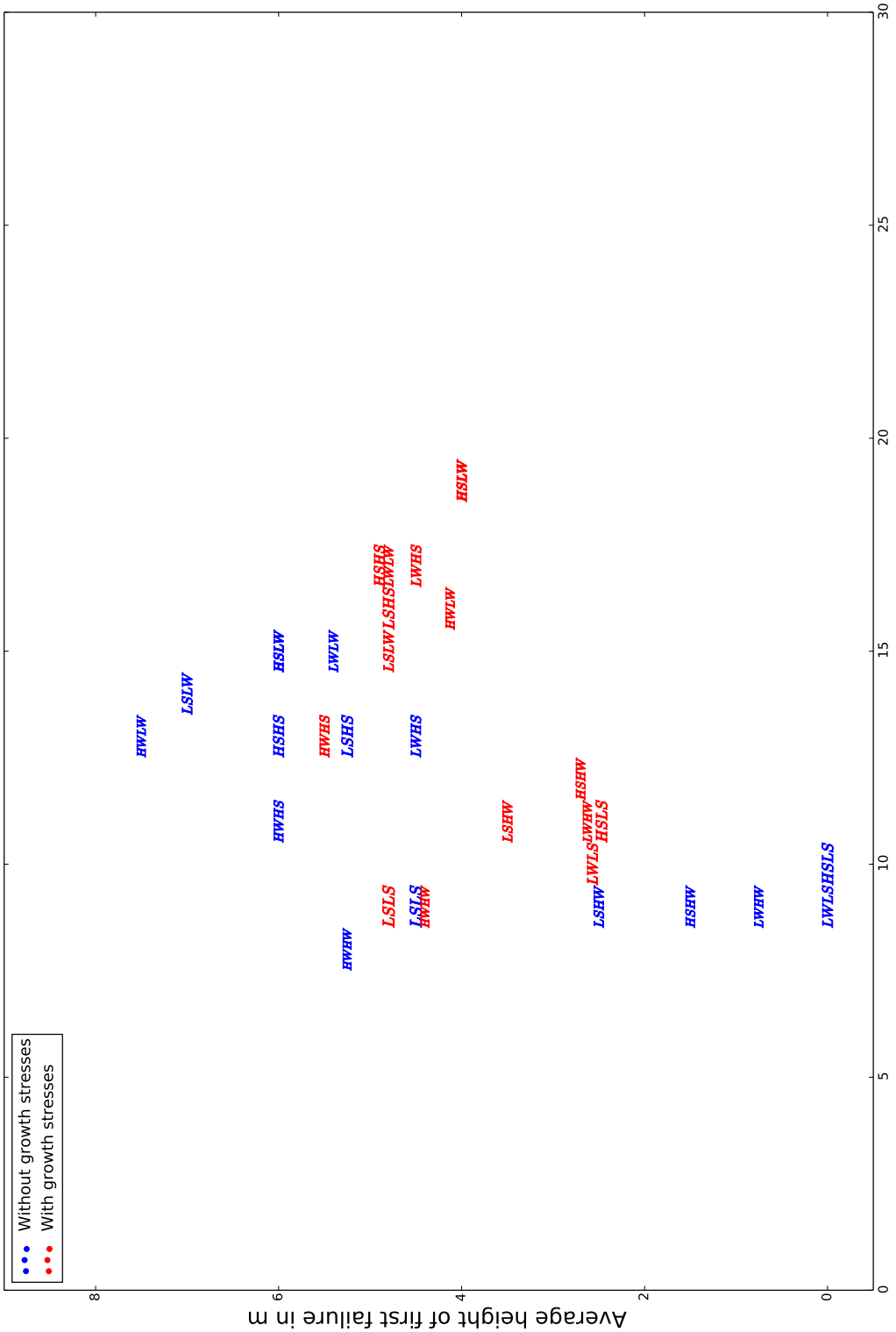

Figure A.5: The height at lowest wind speed at which failure occurs. In the cases where multiple failures occur at the first wind speed failure is observed the heights are averaged. Taken at age 15 for an trees grown at a stocking of 741 stems per hectare.

A.2 Comparison of the magnitude of failure with height and growth stresses

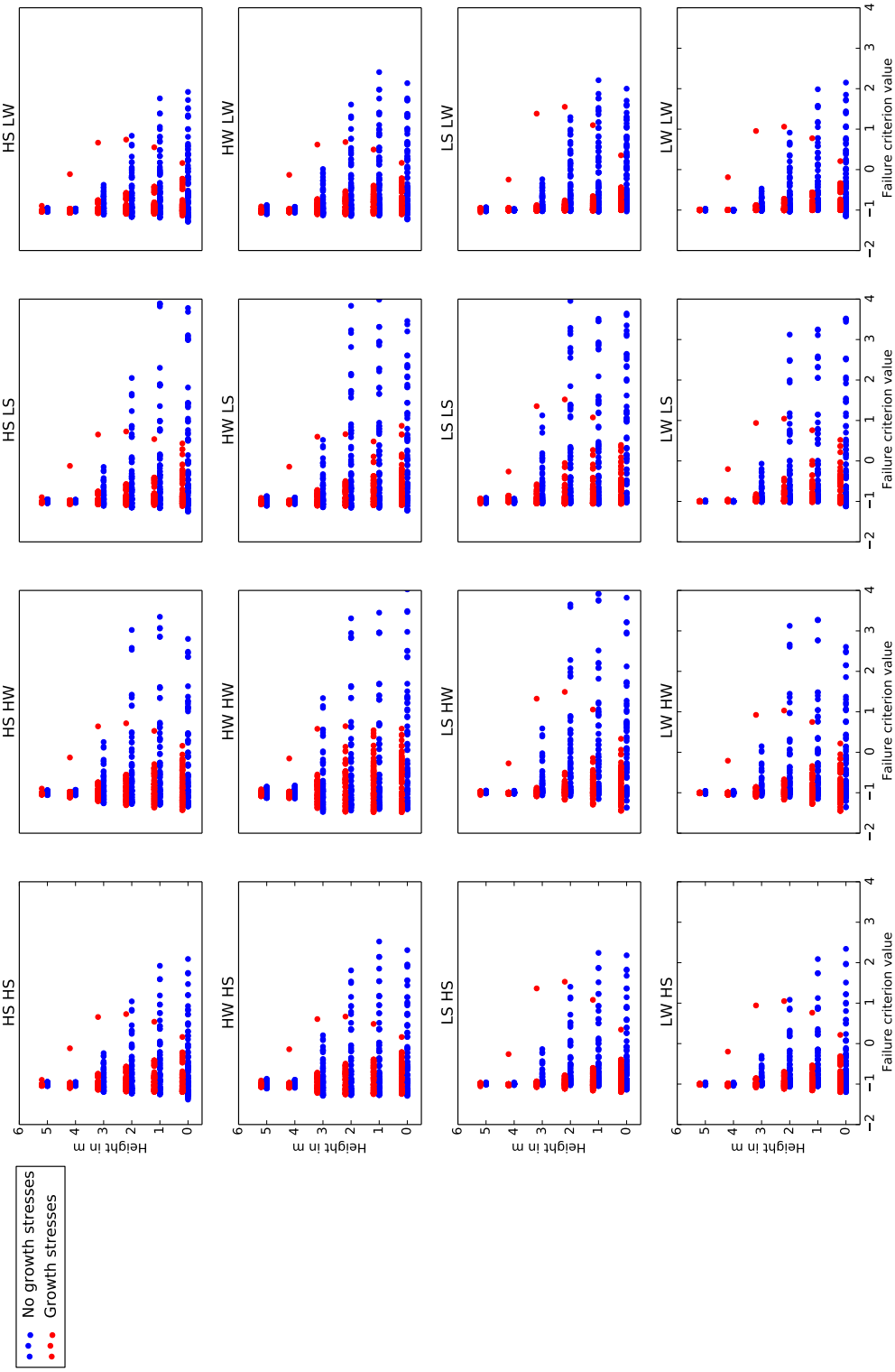

Figure A.6: Comparison of the magnitude of failure and height, with and without growth stresses at age 5 for open grown stems at a windspeed of 20 m/s.

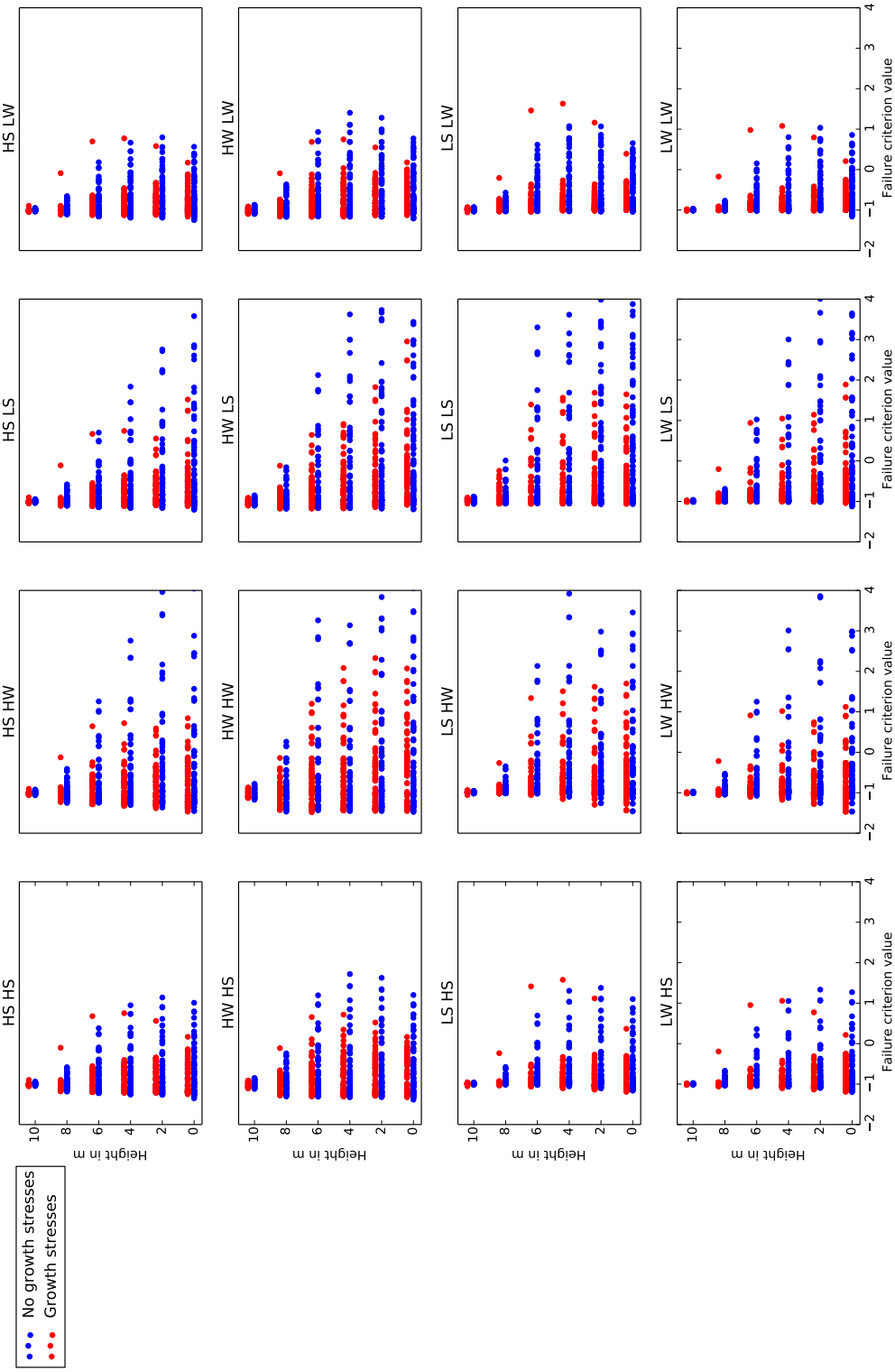

Figure A.7: Comparison of the magnitude of failure and height, with and without growth stresses at age 10 for open grown stems at a windspeed of 20 m/s.

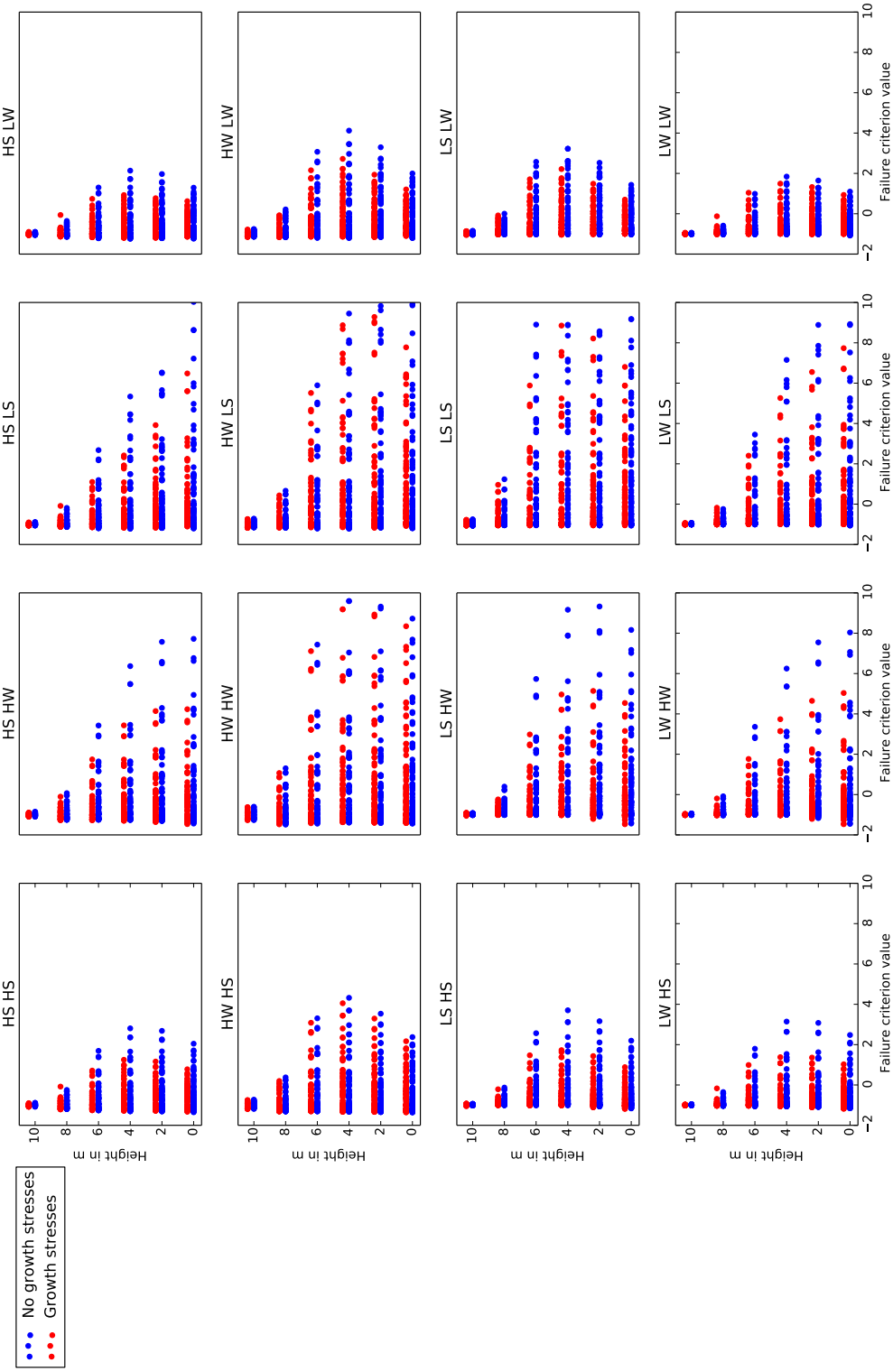

Figure A.8: Comparison of the magnitude of failure and height, with and without growth stresses at age 10 for stems at a stocking of 741 stems per hectare at a windspeed of 20 m/s.

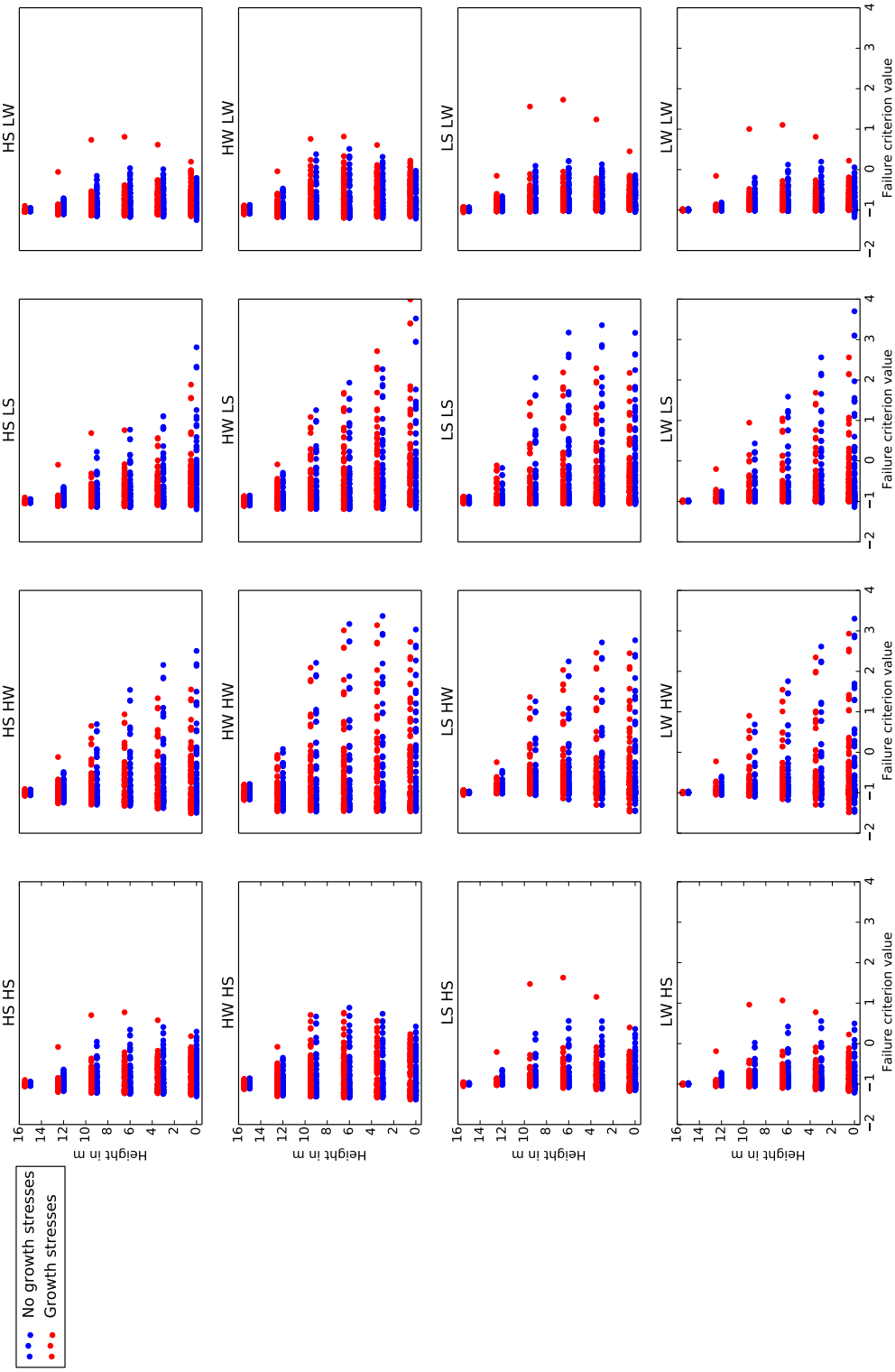

Figure A.9: Comparison of the magnitude of failure and height, with and without growth stresses at age 15 for open grown stems at a windspeed of 20 m/s.

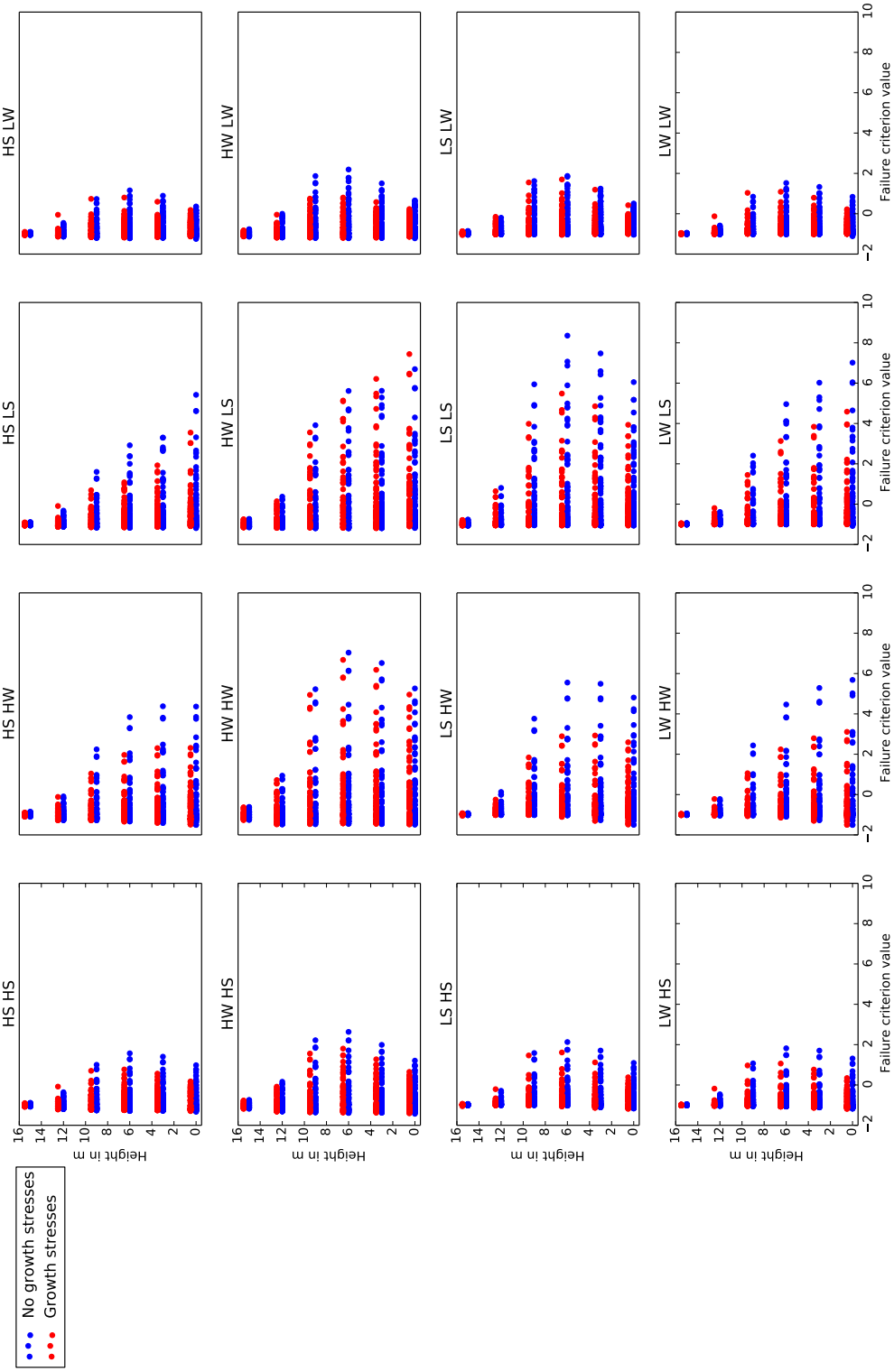

Figure A.10: Comparison of the magnitude of failure and height, with and without growth stresses at age 15 for stems at a stocking of 741 stems per hectare at a windspeed of 20 m/s.

Appendix B

Effect of the TRP for different aged stems, open grown with growth stresses

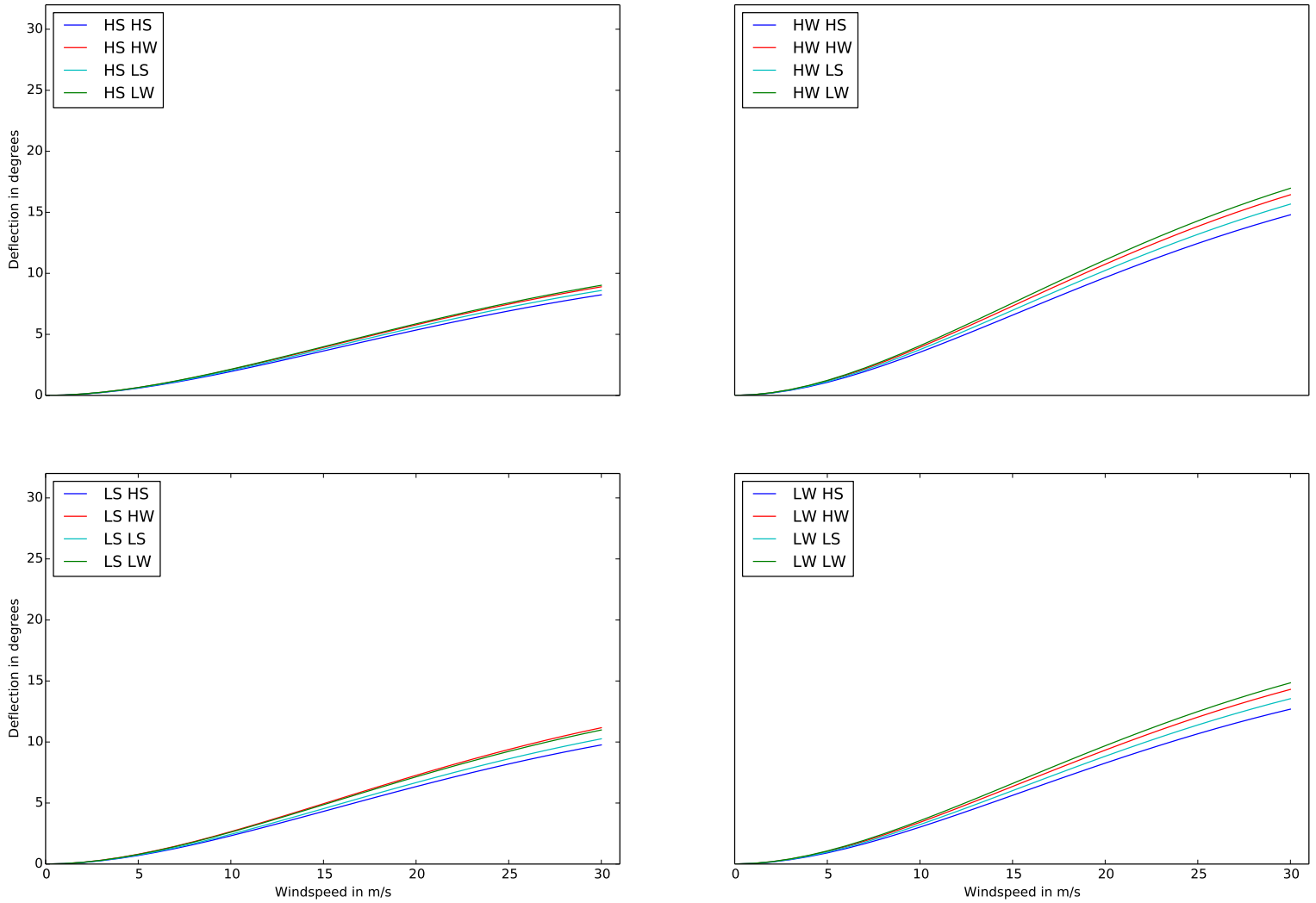

Figure B.1: Deflection in degrees for wind speeds at age 5. Deflection is calculated at the tip of the stem.

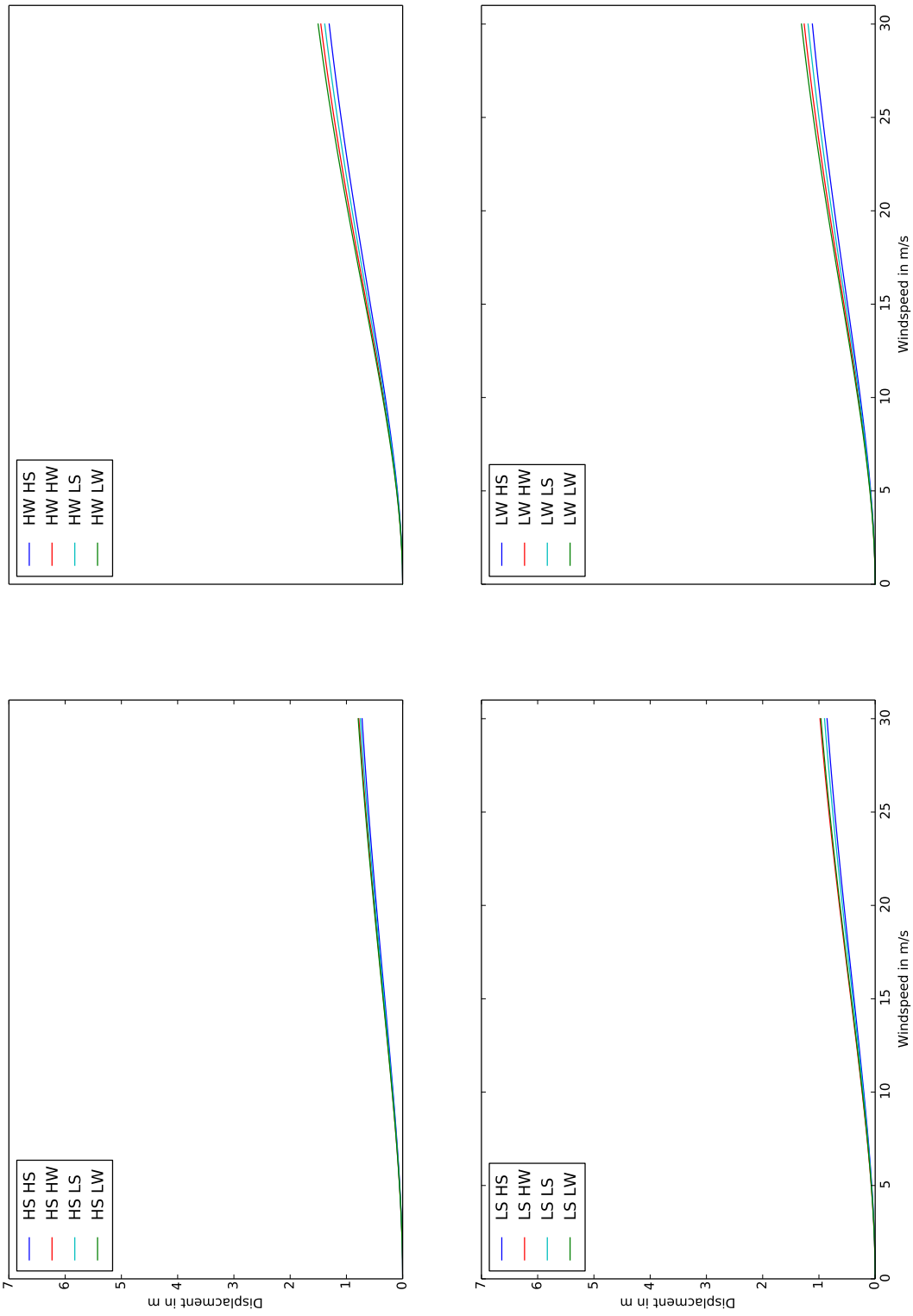

Figure B.2: Displacement in m for wind speeds at age 5. Displacement is calculated at the tip of the stem.

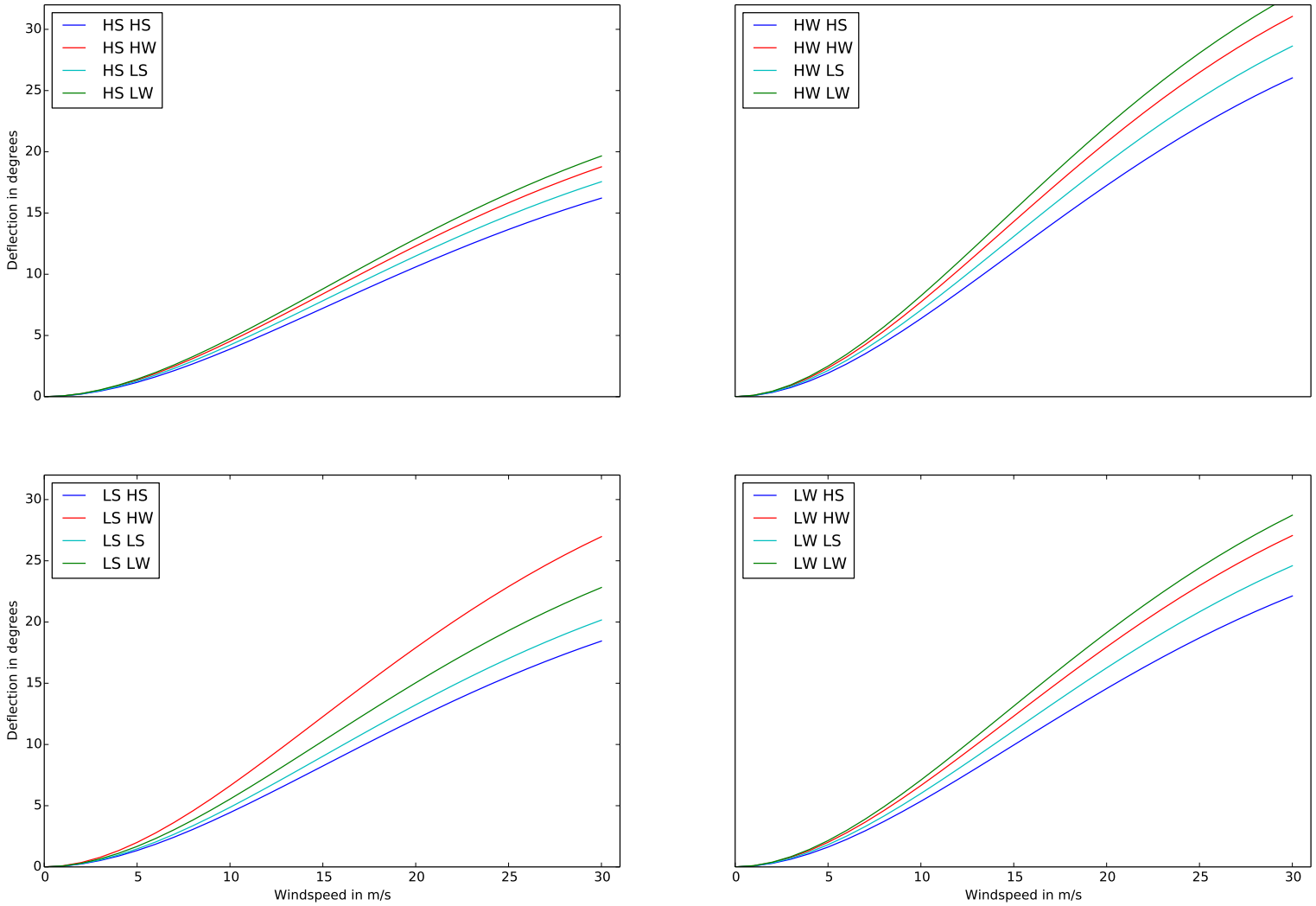

Figure B.3: Deflection in degrees for wind speeds at age 10. Deflection is calculated at the tip of the stem.

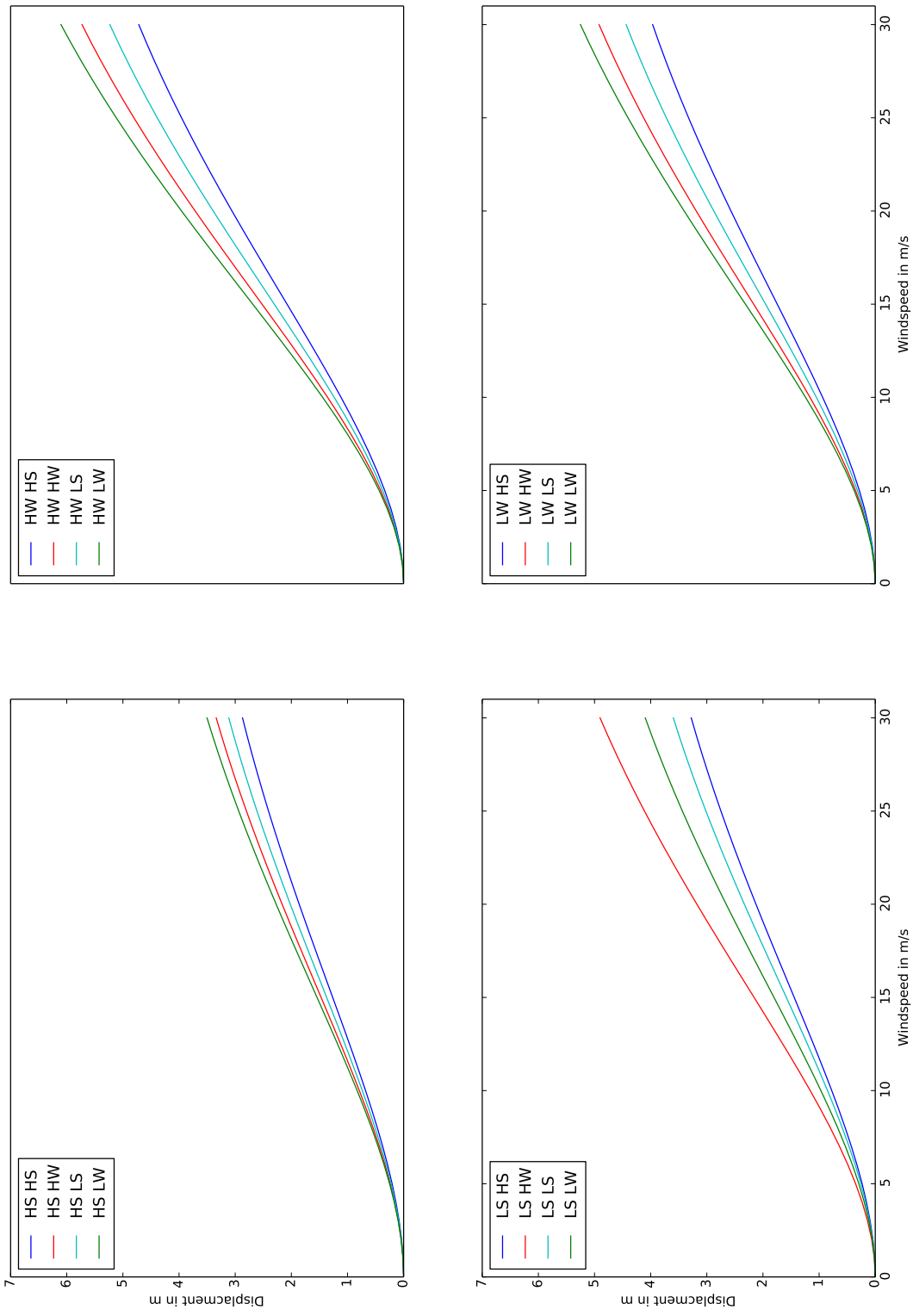

Figure B.4: Displacement in m for wind speeds at age 10. Displacement is calculated at the tip of the stem.

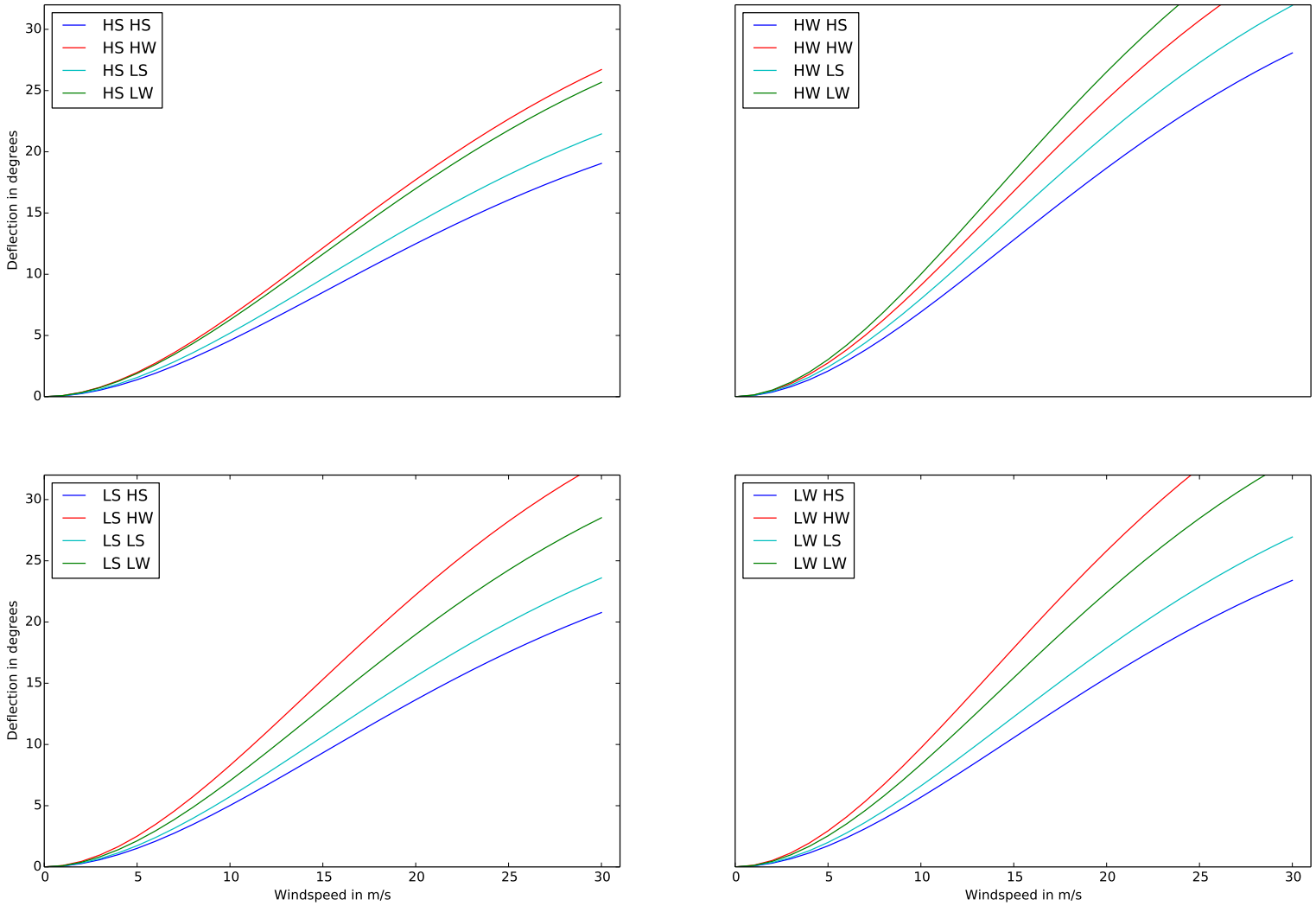

Figure B.5: Deflection in degrees for wind speeds at age 15. Deflection is calculated at the tip of the stem.

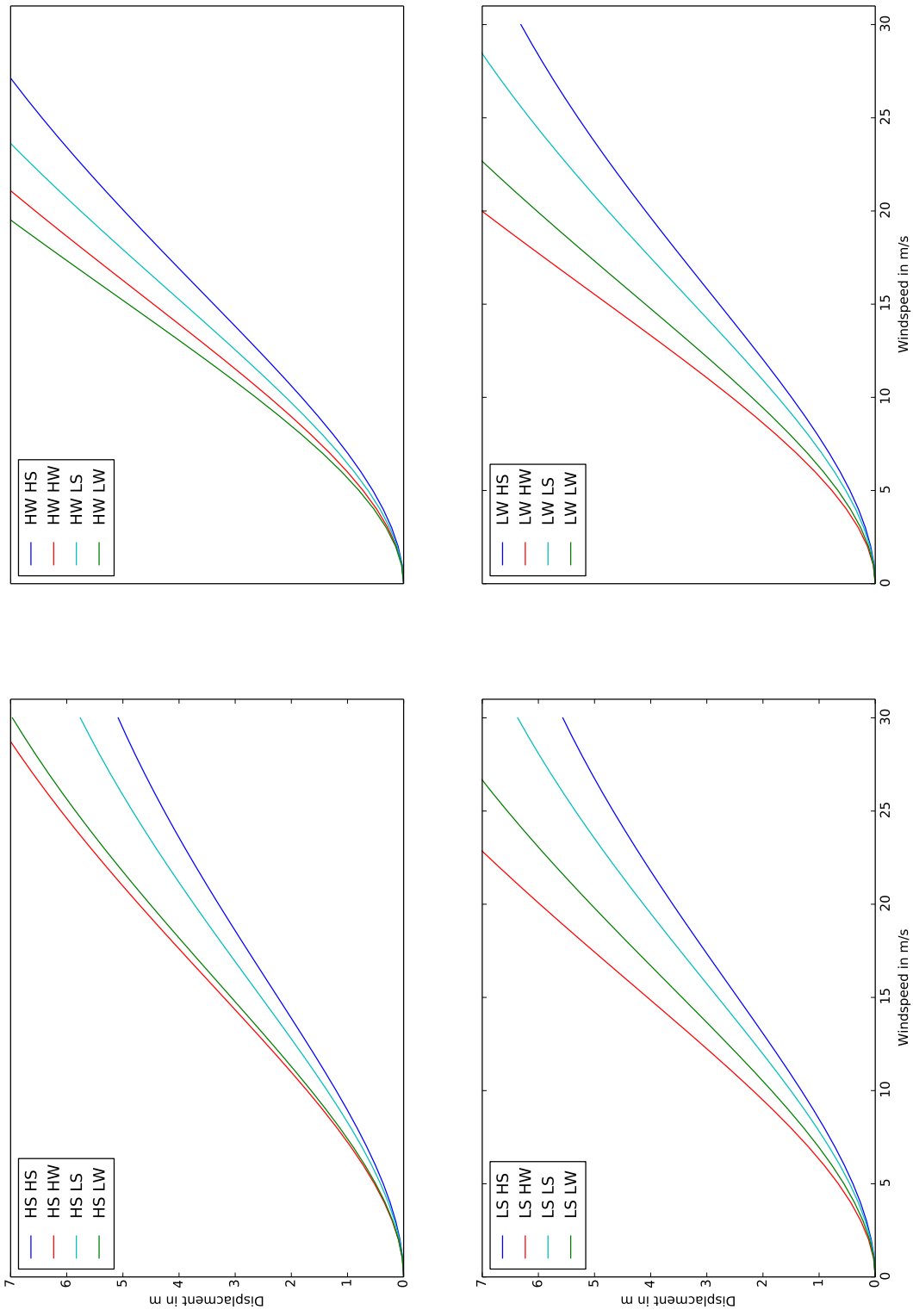

Figure B.6: Displacement in m for wind speeds at age 15. Displacement is calculated at the tip of the stem.

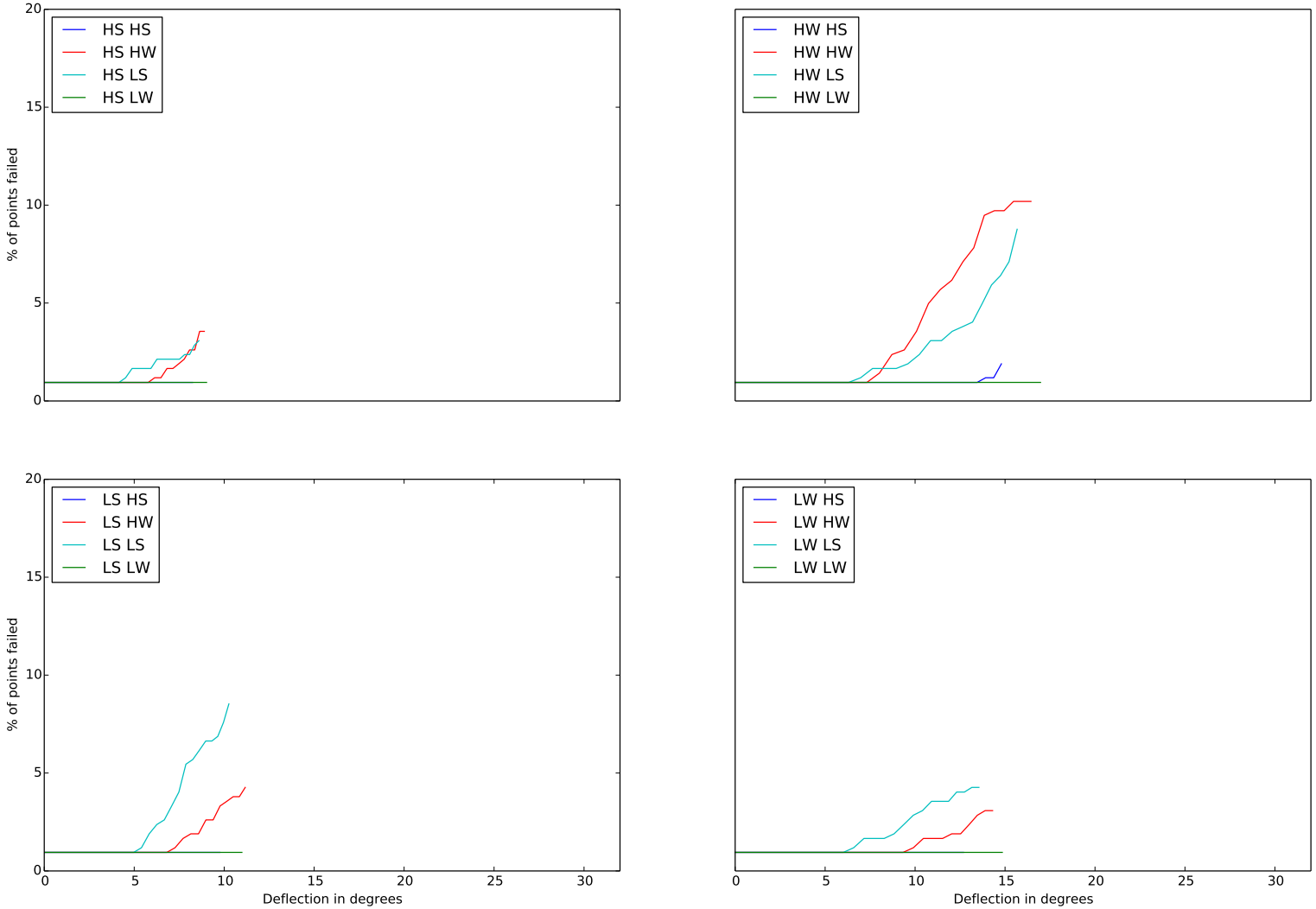

Figure B.7: Proportion of points failed by deflection at age 5. Deflection is calculated at the tip of the stem.

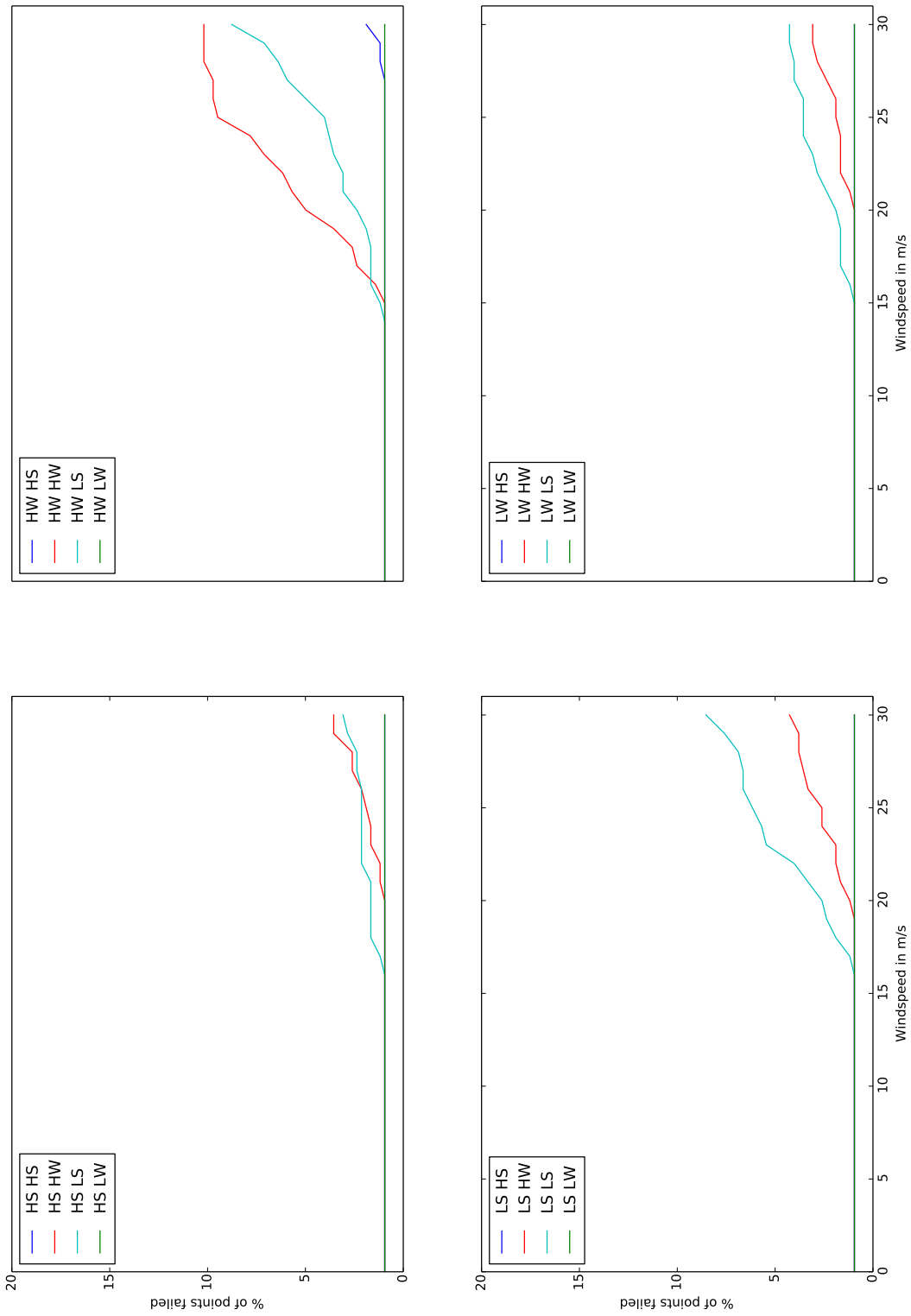

Figure B.8: Proportion of points failed at differing wind speeds at age 5.

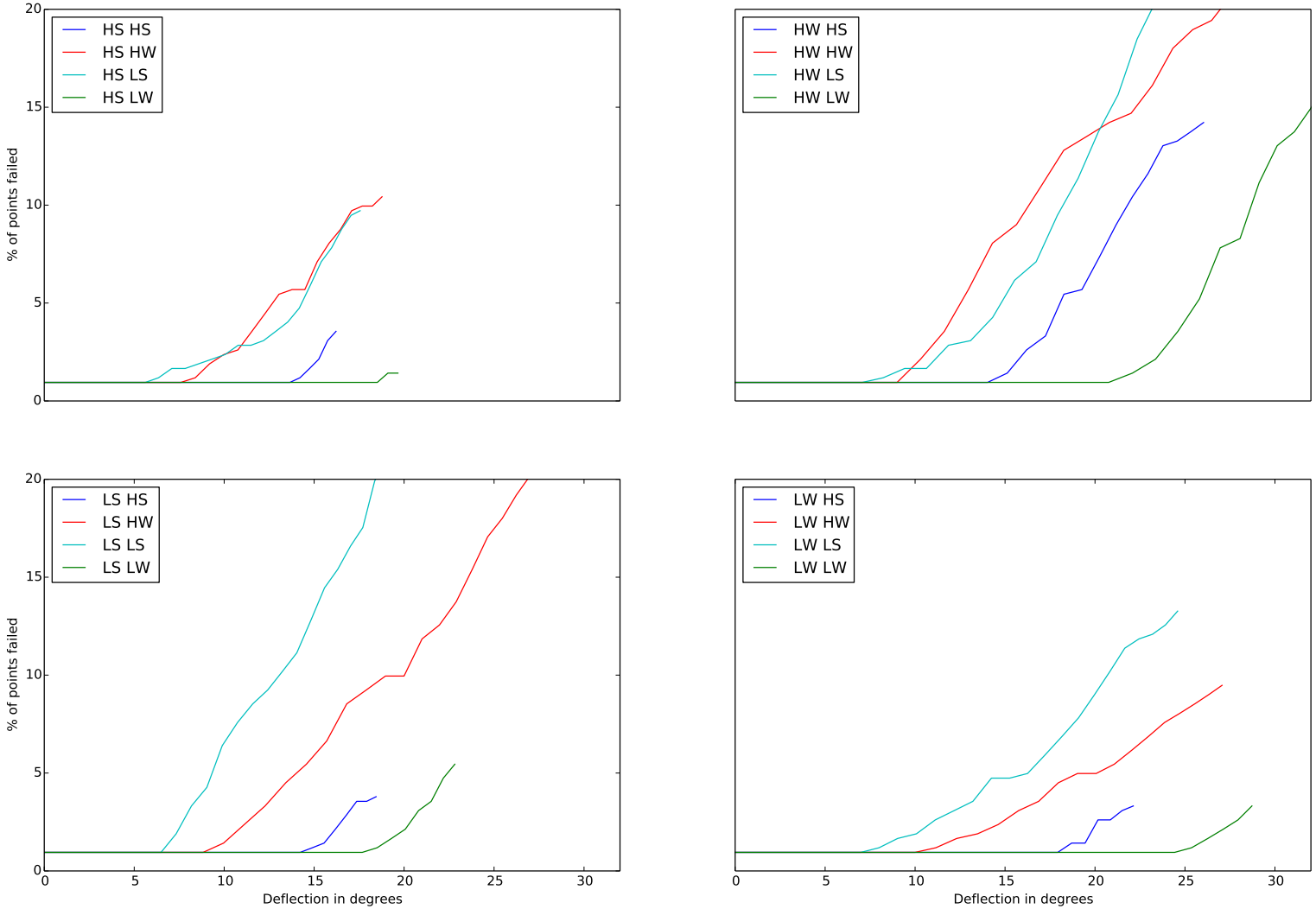

Figure B.9: Proportion of points failed by deflection at age 10. Deflection is calculated at the tip of the stem.

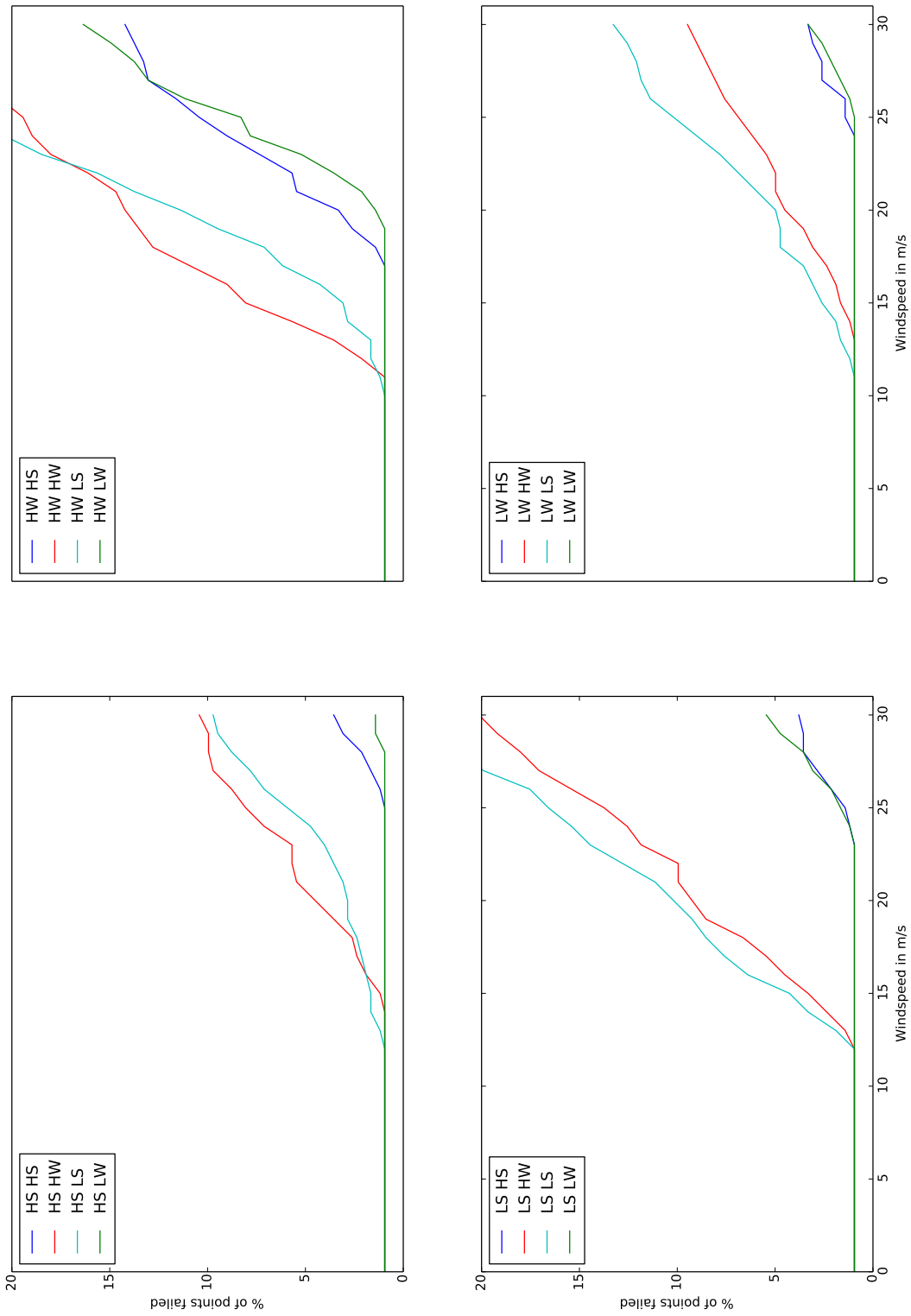

Figure B.10: Proportion of points failed at differing wind speeds at age 10.

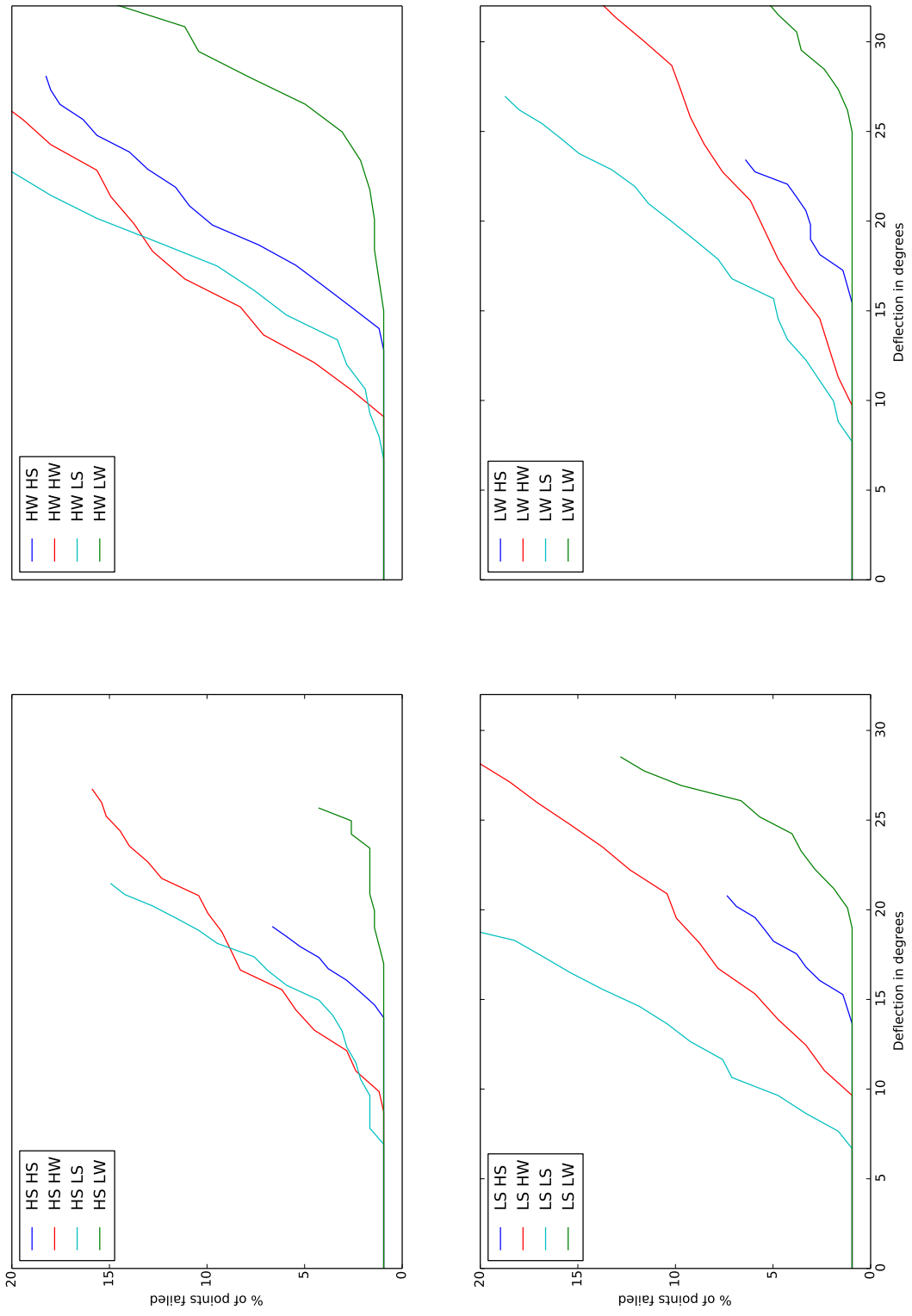

Figure B.11: Total number of points failed by deflection at age 15. Deflection is calculated at the tip of the stem.

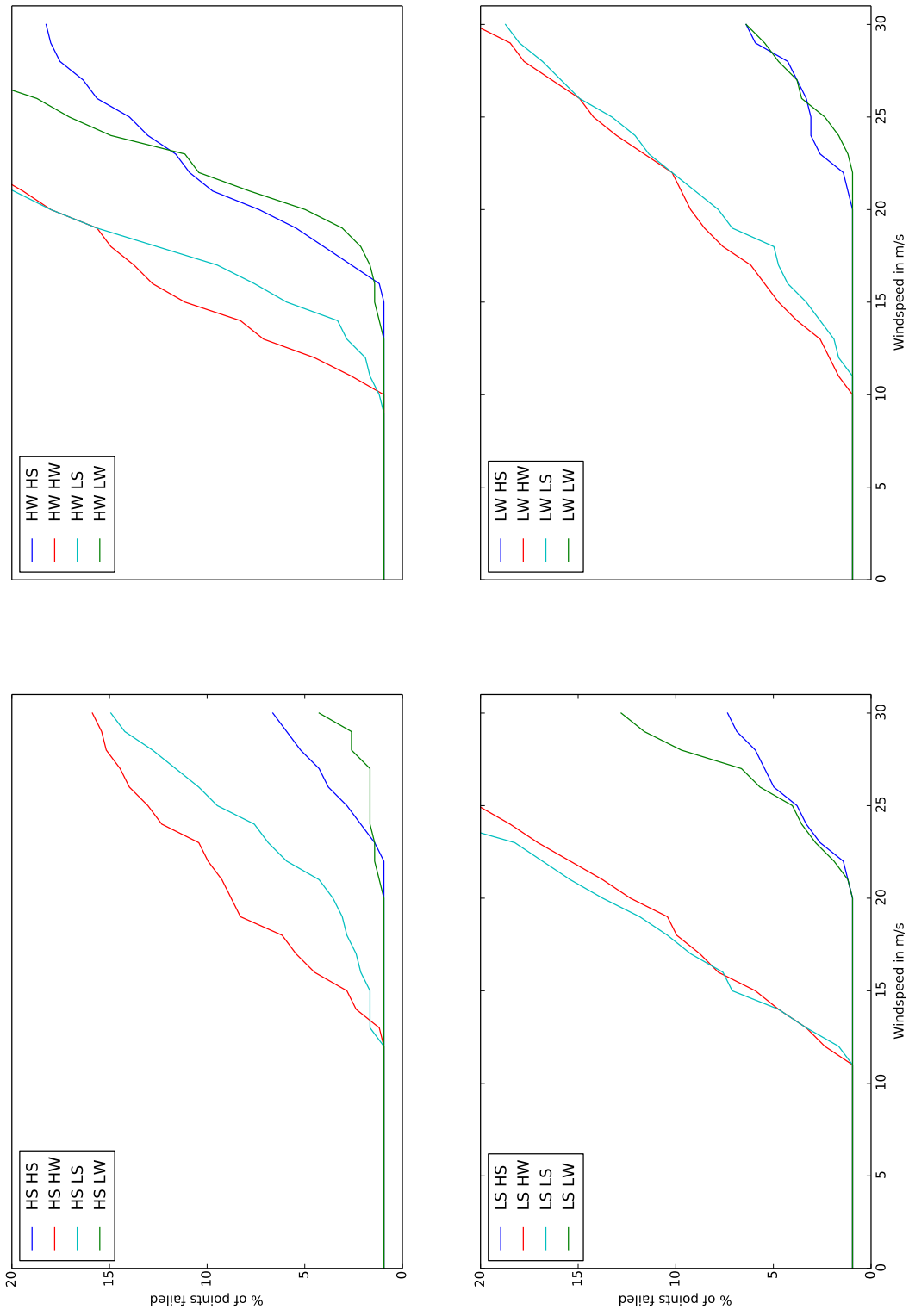

Figure B.12: Proportion of points failed at differing wind speeds at age 15.

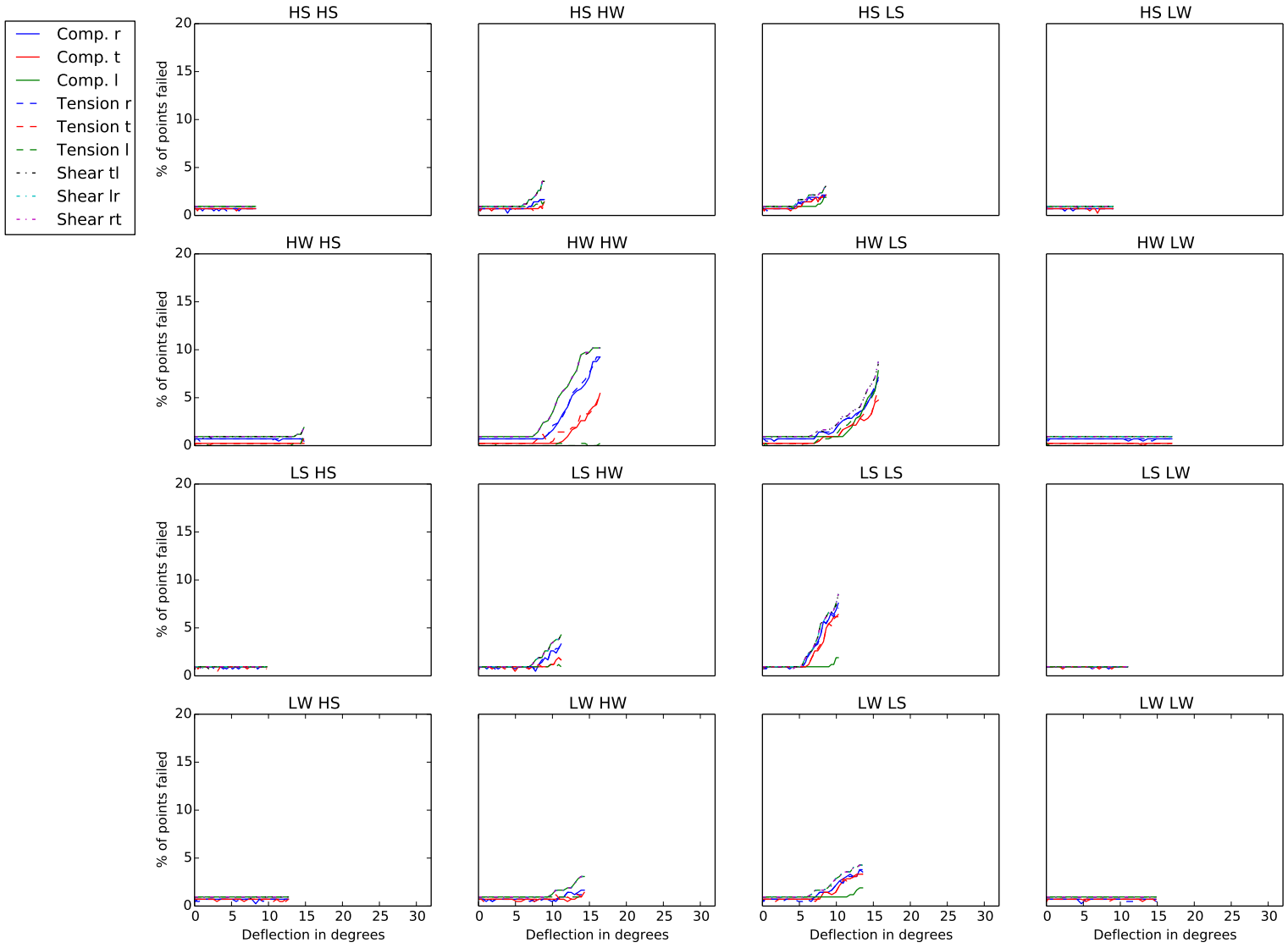

Figure B.13: Proportion of points failed in a given direction at age 5. Deflection is calculated at the tip of the stem.

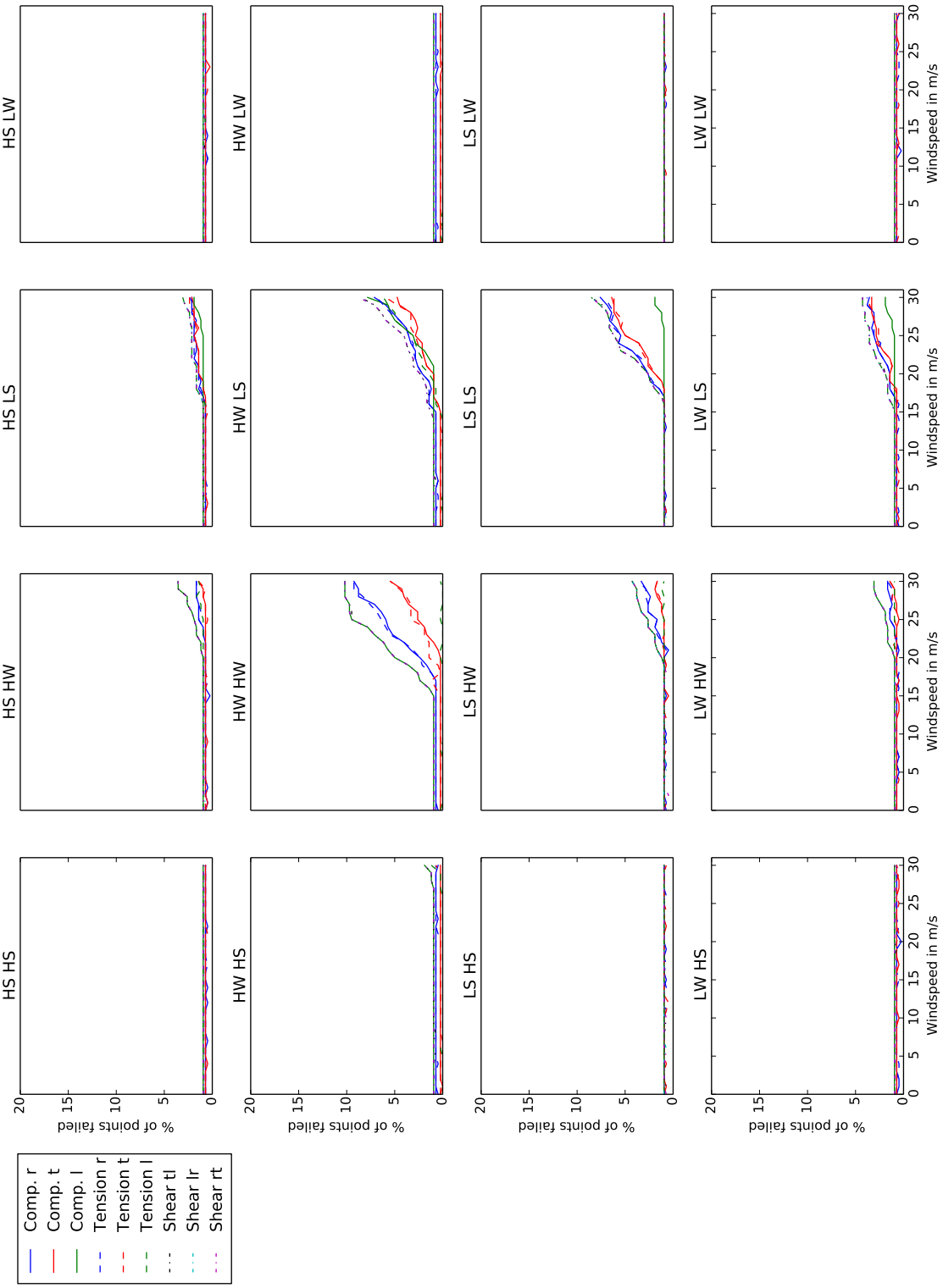

Figure B.14: Proportion of points failed in a given direction at age 5.

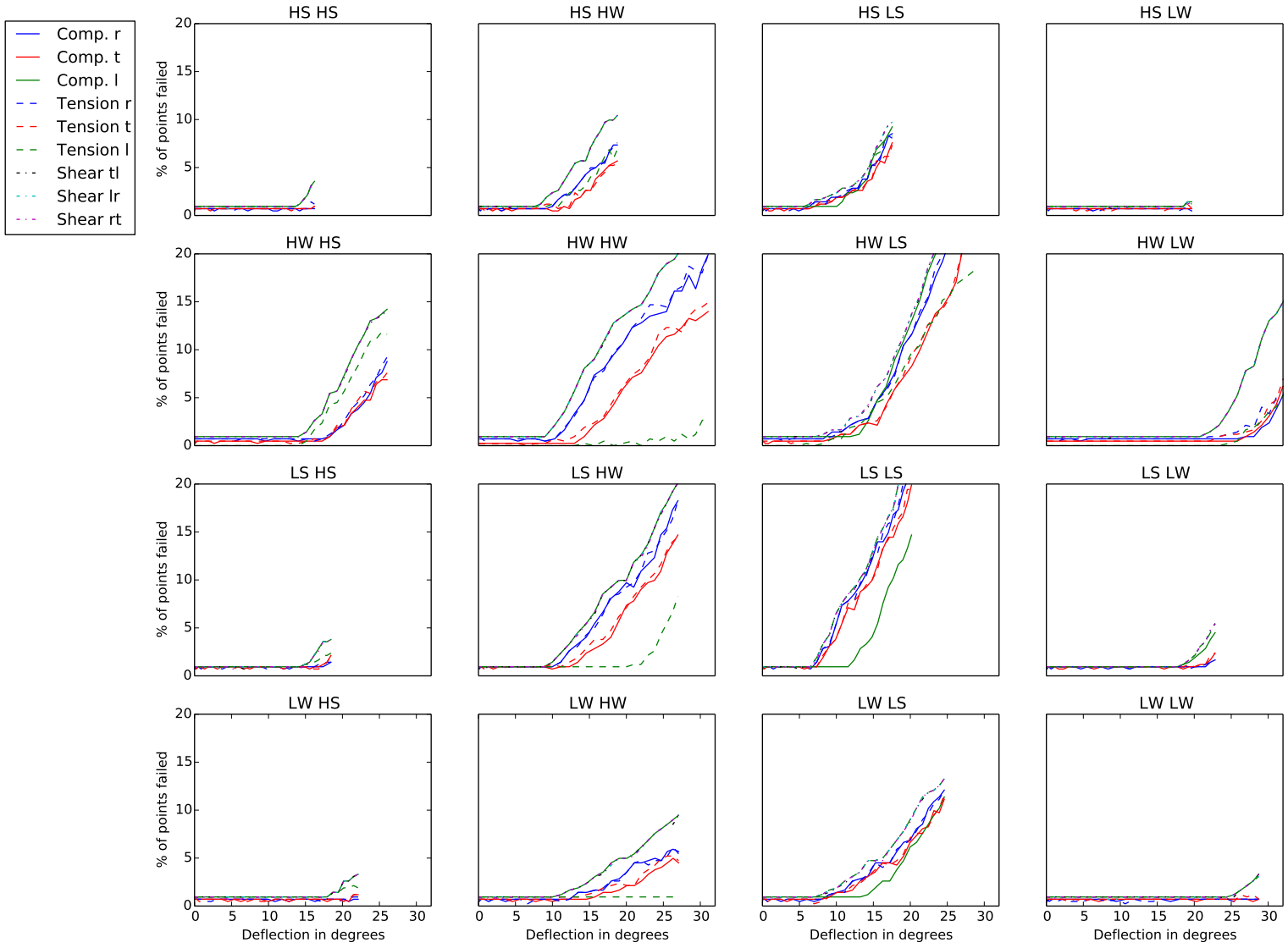

Figure B.15: Proportion of points failed in a given direction at age 10. Deflection is calculated at the tip of the stem.

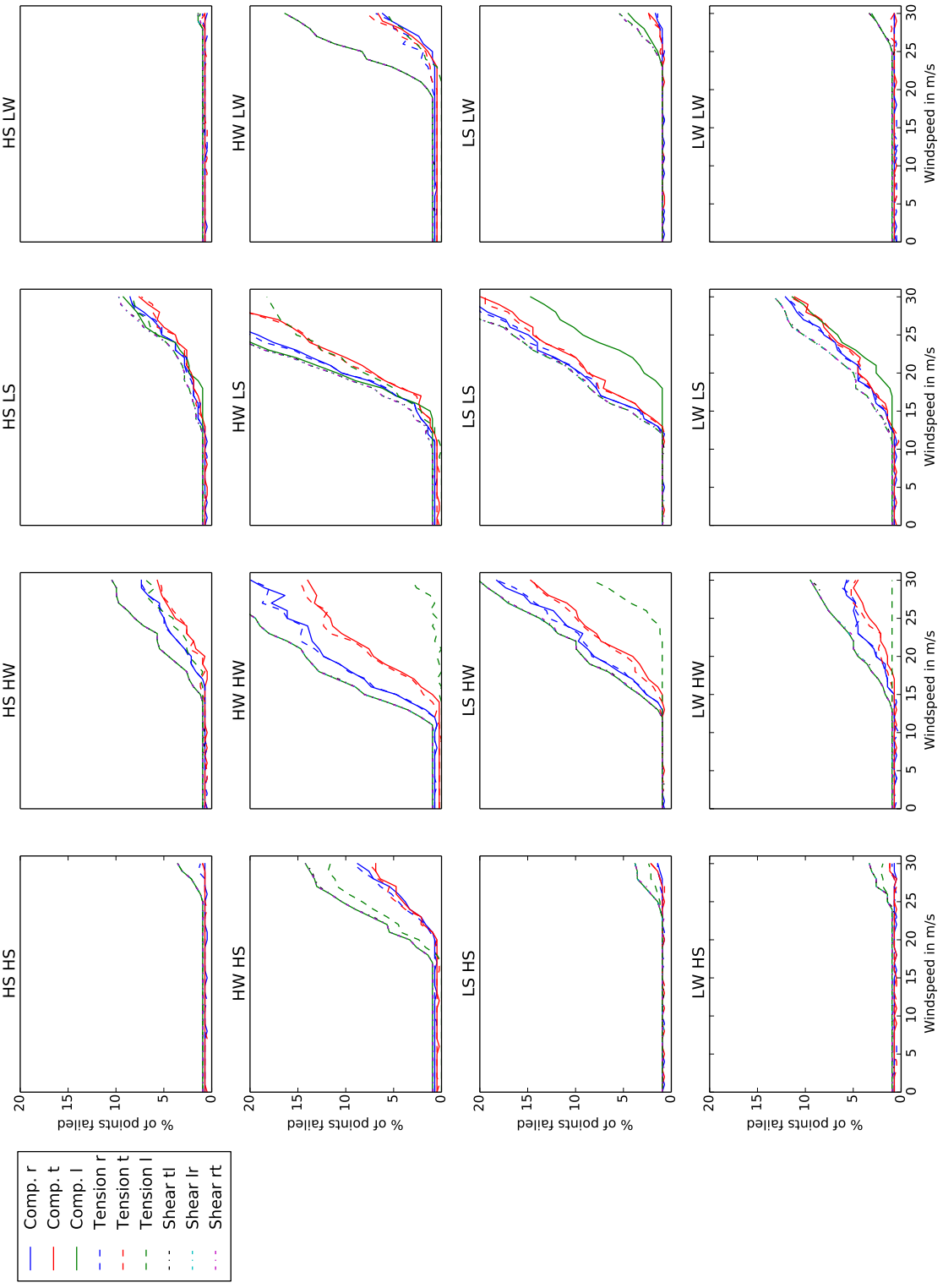

Figure B.16: Proportion of points failed in a given direction at age 10.

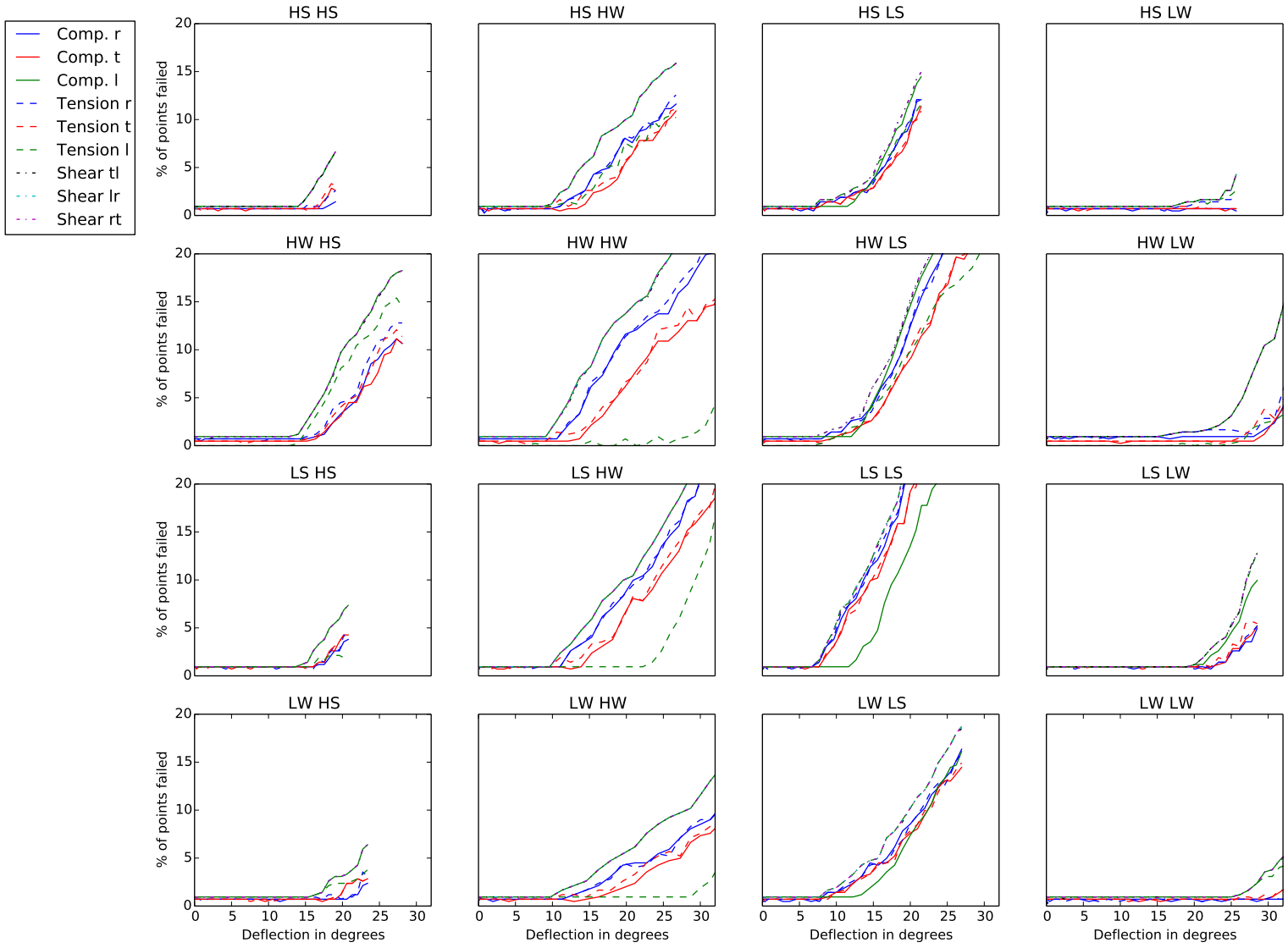

Figure B.17: Proportion of points failed in a given direction at age 15. Deflection is calculated at the tip of the stem.

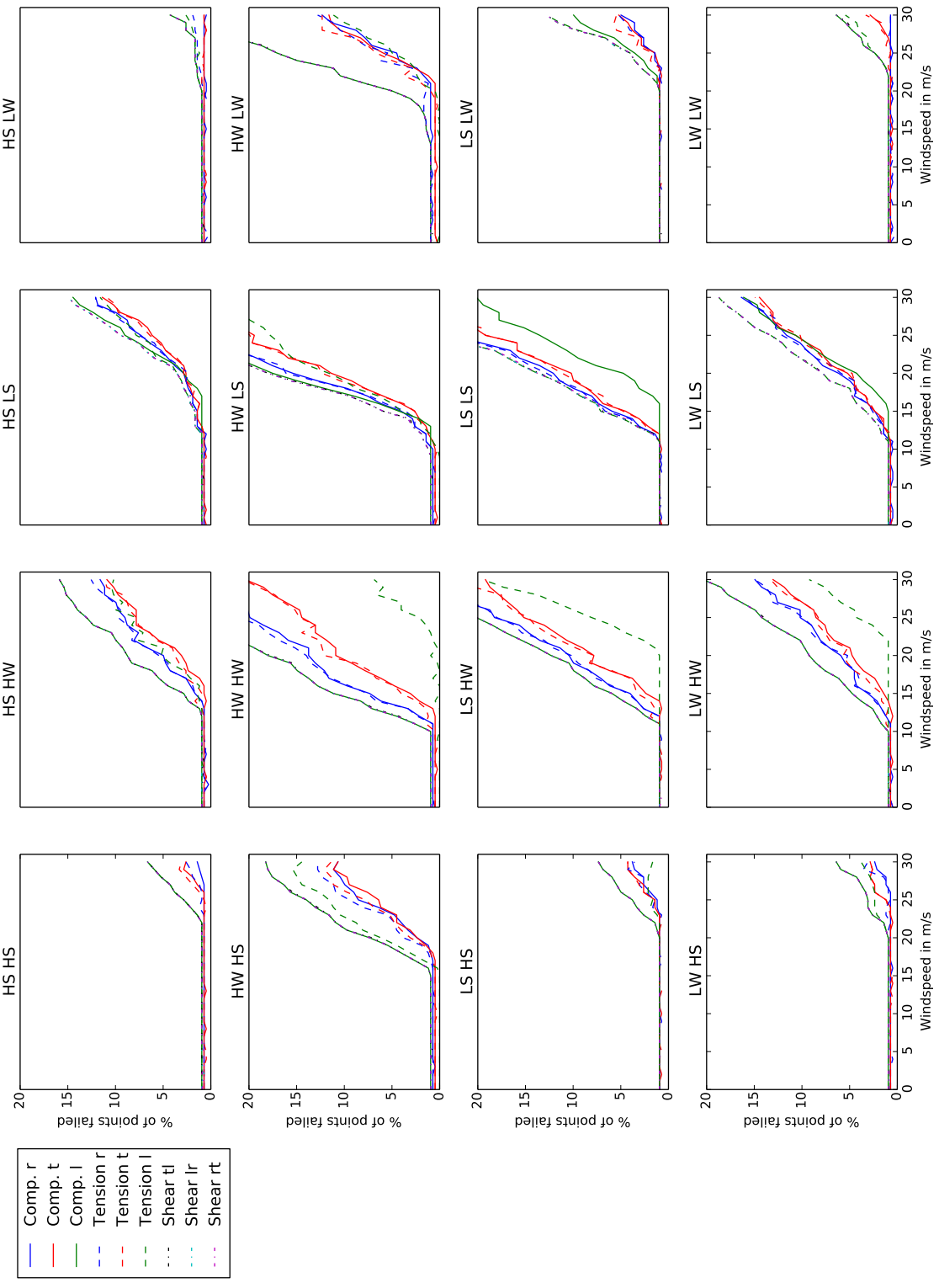

Figure B.18: Proportion of points failed in a given direction at age 15.

Appendix C

Effect of the TRP for different aged stems, 741 stocking with growth stresses

Note that at age 5 there is no difference between open grown and 741 stems per hectare. Refer to Appendix B for these.

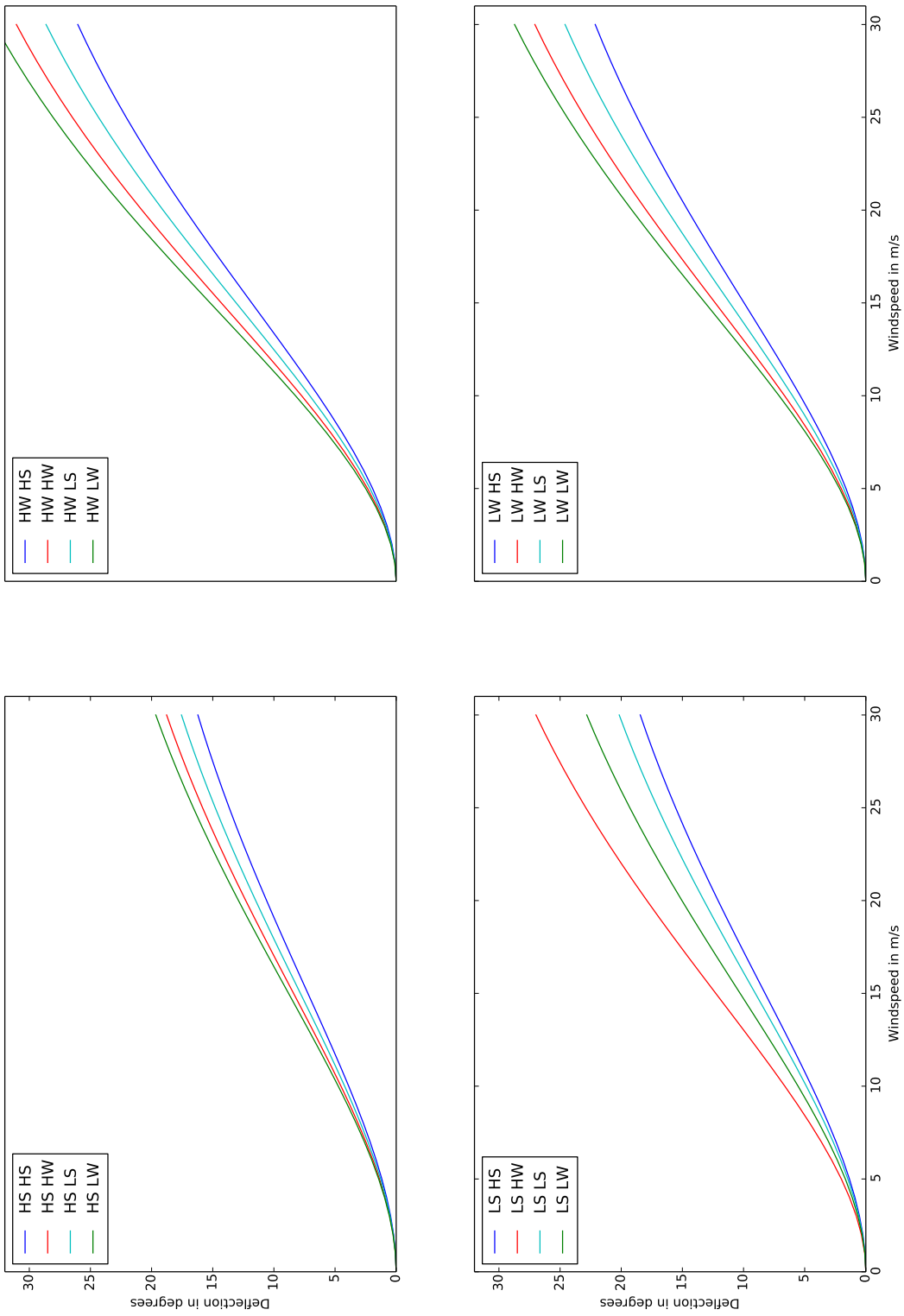

Figure C.1: Deflection in degrees for wind speeds at age 10. Deflection is calculated at the tip of the stem.

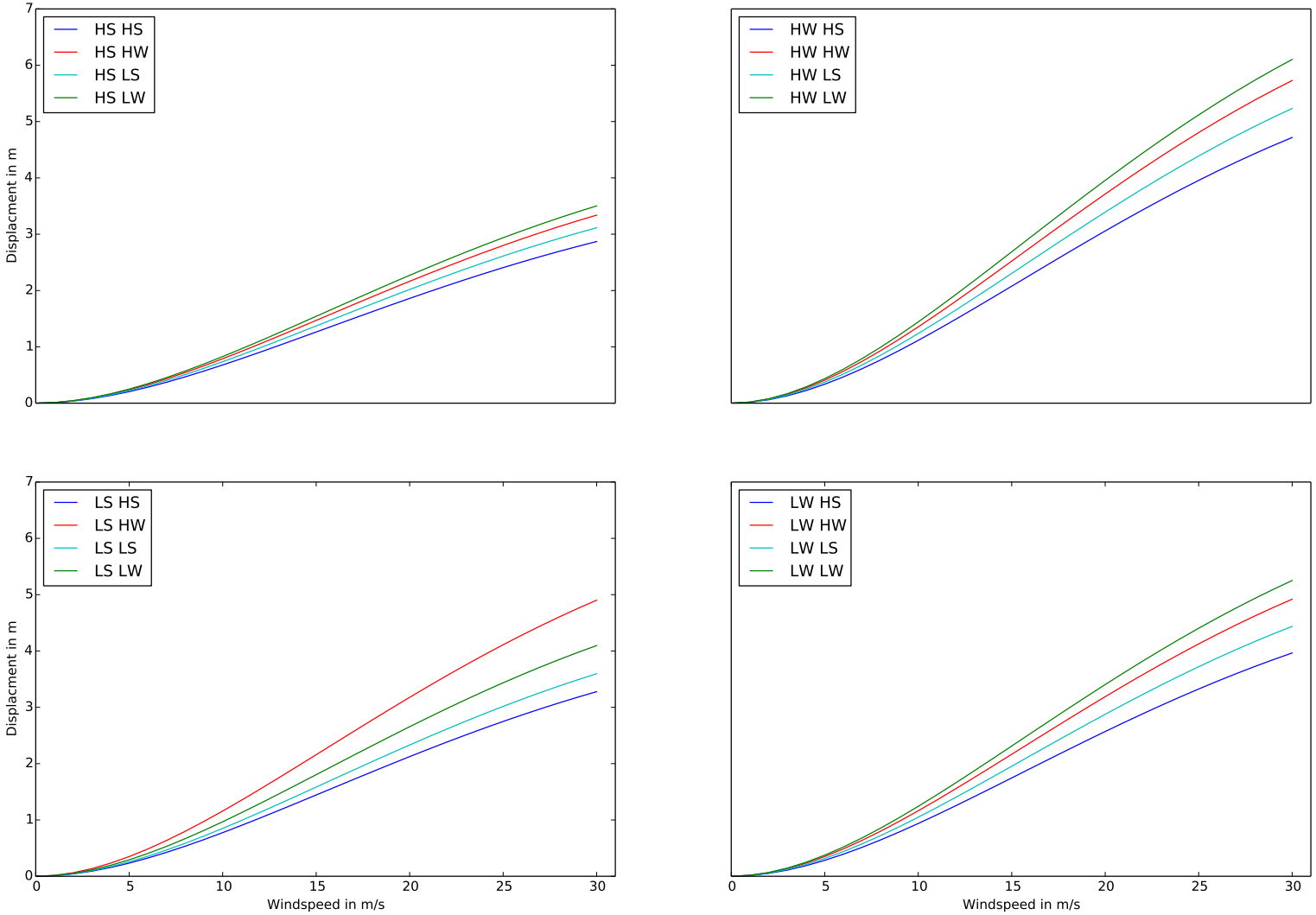

Figure C.2: Displacement in m for wind speeds at age 10. Displacement is calculated at the tip of the stem.

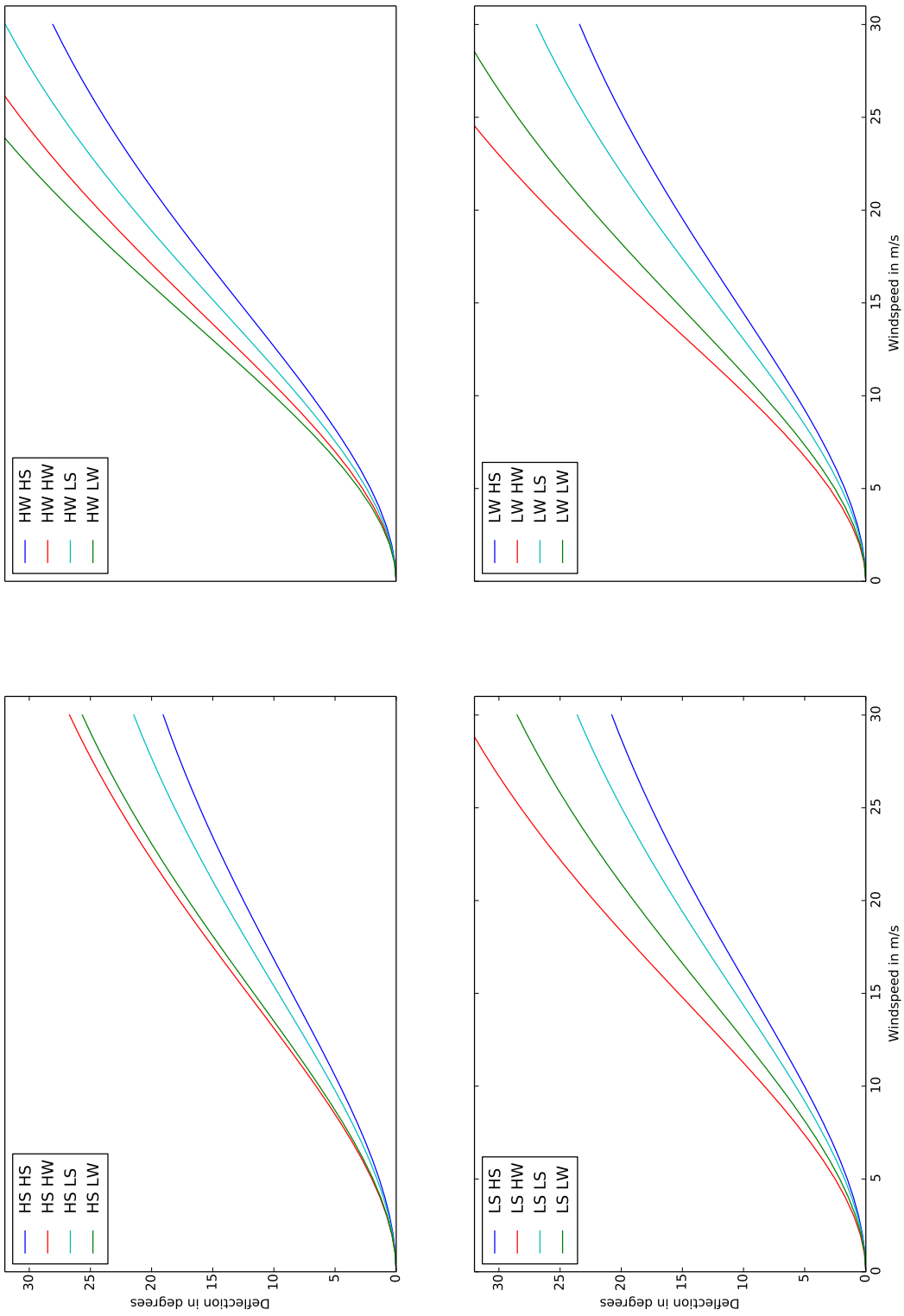

Figure C.3: Deflection in degrees for wind speeds at age 15. Deflection is calculated at the tip of the stem.

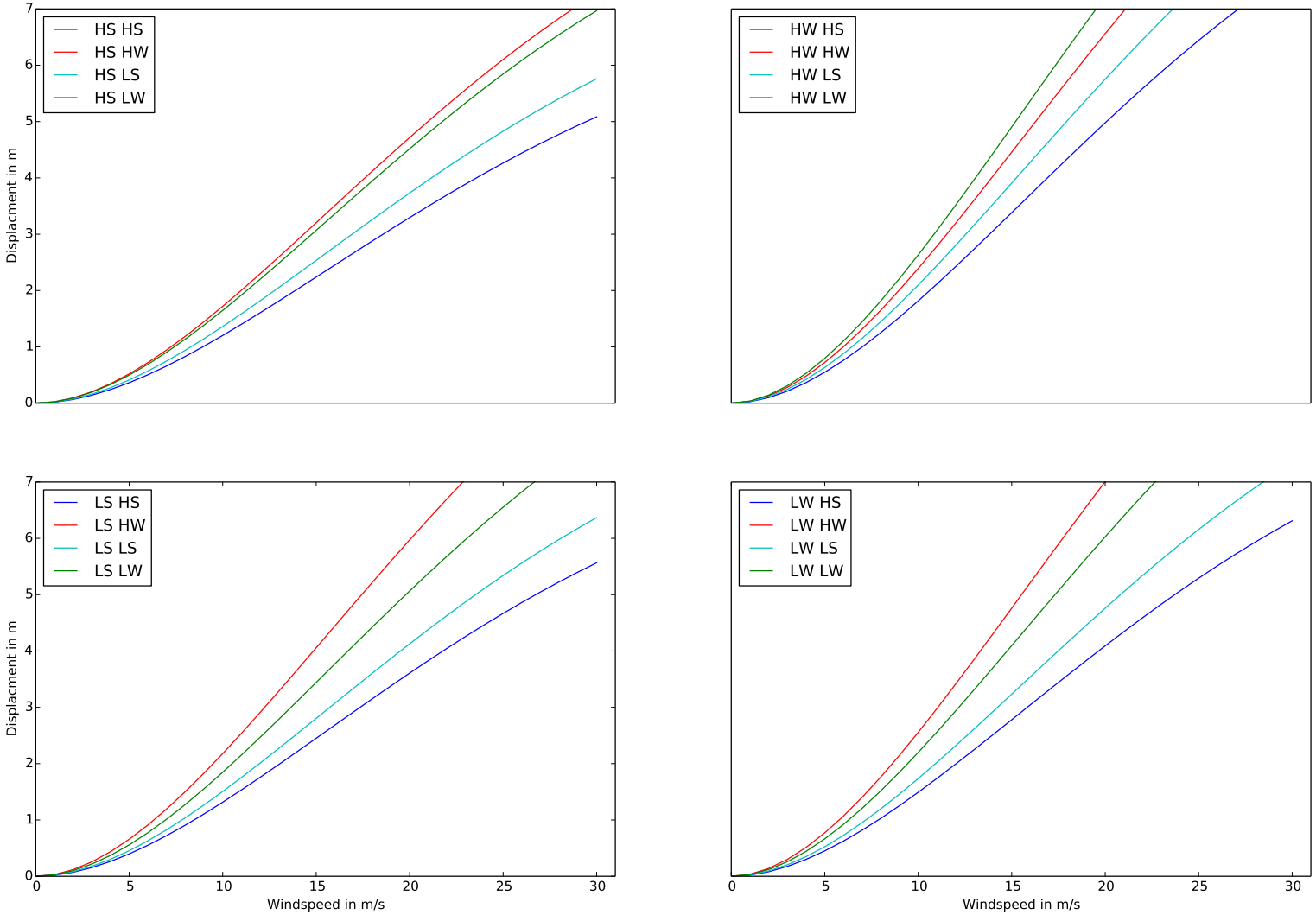

Figure C.4: Displacement in m for wind speeds at age 15. Displacement is calculated at the tip of the stem.

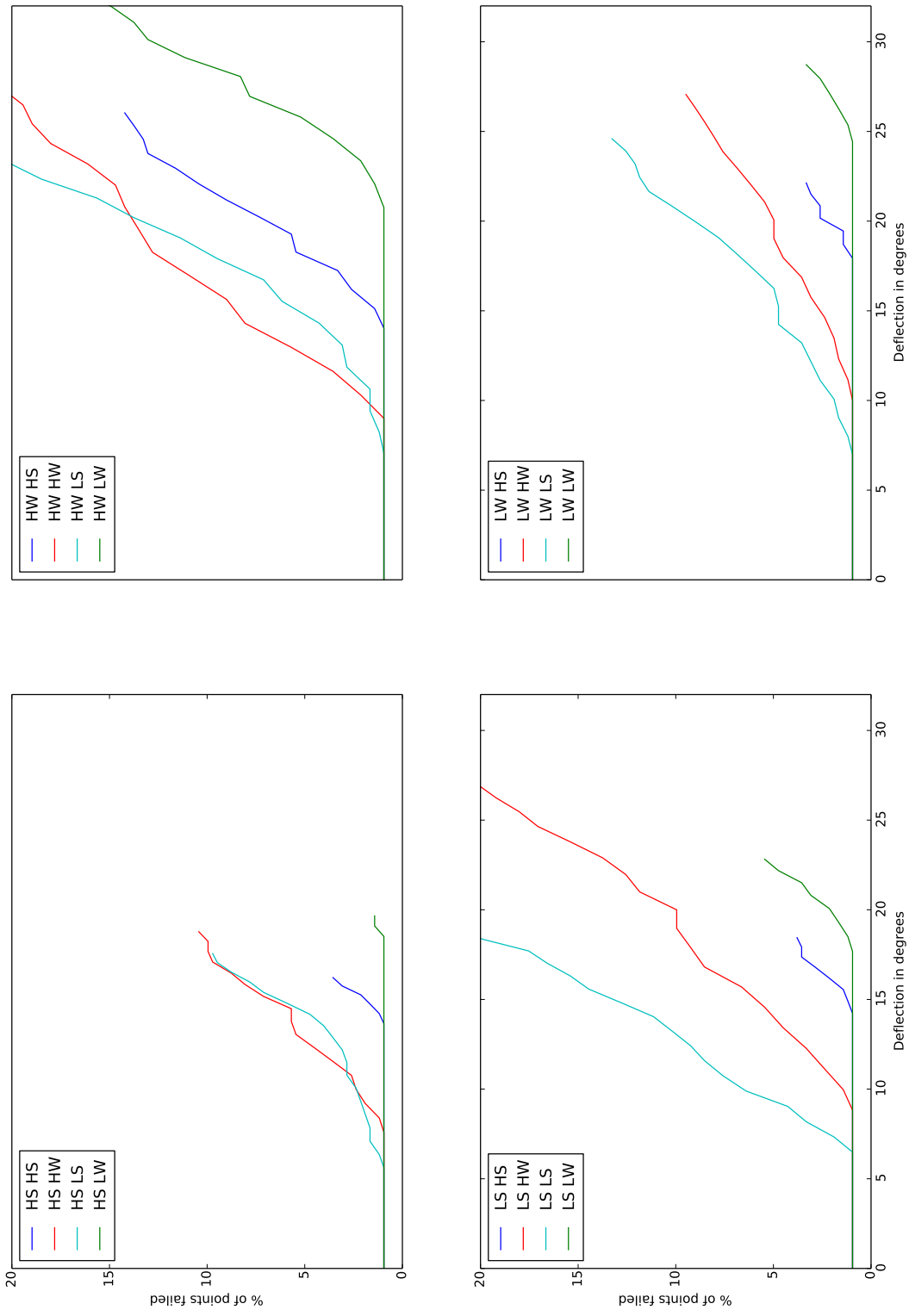

Figure C.5: Proportion of points failed by deflection at age 10. Deflection is calculated at the tip of the stem.

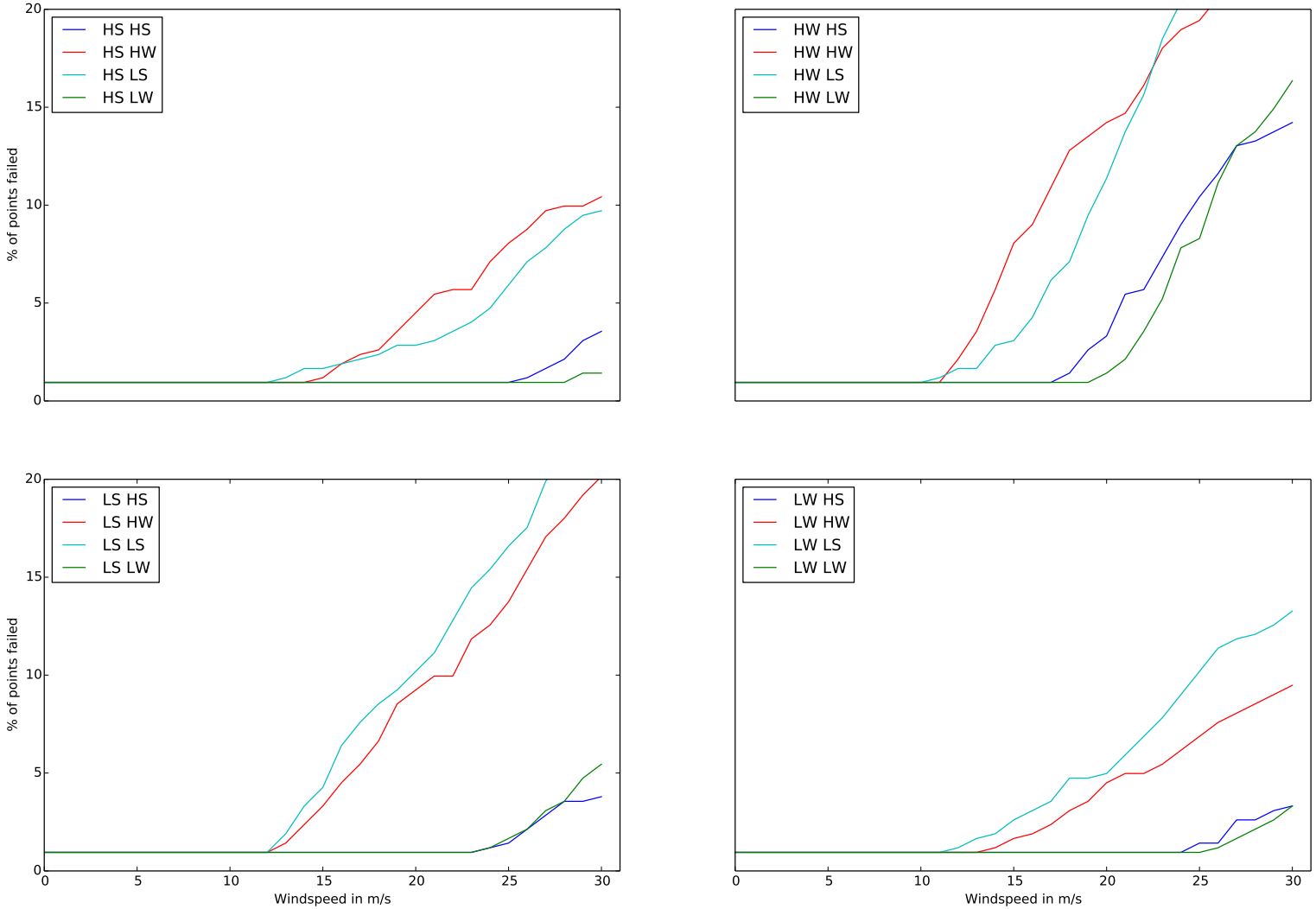

Figure C.6: Proportion of points failed at differing wind speeds at age 10.

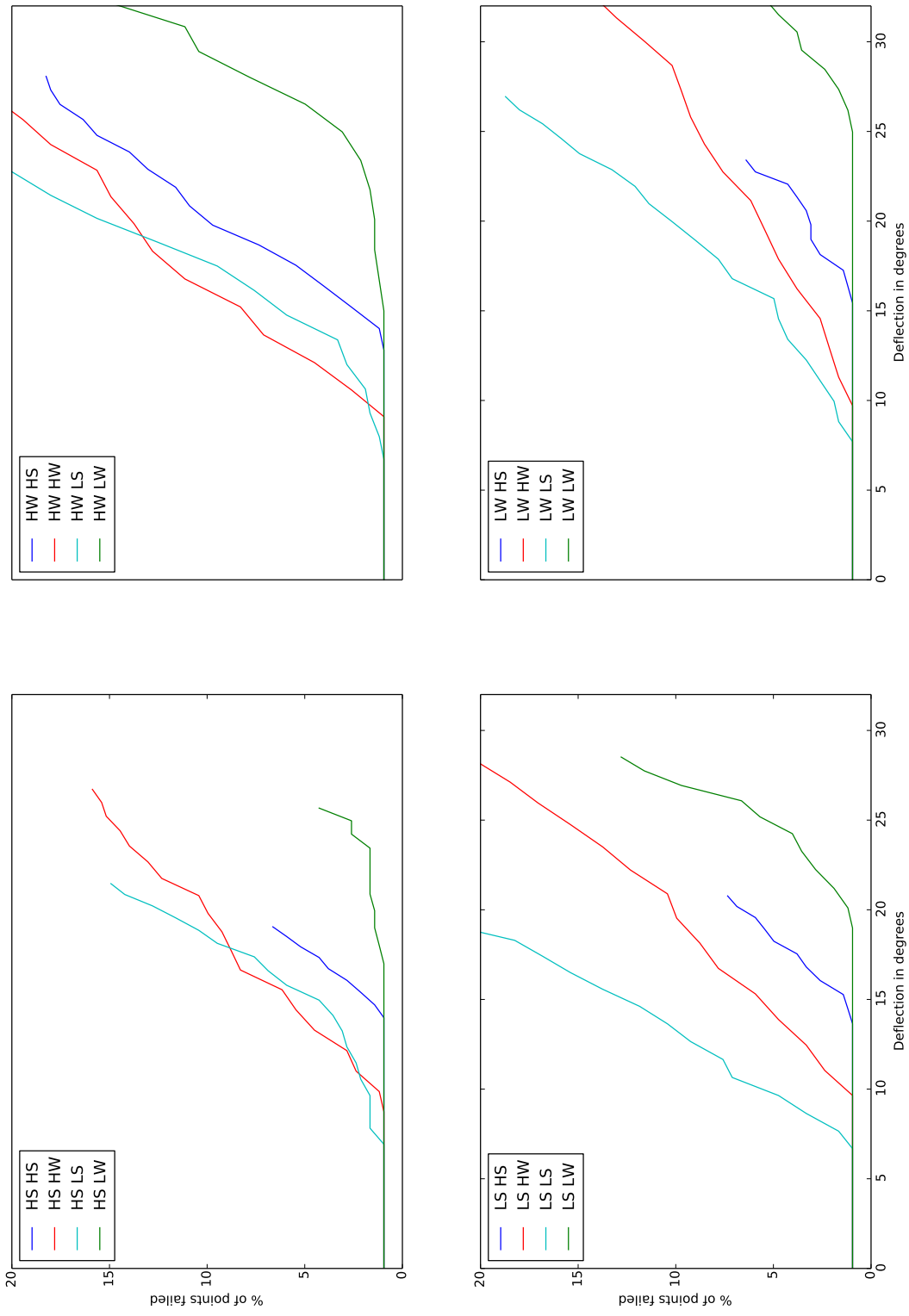

Figure C.7: Total number of points failed by deflection at age 15. Deflection is calculated at the tip of the stem.

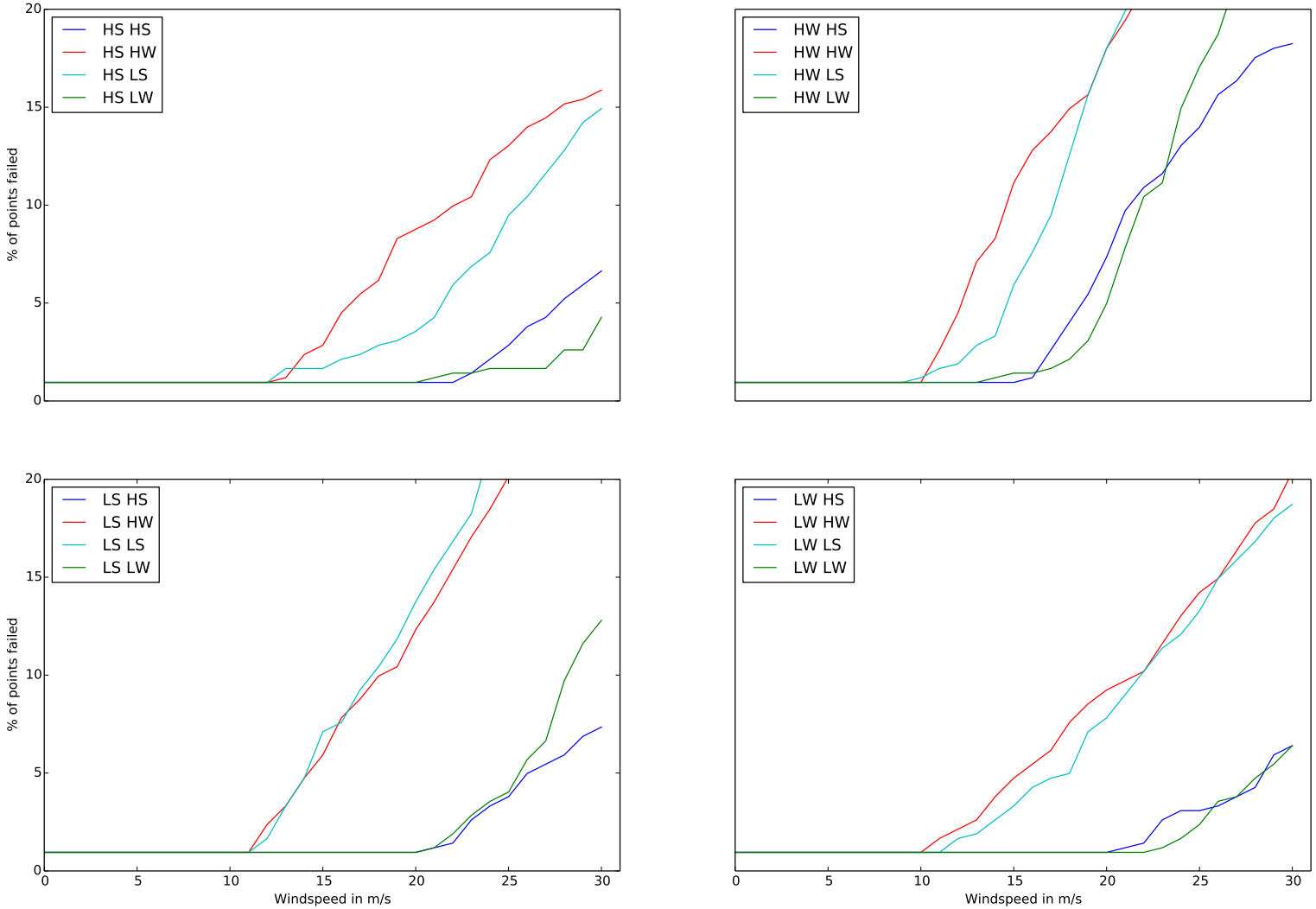

Figure C.8: Proportion of points failed at differing wind speeds at age 15.

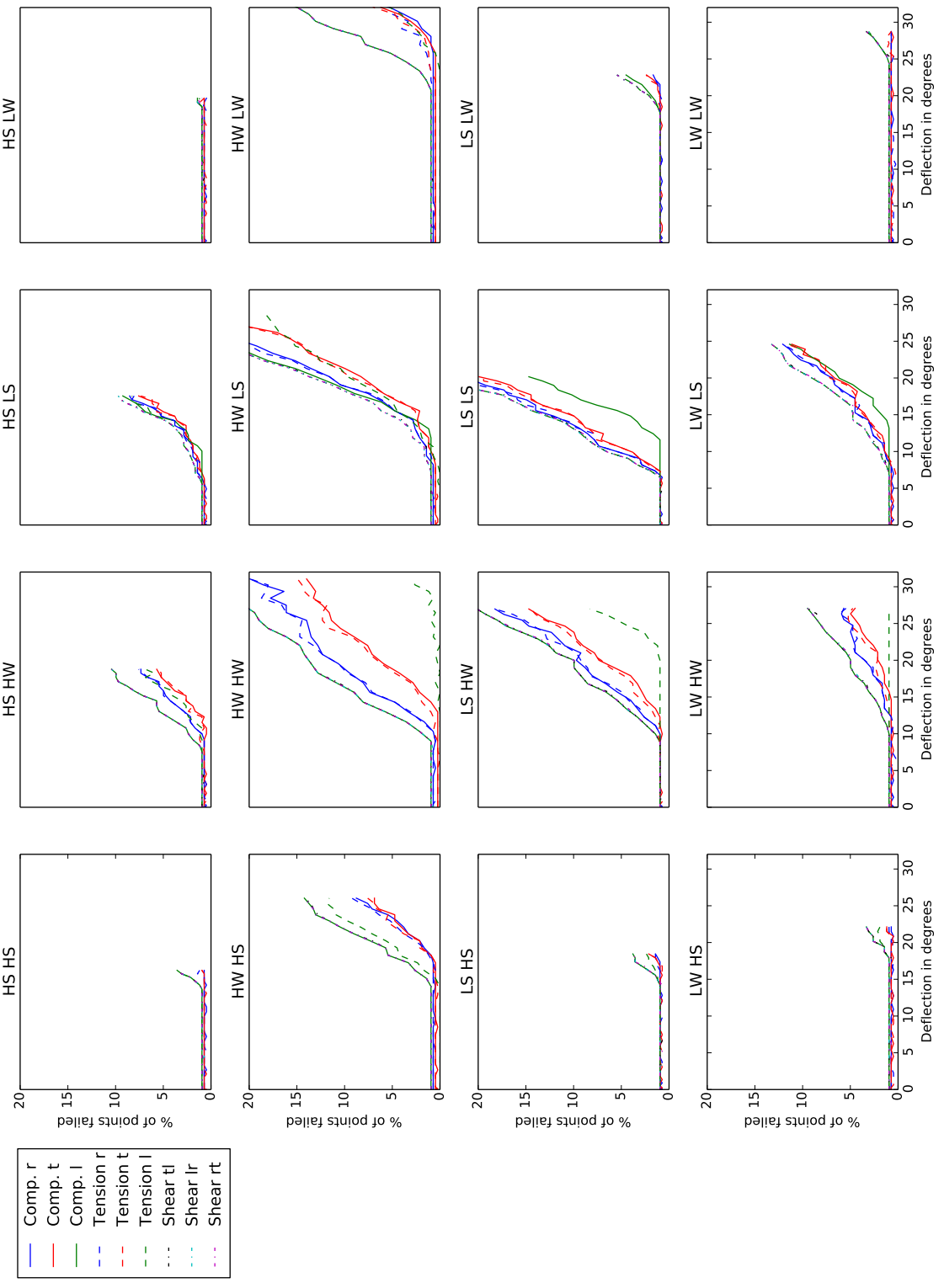

Figure C.9: Proportion of points failed in a given direction at age 10. Deflection is calculated at the tip of the stem.

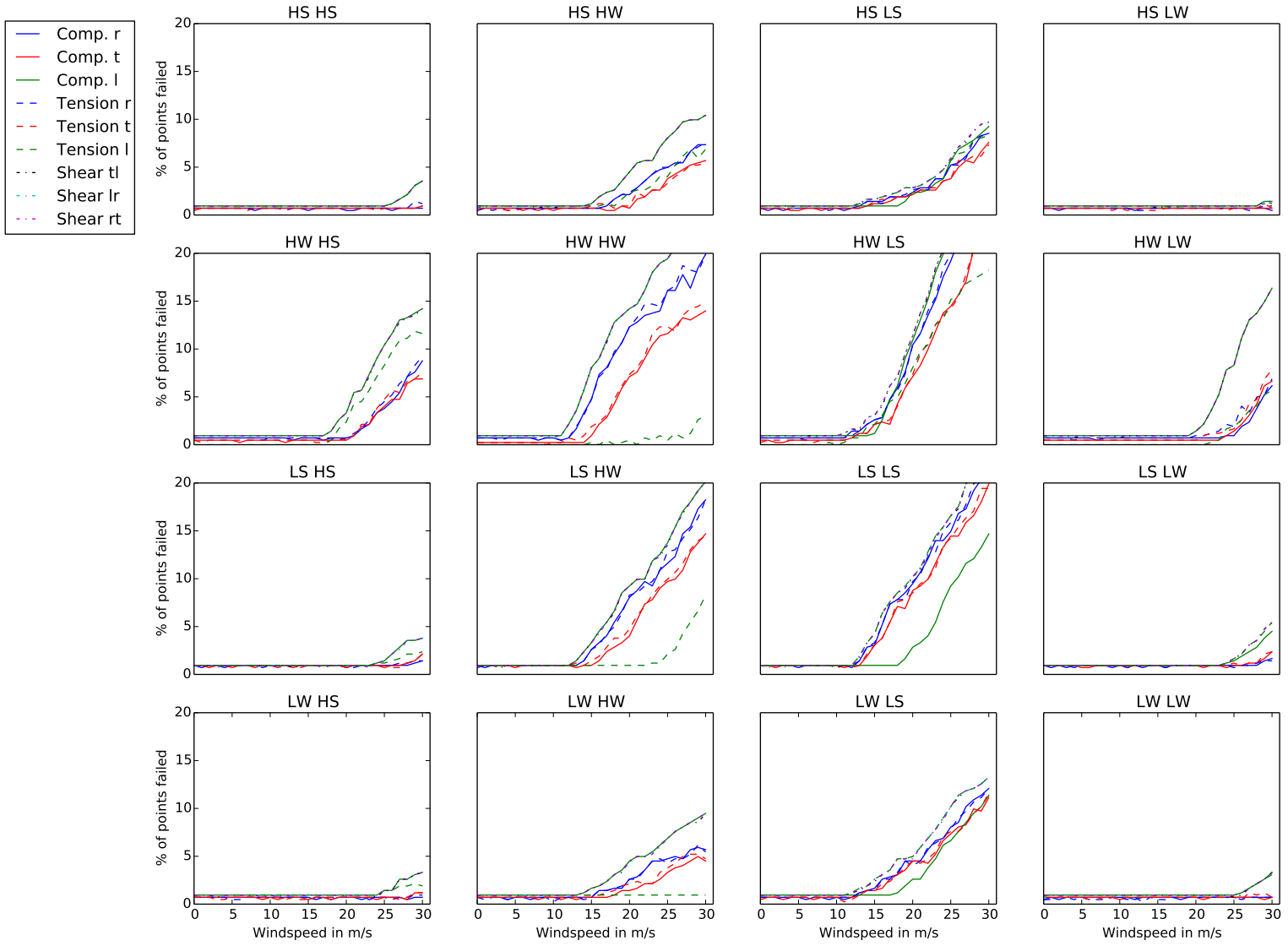

Figure C.10: Proportion of points failed in a given direction at age 10.

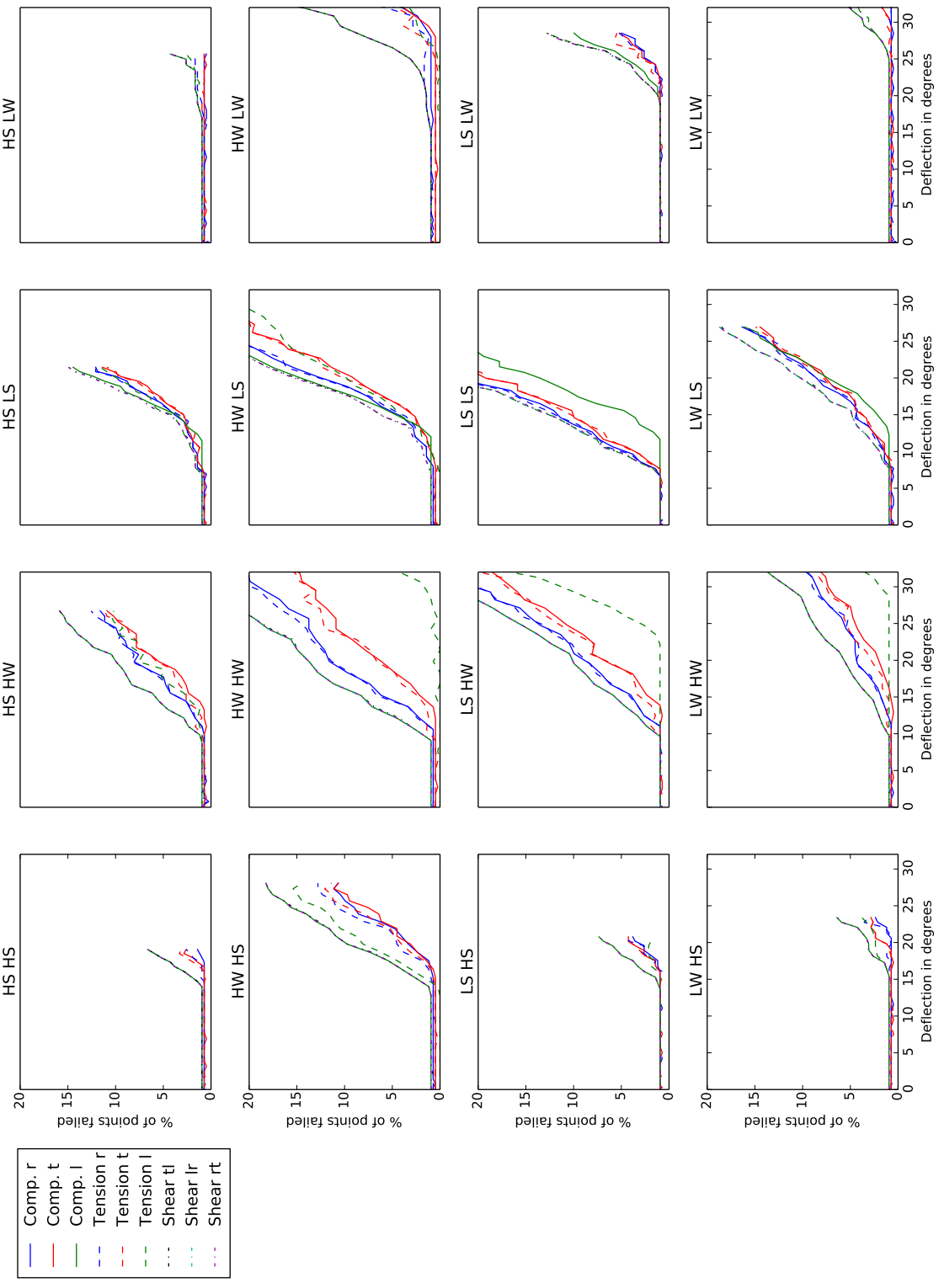

Figure C.11: Proportion of points failed in a given direction at age 15. Deflection is calculated at the tip of the stem.

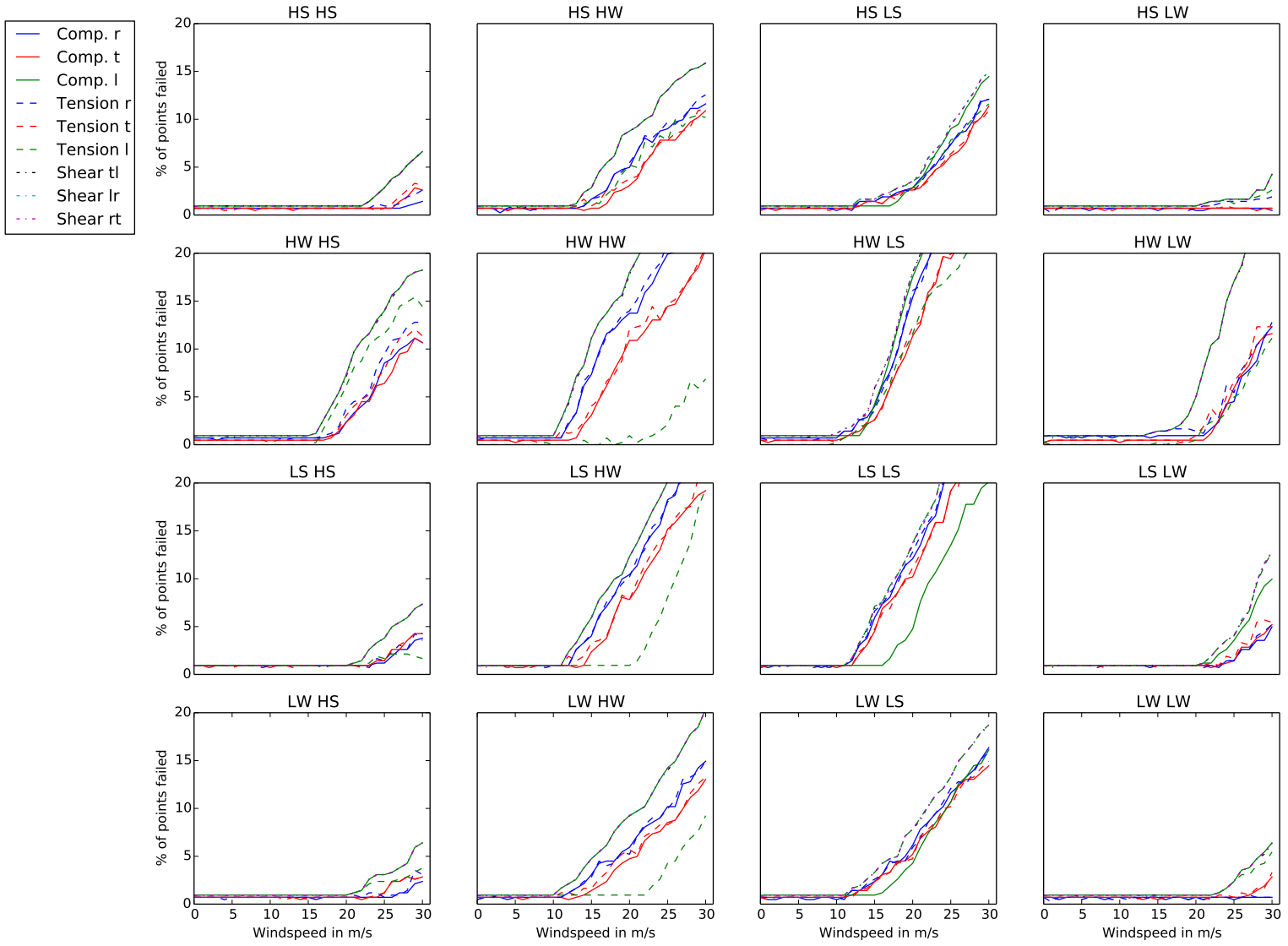

Figure C.12: Proportion of points failed in a given direction at age 15.

Appendix D

Effect of the TRP for different aged stems, open grown without growth stresses

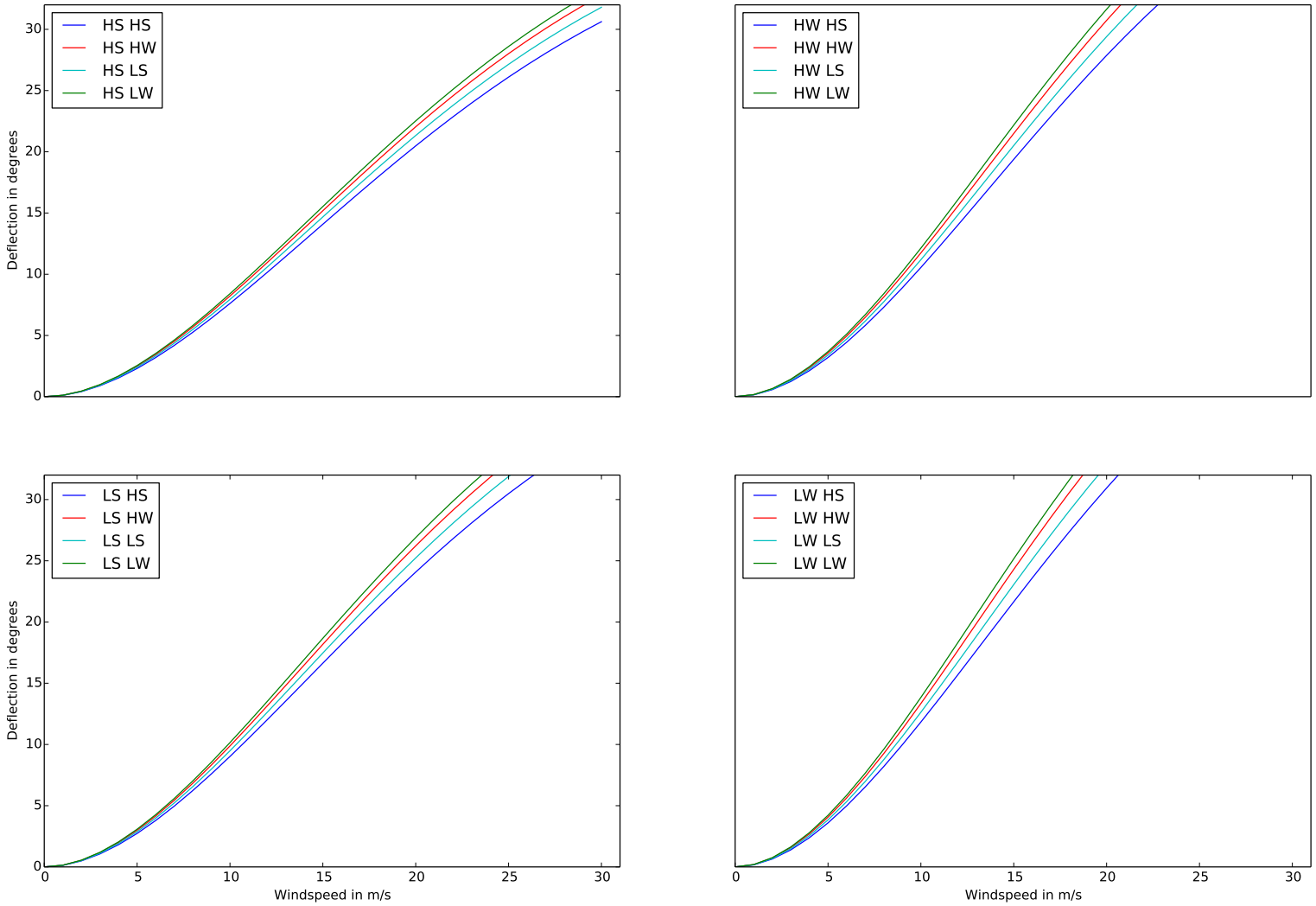

Figure D.1: Deflection in degrees for wind speeds at age 5. Deflection is calculated at the tip of the stem.

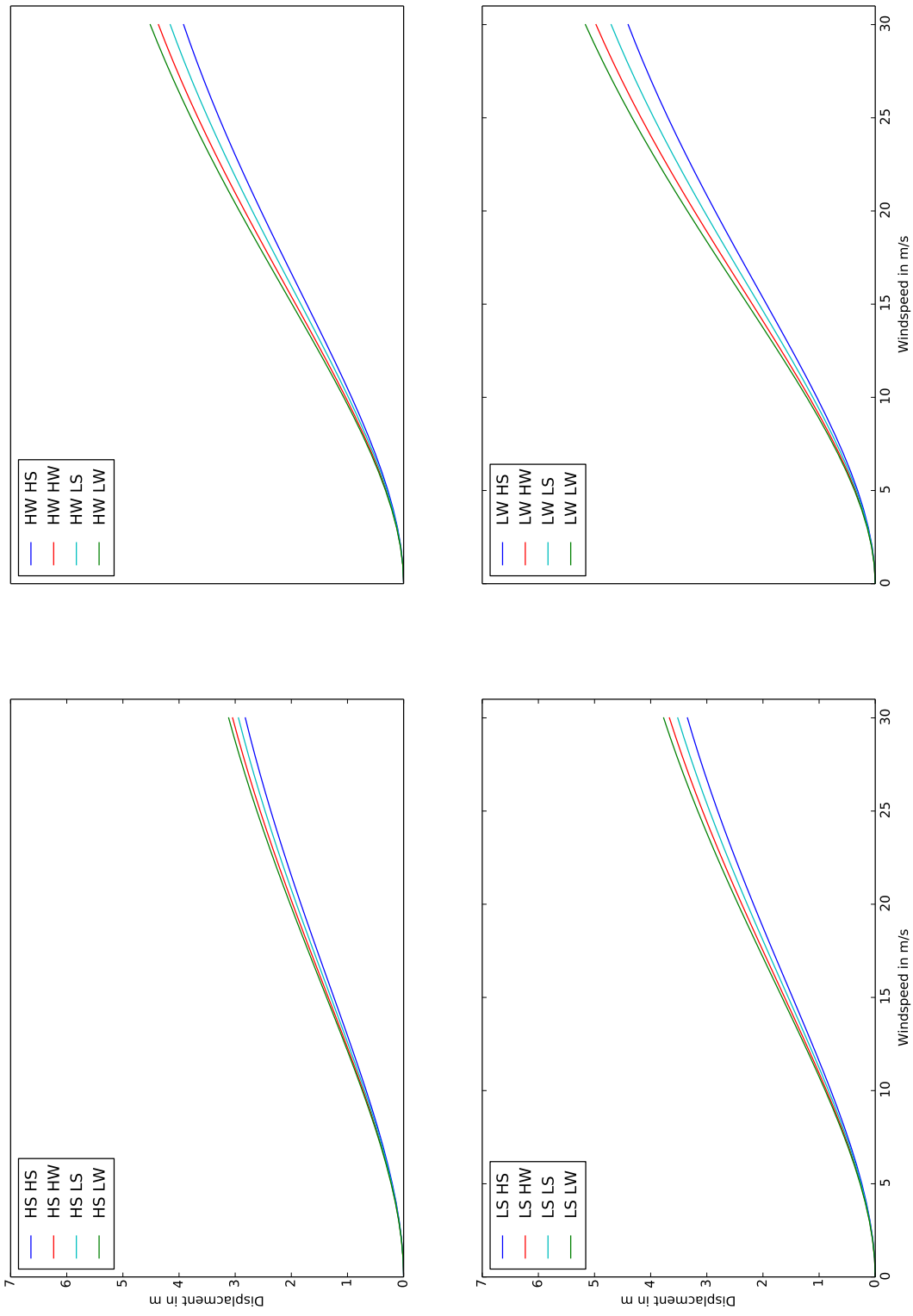

Figure D.2: Displacement in m for wind speeds at age 5. Displacement is calculated at the tip of the stem.

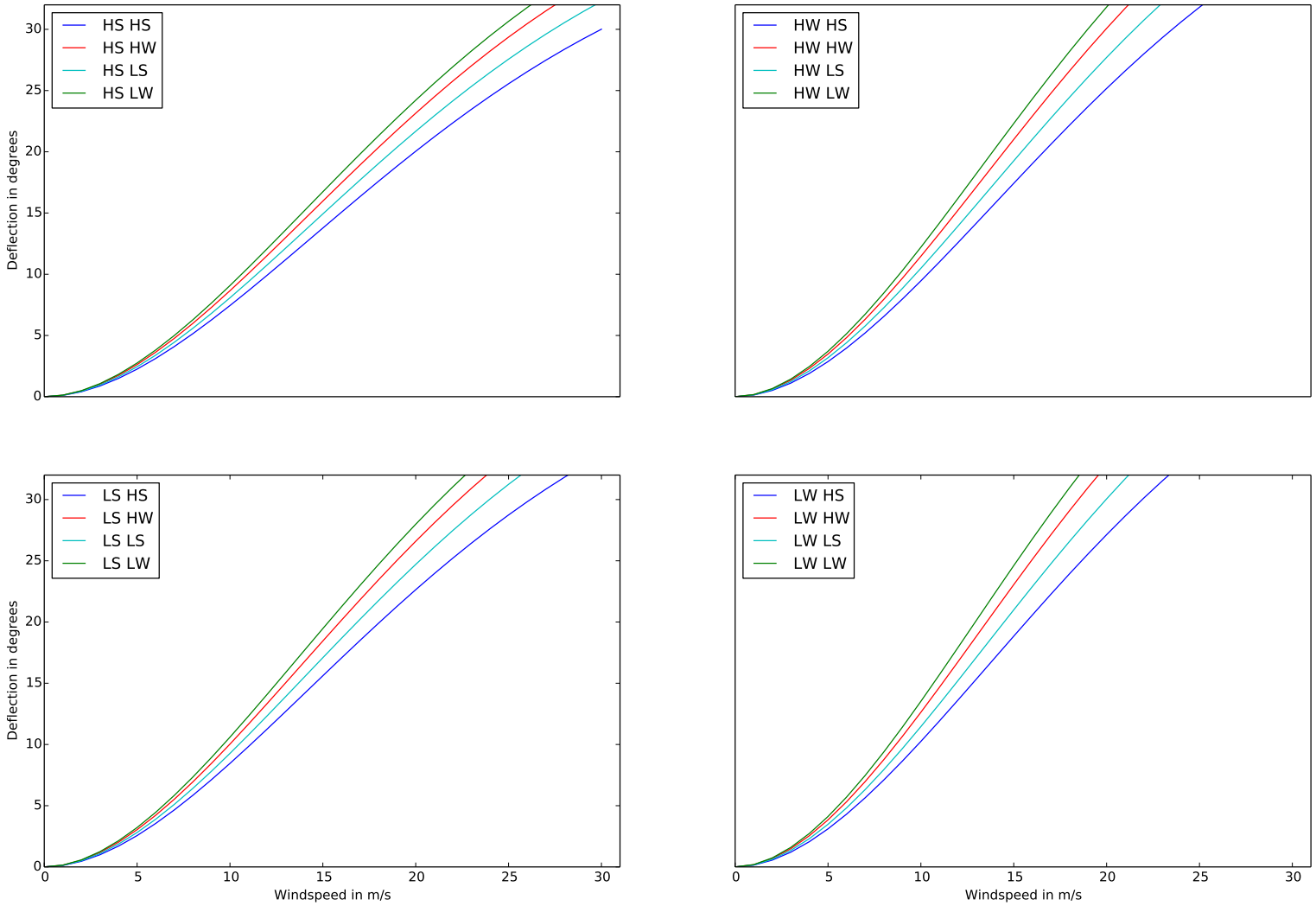

Figure D.3: Deflection in degrees for wind speeds at age 10. Deflection is calculated at the tip of the stem.

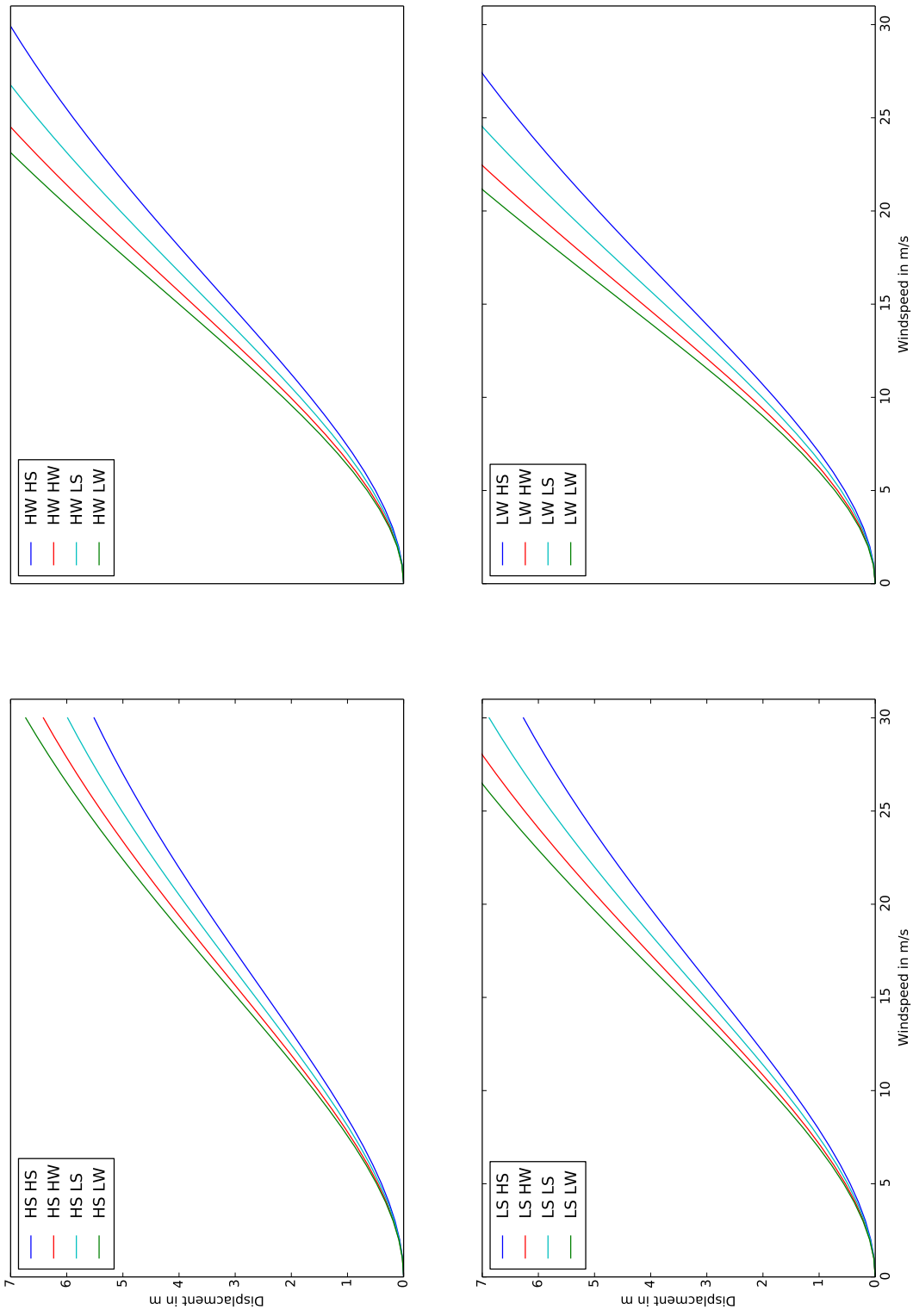

Figure D.4: Displacement in m for wind speeds at age 10. Displacement is calculated at the tip of the stem.

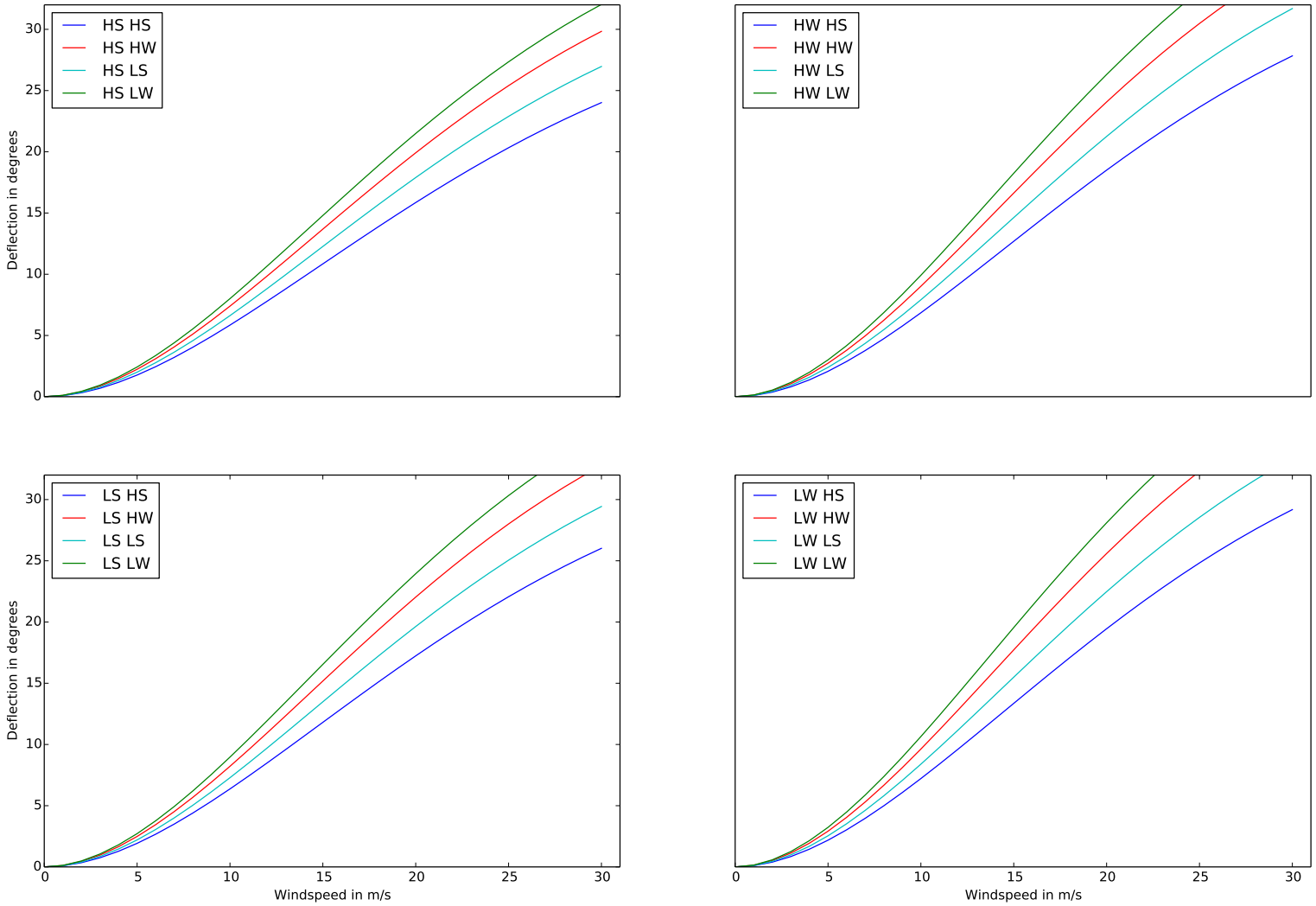

Figure D.5: Deflection in degrees for wind speeds at age 15. Deflection is calculated at the tip of the stem.

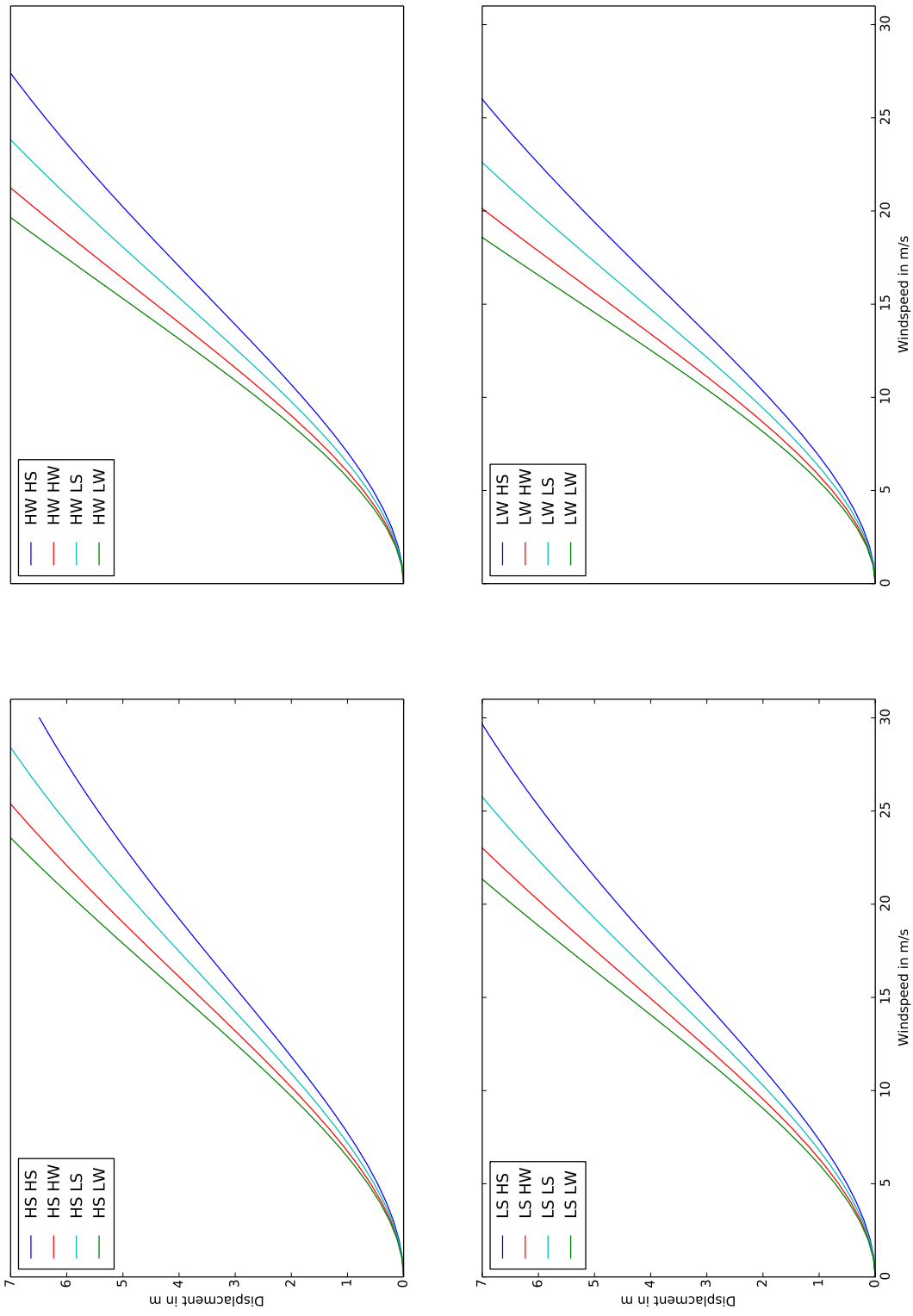

Figure D.6: Displacement in m for wind speeds at age 15. Displacement is calculated at the tip of the stem.

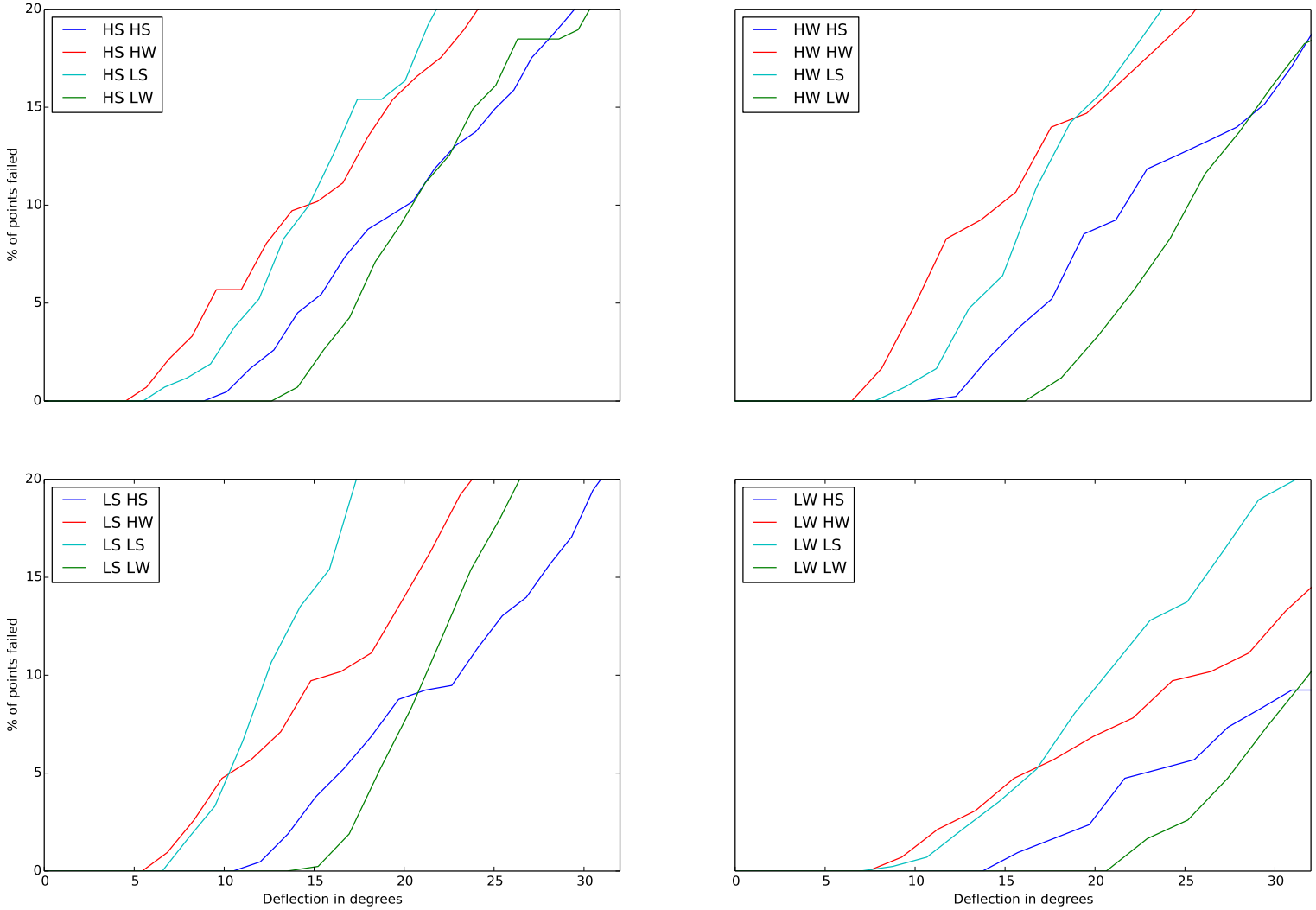

Figure D.7: Proportion of points failed by deflection at age 5. Deflection is calculated at the tip of the stem.

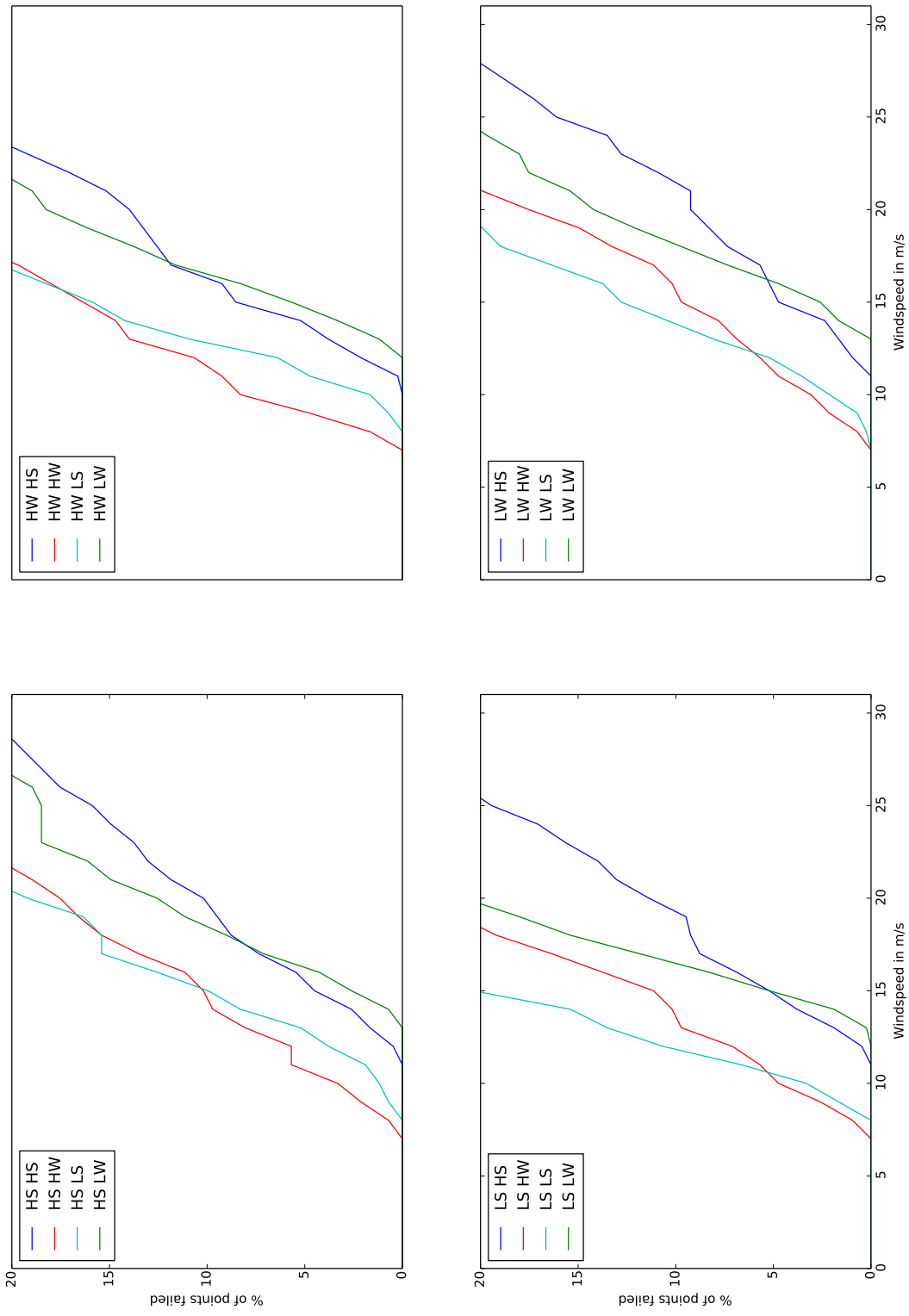

Figure D.8: Proportion of points failed at differing wind speeds wind speed at age 5.

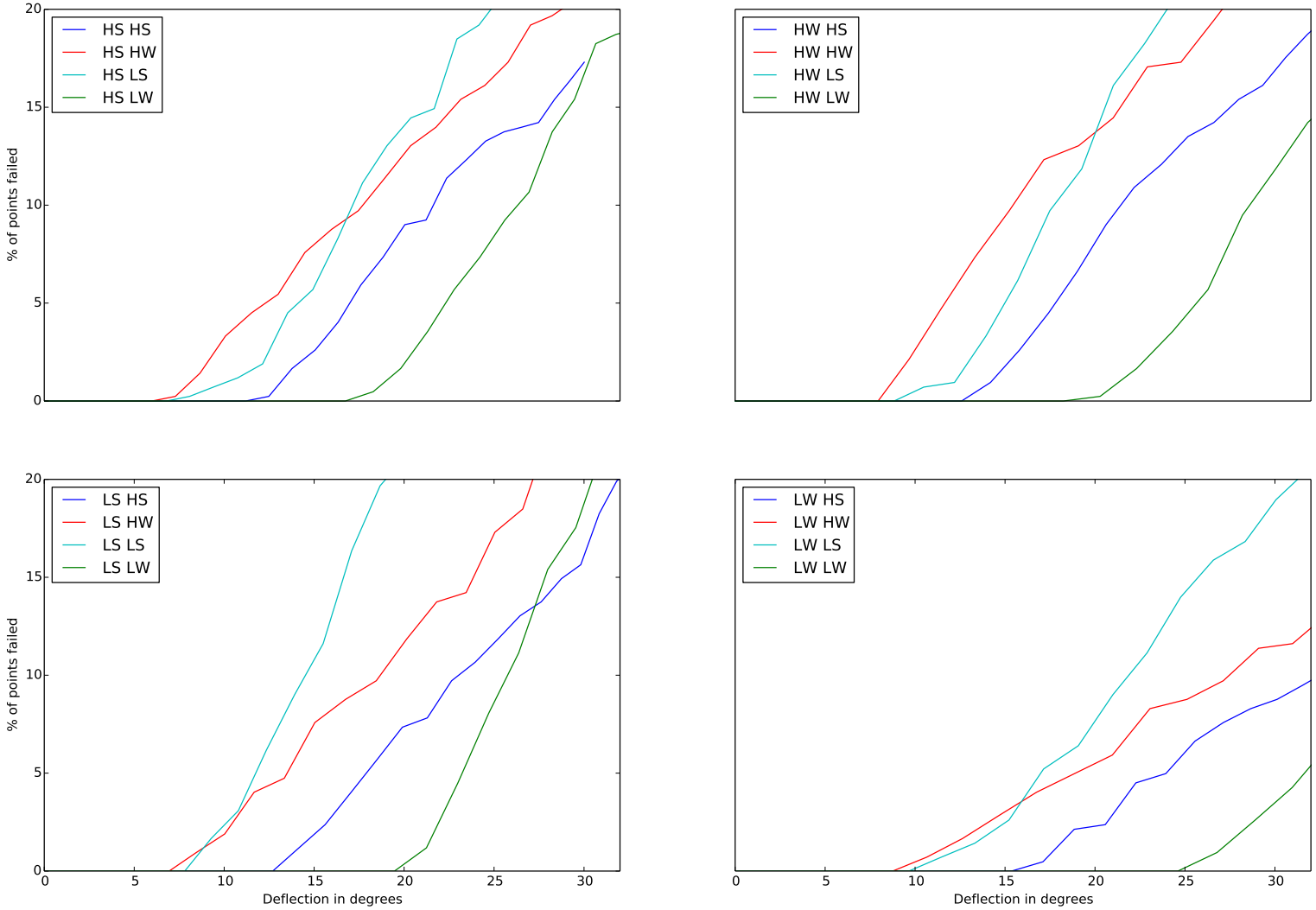

Figure D.9: Proportion of points failed by deflection at age 10. Deflection is calculated at the tip of the stem.

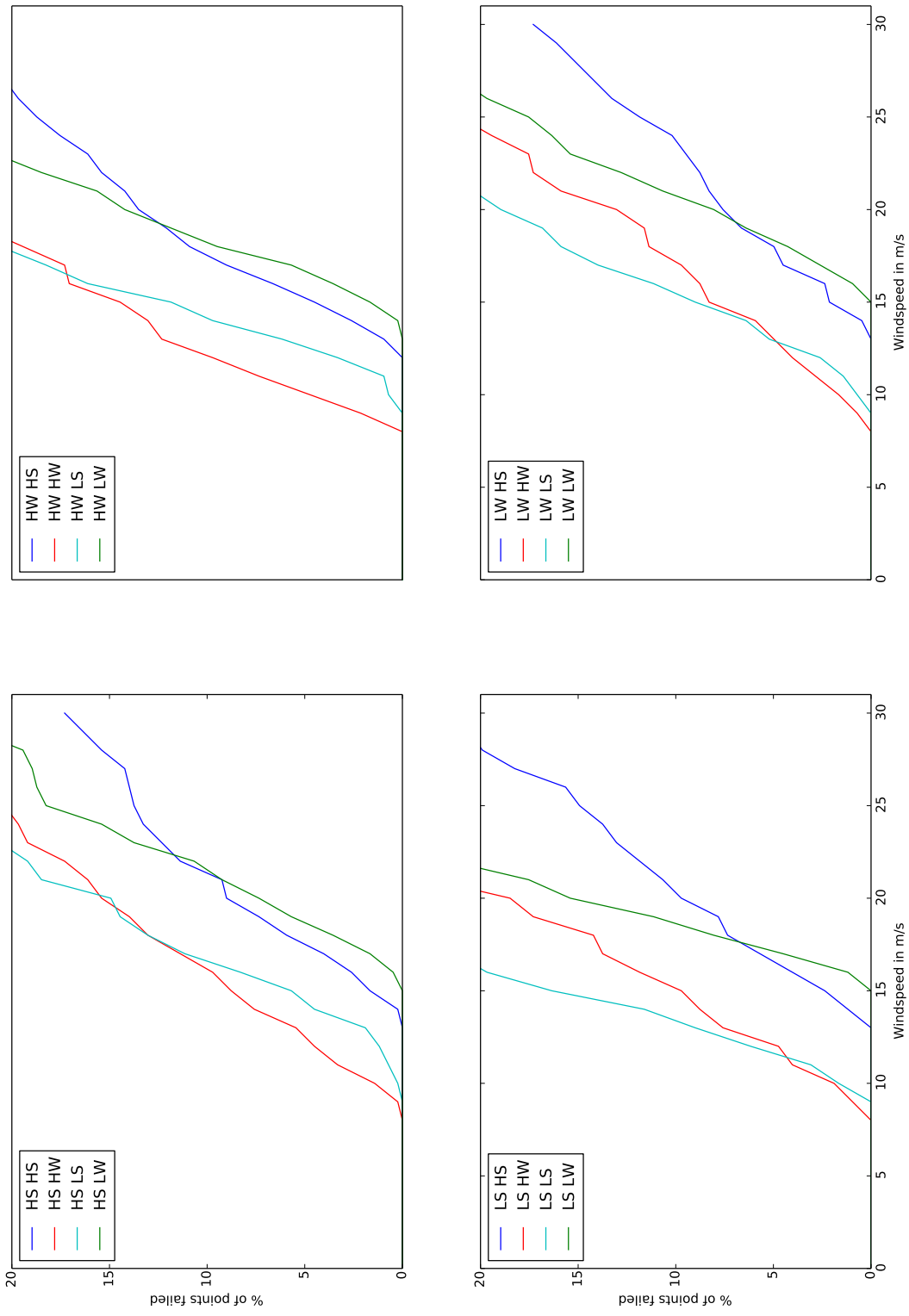

Figure D.10: Proportion of points failed at differing wind speeds wind speed at age 10.

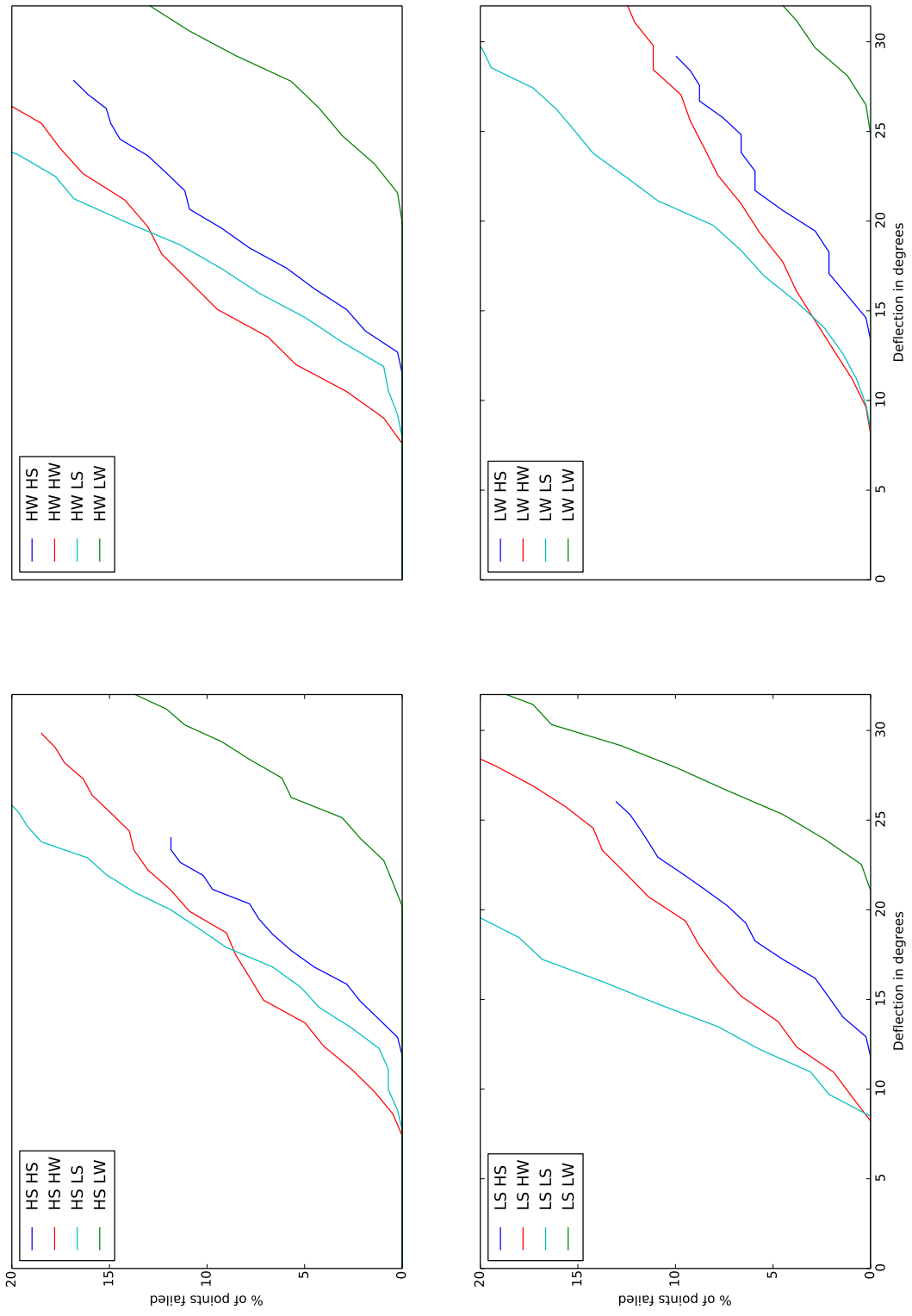

Figure D.11: Total number of points failed by deflection at age 15. Deflection is calculated at the tip of the stem.

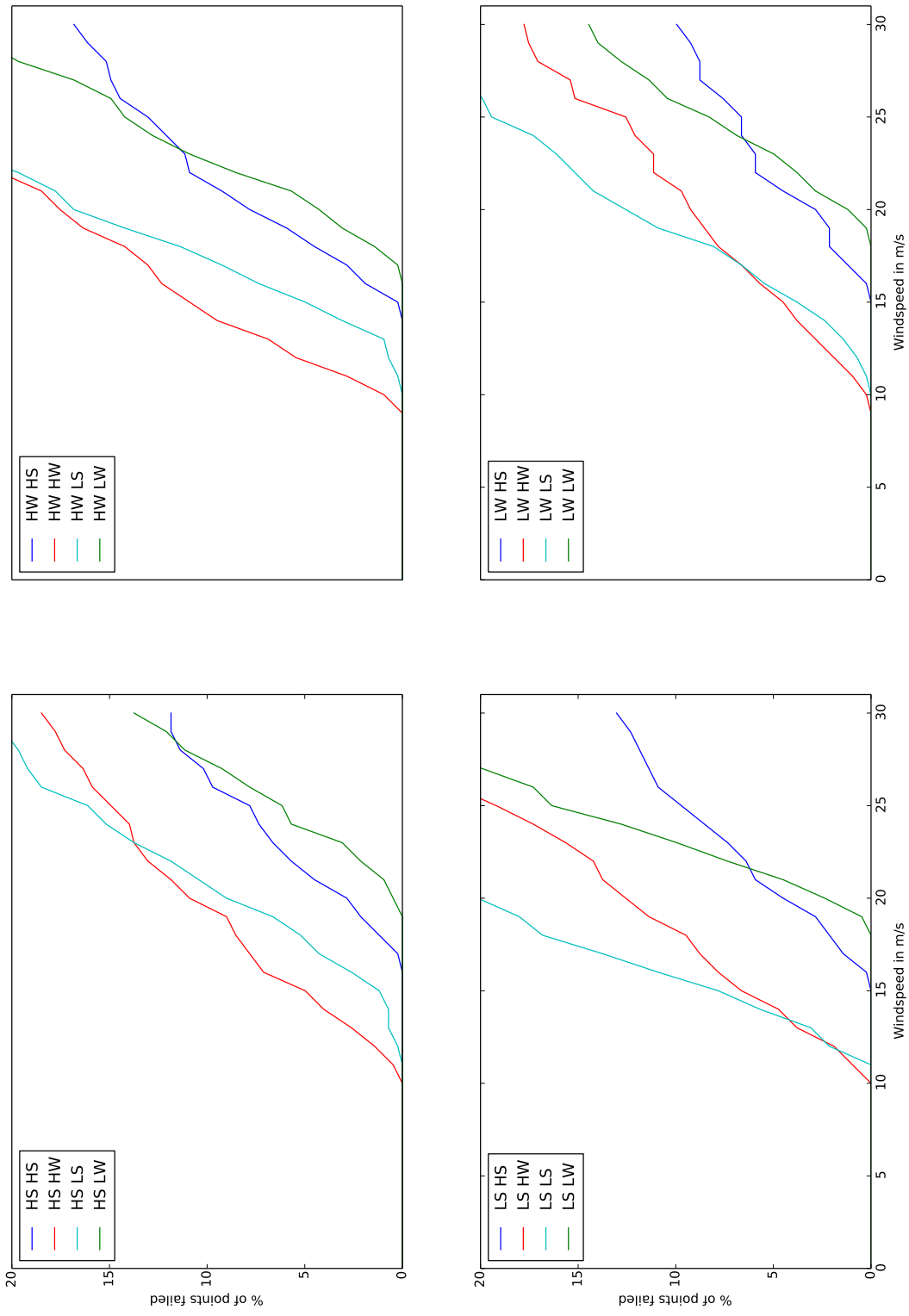

Figure D.12: Proportion of points failed at differing wind speeds at age 15.

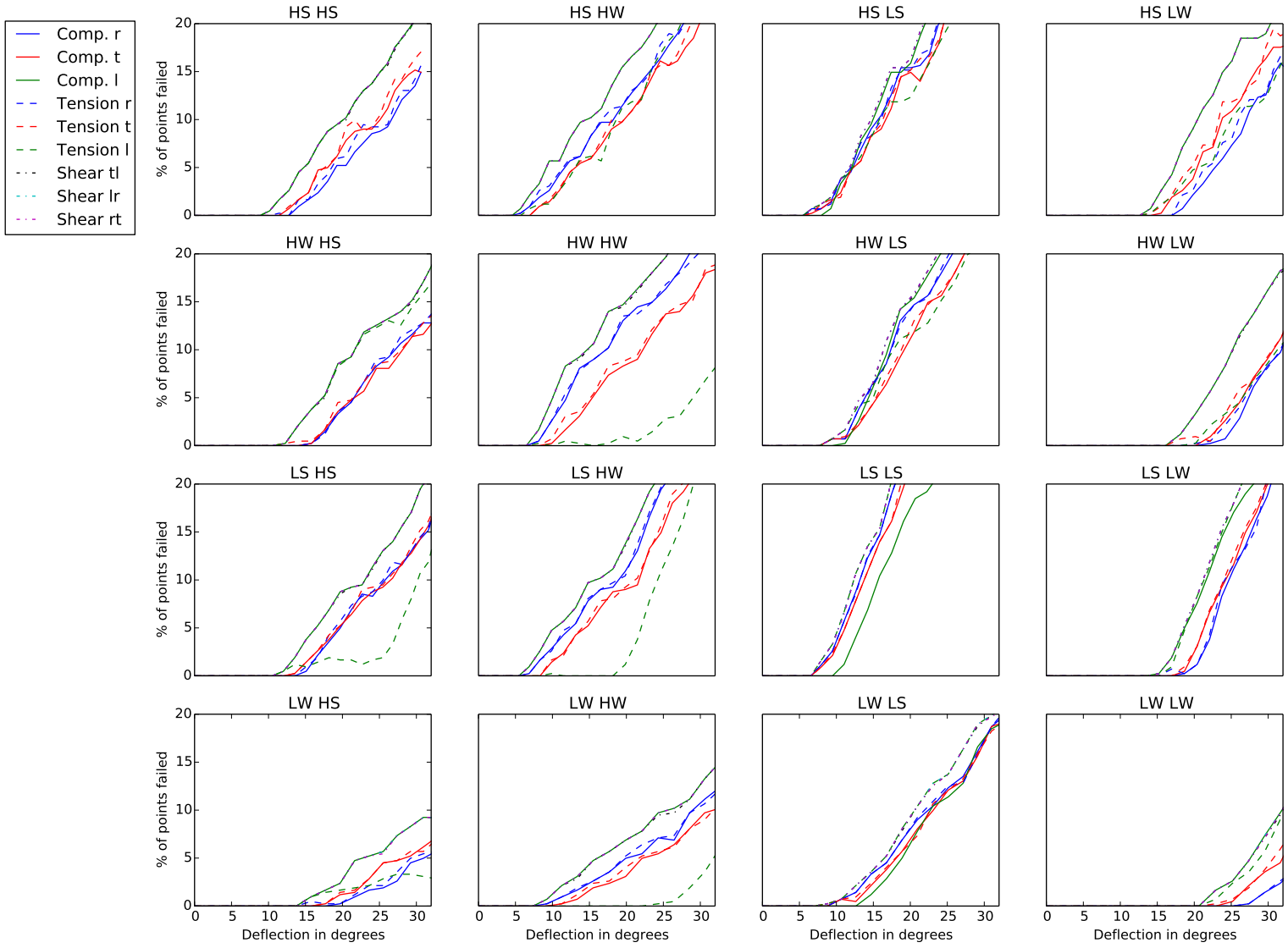

Figure D.13: Proportion of points failed in a given direction at age 5. Deflection is calculated at the tip of the stem.

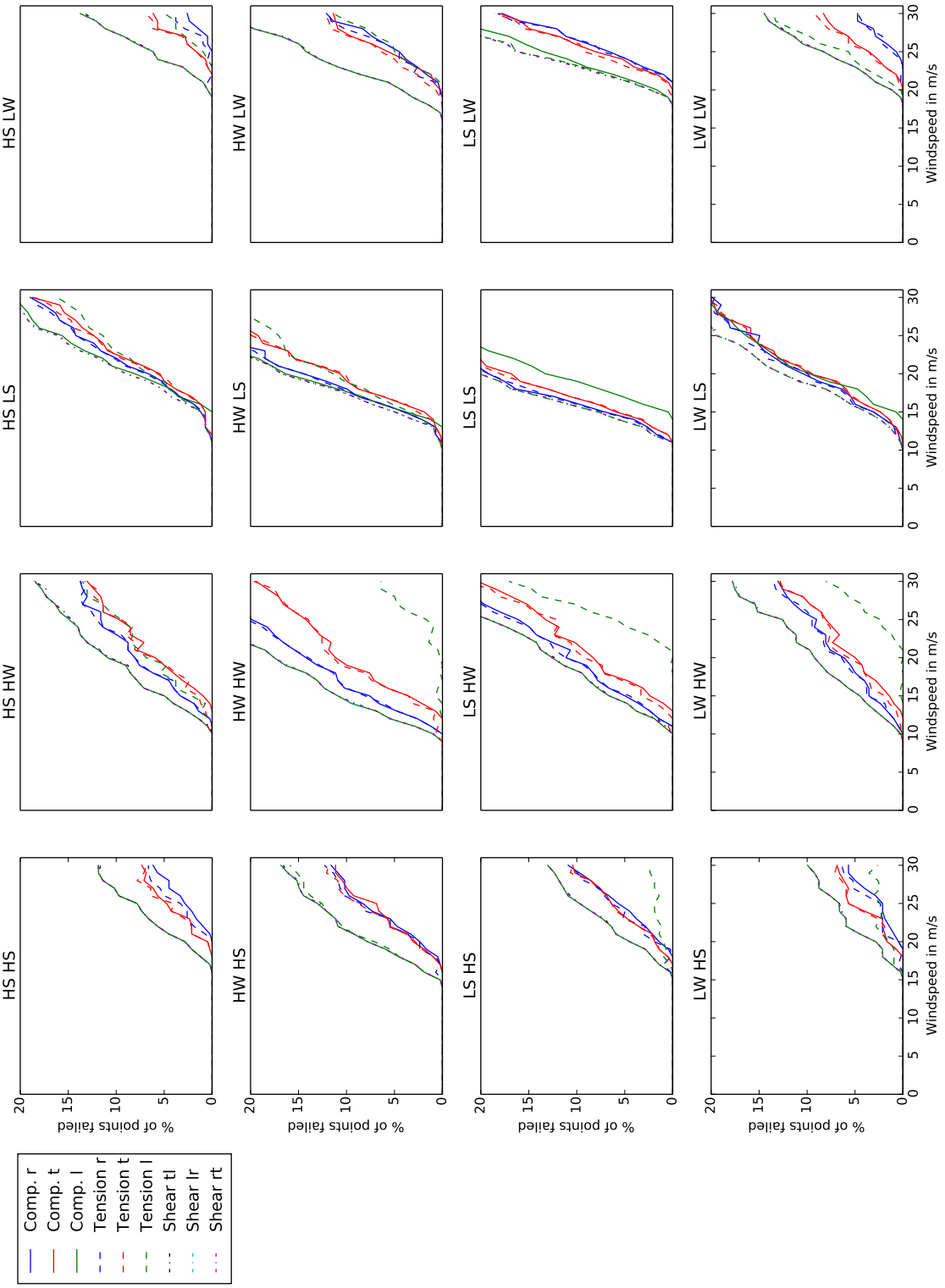

Figure D.14: Proportion of points failed in a given direction at age 5.

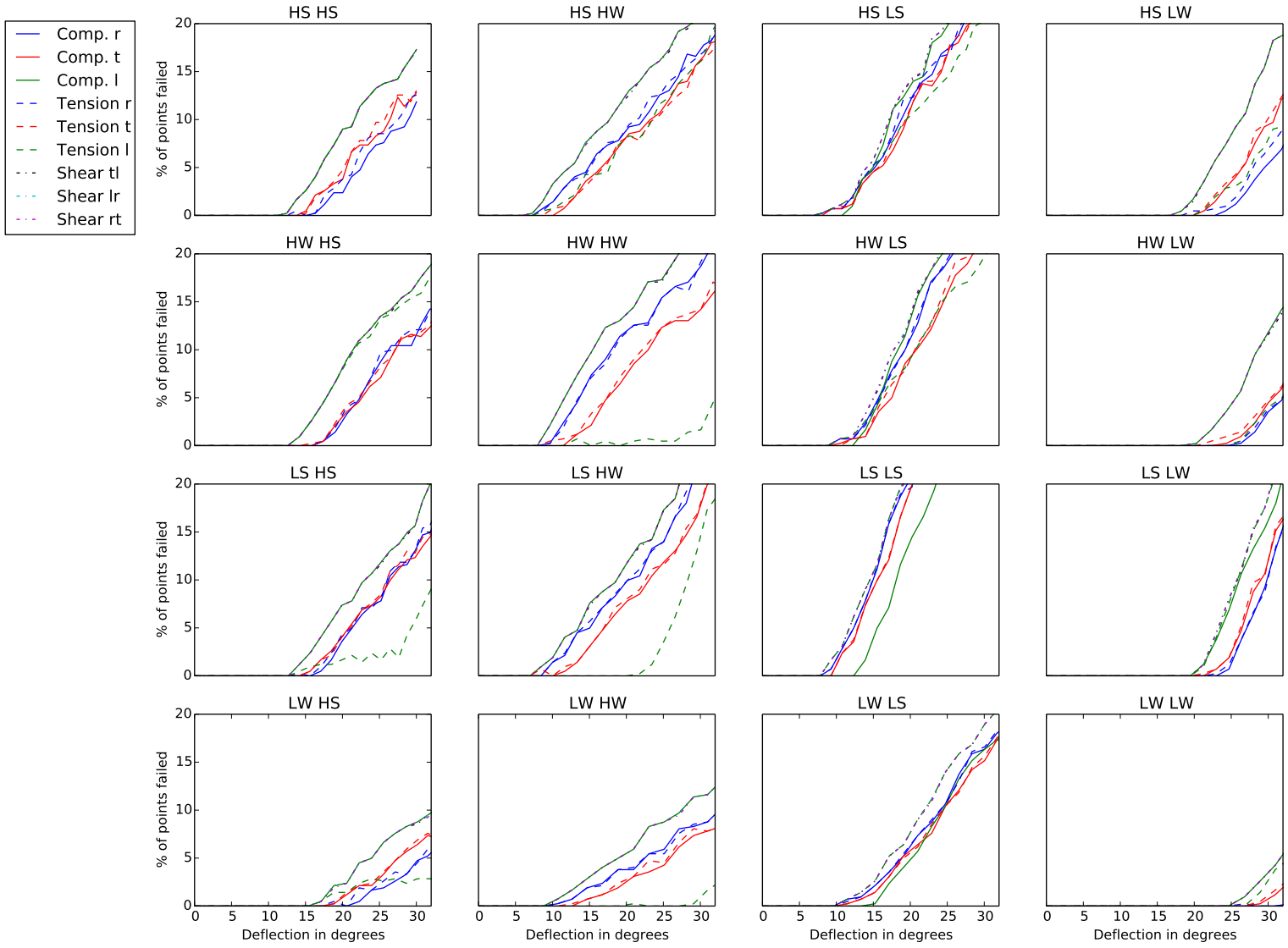

Figure D.15: Proportion of points failed in a given direction at age 10. Deflection is calculated at the tip of the stem.

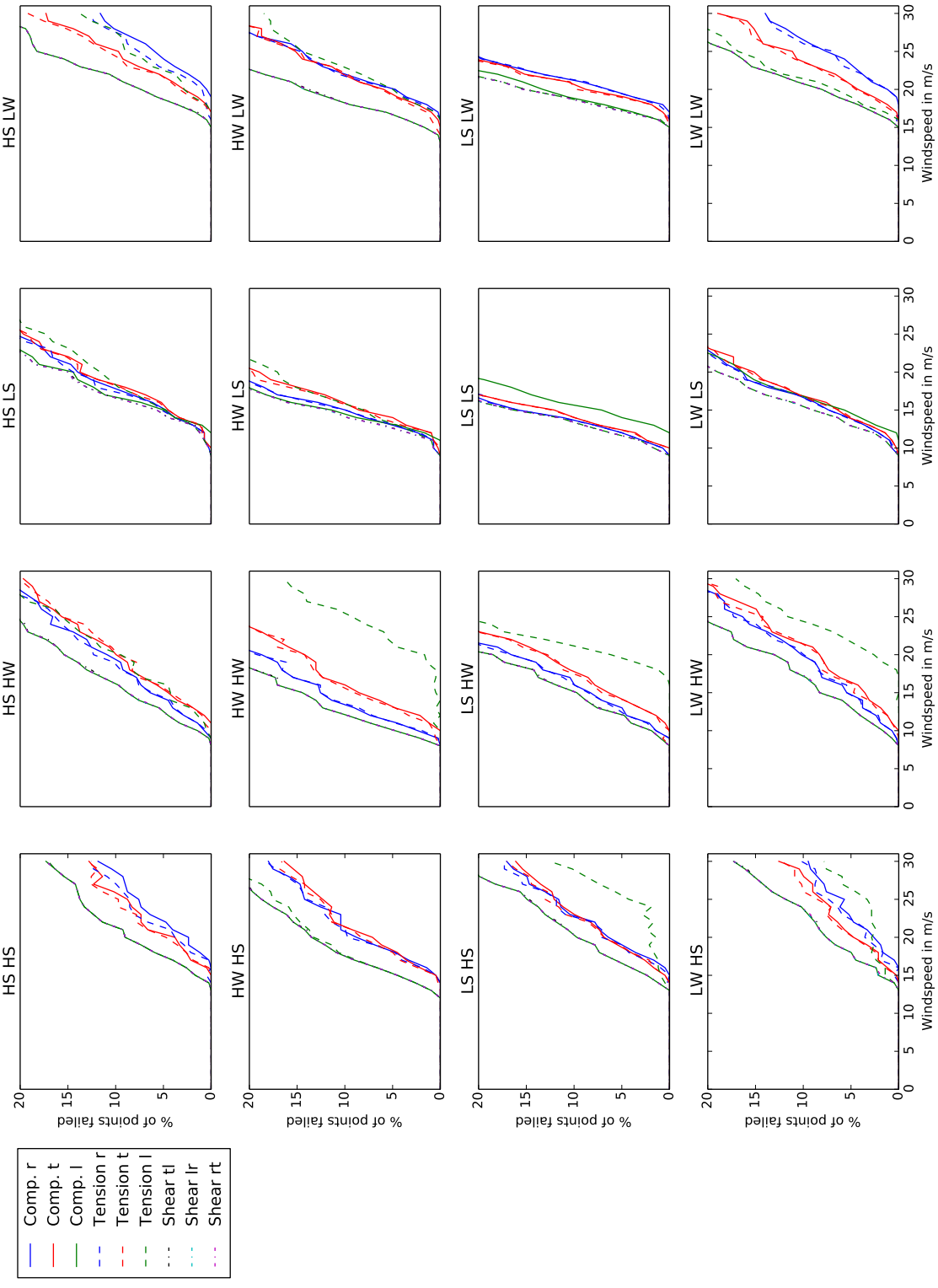

Figure D.16: Proportion of points failed in a given direction at age 10.

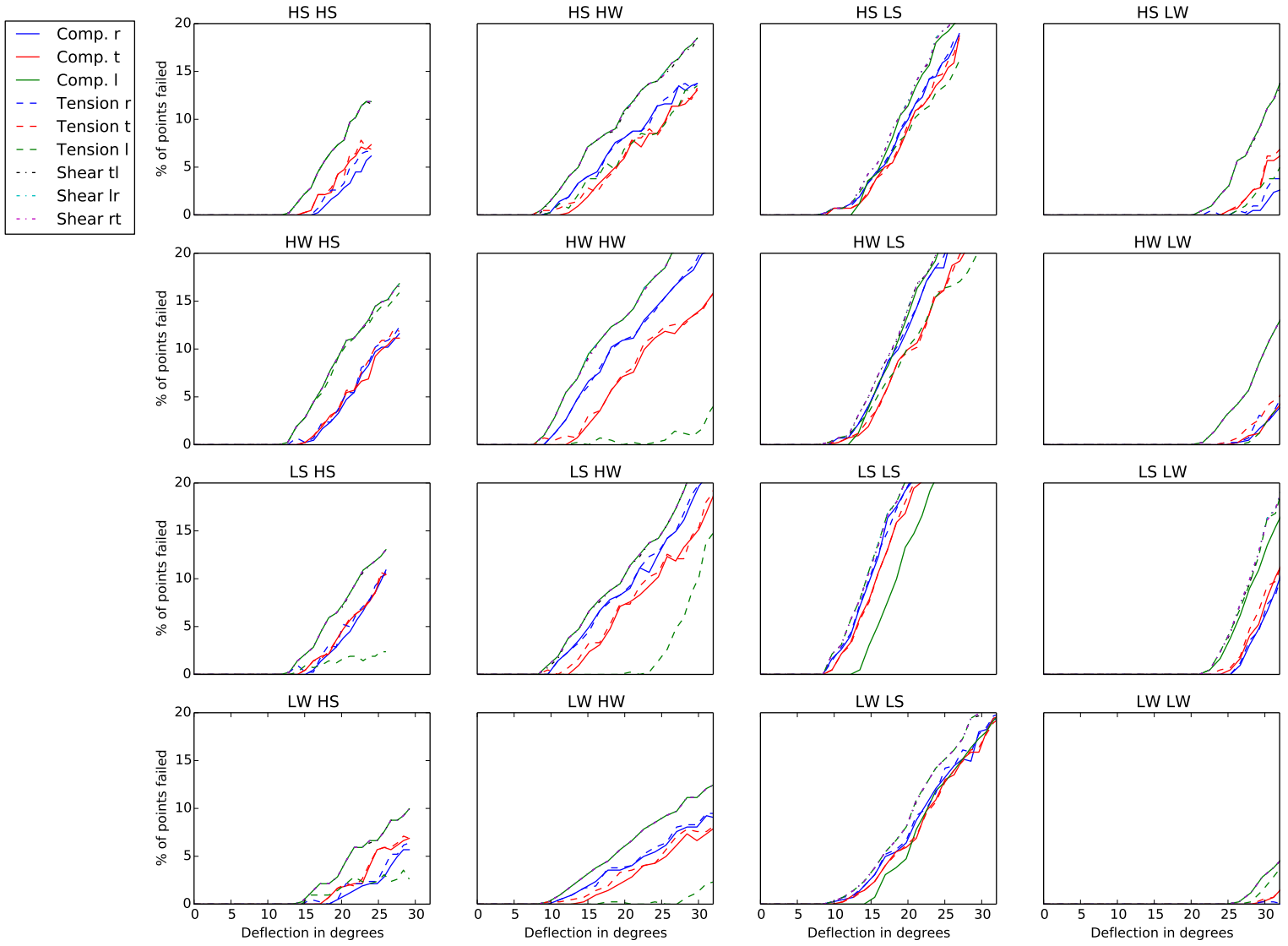

Figure D.17: Proportion of points failed in a given direction at age 15. Deflection is calculated at the tip of the stem.

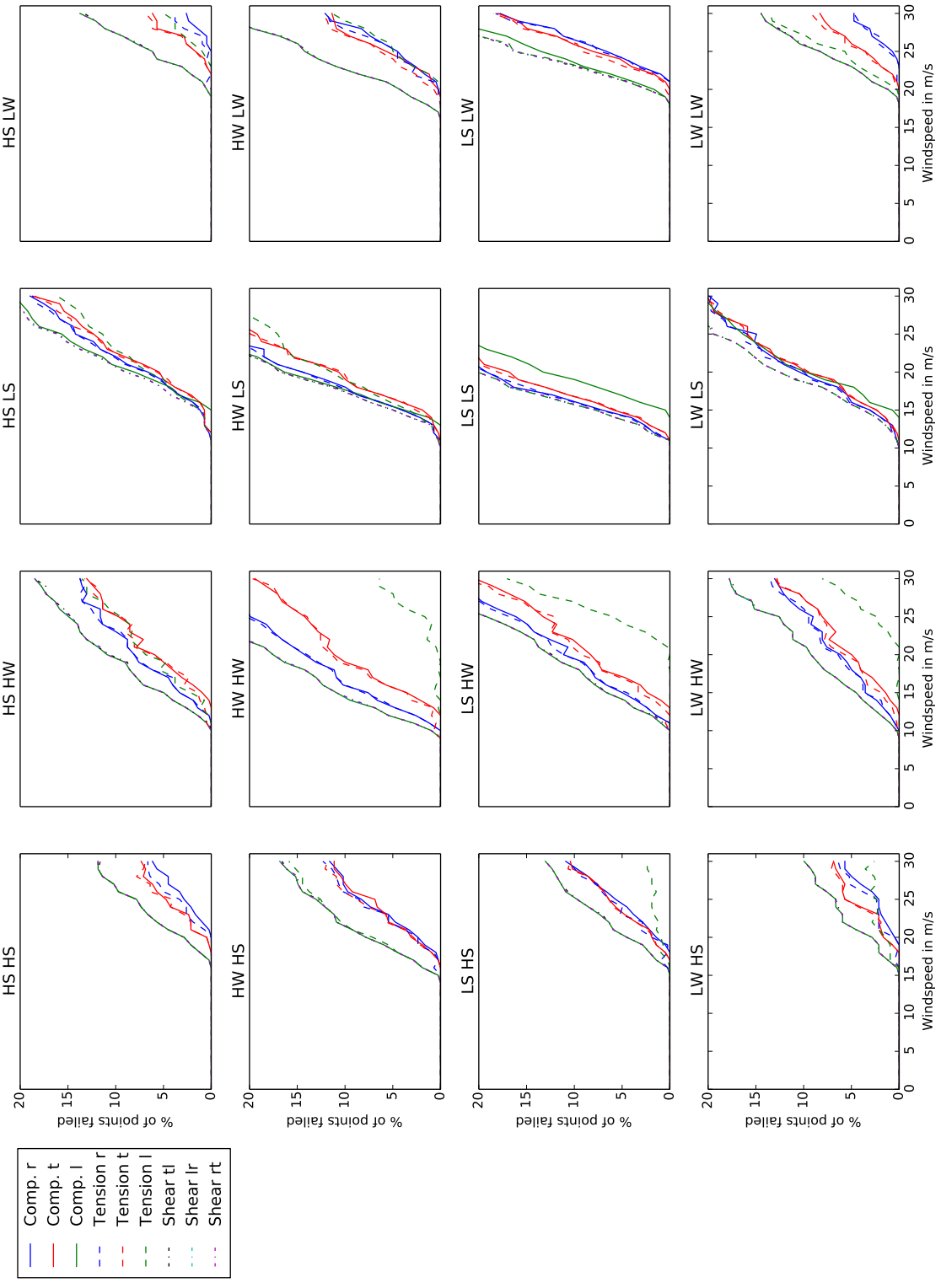

Figure D.18: Proportion of points failed in a given direction at age 15.

Appendix E

Effect of the TRP for different aged stems, 741 stocking without growth stresses

Note that at age 5 there is no difference between open grown and 741 stems per hectare. Refer to Appendix D for these.

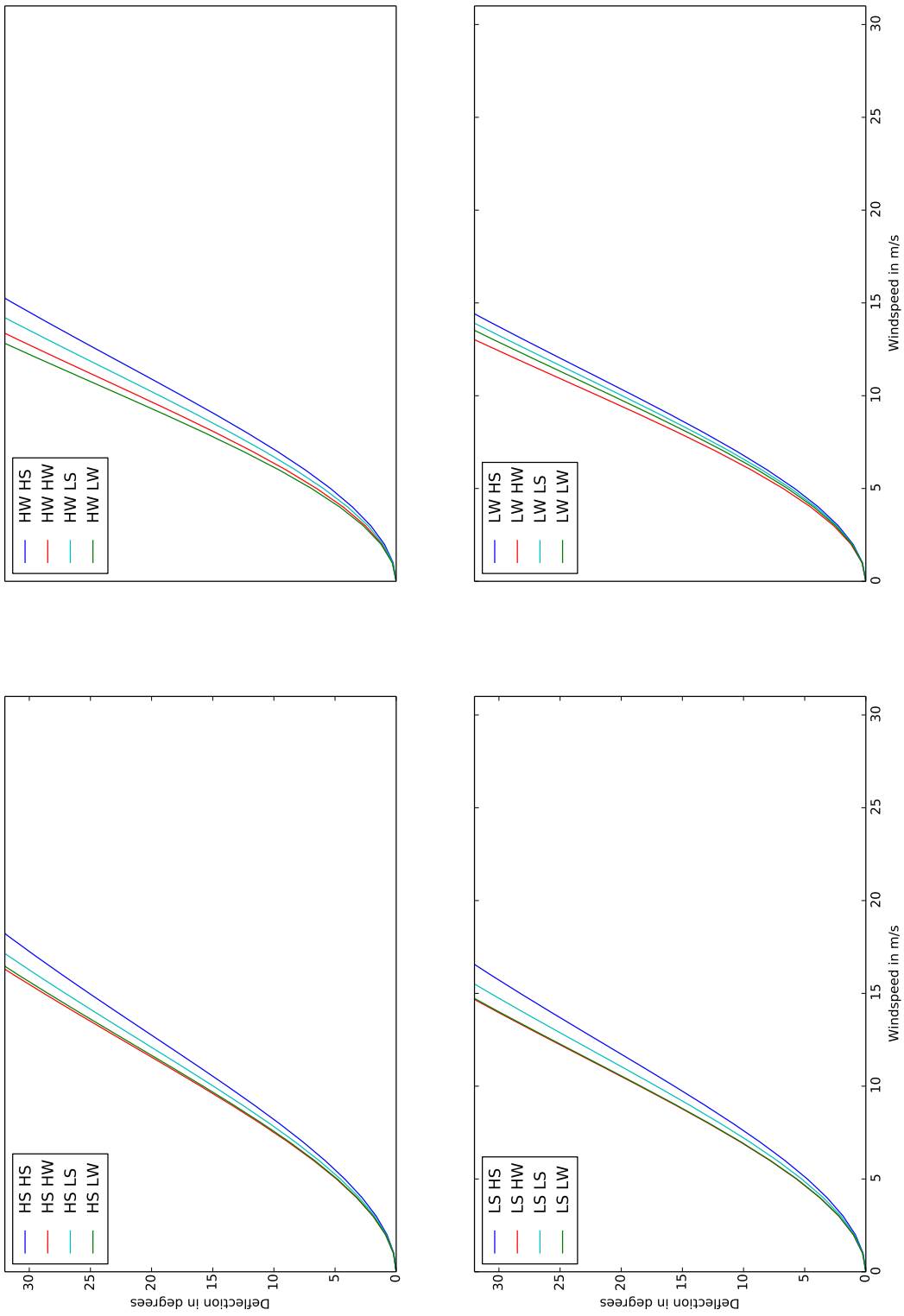

Figure E.1: Deflection in degrees for wind speeds at age 10. Deflection is calculated at the tip of the stem.

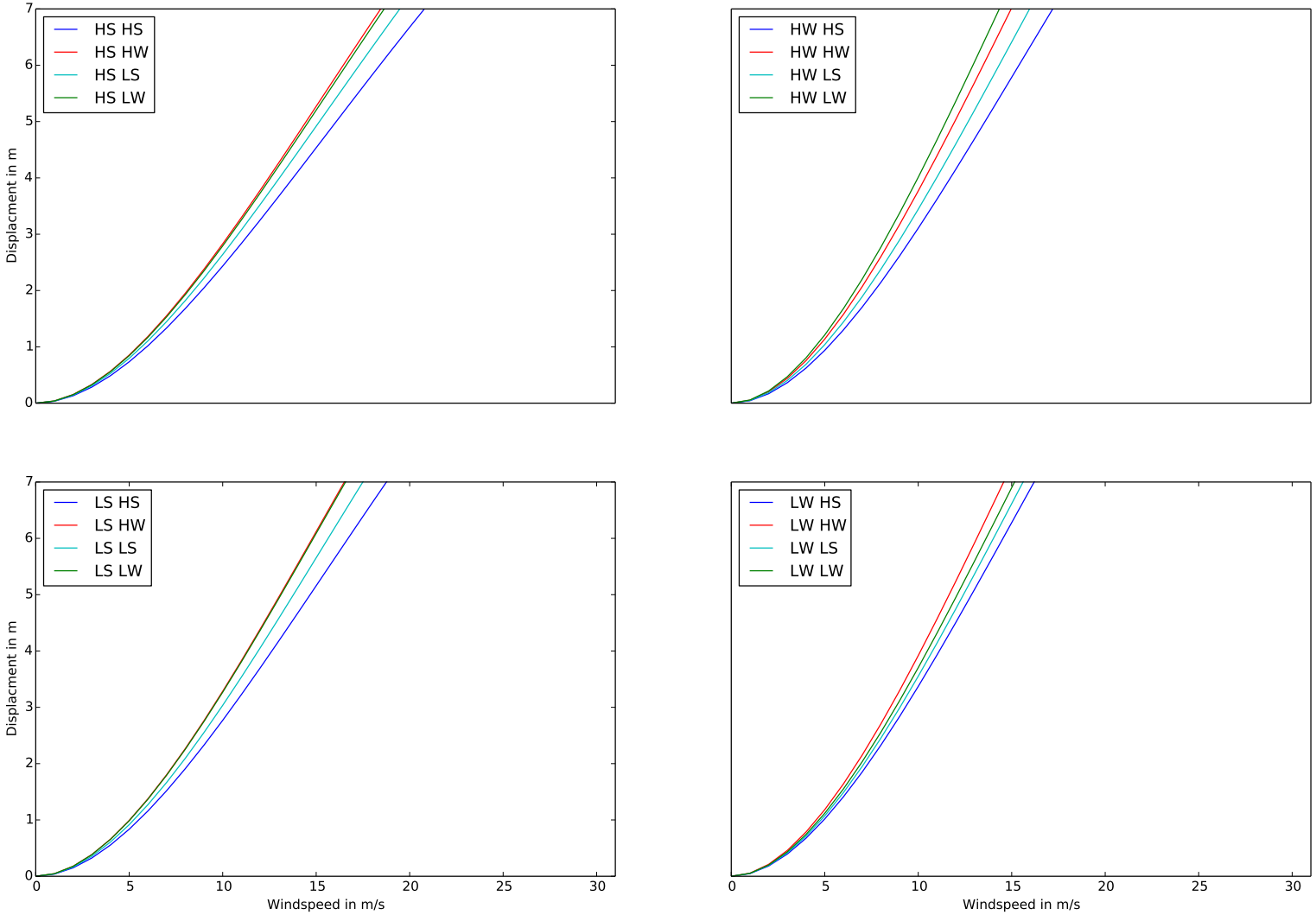

Figure E.2: Displacement in m for wind speeds at age 10. Displacement is calculated at the tip of the stem.

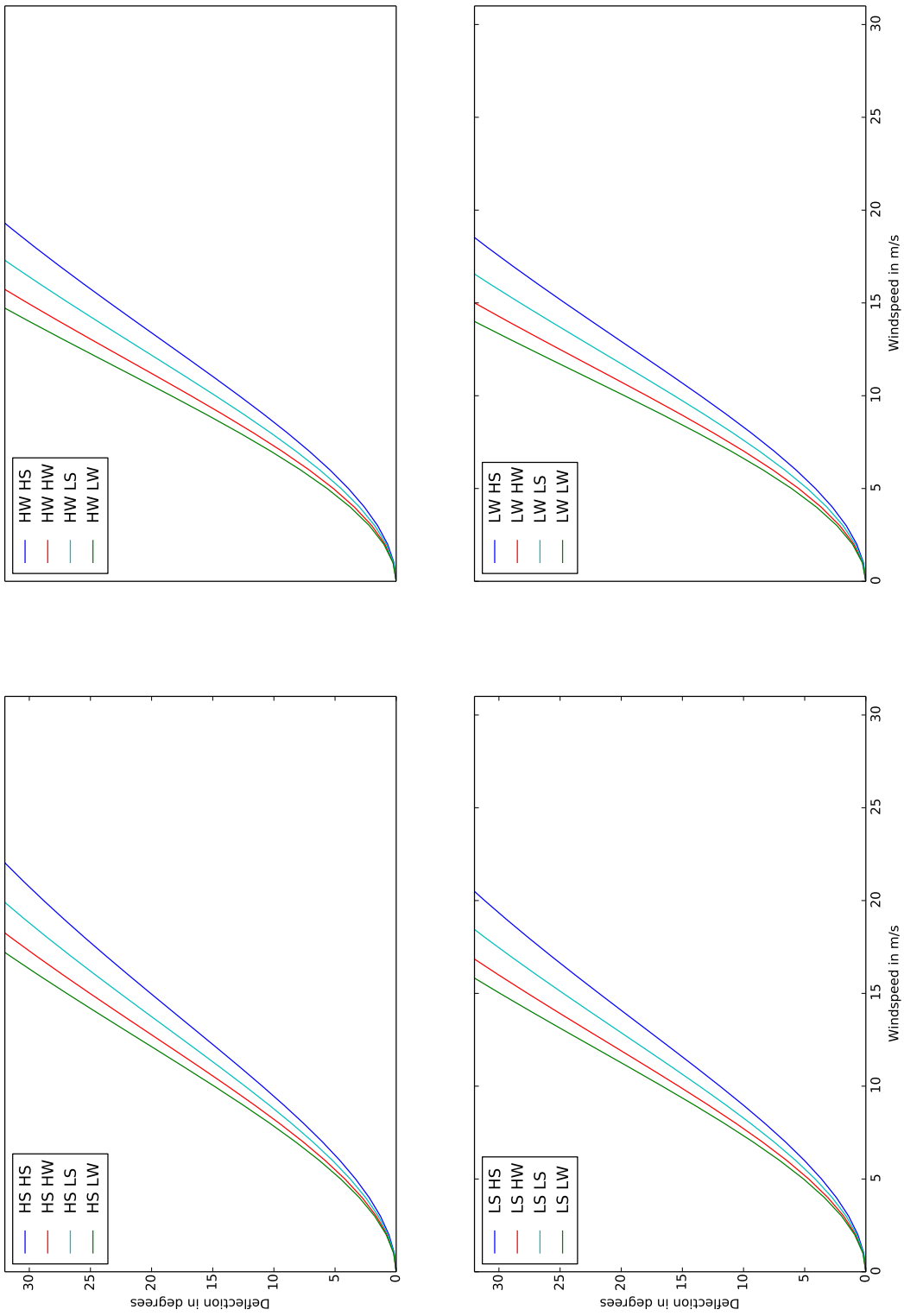

Figure E.3: Deflection in degrees for wind speeds at age 15. Deflection is calculated at the tip of the stem.

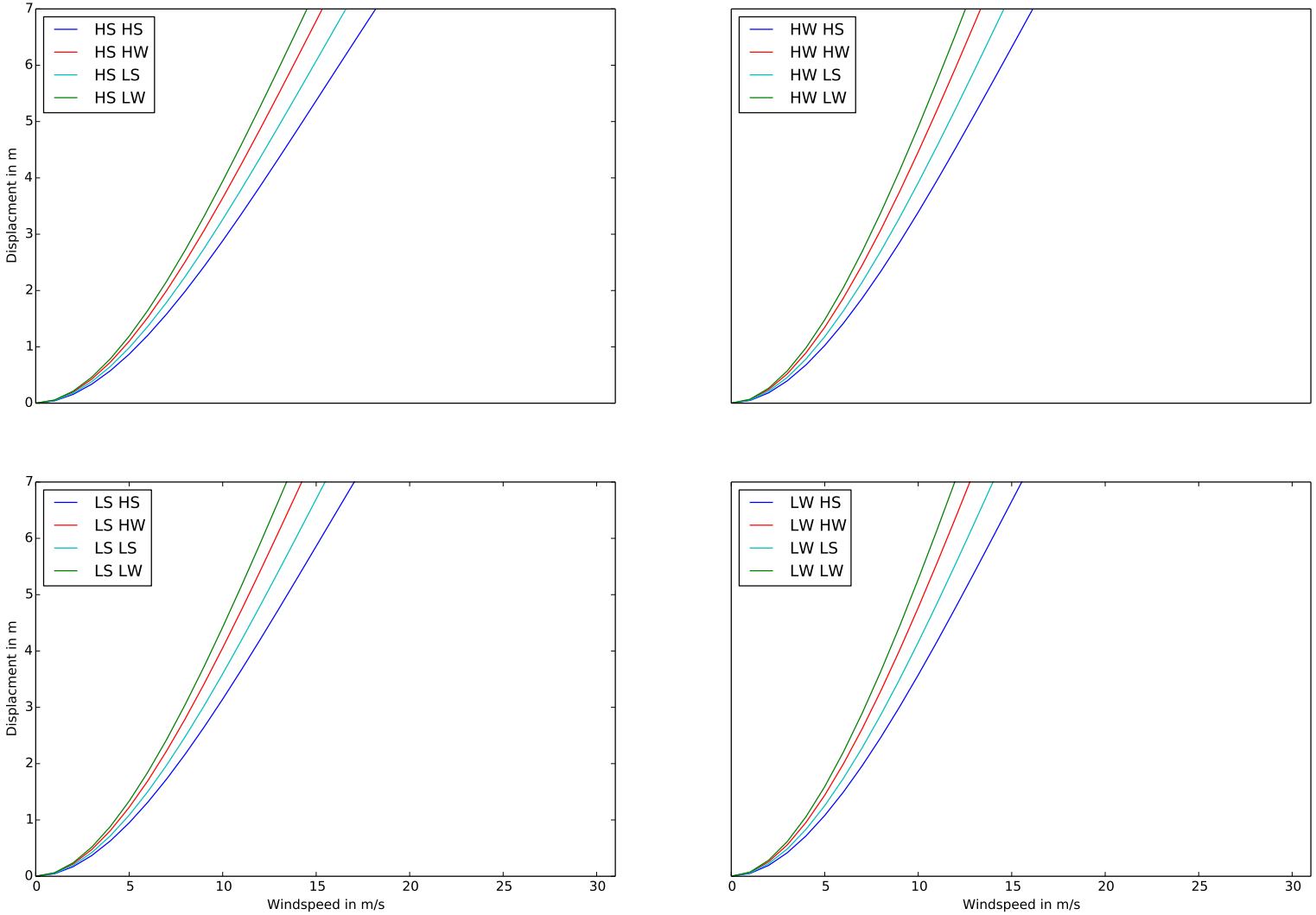

Figure E.4: Displacement in m for wind speeds at age 15. Displacement is calculated at the tip of the stem.

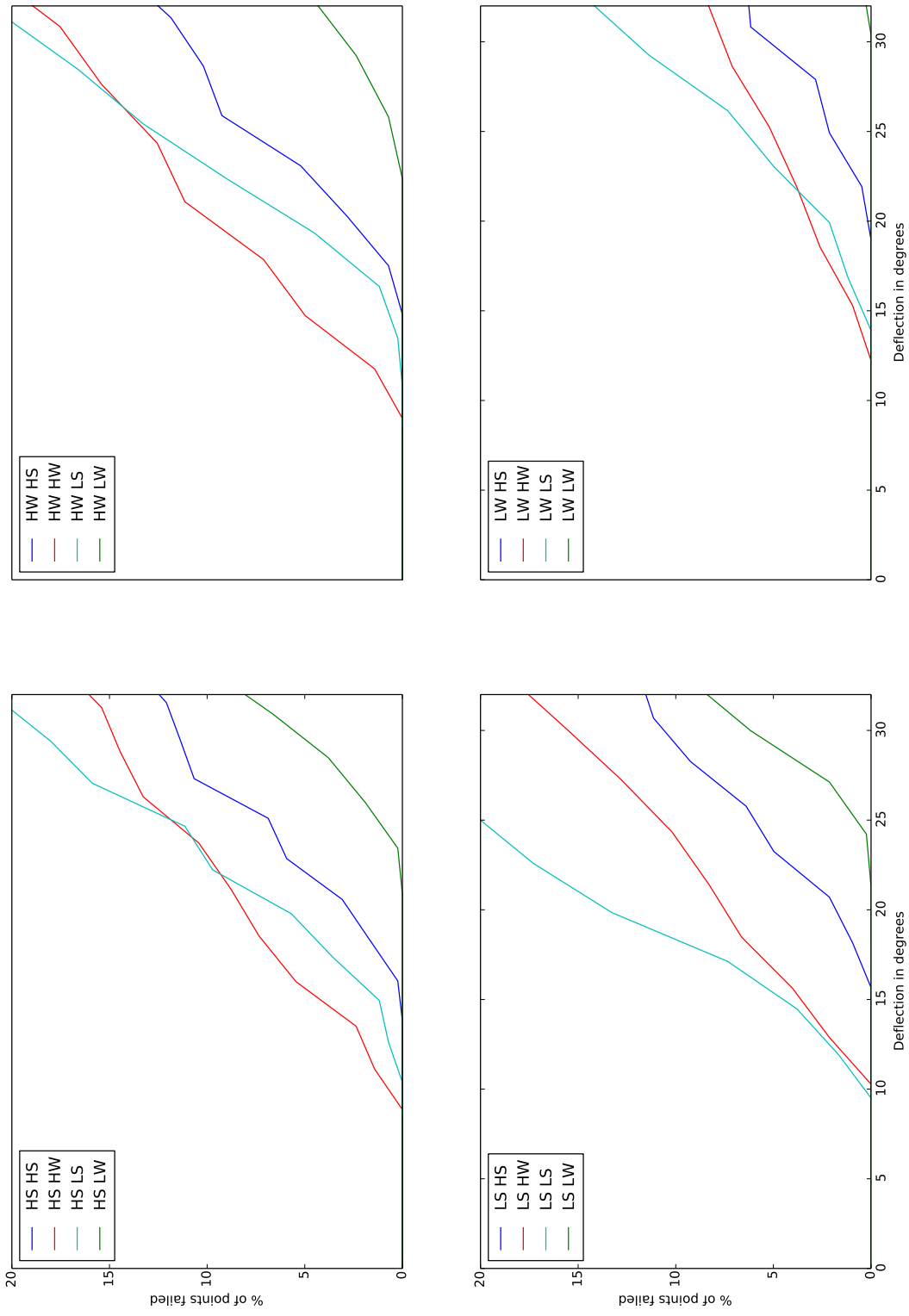

Figure E.5: Proportion of points failed by deflection at age 10. Deflection is calculated at the tip of the stem.

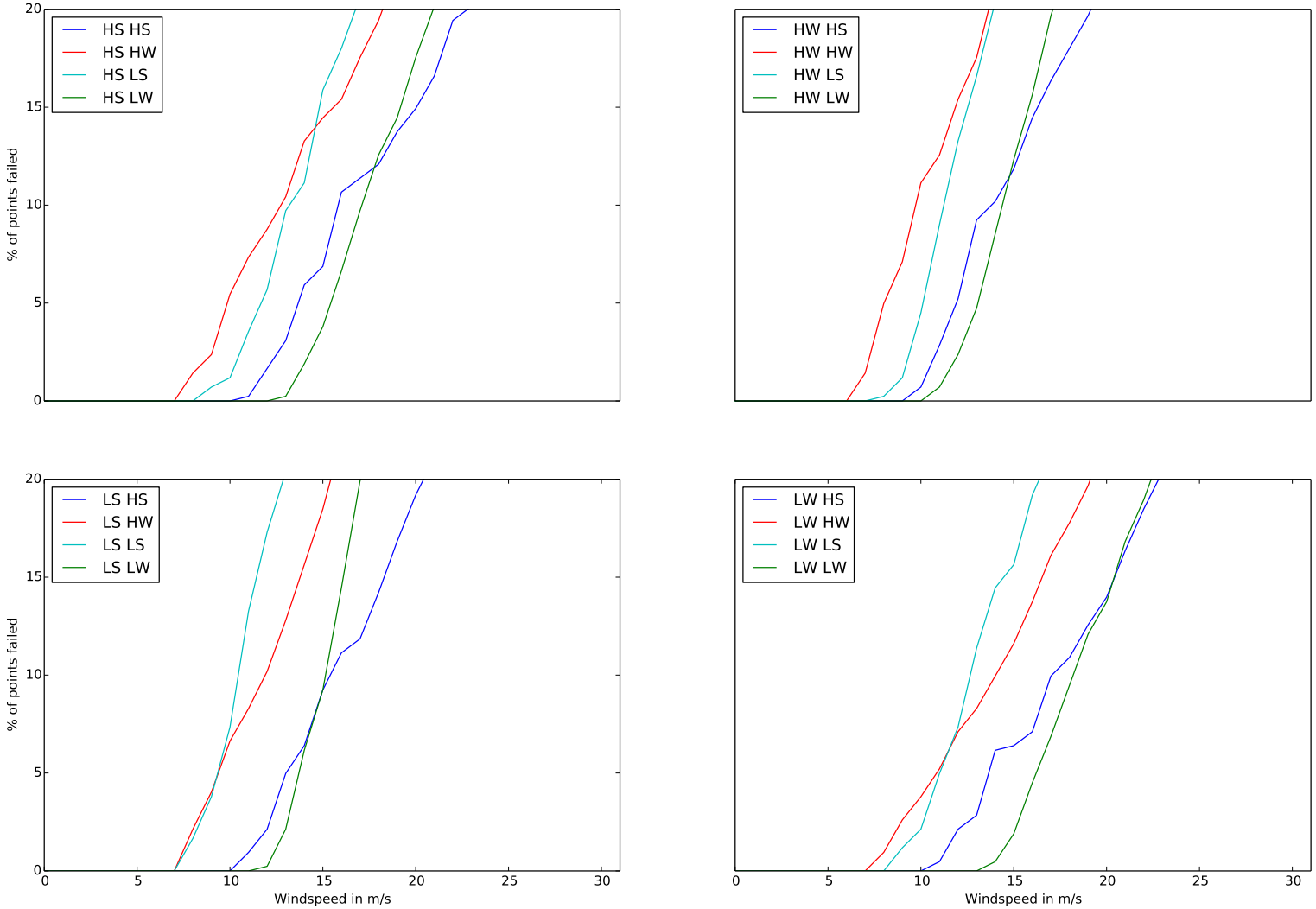

Figure E.6: Proportion of points failed at differing wind speeds at age 10.

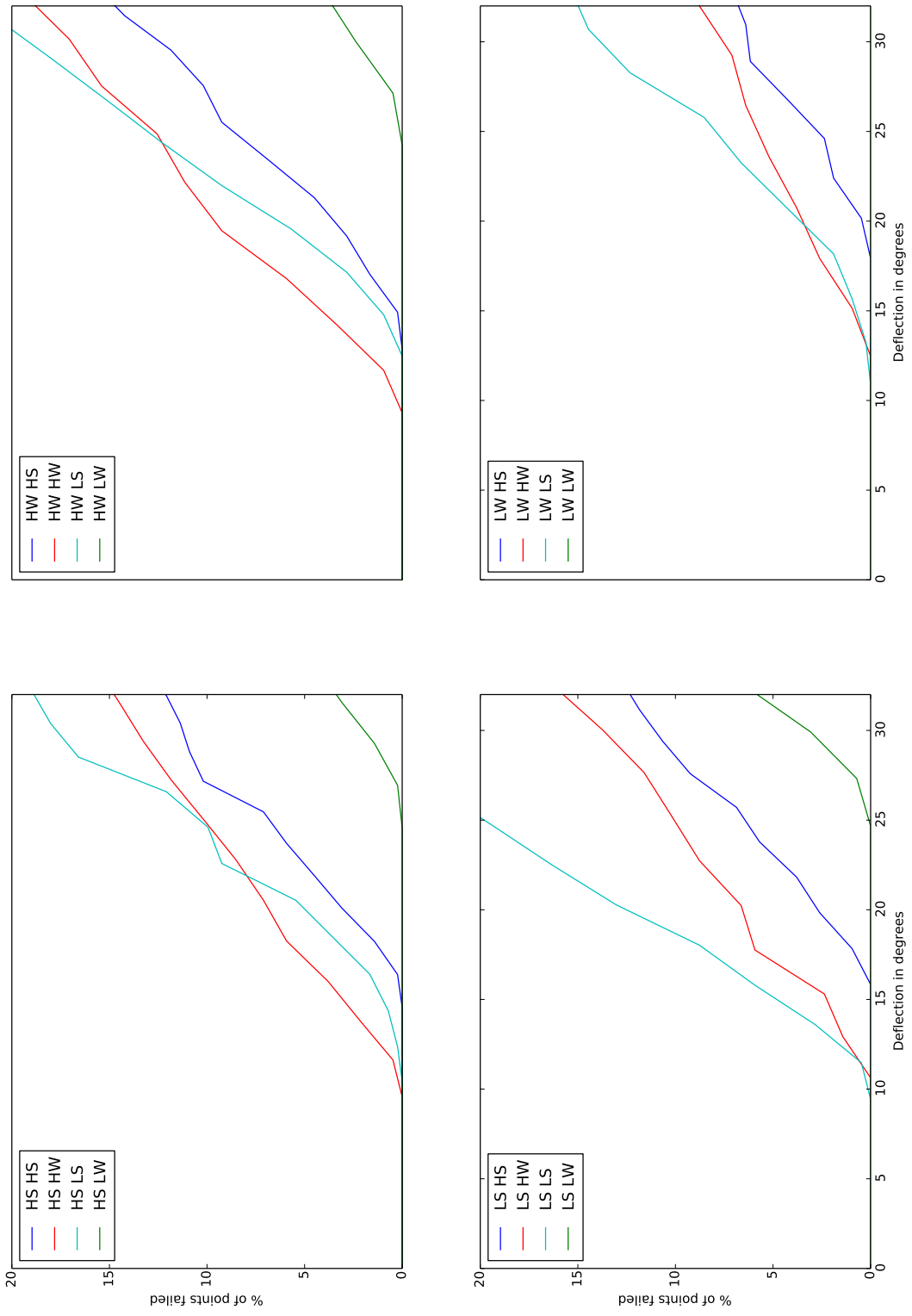

Figure E.7: Total number of points failed by deflection at age 15. Deflection is calculated at the tip of the stem.

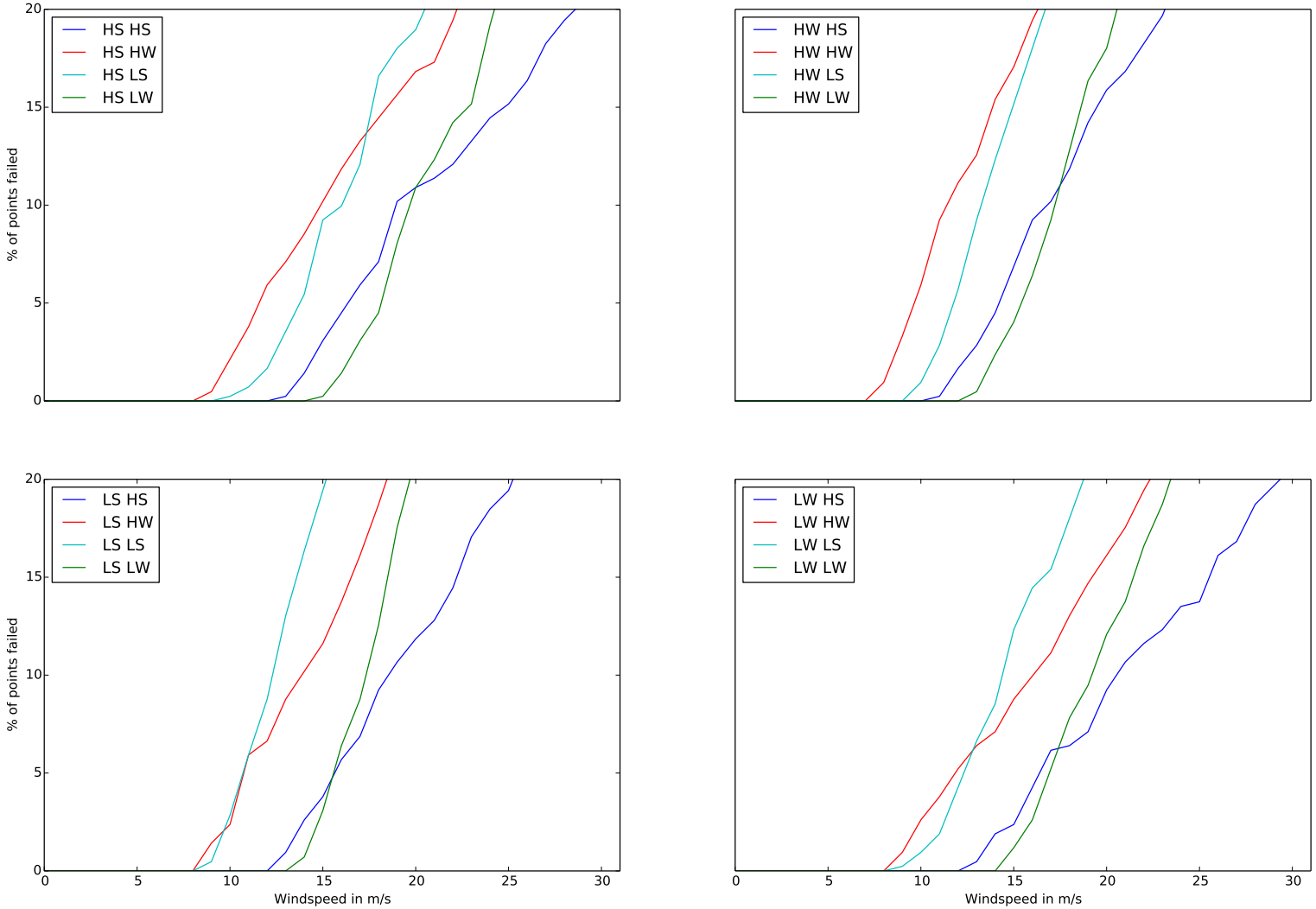

Figure E.8: Proportion of points failed at differing wind speeds at age 15.

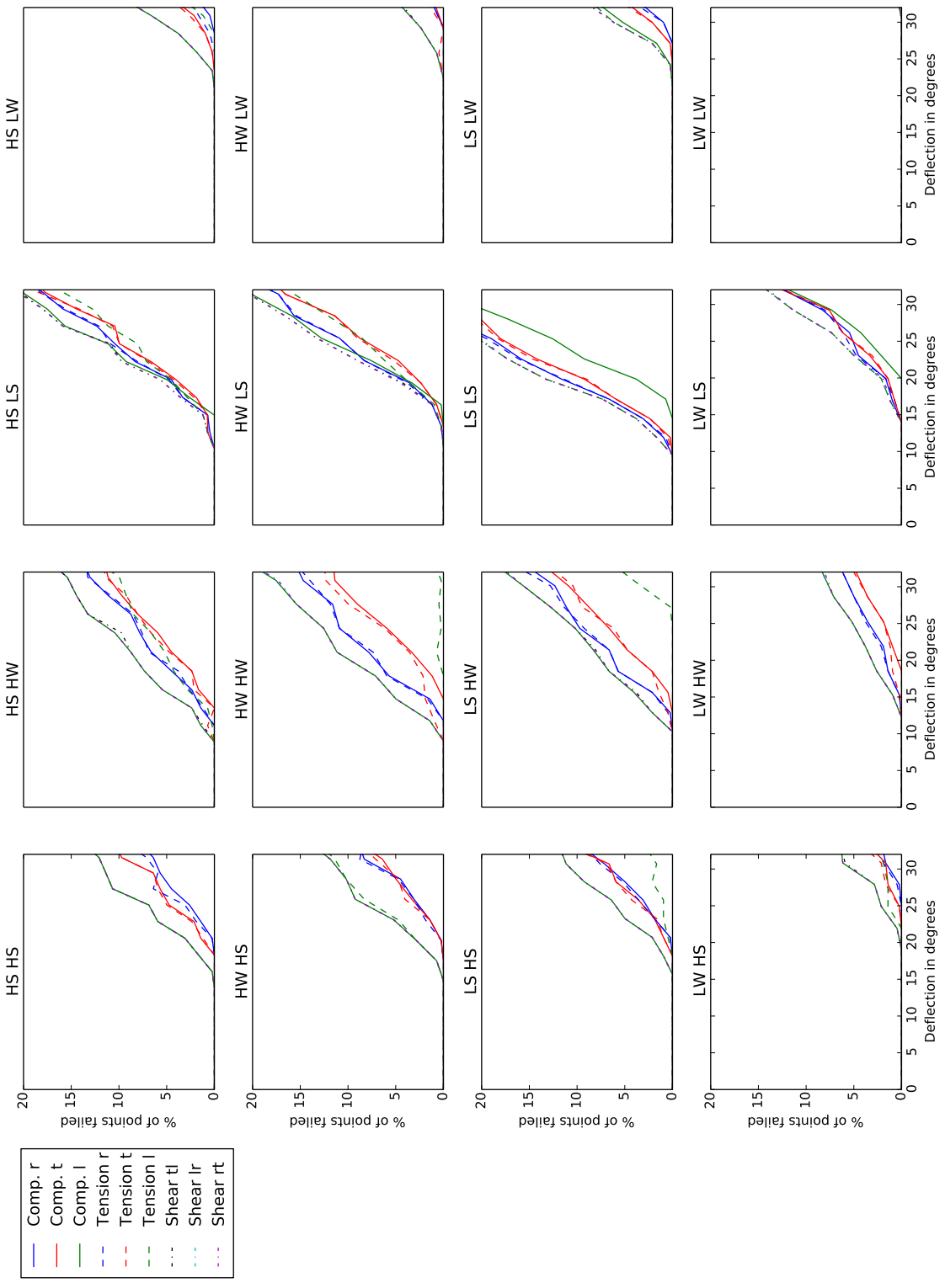

Figure E.9: Proportion of points failed in a given direction at age 10. Deflection is calculated at the tip of the stem.

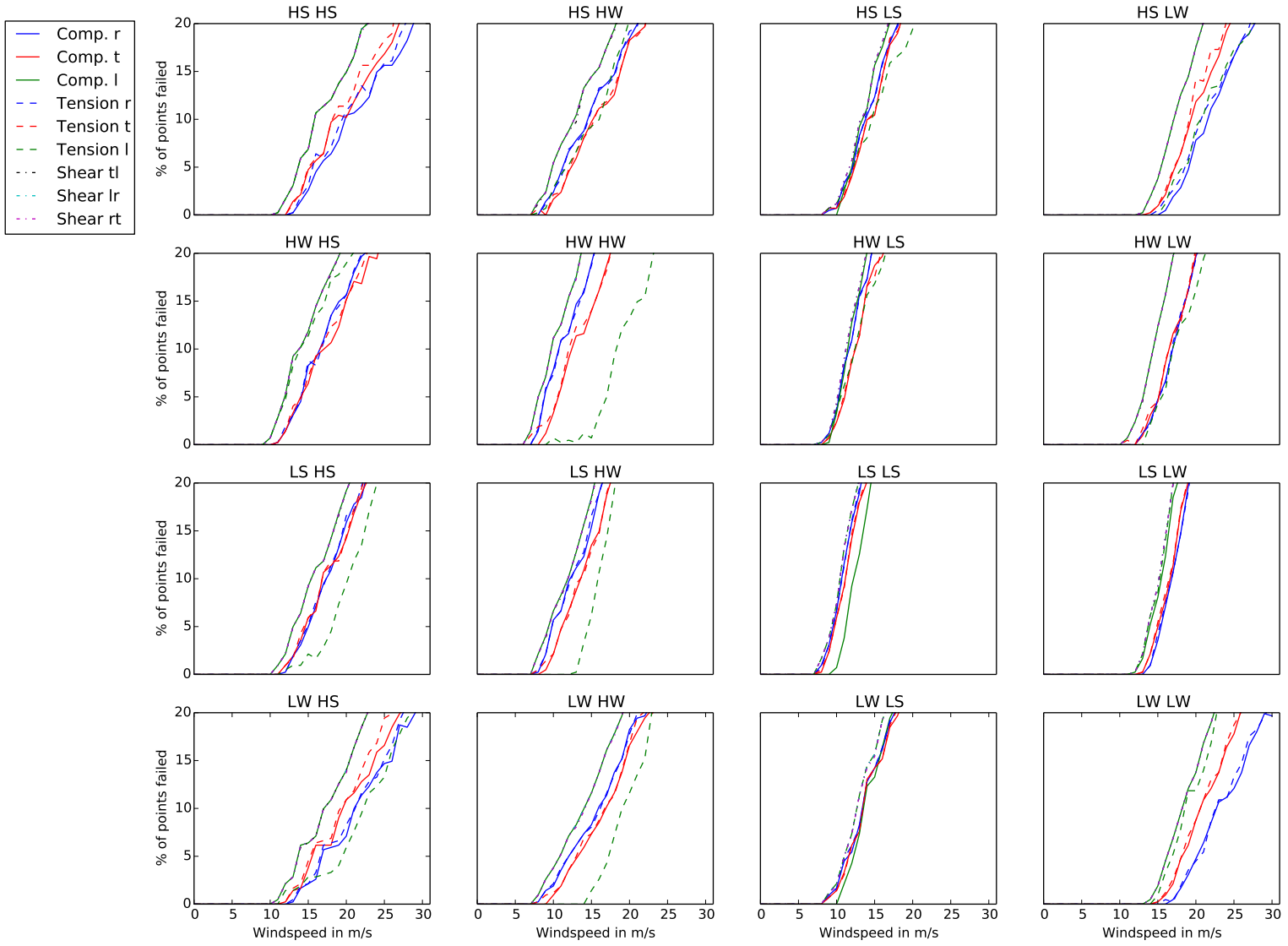

Figure E.10: Proportion of points failed in a given direction at age 10.

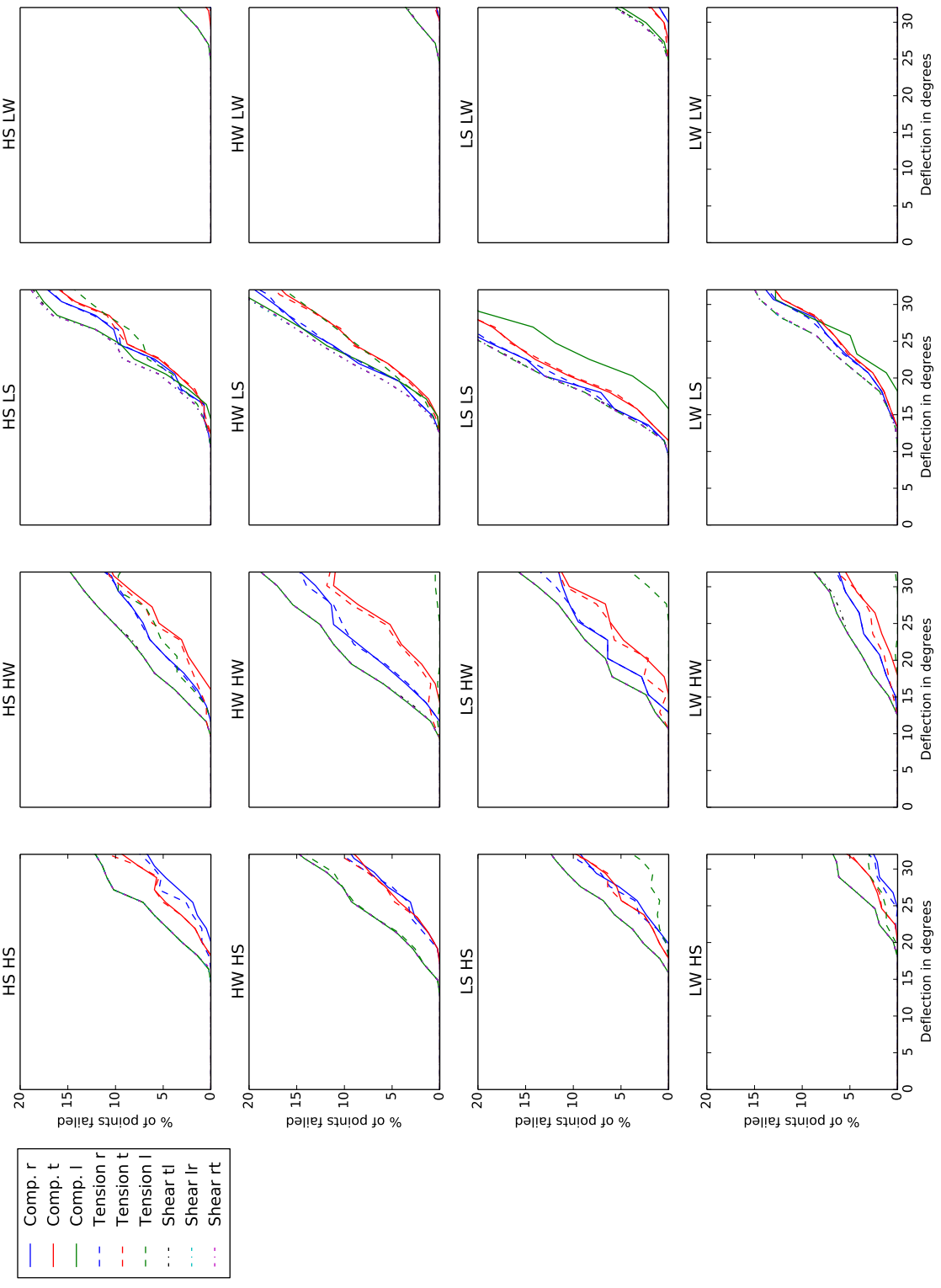

Figure E.11: Proportion of points failed in a given direction at age 15. Deflection is calculated at the tip of the stem.

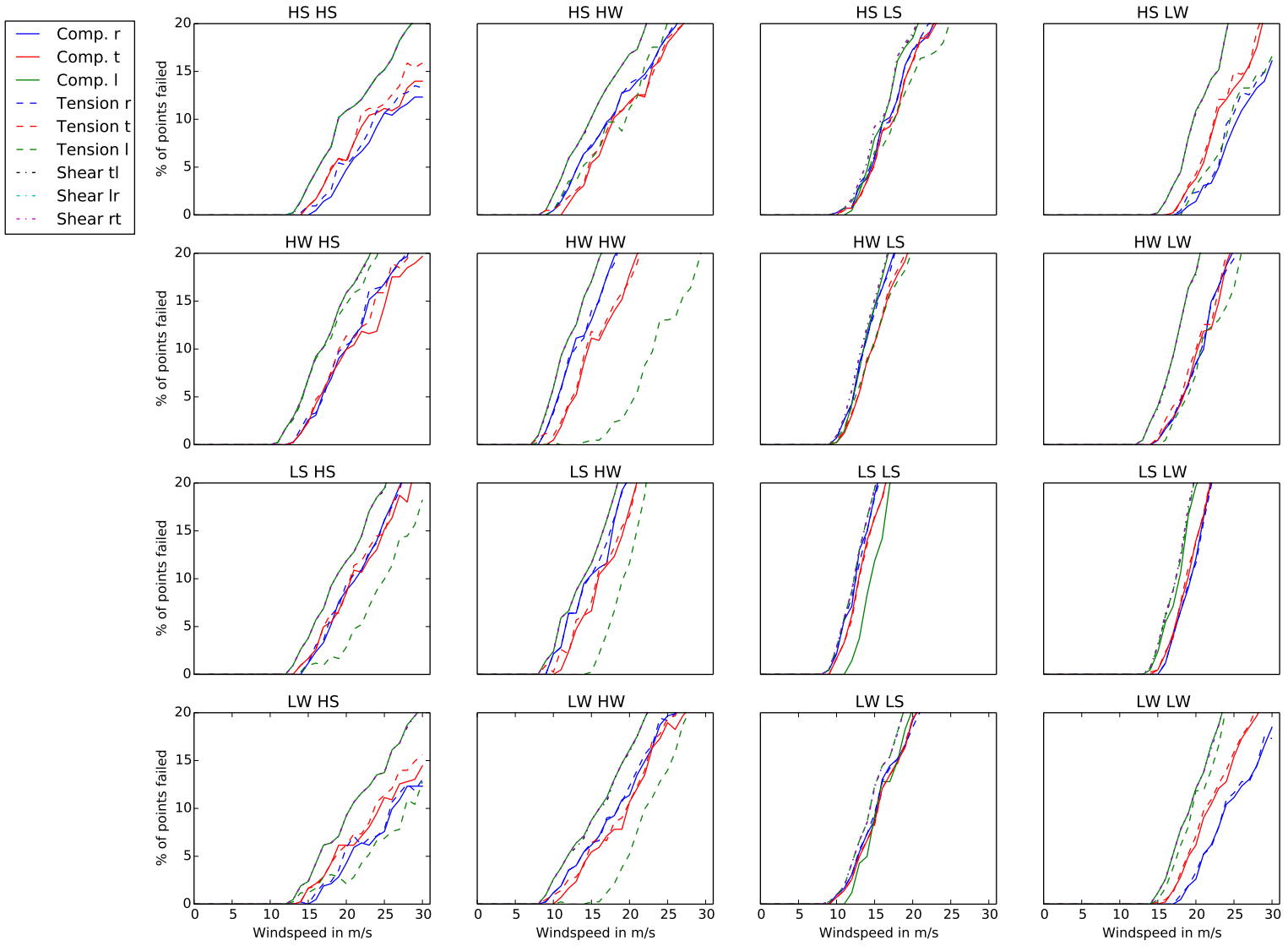

Figure E.12: Proportion of points failed in a given direction at age 15.

Appendix F

Abrevations list for Chapter 2

Table F.1: List of abbreviations used in Chapter 2

Abbreviation	Description
TRP	Typical Radial Pattern
MFA	Micro-Fibril Angle
NZSOF	New Zealand School of Forestry
UTM	Universal Testing Machine
HS	High density high stiffness sample
HW	High density low stiffness sample
LS	Low density high stiffness sample
LW	Low density low stiffness sample
r	Radial direction in the local coordinate system
t	Tangential direction in the local coordinate system
l	Longitudinal direction in the local coordinate system
tl	Tangential longitudinal plane
lr	Longitudinal radial plane
rt	Radial Tangential plane
x	Global horizontal direction, the direction of wind loading
y	Global horizontal direction perpendicular to x
z	Global vertical direction
v	Poisson ratio
E	Elastic modulus
δ_i	Experimental value of i
γ_i	Optimised value of i
θ_i	95% confidence interval of the experimental value of i
$\boldsymbol{\sigma}$	Stress vector
$\boldsymbol{q}$	Vector for failure criterion
$\boldsymbol{P}$	Matrix for failure criterion
$\boldsymbol{F}$	Value of an entry in $\boldsymbol{q}$ or $\boldsymbol{P}$
S	Strength
SE	Standard error

Appendix G

Abrevations list for Chapter 3

Table G.1: List of abbreviations used in Chapter 3

Abbreviation	Value	Description
TRP		Typical Radial Pattern
MFA		Micro-Fibril Angle
NZOF		New Zealand School of Forestry
UTM		Universal Testing Machine
HS		High density high stiffness sample
HW		High density low stiffness sample
LS		Low density high stiffness sample
LW		Low density high stiffness sample
r		Radial direction in the local coordinate system
t		Tangential direction in the local coordinate system
l		Longitudinal direction in the local coordinate system
tl		Tangential longitudinal plane
lr		Longitudinal radial plane
rt		Radial Tangential plane
x		Global horizontal direction, the direction of wind loading
y		Global horizontal direction perpendicular to x
z		Global vertical direction
v		Poisson ratio
E		Elastic modulus
t	5, 10 or 15 years	Age of stem
n	16	Number of sides used to represent the circular stem
h	5, 10 or 15 m	Total height of the stem
i		The value of the constant in question at the centre of the stem
o		The value of the constant in question at the peripheral of the stem
ξ		Value incorporating MFA and its standard deviation

Table G.2: List of abbreviations used in Chapter 3 continued

Abbreviation	Value	Description
ρ		Density of the stem
ρ_c	$5.6kg/m^3$	Density of the canopy
λ		Any constant calculated depending on its position of in the stem
$\boldsymbol{S}$		Compliance matrix in global coordinate system
$\boldsymbol{S_l}$		Compliance matrix in local coordinate system
$\boldsymbol{C}$		Stiffness matrix in global coordinate system
$\boldsymbol{C_l}$		Stiffness matrix in local coordinate system
$\boldsymbol{G}$		Transformation matrix
$\boldsymbol{\sigma}$		Stress in global coordinate system
$\boldsymbol{\sigma_l}$		Stress in local coordinate system
g	$9.81N$	Gravitational force
b, d		Horizontal and vertical radius of the canopy
z_0, z_1		Lower and upper heights of crown effecting the current point
B_s		Force per unit stem volume due to gravity acting on the stem
B_c		Force per unit stem volume due to gravity acting on the canopy
$\boldsymbol{\Omega}$		Domain of the entire stem
$\boldsymbol{\Omega_1}$		Domain of the stem where the canopy's gravitational force acts
S_c		Hight where the canopy starts
h_c		Height of the canopy
r_c		Maximum radius of the canopy
r_s		Radius of the stem at age 15
$\boldsymbol{\Gamma}$		Surface domain of entire stem
$\boldsymbol{\Gamma_1}$		Surface domain of stem where canopy is attached
ω		Wind speed
ρ_{air}	$1.226kg/m^3$	Air density
ς		Canopy drag coefficient

Table G.3: List of abbreviations used in Chapter 3 continued

Abbreviation	Value	Description
M_c		Maximum bending movement
D_{M_c}		Deflection at maximum bending moment
Y_l	0.1	Yield limit for growth stress profile
R		Maximum stem radius at the height of the point being evaluated
r_{core}		Radius of the core of the stem which is assumed to have a constant growth stress profile
IT_{stress}		Initial longitudinal tensile stress from growth stresses
G_s		Imposed growth stress in the longitudinal direction
$\boldsymbol{\sigma_{gs}}$		Imposed growth stress vector
$\boldsymbol{\epsilon}$		Strain in the global coordinate system
W		Strain energy density
$\prod$		Potential energy
$\boldsymbol{u}$		Displacement vector
Ω_{bc1}		Boundary condition one
Ω_{bc2}		Boundary condition two
tol_z		z value which all points below are on the bottom boundary of the mesh
tol		Tolerance required to select only seedling points on bottom boundary
SF_{ten}		Safety factor in the tensile direction
SF_{comp}		Safety factor in the compressive direction

Bibliography

Ancelin, P., Courbaud, B., and Fourcaud, T. (2004). Development of an individual tree-based mechanical model to predict wind damage within forest stands. *Forest Ecology and Management*, 203(1–3):101–121.

Anders Logg, K.-A. M. and Wells, G. N. (2011). *Automated Solution of Differential Equations by the Finite Element Method - The FEniCS Book*. GNU Free Documentation License Version 1.3. www.http://fenicsproject.org/.

Apiolaza, L. A., Butterfield, B., Chauhan, S. S., and Walker, J. C. F. (2011). Characterization of mechanically perturbed young stems: Can it be used for wood quality screening? *Annals of Forest Science*, 68(2):407–414.

Archer, R. (1976). On the distribution of tree growth stresses. Part II: Stresses due to asymmetric growth strains. *Wood Science and Technology*, 10(4):293–309.

Archer, R. (1979). On the distribution of tree growth stresses. Part III: The case of inclined grain. *Wood Science and Technology*, 13(1):67–78.

Archer, R. (1981). On the distribution of tree growth stresses. Part IV: The general case allowign longitudinal and circumferential variation of growth stresses. *Wood Science and Technology*, 15(3):201–209.

Archer, R. (1985). On the distribution of tree growth stresses. Part V: Asymmetric peripheral growth strains with orthotropic material behavior. *Wood Science and Technology*, 19(3):259–276.

Archer, R. (1987). On the origin of growth stresses in trees. Part I: Micro mechanics of the developing cambial cell wall. *Wood Science and Technology*, 21(2):139–154.

Archer, R. (1989). On the origin of growth stresses in trees. Part II: Stresses generated in a tissue of developing cells. *Wood Science and Technology*, 23(4):311–322.

Archer, R. and Byrnes, F. E. (1974). On the distribution of tree growth stresses. Part I: An anisotropic plane strain theory. *Wood Science and Technology*, 8(3):184–196.

Archer, R. R. (1986). *Growth stresses and strains in trees*. Springer series in wood science. Springer-Verlag, Berlin; New York.

Ascher, D., Dubois, P. F., Hinsen, K., Hugunin, J., and Oliphant, T. (1999). *Numerical Python*. Lawrence Livermore National Laboratory, Livermore, CA. http://www.numpy.org/.

Asnacios, A. and Hamant, O. (2012). The mechanics behind cell polarity. *Trends in Cell Biology*, 22(11):584–591.

Astley, R. J., Stol, K. A., and Harrington, J. J. (1998). Modelling the elastic properties of softwood. *Holz als Roh- und Werkstoff*, 56(1):43–50.

AUS/NZS (2010). *Characterization of structural timber - Test methods, AS/NZS 4063.1:2010*. Standards New Zealand.

Barkas, W. W. (1949). *The swelling of wood under stress: a discussion of its hygroscopic, elastic and plastic properties, based on a course of lectures given at Svenska traforskningsinstitutet, Stockholm, Sweden, March 1948*. H. M. Stationery Off.

Barker, J. (1998). The properties of in-grade *Pinus radiata* timber from peeler cores.

Beets, P. N. and Whitehead, D. (1996). Carbon partitioning in *Pinus radiata* stands in relation to foliage nitrogen status. *Tree Physiology*, 16(1-2):131138.

Bodig, J. and Jayne, B. A. (1982). *Mechanics of wood and wood composites*. New York: Van Nostrand Reinhold.

BS (1957). *Methods of testing small clear specimens of timber, BS 373:1957*. BSI British Standards.

Burdon, R. D., Kibblewhite, R. P., Walker, J. C. F., Megraw, R. A., Evans, R., and Cown, D. J. (2004). Juvenile versus mature wood: A new concept, orthogonal to corewood versus outerwood, with special reference to *Pinus radiata* and *P. taeda*. *Forest Science*, 50(4):399–415.

Burgess, S. C. and Pasini, D. (2004). Analysis of the structural efficiency of trees. *Journal of Engineering Design*, 15(2):177–193.

Butterfield, B. and Meylan, B. A. (1980). *Three-dimensional structure of wood*. Chapman and Hall, London, second edition.

Cave, I. and Robinson, W. (1998a). Interpretation of (002) diffraction arcs by means of a minimalist model. *Mircofibril Angle in Wood, International Association of Wood Anatomists*, pages 108–115.

Cave, I. and Robinson, W. (1998b). Measuring microfibril angle distribution in the cell wall by means of x-ray diffraction. *Mircofibril Angle in Wood, International Association of Wood Anatomists*, pages 94–107.

Cave, I. D. and Walker, J. C. F. (1994). Stiffness of wood in fast-grown plantation softwoods - the influence of microfibril angle. *Forest Products Journal*, 44:43–48.

Chauhan, S. S., Sharma, M., Thomas, J., Apiolaza, L. A., Collings, D. A., and Walker, J. C. (2013). Methods for the very early selection of *Pinus radiata* D. Don. for solid wood products. *Annals of Forest Science*, 70(4):439–449.

Chris Eberl, Robert Thompson, D. G. S. B. (2006). Digital image correlation and tracking with matlab. http://www.mathworks.com/matlabcentral/fileexchange/12413-digital-image-correlation-and-tracking.

Contributors, V. (2013). Gphoto2, version 2.5.1. http://www.gphoto.org/.

Coutts, M. P. and Grace, J. (1995). *Wind and trees*. Cambridge University Press, Cambridge; New York.

Domec, J. C. and Gartner, B. L. (2002). Age- and position-related changes in hydraulic versus mechanical dysfunction of xylem: inferring the design criteria for Douglas-fir wood structure. *Tree physiology*, 22(2-3):91–104.

Downes, G. M., Nyakuengama, J. G., Evans, R., Northway, R., Blakemore, P., Dickson, R. L., and Lausberg, M. (2002). Relationship between wood density, microfibril angle and stiffness in thinned and fertilized *Pinus radiata*. *Iawa Journal*, 23(3):253–265.

Dunham, R. A. and Cameron, A. D. (2000). Crown, stem and wood properties of wind-damaged and undamaged Sitka spruce. *Forest Ecology and Management*, 135(1–3):73–81.

England, A. (2000). A dynamic analysis of windthrow of trees. *Forestry*, 73(3):225–238.

Fourcaud, T., Blaise, F., Lac, P., Castera, P., and Reffye, P. (2003). Numerical modelling of shape regulation and growth stresses in trees. *Trees*, 17(1):31–39.

Fourcaud, T., Guillon, T., and Dumont, Y. (2011). Biomechanics of growing trees: Mathematical model, numerical resolution and perspectives. *AIP Conference Proceedings*, 1389(1):734–737.

Gamstedt, E., Bader, T., and Borst, K. (2013). Mixed numerical-experimental methods in wood micromechanics. *Wood Science and Technology*, 47(1):183–202.

Gardiner, B., Byrne, K., Hale, S., Kamimura, K., Mitchell, S. J., Peltola, H., and Ruel, J.-C. (2008). A review of mechanistic modelling of wind damage risk to forests. *Forestry*, 81(3):447–463.

Gardiner, B., Peltola, H., and Kellomki, S. (2000). Comparison of two models for predicting the critical wind speeds required to damage coniferous trees. *Ecological Modelling*, 129(1):1–23.

Gartner, B. L. (1995). *Plant Stems: Physiology and Functional Morphology*. Academic Press., San Diego.

Geitmann, A. (2010). Mechanical modeling and structural analysis of the primary plant cell wall. *Current Opinion in Plant Biology*, 13(6):693–699.

Gibson, L.and Ashby, M. (1997). *Cellular solids: structure and properties*. Cambridge; New York: Cambridge University Press, 2nd edition.

Gillis, P. (1973). Theory of growth stresses. *Holzforschung*, 27(6):197–207.

Gillis, P. P. and Hsu, C. H. (1979). An elastic plastic theory of longitudinal growth stresses. *Wood Science and Technology*, 13(2):97–115.

Green, A. E. and Laws, N. (1966). A general theory of rods. *Proceedings of the Royal Society of London. Series A, Mathematical and Physical Sciences*, 293(1433):145–155.

Guillon, T., Dumont, Y., and Fourcaud, T. (2012a). A new mathematical framework for modelling the biomechanics of growing trees with rod theory. *Mathematical and Computer Modelling*, 55(9–10):2061–2077.

Guillon, T., Dumont, Y., and Fourcaud, T. (2012b). Numerical methods for the biomechanics of growing trees. *Computers & Mathematics with Applications*, 64(3):289–309.

Gustafsson, P. J. (2003). Modelling of mechanical properties of wood and wood-based materials. *Schweizerische Zeitschrift fur Forstwesen*, 154(12):504–509.

Hanhijrvi, A. and Mackenzie-Helnwein, P. (2003). Computational analysis of quality reduction during drying of lumber due to irrecoverable deformation. I: orthotropic viscoelastic-mechanosorptive-plastic material model for the transverse plane of wood. *Journal of Engineering Mechanics*, 129(9):996–1005.

Harrington, J. J. (2002). *Hierarchical modelling of softwood hygro-elastic properties*. Mechanical engineering, University of Canterbury, Christchurch, New Zealand.

Henrik, D. and Gustafsson, P. J. (2013). A three dimensional plasticity model for perpendicular to grain cohesive fracture in wood. *Engineering Fracture Mechanics*, 98:137–152.

Hibbeler, R. (2000). *Mechanics of materials*. New Jersey: Prentice Hall, Fourth edition.

Hill, R. (1950). *The mathematical theory of plasticity*. Oxford: Clarendon Press.

Hofstetter, K. and Gamstedt, E. K. (2008). Hierarchical modelling of microstructural effects on mechanical properties of wood. a review. *Holzforschung*, 63(2):130–138.

Holmberg, S., Persson, K., and Petersson, H. (1999). Nonlinear mechanical behaviour and analysis of wood and fibre materials. *Computers & Structures*, 72(4-5):459–480.

James, K. (2003). Dynamic loading of trees. *Arboriculture and urban forestry*, 29(3):165–171.

Jaouen, G., Almeras, T., Coutand, C., and Fournier, M. (2007). How to determine sapling buckling risk with only a few measurements. *American Journal of Botany*, 94(10):1583–1593.

Jones, E., Oliphant, T., Peterson, P., et al. (2001). SciPy: Open source scientific tools for Python. http://www.scipy.org/.

Kern, K. A., Ewers, F. W., Telewski, F. W., and Koehler, L. (2005). Mechanical perturbation affects conductivity, mechanical properties and aboveground biomass of hybrid poplars. *Tree Physiology*, 25(10):1243–1251.

Kollmann, F. and Cote, W. (1968). *Principles of Wood Science and Technology. Part I Solid Wood*. Springer-Verlag Berlin Heidelberg New York.

Larson, P. (1966). Changes in the chemical composition of wood cell walls associated with age in *Pinus resinosa*. *Forest Products Journal*, 16:37–45.

Lasserre, J.-P., Mason, E. G., Watt, M. S., and Moore, J. R. (2009). Influence of initial planting spacing and genotype on microfibril angle, wood density, fibre properties and modulus of elasticity in *Pinus radiata D. Don* corewood. *Forest Ecology and Management*, 258(9):1924–1931.

Leech, J. W. (1984). Estimating crown width from diameter at breast height for open-grown radiata pine trees in south australia. *Australian forest research*, 14(4):333–337.

Lindström, H., Harris, P., and Nakada, R. (2002). Methods for measuring stiffness of young trees. *Holz als Roh- und Werkstoff*, 60(3):165–174.

Lindström, H., Harris, P., Sorensson, C. T., and Evans, R. (2004). Stiffness and wood variation of 3-year old *Pinus radiata* clones. *Wood Science and Technology*, 38(8):579–597.

Liu, G. R. (2010). *Meshfree methods: Moving beyond the finite element method*. CRC Press, second edition.

Lundh, F. et al. (1995). *Python Imaging Library*. http://www.pythonware.com/products/pil/.

Mackenzie-Helnwein, P., Eberhardsteiner, J., and Mang, H. A. (2003). A multi-surface plasticity model for clear wood and its application to the finite element analysis of structural details. *Computational Mechanics*, 31(1-2):204–218.

Mackenzie-Helnwein, P., Eberhardsteiner, J., and Mang, H. A. (2005a). Rate-independent mechanical behavior of biaxially stressed wood: Experimental observations and constitutive modeling as an orthotropic two-surface elasto-plastic material. *Holzforschung*, 59(3):311–321.

Mackenzie-Helnwein, P. and Hanhijrvi, A. (2003). Computational analysis of quality reduction during drying of lumber due to irrecoverable deformation. II: algorithmic aspects and practical application. *Journal of Engineering Mechanics*, 129(9):1006–1016.

Mackenzie-Helnwein, P., Mllner, H. W., Eberhardsteiner, J., and Mang, H. A. (2005b). Analysis of layered wooden shells using an orthotropic elasto-plastic model for multi-axial loading of clear spruce wood. *Computer Methods in Applied Mechanics and Engineering*, 194(21–24):2661–2685.

Mark, R. E. (1967). *Cell wall mechanics of tracheids.* Yale University Press, New Haven.

Mattheck, C. (1990). Engineering components grow like trees. *Materialwissenschaft und Werkstofftechnik*, 21(4):143–168.

Mattheck, C. (1991). *Trees: the mechanical design.* Springer Verlag, Berlin.

Mattheck, C., Bethge, K., and Tesari, I. (2006). Shear effects on failure of hollow trees. *Trees*, 20(3):329–333.

Mattheck, C. and Kubler, H. (1995). *Wood - The internal optimization of trees.* Springer series in wood science. Springer, Berlin.

Mayer, H., Raupach, M. R., Kohsiek, W., Gardiner, B., Clarke, J. A., Amtmann, R., Crowther, J. M., Jarvis, P. G., and Milne, R. (1989). Windthrow [and discussion]. *Philosophical Transactions of the Royal Society of London. B, Biological Sciences*, 324(1223):267–281.

Mayhead, G. (1973). Some drag coefficients for British forest trees derived from wind tunnel studies. *Agricultural Meteorology*, 12:123130.

Meinzer, F. C., Lachenbruch, B., and Dawson, T. E. (2011). *Size- and Age- Related Changes in Tree Structure and Function*, volume four of *Tree Physiology.* Springer.

Mishnaevsky Jr., L. and Qing, H. (2008). Micromechanical modelling of mechanical behaviour and strength of wood: State-of-the-art review. *Computational Materials Science*, 44(2):363–370.

Moden, C. S. (2008). *Micromechanics of softwoods in the transverse plane: effects on cell and annual ring scales*. PhD thesis, KTH Royal Institute of Technology, Stockholm, Sweden.

Moden, C. S. and Berglund, L. (2008). Elastic deformation mechanisms of softwoods in radial tension: Cell wall bending or stretching? *Holzforschung*, 62(5):562–568.

Moore, J. and Gardiner, B. (2001). Relative windfirmness of New Zealand grown *Pinus radiata* and Duglas-fir: A preliminary investigation. *Forest Ecology and Management*, 31(2):208–223.

Moore, J. and Quine, C. P. (2000). A comparison of the relative risk of wind damage to planted forests in border forest park, Great Britain, and the central North Island, New Zealand. *Forest Ecology and Management*, 135(1-3):345–353.

Morgan, J. and Cannell, M. G. R. (1987). Structural analysis of tree trunks and branches: tapered cantilever beams subject to large deflections under complex loading. *Tree Physiology*, 3(4):365–374.

Niklas, K. J. (1992). *Plant Biomechanics: An Engineering Approach to Plant Form and Function*. University of Chicago Press.

Niklas, K. J. (1997). Mechanical properties of black locust (*Robinia pseudoacacia*) wood: Correlations among elastic and rupture moduli, proportional limit, and tissue density and specific gravity. *Annals of Botany*, 79(5):479–485.

Niklas, K. J. and Spatz, H.-C. (2000). Wind-induced stresses in cherry trees: Evidence against the hypothesis of constant stress levels. *Trees*, 14(4):230–237.

Niklas, K. J. and Spatz, H.-C. (2012). *Plant Physics*. University of Chicago Press.

Ormarsson, S. and Cown, D. (2005). Moisture-related distortion of timber boards of radiata pine: Comparison with Norway spruce. *Wood and Fiber Science*, 37(3):424–436.

Ormarsson, S., Dahlblom, O., and Johansson, M. (2010). Numerical study of how creep and progressive stiffening affect the growth stress formation in trees. *Trees*, 24(1):105–115.

Ozyhar, T., Hering, S., and Niemz, P. (2013). Moisture-dependent orthotropic tension-compression asymmetry of wood. *Holzforschung*, 67(4):395–404.

Papesch, A., Moore, J., and Hawke, A. (1997). Mechanical stability of *Pinus radiata* trees at Eyrewell forest investigated using static tests. *New Zealand Journal of Foresty Science*, 27(2):188–204.

Peltola, H., Kellomki, S., Hassinen, A., and Granander, M. (2000). Mechanical stability of Scots pine, Norway spruce and birch: an analysis of tree-pulling experiments in Finland. *Forest Ecology and Management*, 135(1–3):143–153.

Peltola, H., Kellomki, S., Visnen, H., and Ikonen, V. P. (1999). A mechanistic model for assessing the risk of wind and snow damage to single trees and stands of Scots pine, Norway spruce, and birch. *Canadian Journal of Forest Research*, 29(6):647–661.

Peltola, H. M. (2006). Mechanical stability of trees under static loads. *American Journal of Botany*, 93(10):1501–1511.

Persson, K. (2000). *Micromechanical Modelling of Wood and Fibre Properties*. Structural mechanics, Lund University, Lund, Sweeden.

Qing, H. and Mishnaevsky, L. (2009). 3D hierarchical computational model of wood as a cellular material with fibril reinforced heterogeneous multiple layers. *Mechanics of Materials*, 41(9):1034–1049.

Raffaele, D. A., Riggio, M., Girardi, G., and Piazza, M. (2011). Morphology-based macro-scale finite-element timber models. *Computer-Aided Design*, 43(1):72–87.

Rao, S. (1999). *The Finite Element Method in Engineering*. Boston, Mass.; Oxford: Butterworth Heinemann, third edition.

Reiterer, A., Lichtenegger, H., Tschegg, S., and Fratzl, P. (1999). Experimental evidence for a mechanical function of the cellulose microfibril angle in wood cell walls. *Philosophical Magazine a-Physics of Condensed Matter Structure Defects and Mechanical Properties*, 79:2173–2184.

Rudnicki, M., Mitchell, S. J., and Novak, M. D. (2004). Wind tunnel measurements of crown streamlining and drag relationships for three conifer species. *Canadian Journal of Forest Research*, 34(3):666–676.

Salenon, J. (2001). *Handbook of continuum mechanics: general concepts, thermoelasticity*. Berlin; New York: Springer.

Schniewind, A. P. and Barrett, J. D. (1972). Wood as a linear orthotropic viscoelastic material. *Wood Science and Technology*, 6(1):43–57.

Schopfer, P. (2006). Biomechanics of plant growth. *American Journal of Botany*, 93:1415–1425.

Skaar, C. (1988). *Wood-Water Relations*. Springer Series in Wood Science. Springer-Verlag.

Skatter, S. and Archer, R. (2001). Residual stresses caused by growth stresses within a stem with radially varying spiral grain angle - two numerical solution approaches: 1) Finite element method and 2) Transfer matrix method. *Wood Science and Technology*, 35(1-2):57–71.

Spatz, H.-C. and Bruechert, F. (2000). Basic biomechanics of self-supporting plants: Wind loads and gravitational loads on a Norway spruce tree. *Forest Ecology and Management*, 135(1-3):33–44.

Tabarsa, T. and Chui, Y. (2000). Stress-strain response of wood under radial compression. Part I: Test method and influences of cellular properties. *Wood and Fiber Science*, 32(2):144–152.

Timell, T. E. (1986a). *Compression wood in gymnosperms*, volume two. Springer-Verlag, Berlin; New York.

Timell, T. E. (1986b). *Compression wood in gymnosperms*, volume three. Springer-Verlag, Berlin; New York.

Tsai, S. W. and Wu, E. M. (1971). General theory of strength for anisotropic materials. *Journal of Composite Materials*, 5:58–80.

Waghorn, M. J., Mason, E. G., and Watt, M. S. (2007a). Influence of initial stand density and genotype on longitudinal variation in modulus of elasticity for 17-year-old *Pinus radiata*. *Forest Ecology and Management*, 252(1-3):6772.

Waghorn, M. J., Watt, M. S., and Mason, E. G. (2007b). Influence of tree morphology genetics, and initial stand density on outerwood modulus of elasticity of 17-year-old *Pinus radiata*. *Forest Ecology and Management*, 244(1-3):86–92.

Walker, J. (1993). *Primary wood processing. Principles and practice*. Springer, Dordrecht, first edition.

Walker, J. (2006). *Primary wood processing. Principles and practice*. Springer, Dordrecht, second edition.

Watanabe, U., Norimoto, M., and Morooka, T. (2000). Cell wall thickness and tangential youngs modulus in coniferous early wood. *Journal of Wood Science*, 46(2):109–114.

Watt, M. S., Clinton, P. W., Coker, G., Davis, M. R., Simcock, R., Parfitt, R. L., and Dando, J. (2008). Modelling the influence of environment and stand characteristics on basic density and modulus of elasticity for young *Pinus radiata* and *Cupressus lusitanica*. *Forest Ecology and Management*, 255(3-4):1023–1033.

Watt, M. S., Moore, J. R., Faon, J.-P., Downes, G. M., Clinton, P. W., Coker, G., Davis, M. R., Simcock, R., Parfitt, R. L., Dando, J., Mason, E., and Bown, H. (2006). Modelling the influence of stand structural, edaphic and climatic influences on juvenile *Pinus radiata* dynamic modulus of elasticity. *Forest Ecology and Management*, 229(1-3):136–144.

Watt, M. S., Sorensson, C., Cown, D. J., Dungey, H. S., and Evans, R. (2010). Determining the main and interactive effect of age and clone on wood density, microfibril angle, and modulus of elasticity for *Pinus radiata*. *Canadian Journal of Forest Research*, 40(8):1550–1557.

Watt, M. S. and Zoric, B. (2010). Development of a model describing modulus of elasticity across environmental and stand density gradients in plantation-grown *Pinus radiata* within New Zealand. *Canadian Journal of Forest Research*, 40(8):1558–1566.

Watt, M. S., Zoric, B., Kimberley, M. O., and Harrington, J. (2011). Influence of stocking on radial and longitudinal variation in modulus of elasticity microfibril angle, and density in a 24-year-old *Pinus radiata* thinning trial. *Canadian Journal of Forest Research*, 41(7):1422–1431.

Xinguo, L., Wu, H. X., and Southerton, S. G. (2011). Transcriptome profiling of *Pinus radiata* juvenile wood with contrasting stiffness identifies putative candidate genes involved in microfibril orientation and cell wall mechanics. *BMC Genomics*, 12(1):480.

Xu, P., Donaldson, L., Walker, J., Evans, R., and Downes, G. (2004). Effects of density and microfibril orientation on the vertical variation of low-stiffness wood in radiata pine butt logs. *Holzforschung*, 58(6):673–677.

Yamamoto, H. (1998). Generation mechanism of growth stresses in wood cell walls: Roles of lignin deposition and cellulose microfibril during cell wall maturation. *Wood Science and Technology*, 32(3):171–182.

Yamamoto, H., Yoshida, M., and Okuyama, T. (2002). Growth stress controls negative gravitropism in woody plant stems. *Planta*, 216:280–292.

Yamashita, K., Hirakawa, Y., Nakatani, H., and Ikeda, M. (2009). Longitudinal shrinkage variations within trees of sugi (*Cryptomeria japonica*) cultivars. *Journal of Wood Science*, 55(1):1–7.

Yeh, B. and Schniewind, A. (1992). Elasto-plastic fracture mechanics of wood using the j-intergral method. *Wood and Fiber Science*, 24(3):364–376.

Yoshihara, H. (2009). Prediction of the off-axis stress-strain relation of wood under compression loading. *European Journal of Wood and Wood Products*, 67(2):183–188.